Doctoral theses at NTNU, 2020:227

Ganesh Hiriyanna Rao Ravindra

Hydraulic and structural evaluation of rockfill dam behavior when exposed to throughflow and overtopping scenarios

Doctoral Thesis

Ganesh Hiriyanna Rao Ravindra

ISBN 978-82-326-4802-3 (printed version)
ISBN 978-82-326-4803-0 (electronic version)
ISSN 1503-8181

NTNU
Norwegian University of
Science and Technology

NTNU
Norwegian University of
Science and Technology
Faculty of Engineering
Department of Civil and Environmental Engineering

Doctoral theses at NTNU, 2020:227

NTNU

NTNU
Norwegian University of
Science and Technology

Ganesh Hiriyanna Rao Ravindra

Hydraulic and structural evaluation of rockfill dam behavior when exposed to throughflow and overtopping scenarios

Thesis for the degree of Philosophiae Doctor

Trondheim, August 2020

Norwegian University of Science and Technology
Faculty of Engineering
Department of Civil and Environmental Engineering

NTNU
Norwegian University of
Science and Technology

NTNU
Norwegian University of Science and Technology

Thesis for the degree of Philosophiae Doctor

Faculty of Engineering
Department of Civil and Environmental Engineering

ISBN 978-82-326-4802-3 (printed version)
ISBN 978-82-326-4803-0 (electronic version)
ISSN 1503-8181

Doctoral theses at NTNU, 2020:227

Printed by Skipnes Kommunikasjon as

Preface

This thesis is submitted to the Norwegian University of Science and Technology (NTNU), Trondheim for partial fulfilment of the requirements for the degree of Philosophiae Doctor (PhD).

The work presented in the thesis is the result of a three-year PhD program, which was conducted at the Department of Civil and Environmental Engineering, NTNU, Trondheim. Ass. Prof. Fjóla Guðrún Sigtryggsdóttir has been the main supervisor and Prof. Leif Lia has been the co-supervisor.

The PhD project has been funded by the Norwegian Research Centre for Hydropower Technology (HydroCen) under Work Package 1.2, pertaining to research on embankment dam stability under extreme loading conditions. Part of the research was also supported by Energi Norge AS, Norway.

In accordance with the guidelines of the Faculty of Engineering Science and Technology, the thesis contains an introduction to, and includes, five scientific journal papers and three conference papers (listed on page. XII).

Acknowledgements

Disclaimer: This is the only section of the thesis that has not been subjected to a rigorous peer-review process.

I have on numerous occasions come across the statement '*Life is a journey, not a destination'*. I have come to gain a much deeper understanding of the essence of the statement over the duration of my doctoral studies. I have been very fortunate to have built professional and personal relationships with several colleagues and friends over this period. These very special individuals have taught me invaluable lessons and have helped and supported me in more ways than I can recollect. This is a humble attempt at conveying me deepest appreciations and gratitude.

No series of words could possibly do justice to express my thoughts towards my main supervisor, Ass. Prof. Fjola Gudrun Sigtryggsdottir. She is without a doubt the most genuine, kindhearted, thoughtful and humble person I have had the privilege of knowing. I could not have asked for a better supervisor and a colleague to work with. The whole process of working on a doctoral study becomes simpler and more joyous when the supervisor shares the same level of enthusiasm and exuberance in conduction research. It would not be an overstatement to say that Fjola has been as eager as I have been, if not more in working on this research project. All the long discussion we have had crafting the study, working on writing articles together, travelling to meetings and conferences and just absorbing from her vast technical expertise have in many ways made me a better researcher and most importantly, a better individual. She has made every effort to comfort me and support me during these past years, helping me get through difficult times. Perhaps the best attribute to Fjola is her lovely family. Fjola along with her husband Mr. Eggert Vilberg Valmundsson, and very talented and funny kids Ms. Þorbjörg Gróa Eggertsdóttir and Mr. Valmundur Rósmar Eggertsson have treated me like a family member. I will always be grateful for all the great experiences and memories the family has given me. I firmly hold the position that the most valuable gift a person can give another is an opportunity at life itself. I got the opportunity to work on this project from Fjola and it is no exaggeration when I say I owe everything to her.

As with the main supervisor for the project, I have also been lucky to have Prof. Leif Lia as my co-supervisor for the study. Most know him as an inspiring, humorous and dedicated communicator of hydropower engineering. I also know him as a motor bike and car enthusiast, ski aficionado and most importantly, a very kind and caring human being. I have been a big

fan of Leif ever since I attended his dam engineering course, back when I started out my master studies at NTNU. He possesses a unique skill of communicating technical knowledge to his audience is the most captivating manner. It has been a privilege and an immense learning experience working with Leif these past years. I will forever cherish all our discussions on research, motor bikes (yes, I will get a license soon) and life in general, Thank you.

My supervisor Fjola once told me that having one good friend is worth more than all the wealth in the world. I could not agree with her more on that. I have truly been gifted with many close friends who have played major parts in keeping me going these past years. I would have to start with my dear friend Dr. Marius Rokstad. I once asked Marius why he left his well-paying job at a consultancy firm to get into research, to which he promptly replied, '*Science is fun'*. I have had the privilege to get to know Marius over the past years to be a motivated researcher, highly talented musician and a genuinely caring soul. He inspired me to pick up the guitar and this has enriched my life in many ways. I also feel to proud to have him as a co-author on an article. Marius and his loving wife Mrs. Aline Looten, a talented and dedicated teacher herself, have been exceedingly kind to me and have made my life here more enjoyable. I have never felt home sick as they basically have been more than family.

I have never liked working on the 2nd floor of our department. It as an eerie atmosphere I detest, and I call it the 'dungeon of science'. My office neighbor Ms. Noemi Ambauen has made it much easier working there. We generally begin our workdays with short discussions on deep philosophical issues, pondering at the big questions of life. We also share common interests such as being vegan and being out in nature. Noemi is one of the most accepting and transparent people I have the pleasure of referring to as a friend. I will always cherish our friendship. My dear friend Halvor Kjærås and his entire family in Sandefjord have treated me with much affection for which I will always be thankful. Halvor is a master of several crafts such as science, music and wordplay. I do not know a more creative individual than Halvor and I feel lucky to have him as a friend. I also owe my dear friend Mr. Ola Haugen Havrevoll a thousand thanks as we say in Norwegian. I come to realize the generous nature of Ola more every time I talk with him. Ola has always made me feel welcome and part of the culture here and has helped me find confidence in myself. His picture-perfect family with Kristina, Kåre and Tor have also been an integral part of my life here. Thank you, Ola, for all your support and guidance. I wish to thank Mr. Geir Kiplesund, who is partner on the research project and also a very close friend. Through all our interactions and travels, I have had the pleasure of getting well-acquainted with this kind and caring personality. He has taught me many things about

engineering and has been providing me with daily recommended doses of deep insights and perspectives into life. I feel lucky to have him on the project with us. There is much for me to learn from his vast experience. Thanks also to his lovely family for treating me with fondness.

My many colleagues who are also close friends such as Mr. Eirik Øvregård, Dr. Kaspar Vereide, Dr. Michael Waak, Ms. Livia Pitorac, Dr. Ushanth Navaratnam, Dr. Pierre Yves Henry, Mr. Håkon Sundt, Mr. Jo Halvard have supported me in many ways over this time period. I just want to communicate my heartfelt regards to all of these very special people.

I would also like to sincerely thank faculty members of the department such as Prof. Oddbjørn Bruland, Prof. Knut Alfredsen, Prof. Nils Ruther, Prof. Tor Håkon Bakken, Prof. Sveinung Sægrov for all their support and guidance. All the experimental work we have done as part of the project would not be made possible without the technical and logistical support offered by lab personnel such a Mr. Geir Tesaker, Mr. Thai Mai, Mr. Eirik Nygård and Mr. Vegar Eliassen.

It is not easy carrying the burden of science and this becomes a greater challenge when that burden is three tons of stones and rockfill. Luckily, many master students and assistants have lent hands in carrying all that weight. The blood, sweat and tears offered by Mr. Kofi Opare, Ms. Malin Asbølmo, Mr. Unnar Almarsson, Mr. Nils Smith, Mr. Tellev Lia and Mr. Styrmir Sigurjonsson will never be forgotten.

I very much appreciate the support of Dr. Grethe Holm Midttømme and Mr. Morten Skoglund working at the dam safety section of NVE, Trondheim. Their interest in our research has provided me with much enthusiasm. Special thanks to Dr. Priska Hiller, NVE for her contributions with our research. Her efforts in designing and testing the first lab model greatly helped my further works. And I must apologize to Priska for bothering her with many phone calls and emails with requests for information and advice. The support offered by several dam owning agencies such as Statkraft, BKK and SKL during our field surveys is greatly appreciated. I would also wish to acknowledge the kind invitation offered by Ms. Siri Stokseth, Statkraft to partake in a field visit to Albania. It was a great learning experience.

I would like to thank all the co-authors on the articles. Dr. Oliver Gronz and Mr. Bastian Dost from the University of Trier, Germany and Mr. Øyvind Høydal, NGI, Oslo for all their contributions to our research. It has been a pleasure collaborating with them.

Finally, I would like to convey my appreciations to my parents Mrs. Geeta K, Mr. Ravindra H, my extended family members Ms. Vasundhara K, Mrs. Kamala H, Mr. Anantharamu KV, Mrs. Rashmi R and Mr. Raghavendra H. A and my siblings Ms. Nagashree H R and Mr. Koushik H R. Special shout out to my brother Venkatesh A, who presently works as a geophysicist at Ikon Sciences, USA. He has always set the bar high in the family and has been an inspiring figure, someone to look up to. He taught me to go at life with everything I have, Thanks Venki.

"Because the cosmos is also within us. We are made of star-stuff. We are a way for the universe to know itself."

— Carl Sagan, Cosmos- The shores of the cosmic ocean, 1980

Abstract

Dams are vulnerable to extreme flood events in turn leading to accidental overtopping. This in particular applies to rockfill dams comprised of pervious and erodible material. Obtaining better understanding of behavior of rockfill dam components under extreme loading conditions is of significance from stability and economic standpoints. The aim of the research work forming the basis for the thesis has been to present descriptions of hydraulic and structural behaviors of rockfill dams under throughflow and or overtopping scenarios. Research findings outlining failure mechanisms and stability aspects of ripraps under overtopping scenarios are presented. Results from field surveys conducted to investigate construction aspects of placed ripraps constructed on rockfill dams are described. Further, experimental results demonstrating the hydraulic response of rockfill dam structures exposed to overtopping conditions are provided. Furthermore, behavior of rockfill dam structures coupled with disparate toe configurations subjected to throughflows are described based on experimental model studies. The overarching focus of the research has been to obtain a holistic evaluation of rockfill dam behavior when subjected to extreme loading conditions. This in turn is intended at improving the state of the art in design and construction of these structures.

Summary

Assessment of rockfill dam stability under extreme loading scenarios is an intricate task influenced by significant number of parameters. Ripraps comprising of large natural rock elements are constructed on the downstream slopes of rockfill dams to protect against surface erosion due to overflow. Under throughflow scenarios, rockfill dam stability is primarily influenced by the interaction between the flow and the rockfill material. Further, rockfill dam toes are commonly coupled with the downstream rockfill dam structure to counter the destabilizing effects of throughflow.

The downstream slopes of Norwegian rockfill dams are protected with single layer placed ripraps, comprising of stones placed in an interlocking pattern. Available international literature describing stability aspects of placed ripraps under overtopping conditions is limited. Furthermore, past studies have been limited to describing 1D failure mechanisms in placed ripraps. With an aim of further extending past findings describing unidimensional failure mechanisms in placed ripraps to 2D, experimental data sets accumulated by a past investigation conducted at NTNU, Trondheim through physical modelling investigation conducted on 1:10 scaled model ripraps constructed with angular stones on a steep slope (S = 0.67) were further analyzed with additional tests. Results from the study provide qualitative and quantitative descriptions of a unique failure mechanism in placed ripraps interrelating the disciplines of hydraulic and structural research. Investigation results demonstrated that placed ripraps supported at the toe underwent progressive deformations in 2D when exposed to overtopping flows. The deformation behavior was found to closely resemble the buckling process in a slender-long column pinned at one end and free at the other. These 2D deformations in turn were found to result in total riprap failure commencing at the upstream section of the riprap.

Toe sections of rockfill dams and ripraps are considered critical locations for initiation of progressive dam failure under overtopping conditions. With an objective of investigating construction aspects of rockfill dam toe structures and toe support conditions for placed ripraps, a field survey of nine Norwegian rockfill dams was carried out as part of this doctoral study. As part of the survey, key parameters describing quality of placed riprap construction such as stone sizing, angularity and placement inclination were analyzed. Conformity of placed riprap construction practices with official dam safety guidelines were evaluated. Further, details concerning existing state of toe conditions for the surveyed riprap structures were outlined. Study findings suggest that construction practices adopted for placed ripraps meet the

requirements of official dam safety regulations with respect to sizing of the stones. However, additional recommendations put forward by the dam safety authorities with regards to placement inclination, material uniformity and angularity are not prioritized. Furthermore, detailed survey of riprap toe sections revealed that well-defined toe support measures stabilizing riprap toes are currently not implemented at any of the surveyed rockfill dams.

All past experimental model studies investigating placed riprap stability under overtopping conditions have been conducted with ripraps constrained at the toe section. However, as demonstrated by findings from the field survey, ripraps constructed on the downstream slopes of rockfill dams are generally not provided with any form of toe support. Hence, it is of importance from stability and economical standpoints to understand the failure mechanism in placed ripraps with realistic toe support conditions. Experimental overtopping tests on 1:10 scaled model placed ripraps constructed on a steep slope (S = 0.67) unsupported at the toe section were conducted as part of this study. Employing Smartstone probes, a new technology in stone movement monitoring, laser measurement techniques and Particle Image Velocimetry (PIV) techniques, detailed description of the underlying failure mechanism in placed riprap with unconstrained toe under overtopping conditions is presented. Study findings demonstrate sliding as the underlying failure mechanism in placed ripraps with unsupported toes. Further, placed ripraps with unrestrained toes on an average experience a fivefold reduction in stability, characterized by the critical overtopping magnitude as compared with placed ripraps provided with fixed toe supports. Furthermore, toe support conditions were found to have no effects on either the failure mechanism or the overall stability of dumped ripraps.

Comprehending response of rockfill dam structures when subjected to throughflow facilitates effective design and safety assessment. It is also of relevance for development of numerical models predicting rockfill dam breach process. To obtain a better understanding of non-linear flow through rockfill dams, experimental data sets obtained from model studies conducted as part of the IMPACT (Investigation of Extreme Flood Processes and Uncertainties) project were further analyzed as part of this study. The research project was undertaken during the period 2001-2004 by researchers from a consortium of 11 institutions across Europe, including NTNU, Trondheim. Experimental overtopping investigations were conducted on homogenous rockfill embankments of sizes 0.6 m, 1.2 m and 6 m. Based on statistical analysis conducted on the experimental data sets, a general non-Darcy type power-law describing non-linear flow through homogenous rockfill dams is proposed. Also, performance of the proposed power-law is subjected to a comparative evaluation with some of the well-known power-law relationships

from the available literature employing the experimental data sets. Analysis results demonstrate better correlation between empirical predictions and experimental observations for the proposed non-linear flow law as compared with existing criteria.

A key component of the rockfill dam overtopping system is the rockfill dam toe, constructed in tandem with the downstream rockfill shoulder. Quantitative description of throughflow development in rockfill dams basing on experimental data is seldom found in international literature. Further, experimental corroboration of differences in hydraulic performance of disparate rockfill toe configurations has been rare. Findings from the present study add valuable knowledge to the state of the art on behavior of rockfill dam structures exposed to throughflow. Experimental throughflow tests were conducted on 1 m high rockfill dam models coupled with different toe configurations as part of this study. Investigation outcomes provide qualitative and quantitative descriptions of effects of internal, external and combined toe configurations on throughflow hydraulic properties. Key features describing the hydraulic effects of disparate toe configurations on flow through rockfill dams such as phreatic surface development and internal pore-pressure buildup are evaluated.

Contents

List of papers

***Paper I*: Buckling analogy for 2D deformation of placed ripraps exposed to overtopping.**
Ravindra, G.H.R., Sigtryggsdottir, F.G and Lia, L (2020).
Journal of Hydraulic Research, DOI: https://doi.org/10.1080/00221686.2020.1744745.

***Paper II*: Toe support conditions for placed ripraps on rockfill dams- A field survey.**
Ravindra, G.H.R., Sigtryggsdottir, F.G., Asbølmo, M.F and Lia, L (2019).
Vann 2019 (3), pp. 185- 199.
Retrieval link: https://vannforeningen.no/dokumentarkiv/toe-support-conditions-for-placed-ripraps-on-rockfill-dams-a-field-survey/.

***Paper III*: Failure mechanism in placed riprap on steep slope with unsupported toe.**
Ravindra, G.H.R., Gronz, O., Dost, B and Sigtryggsdottir, F.G.
Engineering Structures, Volume 221, DOI: https://doi.org/10.1016/j.engstruct.2020.111038.

***Paper IV*: Non-linear flow through rockfill embankments.**
Ravindra, G.H.R., Sigtryggsdottir, F.G and Høydal, ØA (2019).
Journal of Applied Water Engineering and Research, 7:4, 247-262.
DOI: https://doi.org/10.1080/23249676.2019.1683085.

***Paper V*: Effects of toe configurations on throughflow hydraulic properties of rockfill embankments.**
Kiplesund, GH., Ravindra, G.H.R., Rokstad, M.M and Sigtryggsdottir, F.G (2020).
Submitted for review in *Journal of Applied Water Engineering and Research*.

The work in these journal papers and manuscripts are also complemented by the following papers presented at international conferences.

- Ravindra, G.H.R., Sigtryggsdottir, F.G., Lia, L (2018). *Evaluation of design criteria for downstream riprap of rockfill dams,* Q. 101- R.71, pp. 1195- 1209, Twenty- sixth International Congress on Large Dams, 4th- 6th July, Vienna, Austria, Published by CRC Press, Taylor and Francis Group.
- Ravindra, G.H.R., Sigtryggsdottir, F.G., Lia, L (2018). *Protection of embankment dam toe and abutments under overtopping conditions,* 3rd International Conference on Protection against Overtopping, 6- 8 June, Grange over Sands, UK.

List of supervised students

Kofi Ntow Opare (2018) *Load measurements at riprap toe* (Master thesis).

Malin Fossum Asbølmo (2019) *Kartlegging av nedstrøms damtå på valgte fyllingsdammer/Field survey of downstream dam toes on selected rockfill dams* (Master project).

Malin Fossum Asbølmo (2019) *Utforming av damtå og betydning for plastring av fyllingsdammer - Kartlegging og modellforsøk/ Significance of toe support conditions on placed riprap stability- Field survey and model studies* (Master thesis).

Unnar Numi Almarsson (Master thesis to be completed in spring 2020) *Fuse plugs in rockfill dams: Design review and model tests* (Joint master thesis between the University of Iceland and NTNU, Trondheim).

Nils Solheim Smith (Master thesis to be completed in spring 2020) *Physical and numerical modelling of extreme flow through rockfill dams* (Master thesis).

Styrmir Sigurjonsson (Master thesis to be completed in spring 2020) *Experimental study on the breaching of rockfill dams* (Master thesis).

List of figures

List of tables

1 Introduction

Water is a necessity for life as we know it, and a basic human right (WHO, 2004). From a historical perspective, prosperity, health and material progress of civilizations have been strongly linked to proficiency in water engineering and in particular, to the ability of storing and directing water. From a current international context, construction and maintenance of reservoir schemes for water retention to satisfy the needs of societies such as water supply, irrigation, flood protection and hydropower represent major investments in many nations. Further, considering projected future impacts of climate change on hydrological regimes, reservoirs will play a pivotal role in facilitating the transition of water-based infrastructure towards a future unfamiliar climate setting.

Reservoir schemes are commonly coupled with dams enabling water storage and regulation. Construction of dams ranks with the earliest and most fundamental of civil engineering activities. As practiced, dam engineering is a highly specialist activity which draws upon many scientific disciplines and balances them with a large element of engineering judgement; dam engineering is thus a uniquely challenging and stimulating field of endeavor (Novak et al., 2001). Embankment dams, constructed with locally excavated earth or rockfill represent 78% of the total number of existing dams worldwide (ICOLD, 2019). Embankment dams comprising of coarse-grained fractional material for over 50% of the dam volume are further classified as rockfill dams, representing 13% of the worldwide dam population (ICOLD, 2019).

A constant trend in society comprises an increase in the safety requirements for all critical infrastructure (Toledo & Morera, 2015). During the last decades, there has been a significant increment of the social demand on dam safety standards, especially in the most developed countries. This has led to new and more demanding dam safety regulations and guidelines (Moran, 2015). This trend is also valid as applied to the Norwegian dam infrastructure. The retroactive enforcement of new and more stringent dam safety regulations (OED, 2009) has necessitated rehabilitation of multitudes of large Norwegian rockfill dams.

Dam safety assessment is a complex task as it is influenced by multitudes of internal and external factors (Sigtryggsdóttir et al., 2016). It is essential to determine the most common causes of dam failure incidents over the decades to identify probable factors which contribute to dam instability. ICOLD statistics (ICOLD, 1995) state overtopping as the main cause of embankment dam failure appearing as the primary factor in 31% of the total number of failures, and is further involved in another 18% of failures as a secondary agent. Hence, equipping

rockfill dams with defense mechanisms to safeguard the dam structure against unanticipated overtopping or leakage events is of paramount importance from a dam safety perspective.

Under overtopping conditions, the downstream slope of a rockfill dam is subjected to highly destabilizing dynamic forces generated due to turbulent throughflow (overtopping of dam core) and or overflow (overtopping of dam crest). Considering throughflow conditions, turbulent flow with high seepage velocities within the embankment structure can result in internal erosion and also destabilize the downstream embankment due to pore pressure build up (Figure 1). Further, under overflow conditions, the downstream slope is inundated with highly turbulent surface flow resulting in preogressive external erosion leading to dam breach.

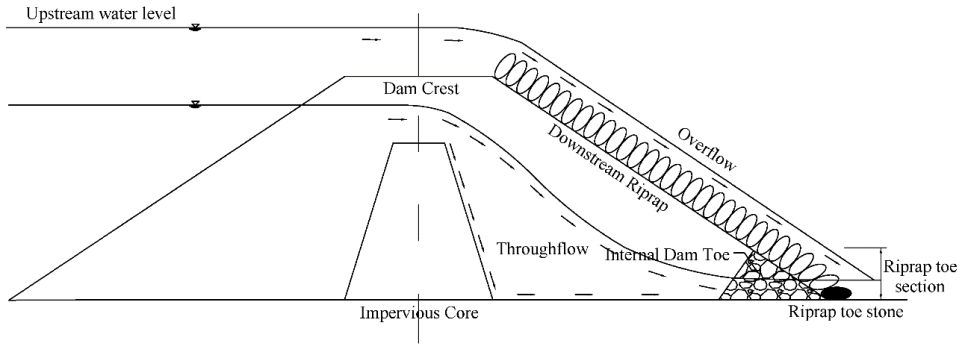

Figure 1. Description of throughflow and overflow scenarios in rockfill dams (Adopted from Ravindra et al. (2019a)).

Ripraps and rockfill dam toes are extensively employed in embankment dam engineering as key components of the overtopping protection system. The Rockfill dam toe comprising of coarser material as compared with the shoulder material is constructed in tandem with the downstream rockfill dam shoulder either as an internal or an external structure. This structure facilitates efficient expulsion of seepage and accidental leakage flows from within the dam structures. This helps in preventing buildup of excess pore pressures leading to slope instability and also assists in minimizing internal erosion due to particle dragging. Hence, the rockfill dam toe is constructed to assure enhanced stability of the downstream shoulder under extremely high through-flow conditions (Moran et al., 2019).

Ripraps are one of the most widely used erosion protection measures for various in-stream hydraulic structures such as embankment dams, spillways, streambeds, river banks, bridge piers and abutments (e.g. Hiller et al., 2019; Thornton et al., 2014; Abt et al., 2013; Khan &

Ahmad, 2011; Siebel, 2007). Ripraps are also used in coastal protection structures such as dikes, embankments and jetties against wave action (Kobayashi & Jacobs, 1985). As applied to rockfill dam engineering, ripraps are constructed on the upstream embankment to protect against erosion resulting because of wave impacts and ice induced forces. Further, ripraps constructed on the downstream slope to protect against erosion due to accidental leakage or overtopping events (Figure 2).

Figure 2. Placed riprap constructed on the downstream slope of dam Oddatjørn, which is a 142 m high rockfill dam constructed in Suldal, Norway (Photo: GHR Ravindra, NTNU).

Obtaining a better understanding of stability aspects of these rockfill dam components under extreme loading conditions is vital for the rockfill dam construction industry. From dam safety and economical standpoints, accumulating technical knowledge on the hydraulic and structural behavior of these structures can lead to safe and economical design, construction and rehabilitation of rockfill dams. With an objective of adding to the international technical expertise on rockfill dam stability, this study was conducted as part of the research project titled 'Embankment dam safety under extreme loading conditions'. The research was initiated by a consortium between the Norwegian Research Centre for Hydropower Technology (HydroCen) and the Norwegian University of Science and Technology (NTNU).

1.1 Organization of the thesis

A brief overview of the structure of the present thesis is provided herein. Chapter 2 summarizes the primary study objectives and the identified research questions to be further addressed in the

thesis. Summaries of the state of the arts in the study disciplines of riprap stability and rockfill dam behavior when subjected to throughflow are presented in Chapter 3. The research methodologies and methods implemented as part of the research project are introduced in Chapter 4. Further, Chapter 5 provides descriptions of the various model setups, testing methodologies and field survey procedures adopted within the research program. Key findings from these investigations are described in Chapter 6. Overarching discussions of the study outcomes are presented as part of Chapter 7 bringing forth a holistic evaluation of the research findings as a whole. Furthermore, answers to the identified research questions and concluding remarks are presented in Chapter 8.

2 Study objectives, scope and research questions

The overarching theme of the research project presented in this thesis is to contribute to the field of rockfill dam engineering through generation of new knowledge aimed at improving dam safety. The investigations are in particular, focused on achieving better understanding of hydraulic and structural response of rockfill dams or dam components under extreme loading circumstances. The research efforts under this theme are directed at conduction of experimental studies aimed at achieving the following research objectives:

***Objective 1*:** Analyzing failure mechanisms and key factors affecting stability of ripraps constructed on the downstream slopes of rockfill dams under overtopping conditions.

Objective 2: Evaluating the hydraulic response of rockfill dams exposed to throughflow scenarios and studying the effects of rockfill toes on throughflow hydraulic properties of rockfill dams.

Pertinent research questions were identified based on literature reviews of the research areas (presented in Section 3 of this thesis) to accomplish the aforementioned objectives and to bridge knowledge gaps in the study disciplines.

***Research question 1*:** What is the 2D failure mechanism in toe supported placed ripraps constructed on steep slopes exposed to overtopping conditions?

***Research question 2*:** Do existing placed ripraps comply with design criteria and recommendations with regards to key parameters describing quality of construction? And are placed ripraps currently provided with any form of toe support?

***Research question 3*:** How do toe support conditions affect the underlying failure mechanisms the stability in placed and dumped ripraps constructed on steep slopes exposed to overtopping?

***Research question 4*:** How can we quantitatively describe non-linear flow through rockfill embankments?

***Research question 5*:** What are the effects of disparate toe configurations on throughflow in rockfill dams?

The study scope is limited to investigating hydraulic and structural behavior of rockfill dam components coupled with the downstream slopes of rockfill dams under throughflow or overflow scenarios.

3 Background

A detailed literature review of the state of the art in a research discipline enables formulation of pertinent research questions by providing valuable insights into the historical development of research methodologies and experimental tools and techniques which have been previously adopted by past research works. The following discussions are aimed at summarizing the state of the art on stability of placed ripraps and on the hydraulic response of rockfill dams under overtopping conditions.

3.1 Placed riprap stability under overtopping conditions

Riprap is defined as an erosion resistant surface cover of large elements such as natural rocks or artificial elements to secure subjacent layers against the impact of hydrodynamic forces due to currents and waves and due to ice induced forces. Riprap on the upstream dam slope is exposed to wave action or currents either perpendicular or parallel to the slope. On the downstream slope, the primary function of riprap is to provide erosion resistance under throughflow and/or overflow conditions. Ripraps can be broadly classified into two categories based on the method of construction; Dumped ripraps comprise of randomly placed stones while placed ripraps are characterized by stones arranged in a specific interlocking pattern. Although dumped ripraps could be considered as a more viable alternative from an economic standpoint, placed ripraps have been found to offer higher degree of stability against overtopping in comparison with dumped ripraps (Hiller et al., 2018). This is attributed to the formation of a bearing structure due to interlocking of stones, which results in increased stability compared to randomly dumped stones.

The stone density (ρ_s), stone size (d), grain size distribution and the embankment slope (S) parameterize the surface layer of dumped ripraps as these parameters in general govern the hydraulic behavior of dumped ripraps. For placed ripraps, an additional parameter needs to be evaluated to discern the overall stability of the riprap structure. The packing factor (P_c) is a generally employed parameters to evaluate the quality of placement of placed ripraps. It should be noted that these parameters are not the commonly used indicators of stability from a structural or geotechnical standpoint. However, these are considered as bridge parameters for correlating the hydraulic and structural stability of ripraps.

The packing factor P_c is adopted to obtain a quantitative measure of density of riprap stone placement as this can have an impact on overall riprap stability. The term packing factor was defined as Equation (1) by Olivier (1967).

$$P_c = \frac{1}{N.{d_{50}}^2} \tag{1}$$

where N represents the number of stones per m^2 surface area of the riprap and d_{50} signifies the median stone size. The median stone size is computed as $d_{50} = (abc)^{1/3}$ averaged over a sample set, where a, b and c represent the longest, intermediate and shortest stone axis respectively. P_c is lower for a densely placed riprap compared to a loosely packed riprap (Hiller et al., 2018).

The research discipline of dumped riprap design under overtopping conditions has advanced since its inception with the classic study of Isbash (1936). Since this early effort to determine the size and thickness of a resistant stone layer, more than 21 stone-sizing relationships for overtopping have been developed (Abt & Thornton, 2014) with major contributions from Chang (1998), Frizell et al. (1998), Abt et al. (1991), Olivier (1967) and others. These studies have been dedicated towards investigating stability of dumped ripraps on moderately steep slopes complying with international construction practice.

Available literature describing the stability aspects of placed ripraps under overtopping conditions is rather limited as compared with the extensive research database available with respect to design and construction of dumped ripraps. Notable contributors to the research area of placed riprap design are Hiller et al. (2018), Peirson et al. (2008), Dornack (2001), Sommer (1997) and Larsen et al. (1986). These past experimental model studies have been aimed at comprehending the underlying 1D failure mechanism in placed ripraps with fixed toe supports exposed to overtopping flows on mild to steep slopes (S = 0.125 to 0.67 with S being the ratio of the vertical to the horizontal slope dimensions). Some of these investigations have also made attempts at juxtaposing stability aspects of placed and dumped ripraps to better understand the fundamental differences in behavior of these structures under overtopping conditions. Within this doctoral study, primary emphasis is laid on better understanding stability of placed ripraps constructed on steep slopes subjected to overtopping flows.

The experimental study conducted by Larsen et al. (1986) was primarily aimed at comprehending the 1D underlying failure mechanisms of placed ripraps exposed to overtopping flows on mild to moderately steep slopes (S = 0.125 to 0.40; S is the ratio of the

vertical to the horizontal slope dimensions). Larsen et al. (1986) found that the successive overtopping of the riprap with increasing discharges resulted in a compaction of the downstream part of the placed riprap (Hiller et al., 2018). A new technique for quantification of the compaction process along the chute length was introduced by Larsen et al. (1986) wherein relative stone displacements were monitored as a function of overtopping magnitude. Relative displacements ($\Delta x\ L_i^{-1}$) of select riprap stones were computed as the ratio of stone displacements along the flow direction (Δx) and the distance between the select stone and the downstream fixed toe structure (L_i). A similar study was later carried out by Sommer (1997) on placed riprap models constructed on slopes S = 0.25 to 0.50. Based on experimental test results, a three step design methodology for placed ripraps was developed by Sommer (1997) taking into account stone displacements. Further, the recent study conducted by Hiller et al. (2018) adopted the technique of relative stone displacement monitoring to analyse the 1D failure mechanism in placed ripraps with fixed toe supports constructed on steep slopes of S = 0.67. Hiller et al. (2018) concluded that unidirectional stone displacements along the chute direction leading to formation of a gap at the upstream section of the riprap was the underlying 1D failure mechanism in placed riprap supported at the toe.

Also, several past experimental studies have documented considerable stability gain for placed ripraps as compared with dumped ripraps. This was quantified to approximately 30% in Peirson et al. (2008) and 80% in Larsen et al. (1986). Hiller et al. (2018) state that placing riprap stones in an interlocking pattern resulted in on an average five times higher stability as characterized by critical overtopping flow magnitude as compared to randomly dumped riprap. This effect has generally been attributed to generation of interlocking forces within the placed riprap structure which offers higher resistance against flow forces, especially at steep slopes.

As an illustration of large-scale application of placed ripraps on rockfill dams, the case of Norwegian rockfill dams can be considered. The Norwegian Water Resources and Energy Directorate (NVE) is responsible for the development of guidelines for construction and monitoring of Norwegian rockfill dams. In order to safeguard dams against accidental overtopping events, dam safety regulations in Norway prescribe construction of single-layered placed ripraps on the downstream slopes of rockfill dams. The individual riprap stones are to be placed in an interlocking pattern with their longest axis inclined towards the dam (OED, 2009; NVE, 2012). The dams are generally classified into four different consequence classes (class 1 through 4). The criteria for the classes reflect the consequences that a possible failure may have for people, the environment and property with Class 4 designating dams with a very

high potential for damage in case of dam failure, Class 3 indicating dams with high damage potential and Class 2 signifying dams with medium damage potential (Midttømme et al., 2012).

As per the recommendations of NVE dam safety guidelines of 2012 (NVE, 2012), placed ripraps need to be constructed on rockfill dam slopes with stones of volume of minimum 0.15 m^3 for dams classified within consequence class 4. To determine the stone size for dams in class 3 and 2, Equation (2) can be used assuming a minimum unit discharge 'q_f' of 0.5 m^3/s for Class 3 and 0.3 m^3/s for Class 2.

$$D_{min} = 1.0 \; S^{0.43} \; q_f^{\,0.78} \tag{2}$$

The proposed design criteria by the NVE is based on large scale field tests and physical modelling investigations carried out by EBL Kompetanse AS (EBL Kompetanse, 2006). Investigations into breach formation mechanisms of rockfill dams subjected to throughflow and overflow conditions were carried out through construction of large-scale rockfill dam structures in an open channel at Rossvatn, Norway and also by conducting overtopping tests on model rockfill structures in a flume (Kjellesvig, 2002 and Sand, 2002). The accumulated data from the tests were employed to arrive at a best-fit design criterion for the design of ripraps of rockfill dams presented as Equation (3).

$$D_{min}=0.43 \; S^{0.43} \; q_f^{\,0.78} \tag{3}$$

The large scale rockfill dams were constructed of coarse rockfill, however, without riprap. The coarse rockfill can at best be considered comparable to dumped ripraps. Application of Equation (2) for the design of placed ripraps was based on the assumption that for a particular size of riprap stones, the stability of placed ripraps would be higher compared to dumped ripraps. Although Equation (2) includes a slope parameter 'S', it was originally developed with data sets obtained from experimental investigation conducted on large scale rockfill dams with downstream embankment slope of S = 0.67 in accordance with Norwegian construction practice. Furthermore, a safety factor of 2.3 is incorporated within Equation (2) over the best-fit Equation (3) proposed by EBL Kompetanse (2006) (Ravindra et al., 2018a).

A literature review into the international state of the art in placed riprap design and construction reveals that description of 2D failure mechanism in placed ripraps under overtopping scenarios is currently not available. Furthermore, all these past studies investigating stability aspects of placed riprap under overtopping conditions have been carried out with ripraps constrained at

the toe section with fixed toe support structures. This entails enhanced resistance against sliding at the riprap toe section. However, several past studies investigating rockfill dam stability aspects under overtopping conditions such as Moran et al. (2019), Javadi and Mahdi (2014) and Moran and Toledo (2011) have demonstrated toe section of rockfill dams as a critical location for initiation of progressive dam failure. Also considering the guidelines offered by the NVE for placed riprap design and construction, protocols addressing specifics on the design aspects of toe support for the riprap structures are currently unavailable.

Thus, this discussion helps in identification of important parameters which could potentially be of significance for placed riprap stability. Since all past experimental research has focused on analyzing 1D failure mechanism in placed ripraps, extension of the findings to 2D could lead to findings which can lead to more effective design of these structures **(*Research Question 1*)**. Further, A large-scale field study documenting existing state of riprap toe construction on rockfill dams is currently unavailable **(*Research Question 2*)**. Furthermore, carrying out experimental overtopping investigations on model placed ripraps with realistic toe support conditions is of significance to obtain representative findings concerning the stability aspects of placed ripraps exposed to overtopping flows. This would also facilitate evaluation of the validity of findings from past research works describing stability of placed ripraps under overtopping conditions **(*Research Question 3*)**.

3.2 Flow through rockfill medium

Under overtopping scenarios, highly turbulent flow through the downstream embankment structure of rockfill dams can result in internal erosion and also destabilize the downstream slope due to dynamic pore pressure generation. Several instances of embankment dam failures resulting as a consequence of flow through the embankment structure are documented in international literature (e.g. Leps, 1975; Cruz et al., 2010 and Foster et al., 2000). Comprehending turbulent throughflow hydraulic properties of rockfill dams facilitates effective safety assessment (e.g. Moran and Toledo., 2011 and Siddiqua et al., 2011; Ferdos and Dargahi., 2016a and Ferdos and Dargahi., 2016b). Furthermore, it is also of relevance for development of numerical models predicting rockfill dam breach process as this can assist in effective design of components of rockfill dam overtopping protection system such as the dam toe resulting in reduced risk of dam failure.

Flow through porous media is generally characterized as either Darcy or non-Darcy type based on confirmation of flow properties with the linear Darcy flow theory (Equation 4) widely

implemented in soil mechanics. Deviations from the linear trend requires the flow to be classified as non-Darcian type.

$$V = K\ i \tag{4}$$

where, V = Bulk flow velocity, K = Coefficient of permeability and i = hydraulic gradient.

Darcian or linear flow through rockfill is seldom encountered in practical applications (Leps, 1975). Wilkins (1955) states that applicability of the linear Darcy flow theory is limited to flow through small grains of the order of 0.5 mm. Flow in rockfill structures depart from the linear flow regime because of the highly porous characteristic of rockfill material resulting in large interconnected void spaces leading to high velocity flows (Siddiqua et al. 2011). Hence, it can be concluded that Darcy's law does not adequately describe throughflow hydraulics in coarse-grained porous media especially at high velocities (e.g. Hansen et al. (1995), Venkataraman and Rama Mohan Rao (1998), Siddiqua et al. (2011) and Ferdos and Dargahi (2016a)).

Pertaining to throughflow hydraulic characteristics of rockfill dams, flow through the core as well as through the sand filter can be considered to be laminar confirming with the linear Darcy flow theory owing to considerably low permeability. However, these low velocity and low magnitude flows do not generally pose considerable threat to the integrity of the rockfill embankment as long as internal erosion is not an issue. But, flow through the transition zone and the supporting fill is more problematic as the state of flow is highly turbulent as a consequence of large permeability resulting in generation of highly destabilizing forces with high internal erosion potential (e.g. Solvik, 1991 and Cruz et al., 2010). Hence, it is of importance to better understand turbulent throughflow hydraulics in rockfill embankments as this can facilitate effective design of rockfill slopes and components of rockfill dam overtopping protection system such as the dam toe.

Description of non-Darcian or turbulent flow through porous media is generally represented as a power-law function (Equation 5), as demonstrated by past investigations such as Izbash (1931), Escande (1953), Wilkins (1955), Scheidegger (1963), Parkins (1966) and Siddiqua et al. (2011).

$$V = a\ i^b \tag{5}$$

where, a and b are empirical coefficients to be determined experimentally. Coefficient a depends on the properties of fluid and porous media such as porosity, particle shape, particle

size, roughness, tortuosity of void structure and viscosity of fluid. Parameter *b is* dependent upon the state of flow or the level of flow turbulence (Siddiqua et al. 2011).

Much literature is available in the study discipline of non-linear flow through rockfill as several past studies have investigated non-Darcian throughflow aspects of rockfill medium adopting theoretical approaches and also through experimental throughflow tests conducting in varying sizes of permeameters. In depth reviews of the available literature within this research discipline are available in studies such as Leps (1975), Venkataraman and Rama Mohan Rao (1998), Sidiropoulou (2007), Cruz et al. (2010) and Salahi et al. (2015). These past research works have resulted in accumulation of various empirical equations describing the non-linear relationship between velocity and gradient of flow through rockfill. Some of the well-established empirical criteria describing non-linear flow through rockfill such as Wilkins (1955) and Engelund (1953) are presented in Table 1.

Wilkins (1955) noted measurement of the surface area of irregular stones (S_o) as a difficult problem. To address this concern, Leps (1975) carried out an investigation to obtain a general empirical relationship to relate parameter m with the median stone size (d_{50}) of the rockfill material. Leps (1975) tabulated the values of parameter m for rock particles of median diameter ranging over a broad interval of d_{50} = 19 mm to 1220 mm which in turn translates to equation 9 (Cruz et al., 2010).

$$m = \frac{d_{50}}{8} \tag{9}$$

Further, several studies have conducted experimental testing programs in permeameters for further validation of performance of the Engelund (1953) approach (Equations 6 and 7) and the Wilkins (1955, 1963) approach (Equation 8). Parkins (1963, 1966) performed tests on d_{50} = 10 mm to 20 mm homogenous angular gravel and concluded that the performance of the Wilkins (1955) approach was satisfactory in predicting the experimental results. Further, a recent study conducted by Siddiqua et al. (2011) on rockfill material with median particle size ranging over d_{50} = 10 mm to 150 mm in a large scale permeameter (D = 0.76 m and L = 2.7 m) further corroborated the performance of the Wilkins (1955, 1963) and the Engelund (1953) approaches in describing non-linear flow through coarse rockfill. The ability of the Engelund (1953) and the Wilkins (1955, 1963) approaches in describing the non-linear throughflow characteristics of rockfill embankments is further evaluated in this article as these are widely implemented in practical applications concerning throughflow hydraulics of rockfill material.

Table 1. Description of well-known empirical relationships describing non-linear flow through porous media.

Research work	Empirical relationship	Remarks
Engelund (1953)	$i = \frac{V^2}{k_t}$ (6) $k_t = \frac{n^3 g\, d_i}{\beta_o\,(1-n)}$ (7)	k_t = turbulent permeability β_o = particle shape coefficient (3.6 for blasted or crushed rock) d_i = characteristic dimension or the representative particle size of the porous medium* n = porosity of the medium
Wilkins (1955)	$V = W\, n\, m^{0.50}\, i^{0.54}$ (8)	n = porosity of the medium m = hydraulic mean radius defined as the ratio of the void ratio (e) to the specific surface area of the stones (S_o) W = material dependent coefficient with a value of 5.243 for crushed rocks**

* A relationship for d_i is presented in publications such as Solvik (1991) and Cruz et al. (2010) as $d_i = 1.7\, d_{10}$. However, some recent studies such as EBL Kompetanse (2006) and Siddiqua et al. (2011) argue on behalf of a different relationship $d_i = 1.22\, d_{20}$.

**Wilkins (1963) based on additional experimental data proposed a revised version of Equation 2.8 with $W = 6.693$.

Furthermore, most past studies have not assessed throughflow hydraulic properties in sufficiently coarse rockfill material of sizes commonly employed in dam construction especially at extremely high turbulence levels. To address this concern, recent studies conducted by Ferdos et al. (2015), Ferdos and Dargahi (2016a) and Ferdos and Dargahi (2016b) have focused on investigating flow through properties in large rockfill with d_{50} = 100 mm to 240 mm at high turbulence levels. Large-scale field studies (in injection wells) and permeameter studies in laboratory settings were undertaken in this regard, aimed at calibration and validation of numerical simulation tools.

Although these different permeameter studies have provided valuable insight into throughflow hydraulics in rockfill material, research into quantitative physical validation of these relationships in actual rockfill dams is currently unavailable in international literature. This is considering the fact that any findings originating from theoretical studies or from experimental investigations conducted in permeameters inevitably require validation within actual rockfill dam models at laboratory and large scales to enhance confidence in the findings for practical implementation. This has been a missing link in the process of development of a sophisticated numerical model simulating rockfill dam breach (Figure 3).

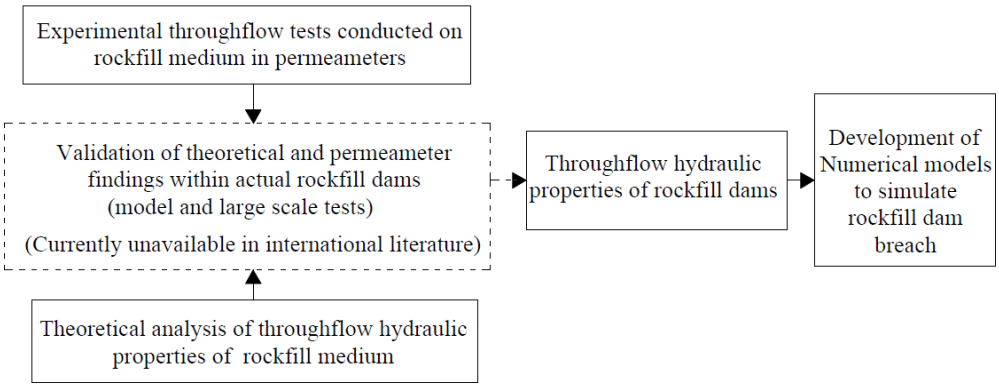

Figure 3. Illustration of processes involved in the development of a numerical rockfill dam breach model and the missing link currently unavailable in international literature (Adopted from Ravindra et al. (2019b)).

Due to the resource intensive nature of experimental testing on rockfill dam models, especially at large scales, research in this area has seldom been conducted in the past. Hence, a comprehensive experimental investigation aimed at providing a realistic description of non-linear flow through homogenous rockfill embankments is required **(*Research question 4*)**. This would also address scaling concerns with regards to flow through rockfill dams and also facilitate further development of numerical dam breach models.

3.3 Flow through rockfill embankments

Under extreme throughflow or overtopping scenarios, rockfill dam failure could result as a consequence of primarily three failure modes, (a) internal erosion, (b) surface erosion and (c) mass slope instability (Moran, 2015). Under throughflow scenarios, highly turbulent flow entering the downstream embankment structure may develop high seepage velocities leading

to transport of fine material downstream leading to internal erosion (e.g. Ravindra et al., 2018 and Moran, 2015). Further, overtopping of the dam crest leading to skimming flow on the downstream slope could lead to progressive surface erosion (e.g. Hiller et al., 2018 and Abt et al., 1991). Furthermore, internal buildup of dynamic pore pressures under such extreme scenarios could lead to significant reduction in the geotechnical stability of the dam and in turn lead to mass slope instability and sliding (Moran, 2015 and Moran and Toledo, 2011).

A prerequisite for effective design of safe rockfill dam structures is having a good understanding of behavior of rockfill dams exposed to throughflow and overflow scenarios. Ability to predict and model flow through rockfill dams can facilitate effective design and dam safety assessment. Numerous past theoretical, numerical and experimental studies have made attempts at quantitatively describing flow through and stability aspects of rockfill dams exposed to extreme scenarios.

Studies such as Javadi and Mahdi (2014), Siddiqua et al. (2013), Garga et al. (1995), Hansen et al. (1995) have conducted experimental investigations on model rockfill dams subjected to throughflow and overflow conditions. The underlying study objective has been to quantitatively describe and in turn predict initiation and progression of failure in rockfill dams from hydraulic and geotechnical standpoints. Further, several past numerical and theoretical investigations such as Larese et al. (2015), Hansen and Roshanfekr (2012), Hansen et al. (2005), Worman (1993), Townsend et al. (1991) and so on have made attempts at development and validation of empirical methodologies and numerical tools for modelling behavior of rockfill embankments subjected to extreme throughflow and or overtopping conditions.

Furthermore, numerous past studies such as Moran et al. (2019), Javadi and Mahdi (2014), Siddiqua et al. (2013), Cruz et al. (2010), Marulanda and Pinto (2000) and Leps (1973) have stated that the toe section of rockfill dams could be a critical location for failure initiation under throughflow scenarios. Rockfill dam toes are commonly coupled with the downstream rockfill dam structure to counter the destabilizing effects of seepage flows entering the downstream dam structure and to stabilize the toe section under extreme situations. Although numerous past studies have investigated rockfill dam behavior when exposed to throughflow and overtopping scenarios, experimental model studies investigating performance of rockfill dams coupled with toe structures are scarce. In this regard, recent studies such as Moran et al. (2019) and Moran and Toledo (2011) have conducted experimental studies on rockfill dam models with external rockfill toes. This was to document the hydraulic and geotechnical effects of an external toe on

the performance of rockfill dams under extreme situations. This research also led to the development and further validation of a design methodology for external toes for rockfill dams.

Apart from this study looking at the efficacy of external toes, experimental studies focusing on investigating the behavior of rockfill dams constructed with disparate toe configurations is currently unavailable in international literature **(*Research question 5*)**. From a dam safety point of view, it is of significance to comprehend the effects of various toe configurations on throughflow properties and in turn, stability aspects of rockfill dams under extreme loading scenarios. Arriving at new knowledge in this regard can facilitate effective design and construction of these structures. This could also enable development and validation of numerical design tools and dam breach models which can further streamline the rockfill dam design process.

4 Research Methodology

The overarching research objective of the present study has been the holistic evaluation of behavior of downstream section of rockfill dams exposed to accidental leakage and or overtopping events. To achieve the study objective, several laboratory experimental testing programs and large-scale field studies have been conducted (Figure 4). Each of these model studies build on knowledge and insights generated during the preceding investigations. The investigation aims presented under were oriented towards addressing several research questions identified in Chapter 3 and fall within the preview of the two principal research objectives presented.

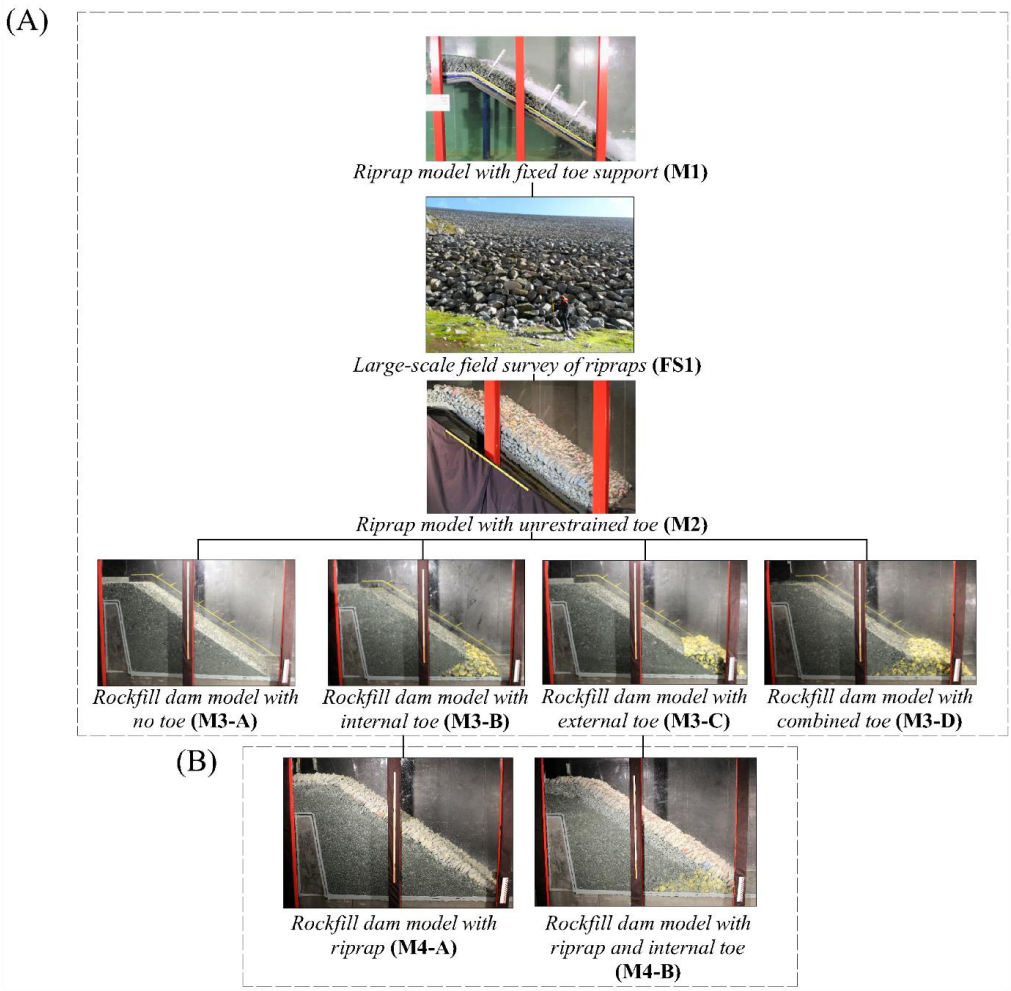

Figure 4. Overview of model tests and field studies conducted as part of the research program.

Details regarding these individual studies are presented in following sections. Findings from part (A) of Figure 4 are presented as part of this doctoral thesis and scientific outcomes from part (B) will be disseminated in the near future in the form of technical articles and reports.

4.1 Investigation methods

As part of the doctoral study, several experimental model studies, field surveys and statistical evaluations were carried out. Research outcomes from each of the investigations address relevant research questions. Findings have been and are planned to be disseminated in the form of several journal publications. A brief overview of the study themes are presented herein.

Model 1 ***(M1)*****- Riprap model with fixed toe support (*Paper I*)**

2D extension of past findings describing unidimensional failure mechanisms in placed ripraps ***(Research question 1) (Objective 1)***.

Field survey 1 ***(FS1)*****- Large-scale field study of ripraps (*Paper II*)**

Documentation of existing state of riprap toe construction on Norwegian rockfill dams ***(Research Question 2) (Objective 1)***.

Model 2 ***(M2)*****- Riprap model with unrestrained toe (*Paper III*)**

Riprap stability investigations with realistic toe support conditions ***(Research Question 3) (Objective 1)***.

Model 3 ***(M3)*****- Rockfill dam models with disparate toe configurations (*Paper V*)**

Presenting quantitative descriptions of effects of toe configurations on throughflow hydraulic properties of rockfill dams ***(Research question 5) (Objective 2)***.

Model 4 ***(M4)*****- Rockfill dam models coupled with riprap and toe structures**

Evaluation of holistic stability aspects of rockfill dam structure coupled with riprap and internal toe. These studies are not included as part of the present doctoral thesis although they comprise a part of the experimental works carried out.

In addition to these experimental studies, ***Paper IV*** presents results from a statistical analysis conducted on experimental data from throughflow investigations conducted on rockfill dam models. Research objective was to provide a realistic description of flow through homogenous rockfill dams through derivation of a general non-Darcy type power-law describing the non-linear throughflow hydraulic response of rockfill embankments subjected to throughflow ***(Research question 4) (Objective 2)***.

Furthermore, as part of the experimental testing program, a series of overtopping tests were conducted on placed riprap models provided with load measuring pressure cells at the toe section. The underlying study objective was to obtain better understanding of the dynamic load generation processes at the toe sections of placed ripraps. This can be considered a major factor influencing placed riprap stability. Ability to quantitatively predict the forces generated at the toe sections of placed ripraps could also facilitate design of efficient toe support measures. The accumulated data is yet to be analyzed and the research outcomes will be disseminated as a journal publication thereafter.

5 Model setups and testing methodology

This section provides descriptions of the various model setups and testing methodologies implemented in the research program. Strategies adopted for conducting the field survey are also presented. Results from the studies are presented in Chapter 6.

5.1 Riprap model with fixed toe support *(M1)* (*Paper I*)

The present doctoral study was initiated in 2017 following the conclusion of the *PLaF* (PLastring av Fyllingsdammer / placed ripraps constructed on rockfill dams) research project. The *PLaF* study funded by EnergiNorge was conducted at NTNU, Trondheim with research emphasis placed on experimental investigation of stability aspects of placed ripraps exposed to overtopping flows (Hiller, 2017). All tests were conducted with ripraps provided with fixed toe supports. The present study was designed to build on the study outcomes from the *PLaF* study to generate pertinent findings regarding placed riprap stability under overtopping events.

As previously stated in section 3.1, all past experimental research on placed ripraps has focused on analyzing the 1D failure mechanism in toe supported placed ripraps on steep slopes exposed to overtopping. Consequently, 2D description of the same was unavailable prior to this study. *Paper I* provides qualitative and quantitative descriptions of 2D deformations in placed ripraps supported at the toe under overtopping scenarios. Experimental data sets accumulated by Hiller et al. (2018) through physical modelling investigation conducted on model ripraps with fixed toe supports constructed with angular stones on a steep slope of $S = 0.67$ were further analyzed along with additional experimental data. Descriptions of the experimental setup, material properties and testing methodology designed by Hiller et al. (2018) are presented herein.

Experimental overtopping tests were conducted by Hiller et al. (2018) on model ripraps constructed in a flume (25 m long, 2 m high and 1 m wide) at the hydraulic laboratory at NTNU (Hiller, 2017). Discharge to the flume was supplied by pumps with a combined capacity of $q = 0.4$ m^2 s^{-1}. A conceptual 1:10 model setup consisting of a single-layered placed riprap section of width 1 m and chute length of $L_S = 1.8$ m constructed over a base frame inclined at 1:1.5 ($S = 0.67$) (Figure 3.2) was designed by Hiller et al. (2018). The test setup was designed assuming Froude similarity. Quarry stones of rhyolite with median diameter of $d_{50} = 0.057$ m and density of $\rho_s = 2710$ kg m^{-3} were used as riprap stones. The stones could be considered angular to sub-angular (average $a\ b^{-1} = 1.7$) and uniformly graded ($C_u = d_{60}\ d_{10}^{-1} = 1.17$). Test ripraps were placed on a 0.1 m thick filter layer comprised of geotextile and angular stones of size $d_{50,F} =$

0.025 m and density $\rho_{s,F}$ = 3050 kg m^{-3}. The dimensions of the filter and the riprap were chosen in accordance with guidelines offered by the Norwegian Water Resources and Energy Directorate (NVE, 2012).

Placed ripraps were constructed by manual placement of stones in an interlocking pattern commencing at the toe progressing upstream to the crest. The test setup required 1200 stones on average. Riprap stones on the slope were deliberately placed with the longest axis (a-axis) inclined at $\beta \approx 60^{\circ}$ with respect to the chute bottom and with an inclination of $\beta \approx 90^{\circ}$ for stones placed on the horizontal crest to account for practical considerations (Figure 5) (Lia et al., 2013). The ripraps were supported at the toe section with a metallic support structure and the entire test setup was elevated from the flume bottom to avoid backwater effects (Figure 5). The experimental setup was situated sufficiently downstream of the inflow section to achieve calm flow upstream of the test ripraps.

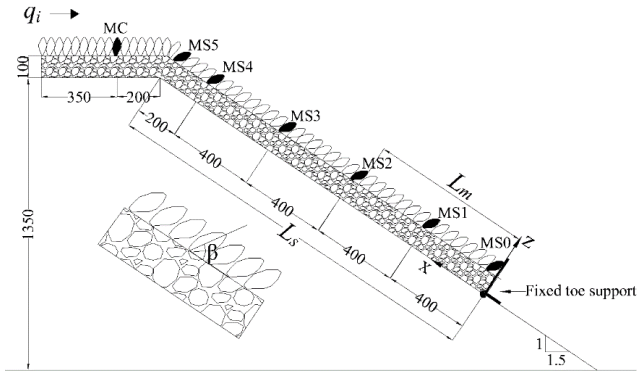

Figure 5. Depiction of experimental setup of model placed riprap supported at the toe. This depiction of the experimental setup is a modified form of Figure 3 from Hiller et al. (2018).

The location co-ordinates of select riprap stones were measured using a laser traverse system in a 3D Cartesian coordinate system with its origin situated at the fixed toe support (Figure 5). The x-axis was aligned in a direction parallel to the chute (33.7º to the flume bottom) pointing in the upstream direction and the z-axis was set perpendicular to the chute. Location coordinates could be measured to an accuracy of ± 0.1 mm in the x-direction and ± 1 mm in the z-direction. The selected stones were located along the centerline of the flume (y = 0.5) at specific positions of x = 0, 0.4, 0.8, 1.2, 1.6 and 1.8 m. The chosen riprap stones were identified as MSm (Figure 5), with m = 0, 1, 2, 3, 4 and 5 for stones located at x = 0, 0.4, 0.8, 1.2, 1.6 and 1.8 m respectively. The marked stone placed on the horizontal crest of the model was labelled MC

(Figure 5). Stone displacements were considered only along the x and z-directions as any possibility of encountering lateral flows prompting stone displacements in the y-direction was ruled out.

5.1.1 Testing methodology

Discharge was supplied to the flume in stepwise increments of q_i = 0.02 - 0.05 m^2 s^{-1} for a specific time interval Δt. 3D location co-ordinates of selected stones were measured prior to and after exposure every discharge step. This procedure was repeated until total failure of the riprap structure was achieved. The overtopping discharge magnitude at which complete collapse or bulk erosion of the riprap occurred was defined as the critical unit discharge (q_c) in this experimental study. Continuous monitoring of erosion of individual stones was not possible due to highly aerated and turbulent flow over the riprap surface. Reference is made to *Paper I* for further details in this regard. Description of key findings from the investigation are presented within Section 6.1 of this thesis.

5.2 Field survey of ripraps *(FS1)* (*Paper II*)

The present field survey was conducted as part of the doctoral study and was intended at investigating toe structures and construction aspects of placed ripraps and riprap toe conditions of existing rockfill dams. To achieve this goal, placed ripraps constructed on nine different Norwegian rockfill dams were surveyed. Key parameters describing quality of placement of riprap and toe stones such as size, shape and inclination were recorded and these have been further analyzed and discussed in *Paper II*. Further, conformity of placed riprap toe construction with official dam safety guidelines are evaluated as part of the present study. Observations from the field survey concerning existing toe conditions for placed ripraps are also presented.

A field survey of placed ripraps on 33 different Norwegian rockfill dams was conducted by Hiller (2016). Findings from *Paper II* add to the findings of Hiller (2016) through investigation conducted to study details concerning toe construction of placed ripraps on nine rockfill dams. Details regarding the dam location, consequence classification, height and length are presented in Table 2. The rockfill dams chosen for the field surveys consisted of varying sizes of dams from 5 m up to 142 m in height (H) and from 70 m to 1400 m in length (L). The criteria for dam selection was presence of well-defined toe structures within the dam structure. The selections included Oddatjørndammen (H = 142 m and L = 466 m) which is the highest rockfill

dam in Norway and Storvassdammen (H = 90 m and L = 1400 m) which is the largest Norwegian rockfill dam by volume. Further, the selection also comprised of dams belonging to different dam safety consequence classes (2 to 4). The variability in dam sizes was considered as an important parameter in order to obtain a representative picture of placed riprap toe construction in rockfill dams.

Table 2. Details of the dams surveyed as part of the study (Ravindra et al., 2019a).

Dam Index	Dam name	Location	Consequence class	Dam height (H) (m)	Dam length (L) (m)
1	Vessingsjø Secondary dam	Tydal, Trøndelag	2	5	70
2	Skjerjevatnet Secondary dam 1	Masfjord, Hordaland*	2	18.7	101.2
3	Skjerjevatnet main dam	Masfjord, Hordaland*	3	29.5	251
4	Nesjø main dam	Tydal, Trøndelag	4	45	1030
5	Fjellhaugvatn dam	Kvinnherad, Hordaland*	2	52	72.8
6	Akersvass dam	Rana, Nordland	4	53	485
7	Førreskar dam	Suldal, Rogaland	3	81	640
8	Storvass dam	Suldal, Rogaland	4	90	1400
9	Oddatjørn dam	Suldal, Rogaland	3	142	466

*Presently known as Vestland.

The nominal stone size (d_n) has been employed to quantify sizing of the riprap stones as this can be considered as the representative size of individual riprap stones (Equation 10). Computation of d_n requires measurements of the longest, intermediate and the shortest axes dimensions of the riprap stones (a, b and c stone axes dimensions). The median stone size (d_{50}) for the stones is further computed as the average of individual nominal stone sizes. Furthermore, the placement angle of the riprap stones with respect to the downstream dam slope is characterized through the parameter (α) (Figure 6), which is the sum of the downstream embankment slope (θ) and the inclination of the longest stone axis with respect to the horizontal (β) (Equation 11).

$$d_n = (abc)^{1/3} \tag{10}$$

$$\alpha = \beta + \theta \tag{11}$$

The field measurements were subdivided into two different measurement phases. The first phase included measurements conducted to study the properties of the riprap section and the second phase was primarily intended at investigating properties of the toe stones and the toe support conditions. During the first phase of measurements, sizing of the riprap stones (a, b and c) and the inclination of the stones with respect to the horizontal (β) were measured for individual stones lying within a random 5 m x 5 m strip of the riprap. The stone dimensions were measured employing standard rulers and the inclinations were measured using a digital inclinometer. During the second phase of the survey, the dimensioning and the placement inclination of toe stones placed along the length of the dam toe were measured at regular distance intervals dependent on the dam length. Also, details regarding existing support conditions for the toe stones were recorded during this phase of the survey. Description of key findings from the investigation are presented within Section 6.2 of this thesis.

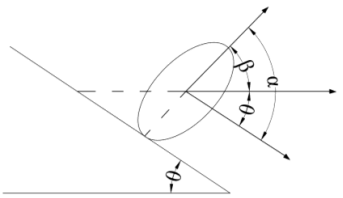

Figure 6. Portrayal of stone inclination with respect to the dam slope (α) as sum of inclination with respect to the horizontal (β) and embankment slope (θ) (Ravindra et al., 2019a).

5.3 Riprap model with unrestrained toe *(M2)* (*Paper III*)

The study described in *Paper III* was aimed at investigating the influence of toe support conditions on stability aspects of ripraps on steep slopes exposed to overtopping flows. A modified version of the experimental setup introduced in Section 5.1 for *Paper I* was put into use to investigate stability and failure mechanism of model placed and dumped ripraps unsupported at the toe section.

As previously stated, the original model designed by Hiller et al. (2018) consisted of a fixed metallic toe support structure fastened to the base frame at the downstream end of the riprap chute providing resistance against sliding of the riprap structure. A modified version of the

model setup was used in the present study, wherein the fixed toe support structure was replaced with a horizontal platform at the downstream extremity of the riprap chute to facilitate construction of placed riprap models with unrestrained toes (Figure 7). The modifications to the experimental rig were so designed as to maintain the original dimensioning of the riprap structure as employed in the preceding investigations to enable comparison of experimental findings. The surface of the horizontal platform was covered with a layer of geotextile to provide realistic friction for the toe stones.

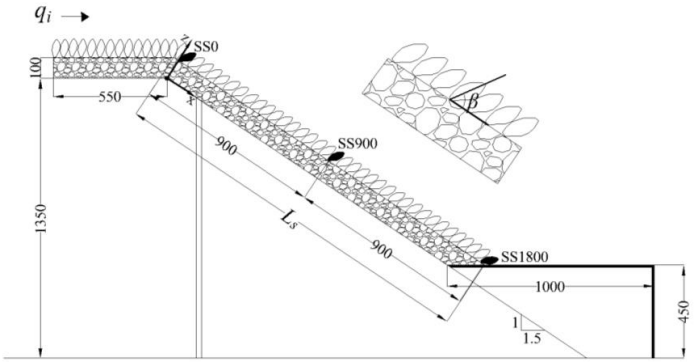

Figure 7. Illustration of experimental setup of model placed riprap with unsupported toe (Adopted from Ravindra et al. (2020b)).

Overtopping tests were carried out with both placed and dumped ripraps to better understand the fundamental differences and similarities in failure mechanisms between the two structures. Placed riprap models were constructed by manual placement of stones in an interlocking pattern commencing at the toe, progressing upstream to the crest. The individual riprap stones were deliberately placed with the longest axis (*a*-axis) inclined at $\beta \approx 60^{o}$ with respect to the chute bottom and at an inclination of $\beta \approx 90^{o}$ on the horizontal crest to account for practical considerations (Lia et al., 2013). It should be noted that the last row of riprap stones, which constitute the toe of the riprap were placed flat on the horizontal platform ($\beta \approx 0^{o}$) (Figure 7). Subsequent rows of stones were placed at incremental inclinations to attain the required stone inclinations of $\beta \approx 60^{o}$. This was also in alignment with the findings from field surveys of riprap toes presented in *Paper II*, wherein mean placement inclinations (β) for the toe stones were found to be much lower in comparison with those for the riprap stones. Further, single layer dumped ripraps were constructed by randomly dumping the riprap stones on the slope with arbitrary orientations and without any interlocking pattern.

Due to flow aeration in the model and the sudden nature of riprap collapse, conventional stone displacement measurement techniques could not be used for monitoring stone motions during these tests. To obtain quantitative descriptions of stone displacement in the tested riprap structures prior to and during riprap failure, new technology in stone displacement monitoring named as Smartstone probes (*Smartstone probe v2.1*), developed at the University of Trier, Germany was adopted within this study. Further, for validation of results obtained by the smartstone sensors, particle image velocimetry (PIV) technique was implemented as part of the investigation in collaboration with University of Trier.

5.3.1 Smartstones

Smartstone sensors are accelerometers designed to be implanted in stones for tracking of parameters describing stone displacements such as accelerations and rotations in time. The module comprises of a triaxial acceleration sensor, a triaxial gyroscope and a geomagnetic sensor (Figure 8). Owing to their non-intrusive nature of operation and flexibility for

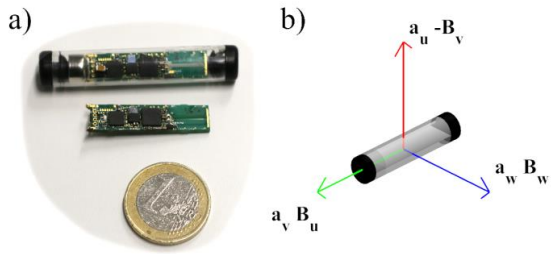

applicability in various engineering and research disciplines, Smartstone technology was found to be an ideal technique for implementation within the present experimental program.

Figure 8. (a) The Smartstone probe in a plastic tube with button cell on the left end and the circuit board with sensors underneath. **(b)** The probe's coordinate system (Adopted from Ravindra et al. (2020b)).

The current version of the smartstone sensor is covered by a 50 mm long and 10 mm wide plastic tube that is closed with two plastic plugs. Energy for recording and data exchange is supplied by a standard 1.5 V button cell (type AG5). The memory size allows for up to 8 minutes of constant movement with 100 Hz sampling rate. Commencement of data acquisition is marked by exceedance of stone movements over a user-defined threshold.

In order to equip select riprap stones with Smartstone probes within the present study, cylindrical holes of diameter 10 mm and length 50 mm were drilled within the stones. The

probes were encased in watertight rubber envelopes and mounted within the cylindrical drill holes. The openings were further sealed using sealing agents. Three riprap stones were mounted with Smartstone probes and placed within the test ripraps at the crown, the center and at the toe sections of the riprap structure for all the tests. This was to monitor stone movements at these locations as this could provide details regarding initiation and progression of riprap failure. The respective stones were identified as SS_0, SS_{900} and SS_{1800} (Figure 7) respectively with the indices representing the distance to the respective stones from the origin along the *x*-direction. The selected stones were located along the centerline of the flume ($y = 0.5$) to address concerns of wall effects.

5.3.2 Particle Image Velocimetry (PIV)

High-speed video footages of the overtopping tests were recorded over the course of the experimental testing program for all the tests. The video footages were in turn subjected to Particle Image Velocimetry (PIV) analysis to enable cross corroboration of investigation results. PIV analysis allows for estimation of the velocity distribution in image pairs. The direction and the velocity of particles in image pairs result from cross-correlation functions. The tool *PIVlab* (Thielicke and Stamhuis, 2014a; Thielicke and Stamhuis, 2014b; Thielicke, 2014; Garcia, 2011), which is available for MATLAB was used to carry out the analysis.

5.3.3 Testing methodology

Due to limitations with the Smartstone probes with respect to battery life and inbuilt memory, adoption of similar testing methodology as adopted within previous investigations to conduct extended overtopping tests was not possible within the present study. Hence, testing methodology was modified to accommodate the limitations of the probes. This was done also considering changes in the behavior of placed riprap models with unsupported toes concerning deformations and critical discharges. Reference is made to *Paper III* for further details in this regard.

To begin with, several pilot overtopping tests with placed and dumped ripraps were conducted without incorporation of the Smartstone probes. The pilot tests on model ripraps were carried out by exposing the riprap structures to incremental overtopping with discharge steps of $\Delta q = 0.02$ m^2 s^{-1}. The discharge levels were maintained constant over regular time intervals of $\Delta t = 1800$ s. The 3D location co-ordinates of several marked stones were measured in between overtopping steps employing the 3D laser traverse system. This procedure was further repeated

over N discharge steps until ultimate riprap collapse was achieved (q_c). Further, for tests conducted with placed and dumped ripraps implanted with Smartstone probes, the riprap structures were directly exposed to the critical discharge (q_c) levels obtained from the pilot tests in order to achieve riprap failure in the shortest possible time. This was to obtain measurements regarding the motion of riprap stones during riprap collapse, also accommodating limitations of the Smartstone probes. In essence, the adopted testing procedure results in measurements describing motion of the riprap stones prior to and during riprap collapse thereby providing a comprehensive description of the underlying failure mechanisms in the tested placed and dumped ripraps. The main outcomes from the study are presented in Section 6.3 of this thesis.

5.4 Rockfill dam models subjected to throughflow (*Paper IV*)

The European research project dubbed IMPACT (Investigation of Extreme Flood Processes and Uncertainties) was undertaken during the period 2001-2004 by a consortium of 11 institutions across Europe. The primary research focus of the project was the assessment and reduction of risks from extreme flooding caused by natural events or the failure of dams and flood defense structures (e.g. Zech and Soares-Frazao, 2007 and Morris and Park, 2007). Several experimental overtopping tests were conducted on earth and rockfill dams of different configurations as part of the research project (Kjetil et al., 2004). Experimental data sets from a single large-scale test conducted on a 6 m high prototype homogenous rockfill dam in Røssvatn, Norway as part of the IMPACT project (EBL Kompetanse, 2003; EBL Kompetanse, 2006; and EBL Kompetanse, 2007) were further analyzed as part of the present doctoral study. Further, in parallel studied conducted by NTNU, Trondheim and SINTEF, Trondheim, model studies on 1:5 and 1:10 scaled models of the large-scale test dam were conducted at the hydraulic testing facility of NTNU, Trondheim (Kjellesvig, 2002 and Sand, 2002). The test dams were composed of uniformly graded rockfill with median particle sizes ranging from d_{50} = 10.2 mm to 350 mm. Experimental data pertaining to throughflow hydraulic behavior of rockfill embankments were accumulated as part of these experimental studies conducted on rockfill embankment models of varying sizes. The data sets were further subjected to a statistical evaluation within *Paper IV* in collaboration with the Norwegian Geotechnical Institute (NGI), Oslo. This was to better understand non-linear flow through actual rockfill embankments. Findings from *Paper IV* are presented in Section 6.4. Technical details regarding the disparate model setups constructed during the IMPACT studies are briefly provided herein.

5.4.1 Large-scale field test experimental setup

The 6 m high homogenous rockfill embankment was constructed in a channel with mean top width of 42.8 m as part of the IMPACT project (EBL Kompetanse, 2006). The cross-sectional geometric outline consisted of crest and bottom widths of 2 m and 20 m respectively with upstream and downstream inclinations of S = 1:1.5 (V: H). The inclination of the embankment side slope was chosen in accordance with Norwegian rockfill dam construction practice (e.g. NVE, 2012). The abutment profiles at the test location were steep resulting in a trapezoidal channel cross-section. The rockfill embankment of volume $V_E \approx 2000$ m^3 was constructed of uniformly graded rockfill material with median stone size of d_{50} = 350 mm. During embankment construction, a set of four piezometers (P_1 to P_4) were installed within the downstream embankment structure at an elevation of 2 m from the channel bottom at a spacing of 4 m along the flow direction for throughflow depth measurements. Images from the test site depicting the test embankment prior to and during testing are presented in Figures 9(a) and 9(b) respectively. Reference is made to *Paper IV* presented within this thesis for detailed information regarding the large-scale experimental setup from the IMPACT study.

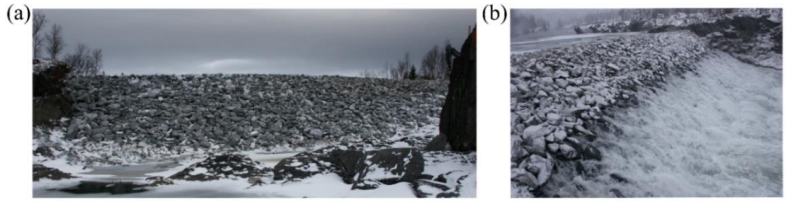

Figure 9. (a) Image of the test rockfill embankment (M1) from the test site downstream of Røssvatn, southern Norway prior to testing; **(b)** Image of the test dam during testing (Image courtesy: EBL Kompetanse (2006) and published in Ravindra et al., 2019b).

5.4.2 Model tests experimental setup

The 1:10 and 1:5 scale models of the large-scale test dam were constructed in flumes available at the hydraulic testing facilities of NTNU, Trondheim (Kjellesvig, 2002 and Sand, 2002). The 0.6 m high dams were constructed in a 2.2 m wide and 10 m long stepped flume and the 1.2 m high dams were constructed in a 4 m wide and 10 m long flume. The top and bottom cross-sectional widths of the 0.6 m high dam were 0.4 m and 2.2 m respectively. Further, top and bottom cross-sectional widths of the 1.2 m high dam were 1.0 m and 2.8 m respectively. All test dams for the 1.2 m high dam models were built with upstream and downstream inclinations of 1:1.5. However, due to limited availability of space within the flume, test dams for model

setup were constructed as partial dam structures with only the downstream embankment built with an inclination of 1:1.5. From a dam safety standpoint, it is of importance to comprehend the throughflow properties within the downstream shoulder of a rockfill dam in comparison with the upstream embankment as the downstream slope of rockfill embankments are exposed to higher degree of destabilizing forces under turbulent throughflow conditions. Also, the large-scale field test model consisted of piezometers installed at the center and within the downstream half of the embankment. Hence, model setups for the 1.2 m high dam, influenced by limited availability of space in the flume, were constructed as half dams with only the downstream half of the embankment structure.

Further, the flume sidewalls for both setups were sloped at 1:1 transforming the flume cross-section to a trapezoidal profile. This was done to account for the steep abutment profile observed at the large-scale dam test location (Figure 9) which resulted in a trapezoidal channel cross-section. For the 0.6 m high dam models, a total of seven piezometers were positioned along the centerline of the dam sections with uniform spacing of 0.3 m for throughflow depth measurements and two piezometers were placed upstream of the test dam sections for water level measurements. For the 1.2 m high dam models, five piezometers with even spacing of 0.5 m were installed within the embankment structures of the test dams and a single piezometer was installed upstream of the test embankments. Reference is made to *Paper IV* and to reports EBL Kompetanse (2006), Kjellesvig (2002) and Sand (2002) for detailed information regarding the model dam experimental setups.

5.4.3 Testing methodology and material properties

A series of seven tests were conducted on the model dams described in earlier discussions. A single throughflow test was conducted on the 6 m high rockfill embankment. Further, a set of six throughflow tests were carried out on the 1:10 and 1:5 models. Technical details regarding the material properties employed for construction of the models are presented in Table 3. Parameters H and W_{cr} represent the height and crest width of the rockfill embankments respectively. S denotes the upstream and downstream embankment slope values. For tests conducted with the 1.2 m high model dams, S represents only the downstream slope as the embankments were constructed as partial dams incorporating only the downstream embankment structures. Details regarding rockfill material properties such as the specific gravity (SG), median stone diameter (d_{50}), coefficient of uniformity (C_u) and porosity are also

presented in Table 3. The testing procedures are described through the parameter ΔQ symbolizing the throughflow discharge intervals.

The test embankments were exposed to incremental throughflow discharges in steps of ΔQ (Table 3). The discharge levels were maintained constant over regular time intervals of 10 minutes to ensure attainment of steady state flow within the dam structure. The process was repeated until the development of total embankment breach characterized by the breach discharge represented as Q_b. However, for the tested dams constructed with large size rockfill with d_{50} > 87.5 mm, ultimate dam breach could not be achieved even with application of maximum flow (Q_{max}) considering capacity of the channel for the large-scale test and the capacities of the flumes for the model tests. The piezometric pressure head measurements at the individual piezometers located within the dam structure were recorded for the corresponding throughflow magnitudes.

Table 3. Details of embankment construction aspects, rockfill material properties and testing procedures (Ravindra et al., 2019b).

Test No.	H (m)	S (-)	W_{cr} (m)	SG (-)	d_{50} (mm)	C_u (-)	n (-)	ΔQ ($m^3 s^{-1}$)	Q_b ($m^3 s^{-1}$)	Q_{max} ($m^3 s^{-1}$)
1	6	1: 1.5	2	2.7	350	1.2	0.40	5	-	30.5
2	0.6	1: 1.5	0.4	3.0	51.4	1.8	0.44	0.005	0.10	0.10
3	0.6	1: 1.5	0.4	3.0	10.8	2.0	0.45	0.005	0.025	0.025
4	0.6	1: 1.5	0.4	3.0	18.5	1.3	0.45	0.005	0.045	0.045
5	0.6	1: 1.5	0.4	3.0	87.6	1.4	0.49	0.01	-	0.15
6	1.2	1: 1.5	1.0	3.0	87.6	1.4	0.49	0.025	-	0.30
7	1.2	1: 1.5	1.0	3.0	203.7	1.7	0.52	0.05	-	0.50

5.5 Rockfill dam models with disparate toe configurations *(M3)* (*Paper V*)

This study described in *Paper V* (Kiplesund et al., 2020) was aimed at investigating the effects of toe configurations on the hydraulic response of rockfill dam exposed to throughflow scenarios. The model studies were conducted within the same flume settings detailed in the previous sections. The basic model setup comprised of the downstream half of a 1:10 scale rockfill dam structure of height H_d = 1 m, bottom width B_b = 1.8 m, top width B_t = 0.3 m (Figure 10(a)) and transverse length L_d = 1 m. The downstream embankment slope was chosen to be S = 1 : 1.5 (H : V) complying with Norwegian rockfill dam construction practice (NVE, 2012). The impervious steel element incorporated in the model setup encompassed the dimensioning

of the central core and the adjacent filter zones (Zone (B), Figure 10(a)). This is because, flow through the core, as well as the adjacent sand filter zone can always be considered to be laminar. Even for large rockfill dams, flow through these regions under throughflow conditions is unlikely to affect the stability of the downstream structure (Solvik, 1991). Since the objective of the experimental study was to investigate the behavior of downstream structure of rockfill dams simulating overtopping of the dam core, an impervious element representing the central core and filter zones was incorporated to simplify model design. All model dimensions were detailed following the guidelines offered by the Norwegian dam safety authorities (NVE, 2012).

Basing on a study of design and constructional aspects of several Norwegian rockfill dams, three discreet rockfill dam toe structures designs were identified, namely the external, internal and combined toe configurations. The external toe configuration represents a trapezoidal rockfill structure constructed on the downstream slope covering the toe region (Zone (F), Figure 10(b)). The internal toe configuration is characterized by a triangular region within the downstream embankment structure comprising of coarse rockfill material (Zone (E), Figure 10(b)). The combined toe configuration represents a coupling of the internal and external toe configurations (Zones (E) + (F), Figure 10(b)). The height of the toe structures were chosen as $H_t = 0.25$ m basing on a literature review of design of several existing Norwegian rockfill dams. The internal toe represents an equilateral triangle with altitude H_t. The external toe dimensions were so chosen as to achieve similar volume of construction as compared to the internal toe and to allow for sufficient length downstream of the dam structure to allow for complete flow development.

The rockfill dam models were constructed on a horizontal support platform of length $L_p = 3$ m, width $W_p = 1$ m and height $H_p = 0.35$ m. This was to elevate the entire test setup from the flume bottom in order to avoid backwater effects (Figure 10). The experimental setup was situated sufficiently downstream of the inflow section of the flume to achieve calm flow upstream of the test models. A series of 10 pressure sensors (P1-P10) were coupled with the experimental setup for measurements of internal pore pressure developments at different locations within the dam structure as shown in Figure 10(a) and also for monitoring of the upstream/downstream water levels during the overtopping tests. The pressure sensors were connected to the platform through a pipe network linked to an array of holes as depicted in Figure 10(c). A series of four holes were provided along the width of the platform at each pressure measurement location for measurement of the average pressure levels and also as a safety precaution against blockage.

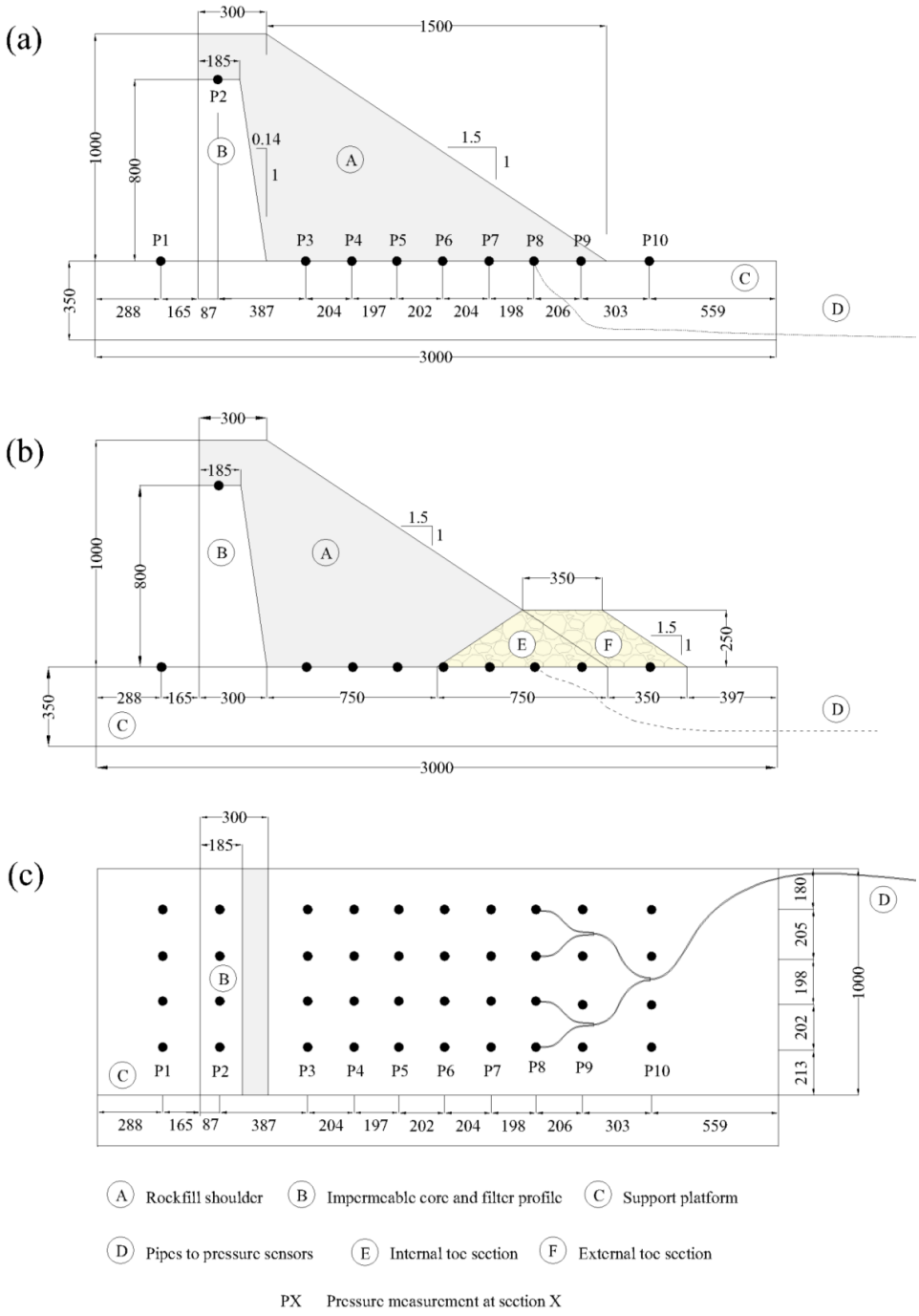

Figure 10. Depictions of the experimental setup with **(a)** planar view of the horizontal platform **(b)** sectional view of the rockfill dam model and **(c)** details regarding the disparate toe configurations.

Two SIEMENS SITRANS P210 sensors with pressure ratings of 0 to 2.5 m water column were employed at locations P1 and P2 and eight SIEMENS SITRANS P210 sensors with pressure ratings of 0 to 1.6 m water column were used at locations P3 to P10. These sensors provide reliable performance with high accuracy of 0.25% of the full-scale value. The sensors were in turn coupled with a data logging system to enable automatic data registration.

The dam shoulder comprised of well-graded rockfill material of density ρ_S = 2720 kg m^{-3}, median particle size $d_{50,S}$ = 0.0065 m and coefficient of uniformity of $C_{u,S}$ = 7.5. The toe sections were constructed employing uniformly graded coarse rockfill of density ρ_T = 2860 kg m^{-3}, median stone size $d_{50,T}$ = 0.052 m and coefficient of uniformity $C_{u,T}$ = 1.42. The material gradations were scaled down from a data base of gradation curves from large-scale rockfill dam constructions with a scaling ratio of 1:10. However, the gradation was biased towards the coarser range of the database. This was due to restrictions with the pumping systems installed in the laboratory, inclusion of very fine particles < 0.5 mm was not possible in the model. Hence, the gradation was carried out with 0.5 mm as the minimum allowed particle size.

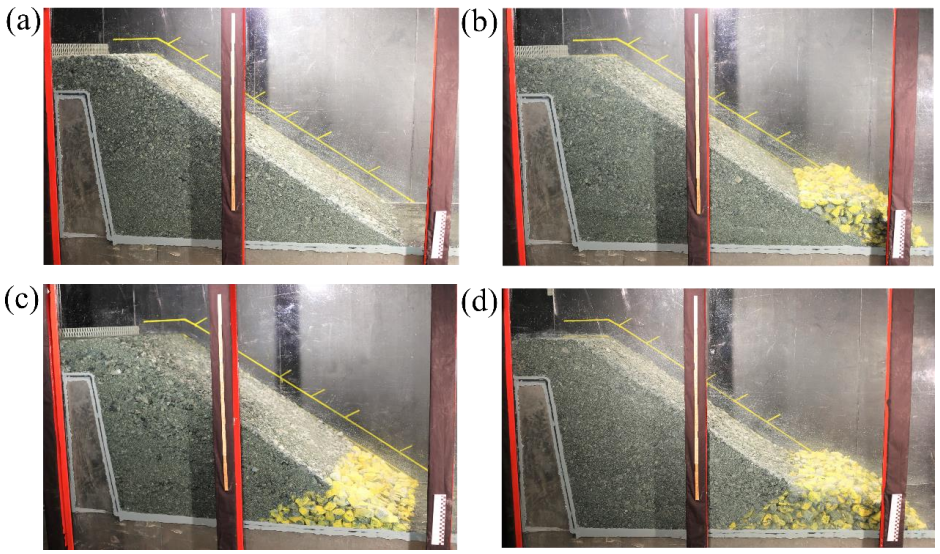

Figure 11. Depictions of the rockfill dams with (a) no toe, (b) external toe, (c) internal toe and (d) combined toe configurations.

The rockfill dam shoulder was built in layers of 0.1 m and were hand compacted using a 0.2 m x 0.2 m tamper weighing 4.54 kg (Figure 11). As a standard method of construction, the tamper was dropped free from a vertical distance of 0.1 m for 10 tampings at each location to achieve

uniform energy of compaction over the entire experimental testing program. The toe sections were constructed by manual placement of stones and were further hand compacted to avoid large voids in the structure.

5.5.1 Testing methodology

The study objective was to provide qualitative and quantitative descriptions of hydraulic responses of the dam structures exposed to incremental throughflow levels and to further evaluate and juxtapose the effects of disparate toe configurations on throughflow development. To accomplish these tasks, A total of twelve throughflow tests were conducted on model rockfill dam structures. A set of three tests were carried out with rockfill dam models without any form of toe. Further, a series of nine tests were conducted on rockfill dams provided with three different toe configurations, three tests per configuration for external, internal and combined toe geometries (Table 4). Main findings from the investigation are detailed in Section 6.5 of the present thesis.

Table 4. Descriptions of toe configurations, testing methodology and critical discharges.

Test no.	Toe configuration	q_i (. 10^{-3} m^3 s^{-1})	N (-)	Δt (s)	q_c (. 10^{-3} m^3 s^{-1})
1	No toe	1.0 - 3.5	6	1800	3.5
2	No toe	1.0 - 3.0	5	1800	3.0
3	No toe	1.0 - 5.0	9	1800	5.0
4	External	1.0 - 3.5	6	1800	3.5
5	External	1.0 - 5.5	10	1800	5.5
6	External	1.0 - 5.0	9	1800	5.0
7	Internal	1.0 - 4.0	7	1800	4.0
8	Internal	1.0 – 5.0	9	1800	5.0
9	Internal	1.0 - 4.5	8	1800	4.5
10	Combined	1.0 - 4.0	7	1800	4.0
11	Combined	1.0 - 3.0	5	1800	3.0
12	Combined	1.0 - 3.0	5	1800	3.0

The rockfill dam models were subjected to incremental levels of overtopping in regular discharge intervals of $\Delta q = 0.5 \cdot 10^{-3}$ m^3 s^{-1} commencing at $q_i = 1 \cdot 10^{-3}$ m^3 s^{-1}. The discharge levels were maintained constant over regular time periods of Δt = 1800 s to allow for flow

stabilization at each overtopping interval. To analyze the development of throughflow patterns, the pore pressure levels within the dam structure were recorded at various locations employing the pressure sensor- data logger setup at an acquisition rate of 100 Hz. Further, high quality images and videos of the tests were acquired. The procedure was repeated until complete erosion of the dam profile was achieved.

6 Summary of results

This section provides a general overview of the research outcomes from the experimental and statistical works conducted as part of the doctoral study. Results from *Paper I* describe a unique 2D failure mechanism in placed ripraps provided with toe supports exposed to overtopping flows. *Paper II* presents findings from a field survey of ripraps looking at practical construction aspects. *Paper III* demonstrates the effects of toe support on overall riprap stability under overtopping scenarios. *Papers IV* and *V* respectively describe flow through hydraulic properties of rockfill embankments and the effects of toe configurations on throughflow development. The model setups and the testing methodologies for the studies are presented within Chapter 5.

6.1 Buckling analogy for 2D deformation of placed ripraps exposed to overtopping (*Paper I*)

3D location co-ordinates of selected placed riprap stones were measured as part of the experimental testing program (Figure 5) prior to and after exposure to incremental overtopping magnitudes (q_i). Data sets from seven overtopping tests were analyzed as part of the study to describe 2D displacements of placed riprap stones exposed to overtopping flows. Table 4 presents a brief overview of the testing procedure and critical unit discharges. Data sets for tests 5 to 7 were obtained from Hiller et al. (2018) with the addition of data sets from four new tests (tests 1 to 4) (Ravindra et al., 2020a). Tests 5, 6 and 7 were referred to as P01, P02 and P04 respectively within the article Hiller et al. (2018).

Table 5. Testing procedure for the documented tests incorporating the discharge q_i given as range, number of discharge steps N, time intervals Δt, initial packing factor P_c and the critical unit discharge q_c representing loading condition at total riprap failure (Ravindra et al., 2020a).

Test	q_i (m^2 s^{-1})	N (-)	Δt (s)	P_c (-)	q_c (m^2 s^{-1})
1	0.05-0.30	9	1800	0.58	0.30
2	0.05-0.20	7	1800	0.56	0.20
3	0.05-0.12	3	1800	0.57	0.12
4	0.05-0.15	4	1800	0.54	0.15
5 (P01*)	0.05-0.24	9	1800	0.56	0.24
6 (P02*)	0.05-0.36	11	3600	0.55	0.36
7 (P04*)	0.10-0.40, 0.35, 0.40	6	3600, 17h	0.53	0.40

*Original labels for the respective tests as employed within Hiller et al. (2018).

As can be inferred from Table 4, the critical unit discharges for the tested ripraps varied over the range q_c = 0.12 m^2 s^{-1} to 0.4 m^2 s^{-1}. Variability in stability of placed ripraps against overtopping has been described by Hiller et al. (2018) as dependent on factors such as the packing density of placement and skill level of labor. All tests were conducted by exposing the ripraps to incremental overtopping in regular discharge and time steps. Test 7 from Table 4 is a special case as riprap failure could not be achieved even after application of the maximum possible unit discharge.

Figure 12 illustrates 2D displacements analysis results from a single test, test 1 presented in Table 4. The plot depicts development of 2D stone displacements as a function of applied overtopping discharge magnitudes ($q_i\, q_c^{-1}$). The horizontal axis of the plot ($L_m\, L_s^{-1}$) represents the distance to the respective selected riprap stones from the riprap stone placed adjacent to the fixed toe structure along the x-axis ($L_m = x_m - x_0$) (Figure 5) normalized over the total riprap length ($L_s = x_5 - x_0$ at $q_i\, q_c^{-1} = 0$). Stone displacements were computed with respect to the position of selected riprap stone adjacent to the fixed toe structure as the displacement of the stone identified as MS0 were moderate in comparison with the displacements measured for the other stones. The vertical axis of the plot represents the progressive stone displacements along the z-axis normalized over the median riprap stone diameter ($\Delta z_m\, d_{50}^{-1}$).

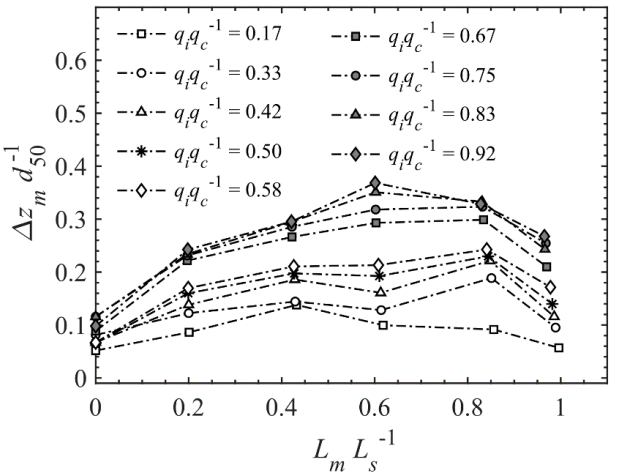

Figure 12. Depiction of 2D displacements of selected riprap stones for test 1 from Table 5 (Adopted from Ravindra et al., 2020a).

From Figure 12, it can be observed that the selected riprap stones underwent progressive displacements in the x-z plane with incremental overtopping. The displacements along the x-

axis can be seen as gradual translation of selected riprap stones in the downstream direction. The magnitude of displacements along the *x*-axis are proportional to the magnitude of overtopping discharge and the distance of the respective stones from the downstream toe, further validating the findings of Hiller et al. (2018). Further, riprap stones undergo progressive displacements along the *z*-direction in a manner directly proportional to the applied overtopping flow magnitude. Also, magnitude of displacements in the *z*-direction are dependent on the distance of the respective selected stones from the toe support as depicted in Figure 12.

Figure 13 presents results from the cumulative statistical analysis carried out with data sets obtained from all the seven tests presented in Table 4. Similar methodology as outlined for test 1 (Figure 12) has been adopted to compute the 2D stone displacements for the remainder of the tests. Figure 12 depicts the mean trends of 2D stone displacements for all the tests represented by average values of $\Delta z_m\, d_{50}^{-1}$ and $L_m\, L_s^{-1}$ computed for the seven tests at uniform intervals of overtopping ($q_i\ q_c^{-1}$ = 0.20). Variability in test results are presented as 95% confidence intervals.

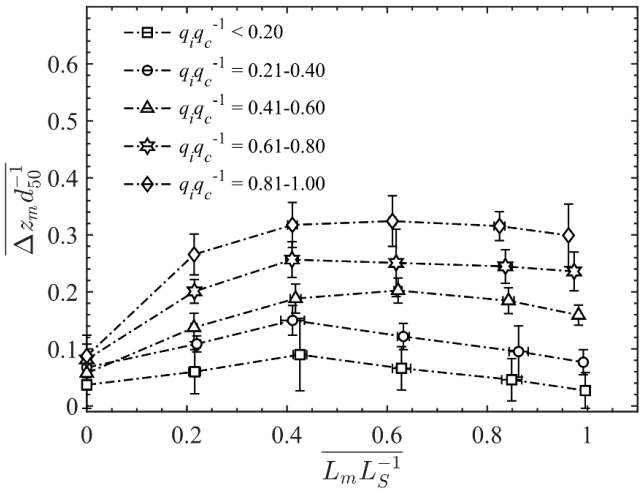

Figure 13. Results from the cumulative analysis carried out on data sets from seven tests representing average stone displacements in 2D. Uncertainty in displacements shown as 95% confidence intervals (Adopted from Ravindra et al., 2020a).

The process of 2D displacements of selected stones previously demonstrated by Figure 12 for test 1 was observed for all seven tests. Cumulative analysis results presented in Figure 13 further corroborate the observations made from Figure 12 of progressive 2D displacements of selected riprap stones as a function of both the overtopping flow magnitude and distance of the

respective stones from the fixed toe structure. Total riprap failure defined as the ultimate collapse of the entire riprap structure in the conducted tests was found to be initiated at the upstream section of the riprap when the maximum displacement of riprap stones along the *x*-axis exceeded the size of the longest axes of the riprap stones at MS5 ($\Delta x_5 \approx a \approx 1.6\ d_{50}$) (Hiller et al., 2018). This further corresponds to displacement of 0.3 - 0.35 times the median stone diameter of riprap stones at MS5 ($\Delta z_5 \approx 0.3\ d_{50}$ to $0.35\ d_{50}$) along the *z*-axis (Figure 13).

The mechanism of progressive 2D deformation of placed riprap stones discussed herein can be thought as being comparable to the mechanism of buckling observed in a slender-long column, pinned at one end and free at the other. A statistical analysis was conducted to demonstrate the similarities between the two mechanisms in the simplest possible manner by implementing the well-established Euler's theory for column buckling.

A non-dimensional equation was derived based on the methodology described within Wang and Wang (2004) with an intention of quantitatively illustrating the buckling modes of placed ripraps by considering a conceptual column with lateral deformations defined as $\Delta z_m\ d_{50}^{-1}$ at a distance of L_m from the pinned end (Equation 12).

$$\left(\frac{\Delta z_m}{d_{50}}\right)_i = A\ \ \frac{q_i}{q_c}\ \sin\left[k \cdot \pi\ \cdot\ \left(\frac{L_m}{L_s}\right)_i \cdot\ f\right] \tag{12}$$

where the term $L_m\ L_s^{-1}$ represents the column length ratio, A is a dimensionless numeric constant, obtained through calibration, $q_i\ q_c^{-1}$ denoting the applied hydraulic load, k denotes the buckling mode (k = 0, 1, 2, ...) and *f is a* numeric constant. It should be noted that $L_m\ L_s^{-1}$ is incorporated in Equation 4.1 as a function of $q_i\ q_c^{-1}$ to account for riprap stone displacements along the *x*-axis with incremental overtopping where the iterative variable i denotes a discharge step (i = 0 for $q_i\ q_c^{-1} = 0$ and $i = n$ for $q_i\ q_c^{-1} = 1$). The term $(L_m\ L_s^{-1})_{i=0}$ represents the original positions of the selected riprap stones prior to being exposed to overtopping.

The term $(L_m\ L_s^{-1})_i$ in Equation 12 can be computed employing Equation 13. The variable $(\Delta x_m\ L_s^{-1})_i$ for a particular overtopping flow can be obtained with the help of the statistically derived Equation 14. Equation 13 is valid for i = 0 to $i = n$ whereas Equation 13 is valid for $i > 0$ and $(L_m\ L_s^{-1})_{i=0}$ represents the initial positions of the riprap stones prior to overtopping exposure and $(\Delta x_m\ L_s^{-1})_{i=0} = 0$ for all stones.

$$\left(\frac{L_m}{L_S}\right)_{i+1} = \left(\frac{L_m}{L_S}\right)_i - \left(\frac{\Delta x_m}{L_S}\right)_{i+1} \tag{13}$$

$$\left(\frac{\Delta x_m}{L_S}\right)_i = \left(\frac{L_m}{L_S}\right)_{i=0} 0.0035 \cdot e^{\left(2.97 \cdot \frac{q_i}{q_c}\right)} \quad (14)$$

Equation 12 was calibrated against experimental data sets to obtain values for the numerical constants A and f. The calibration resulted in Figure 13 with values for calibration constants as $A = 0.38$ and $f = 0.70$ for the first buckling mode ($k = 1$). This corresponded to correlation between the observed and the predicted displacements of $R^2 = 0.89$ and $R^2 = 0.99$ for $\Delta z_m \, d_{50}^{-1}$ and $L_m \, L_s^{-1}$ respectively. Further, Equation 12 with $A = 0.38$, $f = 0.70$ and $k = 1$, was used to compute the continuous profiles of the buckling progression also presented in Figure 14.

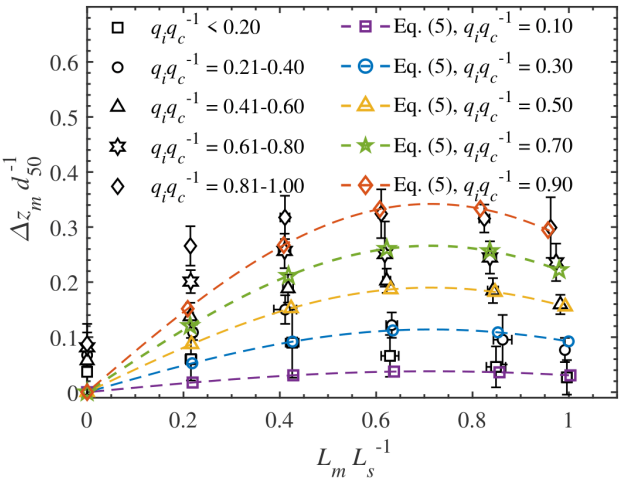

Figure 14. Observed 2D stone displacements from Figure 12 juxtaposed with predicted values from Equation 12 (Adopted from Ravindra et al., 2020a).

6.2 Toe support conditions for placed ripraps on rockfill dams - A field survey (*Paper II*)

The data sets accumulated as part of the field survey of placed ripraps were subjected to a statistical evaluation. Measurements of stone sizes (a, b and c) were used to analyze the size distribution and angularity of the riprap and the toe stones. Further, measurements of inclination of the stones with respect to the horizontal (β) have been employed to compute the angle of placement of the stones with respect to the downstream slope (α).

It is of importance to establish a technical background for the analysis. Comparison of the outcomes from the data analysis with design methodologies for placed ripraps would help bring out the technical significance of the findings. As discussed in Section 3.1, availability of technical literature describing design of placed ripraps is limited. The guidelines available within the Norwegian dam safety regulations and the recommendations of the NVE are some of the very few available official design procedures. Hence, to bring forth the practical relevance of the study findings, the results from the statistical investigation have further been subjected to a comparative evaluation with Norwegian dam safety requirements and recommendations. This would also further help in obtaining a better understanding of compatibility between construction practices and official guidelines. However, it is conveyed that the findings in general would be relevant and applicable for international interpretation.

Table 6 briefly summarizes the official regulations and recommendations concerning design and construction of placed ripraps. Furthermore, main findings from the statistical evaluation regarding conformity of riprap and toe construction practices with official guidelines and recommendations are also presented. To summarize, study findings suggest that construction practices adopted for placed ripraps in general meet the requirements of Norwegian dam safety regulations with regards to sizing and placement of the stones. However, investigation outcomes also show that construction practices adopted at present do not prioritize on addressing additional recommendations put forward by the dam safety authorities with regards to uniformity and angularity of stones used for construction.

Table 6. Summary of official regulations and recommendations with respect to placed ripraps

Parameter	OED (2009) regulations	Additional NVE recommendations	Riprap stones	Toe stones
Minimum stone size (d_{min})	The downstream slope should have slope protection which ensures that the dam can withstand large overtopping due to accidental loads or damage to the dam. Stones within the riprap must have satisfactory size and quality and be arranged in a stable manner.	$d_{min} = 1.0\ S^{0.43}\ q_f{}^{0.78}$ (2) *	All surveyed dams meet requirements of OED and the NVE	All surveyed dams meet requirements of OED and the NVE
Uniformity of stone size (d_{max} /d_{min})		d_{max} / d_{min} < 1.7 *	None of the dams meet the recommendation of the NVE	Vessingsjø secondary dam and Fjellhaugvatn dam meet the NVE recommendation
Angularity		The stones be situated within the bladed to rod shape regimes within the Zingg diagram (Zingg, 1935). This is to ensure optimum interlocking with minimal void formation. **	Majority of the measured riprap stones (67 %) lie outside the NVE specified region within the Zingg diagram	Majority of the measured riprap stones (69 %) lie outside the NVE specified region within the Zingg diagram
Stone placement	The individual riprap stones are to be placed in an interlocking pattern with their longest axis inclined towards the dam.	As stated in the OED (2009) regulations.	Generally in agreement with the regulation	Generally in agreement with the regulation

*Obtained from NVE (2012) and ** from the presentation Hyllestad (2007). The parameters d_{min} and d_{max} denote the minimum and maximum riprap stone sizes; S stands for the downstream embankment slope (S is the ratio of the vertical to the horizontal slope dimensions) and q_f represents recommended minimum design discharge value for the respective dam consequence classifications.

6.2.1 Toe classification

Based on observations from the field study, toe conditions for the surveyed dams were classified into five different categories (Table 7 and Figure 15). The first category of riprap toe construction includes ripraps built with no toe support. This entails that the toe stones were either lying on bare rock surfaces or buried underneath moderate amounts of soil cover. All the surveyed ripraps could be classified under this category as majority of the toe sections were resting on bare rock surfaces or buried with moderate amount of soil cover.

Table 7. Classification of different riprap toe conditions (Adopted from Ravindra et al., 2019a)

Category	Description of toe condition	Dam name
1	No toe support	All surveyed dams (Table 2)
2	Submerged toe	Skjerjevatnet main dam Skjerjevatnet secondary dam 1 (e.g. Figure 15(d))
3	Larger stones at the toe	Fjellhaugvatn dam Storvass dam (Figures 15(a) and (e))
4	Steel rebars	Storvass dam (Figure 15(e))
5	Concrete wall	Akersvass dam (Figure 15(f))

Figure 15. Depiction of existing conditions of placed riprap toe sections. Category 1 at dams **(a)** Fjellhaugvatn dam **(b)** Oddatjørn dam and **(c)** Skjerjevatnet main dam. Category 2 at **(d)** Skjerjevatnet main dam. Category 4 at **(e)** Storvass dam. Category 5 at **(f)** Akersvass dam (Adopted from Ravindra et al., 2019a).

Illustrations of ripraps built with no toe support conditions are presented for dams Fjellhaugvatn, Oddatjørn and Skjerjevatnet main dam in Figure 15(a), 15(b) and 15(c) respectively. Toe stones at Fjellhaugvatn dam and Skerjavatnet main dam were found to be resting on rock surfaces whereas toe stones at Oddatjørn dam were buried under moderate soil cover.

The second category of observed riprap toe conditions at the surveyed dams consists of submerged riprap toe sections. This was the case at certain reaches of riprap toe sections of Skjerjevatnet main dam and Skerjevatnet secondary dam 1. An illustration of the scenario at Skjerjevatnet main dam is depicted in Figure 15(d).

Further, the third classification of riprap toe conditions observed was the placement of larger sized stones at the toe section of the riprap. Fjellhaugvatn dam and Storvass dam fall under this category as larger size stones ($d_{50,\,T}$ / $d_{50,\,RR}$ = 1.53 and 1.45 respectively) were found to be placed at the toe sections of these dams. For the rest of the surveyed dams, stone sizing at the toe and the riprap were found to be comparable.

The fourth category of riprap toe construction observed was the use of steel bars for stabilization of the toe stones. A small section of the riprap toe at Storvass dam was observed to be tentatively supported using reinforcing steel bars (Figure 15(e)) measuring 25 mm in diameter with average outcrop length of 0.3 m. Although majority of the riprap toe sections of Storvass dam were observed to be unsupported, the reinforcing bars were used to tentatively stabilize toe sections of the riprap close to the right abutment where the foundation was observed to be at a steep inclination. The steel rebars were most likely used to facilitate placement of toe stones on the steep foundation.

At Akersvass dam, a small stretch of the riprap toe section was seen to be supported with a concrete wall (Figure 15(f)) and this is classified as the fifth riprap toe state observed as part of this field study. The concrete wall was constructed in tandem with a leakage measuring station and hence, it was evident that riprap toe stabilization was not the primary intention of constructing the structure but rather to facilitate leakage measurements from the dam.

6.3 Failure mechanism in placed riprap on steep slope with unsupported toe (*Paper III*)

Details regarding the experimental testing program are presented within Table 7. The table also presents particulars regarding construction and testing procedures adopted for experiments conducted on placed (P01 - P06) and dumped (D01 - D03) ripraps. The critical overtopping discharge levels for initiation of irreversible riprap failure (q_c) were found to be higher for placed ripraps as compared with dumped ripraps. Unraveling riprap failures were found to be initiated at overtopping discharge magnitudes of q_c = 0.06 m^2 s^{-1} and 0.04 m^2 s^{-1} respectively for placed and dumped riprap (Table 8). This ratio of critical discharge values between placed and dumped ripraps was hence found to be 1.5.

Table 8. Description of the experimental testing procedure (Ravindra et al., 2020b).

Test	P_c (-)	q_i (m^2 s^{-1})	n (-)	Δt (s)	q_c (m^2 s^{-1})
P01*	0.53	0.02 - 0.06	3	1800	0.06
P02	0.53	0.06	1	-	0.06
P03	0.54	0.06	1	-	0.06
P04	0.48	0.06	1	-	0.06
P05	0.49	0.06	1	-	0.06
P06	0.52	0.06	1	-	0.06
D01*	0.91	0.02 – 0.04	2	1800	0.04
D02	0.83	0.04	1	-	0.04
D03	0.74	0.04	1	-	0.04

*Pilot tests conducted without incorporation of the Smartstone probes

Further, the 2D deformations within placed riprap structures were analyzed with respect to incremental overtopping discharge magnitudes using laser measurements of location co-ordinates of six marked stones collected during the pilot tests. Reference is made to *Paper I* (Ravindra, Sigtryggsdottir, et al., 2020) for further details regarding the analysis procedure. Analysis results revealed that the marked riprap stones placed on the riprap chute underwent only minor displacements along and normal to the chute direction (x and z axes respectively) prior to initiation of progressive riprap failure. Further, the toe stones placed on the horizontal platform experienced insignificant downstream displacements along the platform surface.

Furthermore, no definite correlations were found between the stone displacements and the overtopping discharge magnitudes.

6.3.1 Initiation and progression of placed riprap failure

The Smartstone probes were adopted within this study to better understand the mechanisms of failure initiations and progression in placed and dumped ripraps. Also, Particle Image Velocimetry (PIV) analysis using the recorded video footages (provided as a supplementary video file) were also conducted to further validate results derived from measurements obtained from the Smartstones. Cumulative results from analysis conducted implementing these two techniques are presented herein

Detailed analysis of the accelerometer and gyroscope data revealed that riprap failure takes place in uniquely identifiable phases. To illustrate the sequence of events leading up to and further progressing as total riprap collapse, depictions of stone acceleration and orientation measurements for an overtopping test conducted on a model placed riprap are presented as Figure 16). Recorded measurements from the Smartstone placed at the riprap crest (S_0 from Figure 7) from test P05 are portrayed in Figure 16. Further, the individual phases of stone motions within the time series are labelled with capital letters.

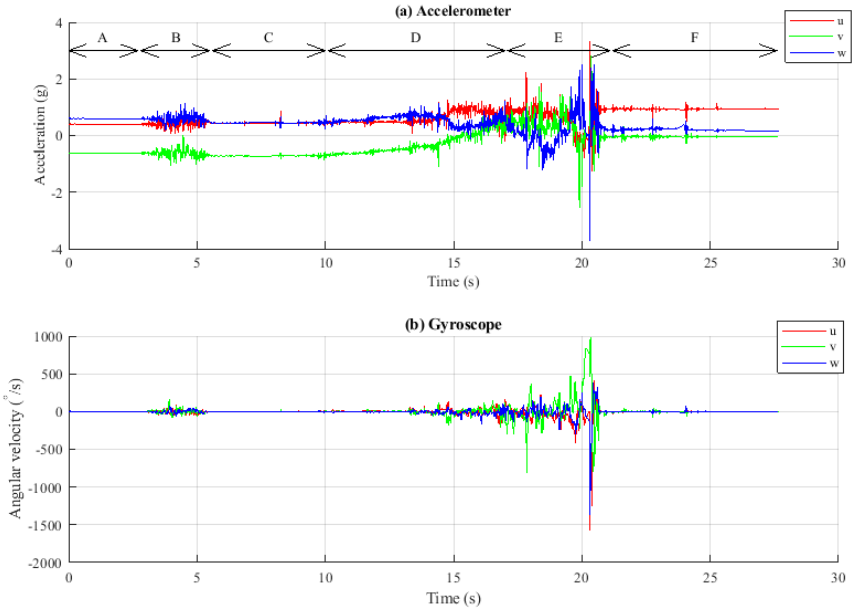

Figure 16. Depictions of **(a)** accelerometer and **(b)** gyroscope measurements from the Smartstone placed at the riprap crest (S_0) from test P05 (Ravindra et al., 2020b).

Phase A: The start of Phase A ($t = 0$) represents the trigger point of the probe subsequent to which the probe initiates the data recording protocol. That is, at $t = 0$, the water flow reaches a magnitude that results in accelerations of the sensor-equipped stone that exceed the threshold of 48 mg. This threshold represents the minimum trigger acceleration value to be experienced by the sensor beyond which data acquisition can commence. This can be due to minor changes in stone inclination by fractions of a degree, as a change of inclination changes the fraction of gravity measured along each probe axis. This effect can be considered a consequence of vibrations generated due to initial flow attack on the stone. The stone does not undergo major displacements during the remainder of phase A. Similar observations were made for Smartstones placed at the center (S_{900}) and at the toe of the riprap (S_{1800}).

Phase B: The hydrodynamic drag and lift forces generated by incremental overtopping flows reaches higher magnitudes resulting in strong vibrations as can be seen from the accelerometer plot in Figure 16. The impinging flow forces and the resulting vibrations further lead to small reorganizations of the stones within the riprap structure, as demonstrated by minor changes in stone inclinations. These are visible within the acceleration plots for the *u* and *w* axes (the blue and red lines) presented in Figure 16. These are on different levels prior to phase B and almost on the same level after phase B. This entails that the stone underwent rotation along the *u*-*w* plane to attain a final configuration for Phase C. This conclusion could also be further corroborated through inspection of the video footage that revealed that during phase B, the riprap layer in its entirety undergoes slight compaction and the stones experience changes in orientation, tilting towards the downstream direction. The Smartstone placed at the center (S_{900}) of the riprap displayed similar behavior. However, the stones placed at the toe (S_{1800}) did not appear to experience significant displacements or rotations during this phase.

Phase C: After this initial readjustment phase leading to compaction of the riprap structure, there is a phase of relative rest with only occasional single small spikes in the acceleration data. In this phase, the overtopping flow magnitude is gradually increasing.

Phase D: The failure begins quite slowly during several seconds with a tilting of the stones in the riprap layer. This tilting is visible by the changing levels of the different acceleration time series. It can be observed that the absolute values at the *v* axis (green line) gradually decrease while the *w* axis values increase (blue line). Thus, the sensor's end indicated by the blue *w* axis moves downwards. This effect is also documented in the video as the whole top layer tilts within this phase of failure initiation.

Phase E: Initiation of progressive sliding collapse of the riprap structure. Reference is made to Paper III (Ravindra et al., 2020b) for detailed description of the sliding process.

Phase F: The riprap stones further collapse to form a pile on top of the horizontal platform. The pile is still overrun by water, resulting in small spikes in measurements. The pile is continually undergoing rearranged as a consequence of flow attack after a pause of several seconds.

Furthermore, dumped ripraps were found to go through a surface erosion process where individual stones were eroded by the action of destabilizing turbulent flow forces. This was in contrast to failure initiation in placed ripraps wherein the riprap structure as a whole was found to undergo a slide.

The acceleration and the gyroscope measurements were subjected to further analysis to derive displacement velocities of the Smartstone during riprap failure. Using integration of the acceleration values, a velocity time series was obtained.

In total, three runs of placed riprap and three runs of dumped riprap were examined. The observations in these two groups are similar within each group and also the differences between the groups are obvious. The general findings are: Placed ripraps collapse were found to occur more abruptly than dumped ripraps. The peak velocities were also found to be higher (between 0.66 and 1.008 m s^{-1}) for placed ripraps as compared with velocities computed for dumped ripraps (between 0.31 and 0.52 m s^{-1}). Also, placed riprap acceleration time series show more frequent and higher magnitude peaks, while the gyroscope time series show less rotations. This in turn entails that placed ripraps are characterized by high degree of vibrations within the riprap structure and that placed ripraps collapse as a unit in the sense that the whole riprap layer slides down the slope as a unified structure. However, for dumped ripraps, less acceleration peaks were visible and significantly higher stone rotations were recorded by the gyroscope. This further suggests that dumped riprap failures entail lower degree of vibrations and that the failure progresses randomly with erosion of individual stones from the slope.

The velocities derived from Smartstone data should be confirmed using different techniques. To accomplish this, Particle Image Velocimetry (PIV) analysis was conducted on the video footage to obtain velocity distributions during the overtopping test. The tool PIVlab (Thielicke and Stamhuis, 2014a; Thielicke and Stamhuis, 2014b; Thielicke, 2014; Garcia, 2011), which is available for MATLAB was employed to carry out the analysis. For each frame, the estimated velocities were stored in a matrix for the horizontal component and a second matrix

for the vertical component. The peak of the time series of the PIV-derived velocities in this cell were compared to Smartstone derived velocities. In all runs that were compared, excellent correlation between the Smartstone derived maximum velocities and the PIV derived peak velocities were observed. Deviations between PIV and Smartstone velocities ranged between 0.01 and 0.06 m s^{-1}.

6.4 Non-linear flow through rockfill embankments *(Paper IV)*

The recorded piezometer data from the tests (Table 3) were employed to compute hydraulic gradients and the corresponding void velocities within the test dams at incremental throughflow magnitudes. Further analysis of the i-V_n trends within the different test dams were conducted over the range of applied through flows for which the test dams were stable. The computed i-V_n trends for the tests are presented in Figure 17(a) and 17(b) for the 0.6 m and 1.2 m high model setups respectively and in Figure 17(c) for the 6 m high large-scale field setup. It can be inferred from the depictions that the computed i-V_n trends for the tests followed non-linear trends in general. Although some degree of variability in the i-V_n trends were observed at different locations within the tested dam structures, the trends in general were in good agreement with each other. The observed variability could be explained as a consequence of local variations in porosity or packing density of rockfill medium at the different piezometric locations due to disparities in manual construction efficiency. The i-V_n trends are presented over a broad range of hydraulic gradients (i = 0.01 to 0.5) for tests conducted with the 0.6 m and the 1.2 m high dam models. But, for the 6 m high rockfill dam (Figure 9), i-V_n trends are presented over a narrower hydraulic gradient range of i = 0.24 to 0.40 as a consequence of unavailable measurements of flow depths for lower throughflow magnitudes as the piezometers were located at 2 m elevation from the dam bottom.

Trend lines of the form $y = a\,x^b$ were added to the individual i-V_n plots demonstrating excellent correlation. Further, values for parameters a and b for the respective tests were extracted as part of the analysis. It was observed that the parameter b for all the tests was consistently placed within the range of 0.48 to 0.55 except for Test 7 (Table 3), wherein a lower value of parameter b = 0.41 was found. The average of the obtained b values was found to be b = 0.51. As stated earlier, parameter b within the power-law (Equation (5)) represents the degree of flow turbulence. The obtained average value of parameter b = 0.51 signifies fully developed turbulent flow regime. This finding is in line with conclusions of several past studies such as Escande (1953), Soni et al. (1978) and Siddiqua et al. (2011) with regards to parameter b that

$b \approx 0.5$ represents post-linear or non-Darcian flow regime. Furthermore, correlation between material properties such as C_u and n and parameter b were evaluated and no definitive relationships could be observed in this regard between the parameters. Considering the anomalous value of $b = 0.41$ for test 7, although the exact reason for the observation is not apparent, the large size of the rockfill particles used for the test ($d_{50} = 0.203$ m) could offer a possible explanation in this regard as the mean stone diameter for this particular test was oversized considering the dam height ($H = 1.2$ m). This could inhibit complete development of flow turbulence resulting in a lower value of b. Furthermore, the porosity of the dam material for test 7, $n = 0.52$ was slightly higher in comparison with other materials which fall within a range of 0.40 – 0.49 and this could also influence flow turbulence levels within the test dam.

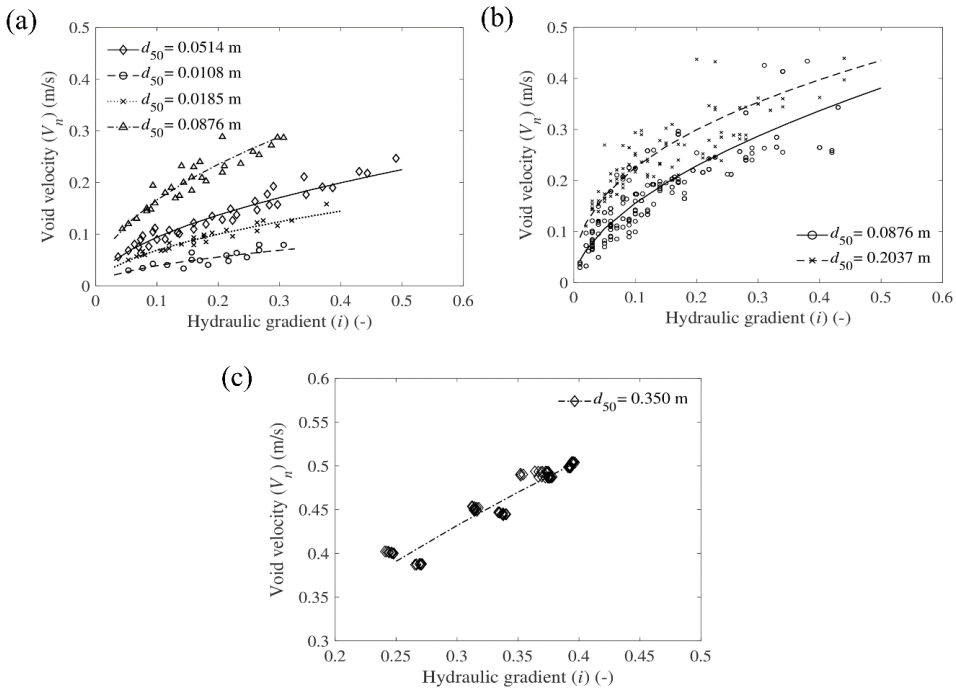

Figure 17. Computed i-V_n trends for **(a)** 0.6 m high dam model **(b)** 1.2 m high dam model and **(c)** 6 m high large-scale dam (Ravindra et al, 2019b).

Further, Figure 18 represents the correlation between parameters a and d_{50} for the respective tests. A clear exponential trend can be observed in this regard quantitatively described by a symmetrical sigmoidal trend line represented as Equation (15). The trend line demonstrated good correlation with the parent dataset with an $R^2 = 0.95$.

$$a = \left(72.987 - \frac{73.613}{\left(1+\left(\frac{d_{50}}{1.136 \cdot 10^{9}}\right)^{0.179}\right)}\right) \tag{15}$$

To obtain a general power-law describing the non-linear i-V_n trend for throughflow in rockfill embankments, the experimentally derived results for parameters a and b were further used to arrive at Equation (16). The value for parameter b is adopted as 0.51 as this represents the average for all tests.

$$V_n = \left(72.987 - \frac{73.613}{\left(1+\left(\frac{d_{50}}{1.136 \cdot 10^{9}}\right)^{0.179}\right)}\right) i^{0.51} \tag{16}$$

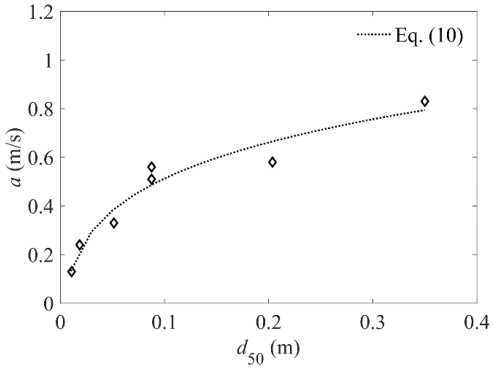

Figure 18. Relationship between parameter a and the mean rockfill particle sizes (d_{50}) (Ravindra et al, 2019b).

The proposed power-law relationship describing the correlation between hydraulic gradient and void-velocity of flow through rockfill embankments (Equation (16)) was further subjected to a comparative performance-based evaluation along with some well-establish power-law relationships from international literature. The Engelund (1953) (Equations (6) and (7)) and the Wilkins (1955, 1963) (Equation (8)) power-law relationships obtained from experimental studies conducted in permeameters, describing non-linear flow through rockfill medium are widely implemented in various disciplines of hydraulic engineering. These criteria have been included in the present study to investigate their validity in describing throughflow properties in actual rockfill embankments.

6.5 Effects of toe configuration on throughflow hydraulic properties of rockfill embankments (*Paper V*)

As described in Section 5.5, pore pressures were measured at different locations within the dam structures (P2-P10) during the tests (Figure 10). In addition, the corresponding upstream water levels (P1) were recorded. The raw pore pressure datasets were subjected to a change point based statistical analysis to obtain representative pore pressure magnitudes at different discharge levels (q_i). Reference is made to *Paper V* for detailed description of the methodology. The pore-pressure development patterns at different locations within the dam structure for Test 1 conducted with no toe (Table 4) are depicted in Figure 19. The pore pressure values depicted for each of the discharge intervals represent the stable values attained after maintaining the discharge magnitude at the respective levels over time periods of Δt = 1800 s. As can be observed, the individual pore-pressure levels within the rockfill shoulder were found to undergo non-linear increments as functions of the applied throughflow magnitudes for Test 1. The non-linear trends in pore-pressure developments were found to be less pronounced at the downstream section of the dam structure. Similar trends were observed for all the tests.

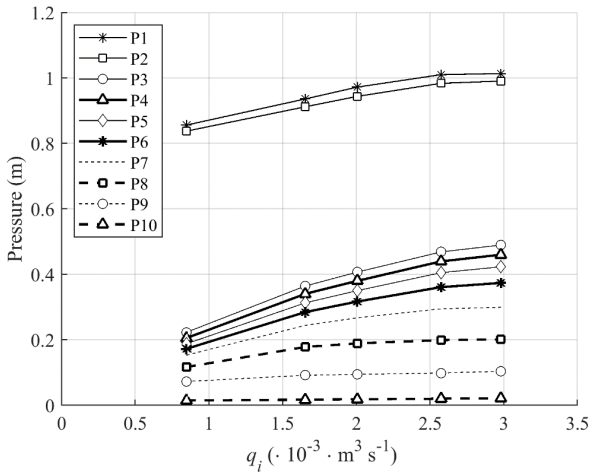

Figure 19. Pore pressure development profiles at different locations within the dam structure for Test 1 from Table 4.

The effects of different toe geometries on phreatic surface developments within the rockfill dam structures were investigated. Figure 20 depicts the positions of the phreatic surfaces within the model dams coupled with different toe configuration as derived from pore pressures measured at the ten pressure sensor locations (P1-P10, Figure 10). As can be observed from

Figure 20, the flow patterns upstream of sensor location P3 were found to be consistent across models. During the tests, the water surface profiles upstream of the dam crest section (P1) were observed to be horizontal in nature as they entered the crest. Hence in Figure 20, the water surface profiles are shown as extensions of pressure measurements from P1 onto the entry surface of the crest using horizontal lines. Further, the drops in pressure from the entry location to P2 were used to plot flow lines with mild gradients over the core-filter element. Furthermore, the flow underwent transitions over the core-filter element and in turn plunged into the downstream dam structure towards P3. The plunge patterns were visually observed to be near vertical drops. This could be explained as a consequence of the steep slope of the core-filter element. A milder slope would lead to more moderate flow patterns.

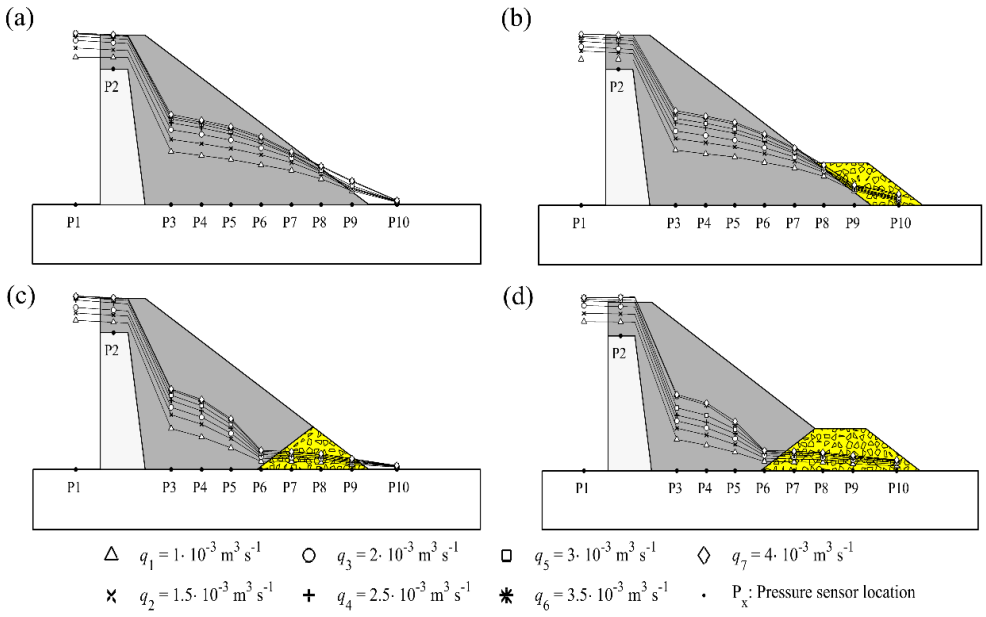

Figure 20. Phreatic surface depictions within model rockfill dams with **(a)** No toe, **(b)** external toe, **(c)** internal toe and **(d)** combined toe configurations as functions of applied throughflow magnitudes (q_i).

Further, for rockfill dam structures with no toe (Figure 20(a)) and with external toe (Figure 20(b)), closely resembling smooth non-linear phreatic surface profiles were observed within the rockfill shoulders. The pore-pressure development was found to be correlated to the applied throughflow magnitudes (q_i). The spacing between the phreatic surfaces were found to undergo decrements with incremental overtopping, owing to the non-linear nature of pore-pressure

developments at each of the sensor locations (Figure 19). From visual observations of Figure 20, the external toe was found to have minor impact on throughflow development within the rockfill shoulder. Results from further quantitative analysis show that adding an external toe introduces friction losses within the toe structure. This results in minor elevations of the phreatic surfaces within the supporting fill, especially towards the downstream section. This in turn leads to reductions in total flow length along the phreatic surfaces. Further, due to the highly porous nature of the toe material, the flow downstream of the shoulder were found to be affected to a minor degree by the external toe configuration. The primary difference in behavior of the two structures was the additional protection offered by the external toe against scouring and erosion at the seepage exit face. Significant damages were observed at the toe sections of the rockfill shoulders for models constructed without toes. This was due to surface erosion resulting as a consequence of the drag forces generated over the seepage exit face and due to occurrence of occasional slides leading to scouring. However, no such damages were observed for dams constructed with external toes.

For dam models built with internal and combined toe configurations, significantly different pore pressure development profiles were obtained as juxtaposed with the dam models built with external toe and with no toe. The phreatic surfaces were found to be located at significantly lower elevations within the shoulders downstream of P3 entailing marked reduction in internal pore pressures. The phreatic surfaces experienced much steeper drops from P3 moving downstream towards P6 (Figure 20) resulting as a consequence of high permeability of the internal toe reaches. The pore-pressure magnitudes downstream of P6 were further seen to experience mild progressive reductions within the toe structures finally exiting the dam structure. The throughflow development patterns within the dam structures constructed with internal and combined toes closely resembled each other. The internal reaches of the high permeability zone give rise to disparate throughflow profiles. The external portion of the combined toe configuration from a theoretical standpoint result in marginal raising of internal pore pressures as described earlier. However, this was not seen from the recorded data, potentially due to variability in permeability of the shoulder material. No damage to the toe sections were observed for either of the toe configurations even at maximum throughflow magnitude.

To further quantitatively describe the previously presented observations, several parameters were quantitatively analyzed. Percentage differences in pore-pressure magnitudes, differences in percentage areas of the dam structures exposed to pore pressure and the length of the phreatic

surface profiles within the dam structures for different toe configurations were analyzed and compared. Reference is made to *Paper V* for in depth discussions in this regard.

6.5.1 Failure initiation

Discharge levels for initiation of dam breach were recorded as part of the experimental testing program. As a key finding, critical locations for breach initiation were always found to be situated over the upstream crest of the dam structures being independent of the flow conditions in the lower reach of the dams. In essence, none of the tested dams experienced irreversible dam breach at the toe section even with the application of maximum throughflow magnitude which could be accommodated through the crest. Significant damage to the toe sections were observed for dams constructed with no toe. However, ultimate breach initiation leading to erosion of the dam structure were always found to be initiated at the overtopped upstream crest section.

Furthermore, no clear correlations were found between the magnitude of maximum throughflow required for initiation of dam breach and the toe configurations employed (Table 4). This in turn suggests that the amount of throughflow entering the dam structure is primarily dependent on properties of the dam crest such as the dimensioning and the permeability rather than on the downstream flow conditions. This also suggests that stability of rockfill dams under overtopping situations with unprotected downstream slopes is determined by features of the dam crest. However, during piping scenarios leading to entry of highly turbulent, large magnitude pressure flows into the dam structure, the rockfill dam toe could greatly help stabilize the dam structure. Further investigations in this regard are highly recommended.

7 Discussions

Two principle research objectives for the doctoral study were defined earlier within the thesis. ***Objective 1*** was oriented towards obtaining a holistic description of stability and failure mechanisms in ripraps exposed to overtopping. Further, ***Objective 2*** was focused on evaluating the hydraulic response of rockfill embankments subjected to throughflow scenarios. The present section is aimed at providing overarching interpretations of key research findings from the study with emphasis on addressing the laid-out research objectives.

7.1 Holistic evaluation of riprap stability under overtopping conditions (*Objective 1*)

The main research outcomes from *Papers I* to *III* are discussed within the present sub-section. The objective of these discussions is to bring out the significance of the research on ripraps and to provide an overarching evaluation of the relationship between the different studies. These are in turn intended at presenting a holistic evaluation of the research program on ripraps as a whole.

7.1.1 2D deformation behavior in toe supported placed ripraps on steep slopes (*Paper I*)

Several past research works such as Hiller et al. (2018), Dornack (2001), Sommer (1997), Larsen et al. (1986) and Siebel (2007) have described 1D failure mechanism in placed riprap provided with toe support exposed to overtopping flows. These studies have introduced novel techniques and methodologies for detection of riprap stone displacements. These have also provided valuable insight into the longitudinal compaction process occurring within the riprap structure. Findings related to 2D deformations in placed ripraps with toe support (***M1***) under overtopping conditions obtained from the present research work add to the available international literature on the research topic. The results obtained from the study demonstrate that toe supported placed ripraps constructed on steep slopes exposed to overtopping flows undergo a 2D buckling process analogous to the buckling profile of a long-slender column under compression pinned at one end and free at the other end (Figures 13 and 14). This can be explained as a direct consequence of the interlocking forces generated between the individual riprap stones forming a bearing structure capable of withstanding certain degree of deformations. Placed ripraps supported at the toe exposed to overtopping undergo initial

compaction to form a unified riprap structure. Further increment in the applied hydraulic loading which in turn results in higher drag and lift forces on the riprap structure. The drag forces lead to compaction of the riprap along the chute length and a combined effect of the bending moments and in part, the hydraulic lift forces generated within the riprap structure lead to out of plane deformations. This process eventually leads to ultimate structural collapse of the riprap structure.

Numerous past studies investigating placed riprap stability have concluded that the erosion of single stones in a placed riprap does not necessarily result in the loss of the structural integrity of the placed riprap structure (Hiller et al., 2018; Dornack, 2001; Sommer, 1997; Larsen et al., 1986). The findings of this study provide evidence in support of this statement. Since placed ripraps exposed to overtopping loads form a unified structure as a consequence of the generated interlocking effect, detachment of a single loosely placed stone from the structure does not necessarily entail loss of structural integrity as the configuration of the neighboring stones can still offer a considerable degree of resistance against the destabilizing force. This in turn entails that placed riprap stability is not governed by individual riprap elements but rather that the unified structure formed due to interlocking of the ripraps stones as a whole resists the applied hydraulic loading. This behavior is comparable to the response of structural elements, such as a masonry structure acted on by external loading.

The qualitative and quantitative descriptions of the unique failure mechanism observed in toe supported placed ripraps further relate the fields of hydraulic and structural engineering. This provides a fresh perspective on design and construction of placed ripraps and hydraulic structures in general. Design approaches currently employed in hydraulic engineering generally place emphasis on the geometrical and flow boundary conditions, material characteristics and fluid properties. However, design methodologies taking into account the multilayered behavior of these structures are seldom encountered. Findings of the present study document the fact that stability of toe supported placed ripraps constructed on steep slopes is a predictable mechanism following the principles of an established structural theory. This leads to the possibility of incorporation of buckling as a failure mechanism within the design process, which can enhance the effectiveness of the process as numerous design parameters such as stone size and chute length, can be strategically designed to accommodate or impede the formation of buckling in ripraps.

This method of interrelating knowledge from different research disciplines should in general be applicable to every scientific branch. Perhaps the most significant takeaway from the results presented within the study evaluating buckling in placed ripraps could be that no research discipline is self-sufficient. In other words, drawing from gathered knowledge within different research areas can only strengthen and reinvigorate our scientific quest.

7.1.2 Significance of toe support on riprap stability (*Papers I to III*)

The fundamental objective of experimental hydraulic research is to obtain accurate and realistic descriptions of behavior of structures and processes occurring within these structures as applicable to prototype scales. In order to obtain realistic portrayal of riprap stability under overtopping scenarios, it is of essence to incorporate, as far as possible, test conditions closely resembling those found in the prototype scale. The 2D deformation behavior in placed ripraps resembling column buckling was found in model placed ripraps provided with fixed toe supports (Figures 13 and 14). However, field survey of placed ripraps constructed on rockfill dams clearly demonstrated the fact that existing placed riprap structures are not provided with any form of systematized or well-designed toe supports (Figure 15). Incorporation of this finding into the experimental model studies in the lab gave rise to new results regarding riprap stability in general. In contrast to the 2D deformations observed in placed ripraps provided with toe support (***M1***), placed ripraps unsupported at the toe section (***M2***) were found to undergo sliding failure at a significantly lower overtopping magnitude (Figure 16).

Placed riprap stones experience minor degree of reorientations and displacements along the downstream chute direction following initial exposure to overtopping flows. Upon initial exposure to overtopping, the incremental hydraulic drag and lift forces and the resulting vibrations lead to rearrangements of the individual stones wherein the riprap structure undergoes compaction to fill the voids. Following these initial readjustments, the individual stones achieve a stable configuration leading to the formation of a unified riprap structure due to generation of interlocking forces between the individual stones. Upon further increment in overtopping magnitude, the riprap structure is exposed to higher destabilizing hydraulic forces. These are in part transferred on to the underlying filter layer as frictional forces. A part is also directed towards the riprap toe where the static frictional forces setup between the toe stones and the geotextile membrane laid on the horizontal platform increase in magnitude to counter the incremental hydrodynamic forces transferred towards the toe. Furthermore, initiation of riprap collapse marks the point of time at which the magnitude of the impacting hydrodynamic

forces exceed the limiting values of the static frictional forces between the toe stones and the horizontal platform and also the riprap-filer interface. This frictional yield results in displacements of the toe stones and following this event, the riprap structure in its entirety undergoes a progressive slide on the underlying filter layer, further forming a pile on the flume bottom.

Juxtaposition of these two disparate failure mechanisms in placed ripraps helps bring out the importance of toe support conditions in discerning the failure mechanism in placed ripraps. In case of a constrained toe structure as employed in ***M1*** (Figure 4), the riprap structure is likely to fail as a consequence of structural collapse or buckling as the toe support structure provides unlimited resistance stabilizing the toe, in turn eliminating the possibility of sliding of the riprap structure. Under such conditions, the riprap structure experiences some degree of compaction during initial stages of overtopping exposure and further, following the formation of a unified riprap structure, incremental overtopping flows give rise to development of progressive 2D deformation profiles in ripraps resembling the buckling process in a slender-long column. However, in case of an unrestrained toe, the placed riprap section slides along the steep slope as a result of limited frictional resistance offered at the toe section. Hence, findings from the present doctoral study demonstrates that the configuration of the toe section of placed riprap as a key factor influencing the overall failure mechanism. Further, Hiller et al. (2018) investigated 1D displacement of riprap stones in ***M1*** (Figure 4) and showed that compaction of the riprap structure at the downstream end leads to formation of a gap at the upstream crest of the riprap. However, this was not observed within ***M2*** (Figure 4) as the limited frictional forces setup at the interface between the toe stones and the horizontal platform do not allow for such a high degree of compaction to occur. The riprap structure experiences sliding failure due to toe yield before any major compaction or 2D deformation of the riprap structure could occur.

In contrast, failure mechanism in dumped ripraps was found to be similar between model setups ***M1*** and ***M2*** (Figure 4). The riprap stones were found to undergo a surface erosion process where individual stones were eroded by the action of destabilizing turbulent flow forces. This contrasted with failure initiation in placed ripraps with unsupported toes (***M2***) wherein the riprap structure as a whole was found to undergo a slide. This difference in the failure mechanisms can be described as due to the absence of interlocking forces between individual riprap stones. Since dumped ripraps comprise of randomly arranged stones, individual stones are not interlocked with the adjacent elements. When the dumped riprap structure is exposed to overtopping flow forces, the individual stones counter the flow attack primarily through self-

weight of the individual elements and the bottom frictional forces generated at the riprap-filter interface. Failure initiation marks the instant at which the magnitude of the destabilizing hydrodynamic forces exceed the resultant of the stabilizing self-weight and the frictional forces. Hence, dumped riprap failure can be stated as the resultant of progressive unraveling erosion of individual riprap elements whereas placed riprap failure entails sudden slide of the entire riprap structure. This clearly documents the fact that toe support conditions can have significant influence on underlying failure mechanism in placed ripraps but dumped riprap failure mechanism is unaffected by toe support conditions.

This also provides an explanation for higher velocities measured for stone displacements in placed ripraps during failure as compared to dumped riprap stones. Placed ripraps experience an instantaneous slide following toe yield wherein the riprap structure moves down the slope as a unit. Whereas dumped riprap failure entails erosion of discreet riprap elements wherein individual stones suffer collisions with one another during the erosion process thereby resulting in loss of kinetic energy. Further, placed riprap failures were found to be initiated at higher overtopping magnitudes as compared with dumped ripraps. As a combined effect of these two causes, placed riprap stones travel on the slope at higher velocities than dumped riprap stones.

The critical overtopping discharge magnitudes for initiation of riprap collapse (q_c) were found to be q_c = 0.06 m^2 s^{-1} and 0.04 m^2 s^{-1} for placed and dumped riprap respectively within ***M2*** (Table 5). This in turn entails that placed ripraps unsupported at the toe offer 1.5 times higher stability, characterized by the critical overtopping magnitude as compared with dumped riprap. Past experimental studies conducted on placed riprap models provided with fixed toe supports such as Hiller et al. (2018), Peirson et al. (2008), Dornack (2001) and Larsen et al. (1986) have also demonstrated that placed ripraps offer higher stability as compared to dumped riprap, especially at steep slopes. Hiller et al. (2018) documented average critical overtopping magnitudes of q_c = 0.30 m^2 s^{-1} and 0.04 m^2 s^{-1} respectively for placed and dumped ripraps resulting in a ratio of average critical discharge values of 7.5. The fivefold reduction in placed riprap stability in terms of average critical overtopping discharge magnitude required to achieve placed riprap from q_c = 0.30 m^2 s^{-1} within Hiller et al. (2018) to q_c = 0.06 m^2 s^{-1} within the present study can be attributed to the absence of a toe support structure. However, dumped riprap stability can be stated as being unaffected by toe support conditions as the critical discharge for failure initiation remained constant at q_c = 0.04 m^2 s^{-1} between model setups. These findings further add to the earlier statement that toe support conditions can have considerable impacts on placed riprap stability and not on the stability aspects of dumped

ripraps. A brief summary of key findings regarding critical discharge magnitudes and failure mechanisms across model setups both for placed and dumped ripraps are presented in Table 9 for ease of reference.

Table 9. Summary of critical discharges and failure mechanisms across model setups

Sl. no	Riprap type	Toe support condition	Model setup	Avg. Critical discharge (q_c) m^3 s^{-1}	Failure mechanism
1	Placed	Fixed toe support	M1	0.30	2D buckling like deformations
2	Placed	Unsupported	M2	0.06	Sliding
3	Dumped	Fixed toe support	M1	0.04	Surface erosion
4	Dumped	Unsupported	M2	0.04	Surface erosion

Findings from this doctoral study establishes that toe conditions for placed ripraps plays a pivotal role in discerning the underlying failure mechanism and also, overall riprap stability. Dumped riprap stability was found to be unaffected by toe conditions. This finding has significant practical relevance, especially in light of the outcomes from the field survey which suggests that existing placed ripraps are unsupported at the toe. It should be noted that placed riprap construction is resource intensive in terms of material requirements and manual and mechanical labor in comparison with dumped riprap construction. Placed ripraps can result in considerable gain in stability. However, study findings suggest that toe support conditions can determine the magnitude of stability increment. In other words, implementation of toe support onto existing placed ripraps could lead to much significant stability gains. Since multitude of rockfill dams are poised to be upgraded in the near future, arriving at design criteria and construction methodologies is of significance from placed riprap stability standpoint. Hence, further research addressing this vital feature influencing placed riprap stability is highly recommended.

7.1.3 Smartstones

The Smartstone probes represent state of the art technology in stone movement monitoring. Adoption of this sophisticated technique within the experimental model setup facilitated in obtaining better understanding of the failure mechanism in placed and dumped ripraps exposed to overtopping. The probes were found to be versatile and reliable with broad ranging capabilities. A major advantage of the technique is concerning elimination of undesirable

effects on flow hydraulics within the model. Results from the present study clearly demonstrate that the Smartstones probes are capable of capturing several important details regarding initiation and progression of failure in ripraps such as acceleration and angular velocities of the stones thereby providing an overarching picture of the underlying failure mechanisms. However, the probes currently face limitations with regards to limited battery life and internal memory capabilities. Further improvements to the probes addressing these limitations could greatly enhance potential for implementation of the probes within practical and experimental applications.

7.2 Flow through rockfill dams (*Objective 2*)

The present sub-section is intended at providing a broader perspective on the main results from *Papers IV* and *V* dealing with the hydraulic behavior of rockfill dams subjected to throughflow conditions.

7.2.1 Effects of toe configurations on throughflow (*Paper IV*)

Research activities conducted as part of this doctoral study forming the basis for *Papers I* and *III* were primarily aimed at investigating stability aspects of riprap structures subjected to overtopping. Further development of the research program was designed around the premise of obtaining a holistic evaluation of rockfill dam stability when subjected to throughflow and overflow scenarios (Figure 4). Considering the various phases involved in rockfill dam overtopping, it is evident that the first phase would be exposure of the dam shoulder to throughflow. Hence, to obtain a better understanding of response of rockfill dam shoulders comprised of uniform material subjected to throughflow, pertinent data sets accumulated as part of the IMPACT project were further analyzed as detailed in Section 4.4 (*Paper IV*). Statistical evaluation of the data (Figures 17 and 18) gave rise to a general non-linear power law (Equation 16) describing the velocity-gradient relationship within the dam structures. This essentially signifies that flow through rockfill structures is a predictable process which can be characterized and quantified to form a general flow law. This further provides a description of the interaction between externa hydraulic loading and the response of the dam structure.

Research outcomes from *Paper IV* are of significance also considering the fact that existing non-linear flow laws widely implemented in rockfill engineering applications were originally developed in the 1950's and the 1960's (Table 1) through small scale permeameter studies. Validity of these relationships were not tested in applications relating to real rockfill dam

structures and especially at large scales. Findings from *Paper IV* address these concerns as data sets from model studies encompassing rockfill dam models of board ranging sizes of 0.6 m to 6 m in height and constructed with material of sizes d_{50} = 10.2 mm to 350 mm were evaluated to arrive at Equation (16). The performance of Equation (16) with respect to its ability to predict experimental data was juxtaposed with existing relationships (Equations (6), (7) and (8)). Study outcome revealed higher correlation between predictions and observations for Equation (16) as compared with existing relationships.

Development of a sophisticated numerical model capable of simulating rockfill dam breach has been considered an uphill task owing to the complexity of the task at hand. Multitudes of external and intrinsic factors affect dam breach initiation and progression. Findings from the present doctoral study provides valuable information in this regard for implementation of non-linear throughflow characteristics of rockfill dams comprising of uniform material within these numerical models.

7.2.2 Effects of toe configurations on throughflow (*Paper V*)

Building on the results from the study, a new experimental program was devised to further our understanding of throughflow aspects of rockfill dams regarding effects of disparate toe configurations on throughflow development (Models **M3-A** to **D,** Figure 4). Widely implemented rockfill dam toe types such as the external, internal and combined toe configurations were investigated. Study outcomes provide quantitative and qualitative descriptions of throughflow development in rockfill dams coupled with different toe configurations as a function of throughflow magnitude (Figure 20).

Quantitative description of throughflow development in rockfill dams basing on experimental data is seldom found in international literature. Further, experimental corroboration of differences in hydraulic performance of disparate rockfill toe configurations has been rare. Findings from *Paper V* add valuable knowledge to the international literature on behavior of rockfill dam structures exposed to throughflow. Investigation results enable effective engineering decision making with regards to ideal choice of rockfill dam toe design based on site-specific design restrictions. This facilitates rockfill dam design process and can further help strengthen the design both from economical and stability standpoints. Considering research applications, data sets accumulated as part of the experimental testing program could be further employed for validation of theoretical studies conducted in the past within the study discipline. Furthermore, the data sets could be valuable for calibration and validation of

numerical models predicting throughflow behavior in rockfill embankments. Enhancement of capabilities of commercially available numerical seepage models could be of high interest for researches and also for agencies involved with rockfill dam design and safety assessment.

7.3 Study limitations and recommendations for future investigations

This study provides a step forward in the study discipline of overtopping protection of rockfill dams, addressing key research questions. There are however possibilities for further expansion of research from this study to further bridge knowledge gaps in the study area.

1. Experimental overtopping tests with model setups *M1* and *M2* were conducted on special placed riprap structures constructed on a steep slope (S = 0.67) with angular stones ($a\ b^{-1}$ = 1.7) placed at an angle of β = 60º. Validity of experimental results considering riprap models built with different material and site-specific properties should be further looked into to address scaling concerns and to improve confidence for general applicability of study findings.

2. Toe support for placed ripraps has been shown to significantly augment placed riprap stability. However, design criteria outlining technical details regarding design of toe supports for placed ripraps is currently not available within international literature or national dam safety guidelines. Further experimental testing in this regard is highly recommended as part of future studies to arrive at well-defined toe stabilizing methods for placed ripraps.

3. Carrying out large-scale overtopping field tests with ripraps constructed on rockfill dam structures are recommended to evaluate the validity of the observed failure mechanisms at larger scales and to better understand the combined influence of throughflow and overflow on placed riprap stability at larger scales.

4. The non-linear power law relationship describing the throughflow velocity and gradient relationship within rockfill embankments (Equation 16) was derived with tests conducted on dam models constructed with well-graded material with coefficient of uniformity (C_u) varying within the range 1.2 – 2.0. Derivation of a general power law

for description of non-linear flow through dams constructed using well-graded rockfill is recommended in future investigations.

5. Findings from *Paper V* describe internal toe configurations as an efficient formation to deal with internal pore pressure build up during accidental throughflow scenarios. Well-defined methodologies providing technical details regarding design of internal toe structures for rockfill dams are currently not found in international literature. Further research to arrive at guidelines outlining sizing of material and dimensioning of such toe structures is recommended.

6. Experimental model studies in *Paper V* were conducted with rockfill dams comprising of well-graded material (C_u = 7.5) with mean grain size of d_{50} = 6.5 mm and minimum particle size of 5 mm. Conducting similar studies with material of varying material properties would facilitate further validation of the study findings. In particular, inclusion of finer material could significantly influence experimental results and is highly recommended in future investigations.

7. The various phases of this doctoral study have made efforts to add to our understanding of behavior of various constituents of rockfill dams subjected to extreme loading scenarios. However, the ultimate objective of the work has been to obtain a holistic evaluation of rockfill dam stability. In order to accomplish this task, experimental tests on realistic rockfill dam models consisting of key components such as the rockfill dam shoulder, dam toe and riprap would be necessary. These are being conducted as part of the follow up of the present doctoral study. Further disseminations describing rockfill dam stability as a whole would lead to enrichment of our understanding of the research area.

8 Answers to research questions and concluding remarks

Pertinent answers to the research questions identified as part of the thesis are summarized herein along with some final concluding remarks.

8.1 Answers to research questions

Several research questions were identified based on the literature review conducted to fathom the state of the art in the research disciplines. The experimental and statistical evaluations conducted as part of the present study have been aimed at addressing these to add to our understanding of the issues. This section provides responses to the identified research questions.

Research question 1: What is the 2D failure mechanism in toe supported placed ripraps constructed on steep slopes exposed to overtopping conditions?

Toe supported placed riprap structures constructed on steep slopes undergo progressive deformations in 2D when exposed to overtopping flows. The deformation behavior closely resembles buckling of a slender-long column pinned at one end and free at the other. These progressive deformations ultimately lead to total riprap failure at the upstream section of the riprap

Research question 2: Do existing placed ripraps comply with design criteria and recommendations with regards to key parameters describing quality of construction? And are placed ripraps currently provided with any form of toe support?

According to the survey, the general practices adopted for construction of placed ripraps on Norwegian rockfill dams prioritize sizing of the stones. Other parameters such as stone angularity and uniformity are generally not paid attention to.

Furthermore, well-defined toe support measures stabilizing riprap toes are currently not implemented at any of the surveyed rockfill dams.

Research question 3: How do toe support conditions affect the underlying failure mechanisms and the stability in placed and dumped ripraps constructed on steep slopes exposed to overtopping?

Sliding was found to be the underlying failure mechanism in placed ripraps with unsupported toes constructed on steep slopes exposed to overtopping. Placed ripraps with unrestrained toes experience a fivefold reduction in stability, characterized by the critical overtopping magnitude as compared with placed ripraps provided with fixed toe supports. Further, surface erosion of individual riprap stones represents the underlying failure mechanism in dumped ripraps both with and without toe support. Furthermore, toe support conditions have minimal effects on the overall stability of dumped ripraps.

Research question 4: How can we quantitatively describe non-linear flow through rockfill embankments?

Non-linear flow through homogeneous rockfill embankments constructed with uniformly graded material can be quantitatively described in the form of a non-Darcy type power law. This empirical equation derived based on experimental investigations relates throughflow velocities to gradient developments within rockfill embankment structures.

Research question 5: What are the effects of disparate toe configurations on throughflow in rockfill dams?

Rockfill dam models coupled with external, internal and combined toe configurations were subjected to throughflow conditions. Both the internal and the combined configurations lead to significant lowering of phreatic surfaces and in turn, pore pressures within the rockfill shoulder as for a particular throughflow magnitude as compared with a dam with no toe. The external toe configuration has minimal effects on throughflow development. All toe configurations protect the toe section against scouring and erosion at the seepage exit face. The crest section of a rockfill dam is a critical location of initiation of surface erosion. The crest features also govern the maximum throughflow which can enter the dam structure.

8.2 Concluding remarks

The aim of the research work forming the basis for the thesis has been to add to the state of the art on stability of rockfill dams exposed to extreme loading. Several experimental model studies, field surveys and statistical analysis were carried out as part of this doctoral study. Research outcomes from the investigations present descriptions of hydraulic and structural behaviors of rockfill dams and or dam components under throughflow and or overtopping scenarios. These are further intended at facilitating development of design and construction methodologies thereby enhancing rockfill dam safety.

One of the primary findings from this study is that toe supported placed ripraps constructed on steep slopes exposed to overtopping flows undergo buckling like 2D deformations, ultimately leading to riprap failure. A large-scale field survey of placed riprap built on nine Norwegian rockfill dams was conducted as part of this doctoral study. The study helped document the fact that placed ripraps constructed on existing rockfill dams are not provided with well-defined toe support measures. Further, to achieve a more realistic picture of riprap stability, experimental overtopping tests were conducted on placed ripraps unsupported at the toe section. Study findings demonstrated sliding as the underlying failure mechanism in placed ripraps with unsupported toes. Placed ripraps with unrestrained toes on an average were found to suffer a fivefold reduction in stability, characterized by the critical overtopping magnitude as compared with placed ripraps provided with fixed toe supports. Furthermore, toe support conditions were found to have no effects on either the failure mechanism or the overall stability of dumped ripraps.

Throughflow data sets were accumulated from experimental studies conducted on homogeneous rockfill dams of sizes varying from 0.6 m to 6 m composed of uniform material as part of the IMPACT project. Subjecting the datasets to a statistical analysis, a general non-Darcy type power-law describing the non-linear relationship between throughflow velocities and gradient developments was derived. Further, experimental throughflow tests were conducted on 1:10 scale, 1 m high rockfill dam models coupled with different toe configurations as part of this study. Investigation outcomes provide qualitative and quantitative descriptions of effects of internal, external and combined toe configurations on throughflow hydraulic properties.

The experimental research conducted as part of this doctoral study to better understand placed riprap stability under overtopping conditions helps identify toe support conditions as an important parameter influencing overall placed riprap stability. This was also found to play a discerning role with regards to the underlying failure mechanism in placed ripraps. Coupling placed riprap structures with toe supports could result in significant stability gain and also lead to a predictable buckling like failure mode. Further, material properties such as angularity of the stones could have direct influence on the interlocking forces generated between the stones and in turn, on overall placed riprap stability.

These findings are of particular significance considering outcomes from the field survey which suggests that existing placed ripraps are unsupported at the toe. Placed riprap construction is a

more resource intensive activity as compared with dumped riprap construction. Further, multitude of rockfill dams are poised to be upgraded in the near future. Hence, arriving at efficient design and construction methodologies to provide toe supports for placed ripraps could lead to large stability and economic gains.

Further, research works conducted as part of this doctoral study investigating flow through rockfill dams improves our understanding of the interaction between throughflow and rockfill dams. The study also presents findings regarding the effects of disparate toe configurations on throughflow development. Investigation results enable effective engineering decision making and can further help strengthen the design process of rockfill dams both from economical and stability standpoints. Furthermore, ability of predicting the response of rockfill dams when subjected to extreme throughflow conditions facilitates development of numerical modelling tools for dam breach predictions. Enhancement of capabilities of commercially available numerical seepage models could be of high interest for researches and also for agencies involved with rockfill dam design and safety assessment. Data sects collected as part of the various research works presented as part of this study aim at supplementing development, calibration and validation of such numerical modelling tools.

Bibliography

Abt, S R, & Thornton, C. I. (2014). Riprap Design for Overtopping – Man Do I Need a Martini! *World Environment and Water Resources Congress 2014*, *1936*, 1191–1198.

Abt, Steven R., Thornton, C. I., Scholl, B. A., & Bender, T. R. (2013). Evaluation of overtopping riprap design relationships. *Journal of the American Water Resources Association*, *49*(4), 923–937.

Abt, Steven R, Terry L, J., & Members, A. (1991). Riprap Design for Overtopping Flow. *Journal of Hydraulic Engineering*, *119*, 959–972.

Chang, H. H. (1998). Riprap Stability on Steep Slopes. In *International Journal of Sediment Research* (Vol. 13, pp. 40–49).

Cruz, P. T., Materon, B., & Freitas, M. (2009). *Concrete Face Rockfill Dams*. CRC Press.

Cruz, P. T., Materon, B., & Freitas, M. (2010). *Concrete Face Rockfill Dams*. CRC Press, Taylor and Francis Group.

Dornack, S. (2001). Uberstrombare Damme-Beitrag zur Bemessung von Deckwerken aus Bruchsteinen/ Overtopping dams-Design criteria for riprap. *PhD Thesis, Technische Universitat Dresden*.

EBL Kompetanse, A. (2003). *Stability and Breaching of Dams Report on Sub-Project 1 Shear Strength of Rockfill and Stability of Dam Slopes*.

EBL Kompetanse, A. (2006). *Stability and breaching of embankment dams, Report on Sub-project 2: Stability of downstream shell and dam toe during large through-flow*.

EBL Kompetanse, A. (2007). *Stability and Breaching of Embankment Dams Report on Sub-Project 3 (SP3) Breaching of Embankment dams*.

Engelund, F. (1953). On the laminar and turbulent flows of groundwater through homogeneous sand. *Trans. Dan. Acad. Tech. Sci., 3*, 1–105.

Escande, L. (1953). Experiments Concerning The Infiltration Of Water Through A Rock Mass. *Proceedings of the Minnesota International Hydro Convention*.

Ferdos, F., & Dargahi, B. (2016a). A study of turbulent flow in large-scale porous media at

high Reynolds numbers. Part I: numerical validation. *Journal of Hydraulic Research*, *54*(6), 663–677.

Ferdos, F., & Dargahi, B. (2016b). A study of turbulent flow in large-scale porous media at high Reynolds numbers. Part II: flow physics. *Journal of Hydraulic Research*, *54*(6), 678–691.

Ferdos, F., Worman, A., & Ekstrom, I. (2015). Hydraulic Conductivity of Coarse Rockfill used in Hydraulic Structures. *Transport in Porous Media*, *108*, 367–391.

Foster, M., Fell, R., & Spannagle, M. (2000). The statistics of embankment dam failures and accidents. *Canadian Geotechnical Journal*, *37*(1992), 1000–1024.

Frizeii, K. H., Ruff, J. F., & Mishra, S. (1998). Simplified Design Guidelines for Riprap Subjected To Overtopping Flow. *In Proceedings of the Annual Conference of the Assoc. Of State Dam Safety Officials.*, 301–312.

Garcia, D. (2011). *RESEARCH ARTICLE A fast all-in-one method for automated post-processing of PIV data*. 1247–1259.

Garga, V. K., Hansen, D., & Townsend, D. R. (1995). Mechanisms of massive failure for flowthrough rockfill embankments. *Canadian Geotechnical Journal*, *32*(6), 927–938.

Hansen, D., Garga, V. K., & Townsend, D. R. (1995a). Flowthrough Rockfill Embankments: Behavior in Subzero Temperatures. *Journal of Cold Regions Engineering*, *9*(December), 195–218.

Hansen, D., Garga, V. K., & Townsend, D. R. (1995b). Selection and application of a one-dimensional non-Darcy flow equation for two-dimensional flow through rockfill embankments. *Canadian Geotechnical Journal*, *32*(2), 223–232.

Hansen, D., & Roshanfekr, A. (2012). Assessment of Potential for Seepage-Induced Unraveling Failure of Flow-Through Rockfill Dams. *International Journal of Geomechanics*, *12*(5), 560–573.

Hansen, D., Zhao, W. Z., & Han, S. Y. (2005). Hydraulic performance and stability of coarse rockfill deposits. *Proceedings of the Institution of Civil Engineers*, *WM4*, 163–175.

Hiller, Priska H. (2017). Riprap design on the downstream slopes of rockfill dams,. *Doctoral Thesis, Norwegian University of Science and Technology, Trondheim*.

Hiller, Priska H, Aberle, J., & Lia, L. (2018). Displacements as failure origin of placed riprap on steep slopes. *Journal of Hydraulic Research*, *56*(2), 141–155.

Hiller, Priska H, Lia, L., & Aberle, J. (2019). Field and model tests of riprap on steep slopes exposed to overtopping. *Journal of Applied Water Engineering and Research*, *7*(2), 103–117.

Hiller, Priska Helene. (2016). *Kartlegging av plastring på nedstrøms skråning av fyllingsdammer*.

Hyllestad, E. (2007). *Retningslinjer for fyllingsdammer. Presentasjon under EBLs vårmøte 23.5.2007: Norges vassdrags- og energidirektorat.*

ICOLD. (1995). Dam Failures - statistical analysis. *Bulletin 99*, 73.

ICOLD. (2019). *World Register of Dams*.

Isbash, S. (1936). Construction of Dams by Depositing Rock in Running Water. *International Congress on Large Dams*.

Izbash, S. V. (1931). O filtracii v krupnozernistom materiale. *Izv. Nauchno Issled. Inst. Gidro-Tekh. (NILG)*.

Javadi, N., & Mahdi, T.-F. (2014a). Experimental investigation into rockfill dam failure initiation by overtopping. *Natural Hazards*, *74*, 623–637.

Javadi, N., & Mahdi, T. F. (2014b). Experimental investigation into rockfill dam failure initiation by overtopping. *Natural Hazards*, *74*(2), 623–637.

Khan, D., & Ahmad, Z. (2011). Stabilization of Angular-Shaped Riprap under Overtopping Flows. *World Academy of Science, Engineering and Technology, International Journal of Civil, Environmental, Structural, Construction and Architectural Enfineering*, *5*(11), 550–554.

Kiplesund, G. H., Ravindra, G. H. R., Rokstad, M. M., & Sigtryggsdottir, F. G. (2020). Effects of toe configuration on throughflow hydraulic properties of rockfill dams. *Journal of Applied Water Engineering and Research (Submitted)*.

Kjellesvig, H. M. (2002). *Stability and Failure Mechanisms of Dams, Data Report No. 1*.

Kjetil, V., Løvoll, A., Höeg, K., Morris, M., Hanson, G. J., & Hassan, M. A. (2004). Physical modeling of breach formation: Large scale field tests. *Preceedings Of Dam Safety*, 1–16.

Kobayashi, N., & Jacobs, B. K. (1985). Riprap Stability Under Wave Action. *Journal of Waterway, Port, Coastal, and Ocean Engineering*, *111*(3), 552–566.

Larese, A., Rossi, R., Oñate, E., Toledo, M. Á., Morán, R., & Campos, H. (2015). Numerical and Experimental Study of Overtopping and Failure of Rockfill Dams. *International Journal of Geomechanics*, *15*(4), 04014060.

Larsen, P., Bernhart, H. H., Schenk, E., Blinde, A., Brauns, J., & Degen, F. P. (1986). Uberstrombare Damme, Hochwasserentlastung uber Dammscharten/ Overtoppable dams, spillways over dam notches. *Unpublished Report Prepared for Regierungsprasidium Karlsruhe*, *Universita*.

Leps, T M. (1973). Flow through rockfill. *John Wiley and Sons*, 87–107.

Leps, Thomas M. (1975). Flow through rockfill: In Embankment-dam Engineering. In P. SJ & H. RC (Eds.), *John Wiley and Sons INC., Pub., NY, 1973, 22P* (Vol 12, No).

Lia, L., Vartdal, E. A., Skoglund, M., & Campos, H. E. (2013). Riprap protection of downstream slopes of rockfill dams-a measure to increase safety in an unpredictable future climate. *European Club Symposium of the International Comission on Large Dams*.

Marulanda, A., & Pinto, N. L. de S. (2000). Recent experience on design, construction, and performance of CFRD dams. In *Concrete Face Rockfill Dams* (pp. 279–299). Barry Cooke.

Midttømme, G. H., Isomäki, E., Meyer, A. E., & Bartsch, M. (2012). Regulations and guidelines for dam safety in Finland , Norway and Sweden. *ICOLD, European Club*.

Moran, R. (2015). Review of embankment dam protections and a design methodology for downstream rockfill toes. *Dam Protections against Overtopping and Accidental Leakage - Proceedings of the 1st International Seminar on Dam Protections Against Overtopping and Accidental Leakage*, 25–39.

Morán, R, & Toledo, M. A. (2011). Reserarch into protection of rockfill dams from overtopping using rockfill downstream toes. *Canadian Journal of Civil Engineering*, *38 (12)*(April), 1314–1326.

Moran, Rafael. (2015). Review of embankment dam protections and a design methodology for downstream rockfill toes. *Dam Protections against Overtopping and Accidental*

Leakage - Proceedings of the 1st International Seminar on Dam Protections Against Overtopping and Accidental Leakage, 25–39.

Morán, Rafael, Toledo, M. Á., Larese, A., & Monteiro-alves, R. (2019). *A procedure to design toe protections for rock fi ll dams against extreme through- fl ows*. *195*(May), 400–412.

Morris, M. W., & Park, H. (2007). Breach formation : Field test and laboratory experiments Formation d ' une brèche dans une barrage : Test sur le terrain et expériences en laboratoire. *Journal of Hyd. Research*, *45*(September 2011), 9–17.

Novak, P., Moffat, A., Nalluri, C., & Narayanan, R. (2001). *Hydraulic Structures*. Spon Press, Taylor and Francis Group.

NVE. (2012). Veileder for fyllingsdammer. *Norwegian Water Resources and Energy Directorate*, 21–25.

OED. (2009). *Forskrift om sikkerhet ved vassdragsanlegg (Damsikkerhetsforskriften). Oljeog energidepartementet.*

Olivier, H. (1967). Through and Overflow Rockfill Dams-New Design Techniques. *Proceedings of the Institution of Civil Engineers*, 433–471.

Parkins, A. K. (1963). Rockfill dams with inbuilt spillways. *Water Res. Edn. Aust., Bulletin No.6*.

Parkins, A. K. (1966). Rockfill structures subjected to water flow. *Journal of Soil Mech. Found. Div. ASCE*.

Peirson, W L, Figlus, J., Pelles, S. E., & Cox, R. J. (2008). Placed rock as protection against erosion by flow down steep slopes. *Journal of Hydraulic Engineering*, *134*(9), 1370–1375.

Peirson, William L, Jens, F., Steven E, P., & Ronald J, C. (2008). Placed Rock as Protection against Erosion by Flow down Steep Slopes. *Journal of Hydraulic Engineering*, *134*, 1370–1375.

Ravindra, G. H. R., Gronz, O., Dost, B., & Sigtryggsdottir, F. G. (2020). Failure mechanism in placed riprap on steep slope with unsupported toe. *Engineering Structures (In Review)*.

Ravindra, G. H. R., Sigtryggsdottir, F. G., Asbølmo, M. F., & Lia, L. (2019). Toe support conditions for placed ripraps on rockfill dams- A field survey. *Vann*, *3*.

Ravindra, G. H. R., Sigtryggsdottir, F. G., & Høydal, Ø. A. (2019). Non-linear flow through rockfill embankments. *Journal of Applied Water Engineering and Research*.

Ravindra, G. H. R., Sigtryggsdottir, F. G., & Lia, L. (2018a). Evaluation of Design Criteria for Downstream Riprap of Rockfill Dams. *Proceedings of the 26th Congress on Large Dams*.

Ravindra, G. H. R., Sigtryggsdottir, F. G., & Lia, L. (2020). Buckling analogy for 2D deformation of placed ripraps exposed to overtopping. *Journal of Hydraulic Research*.

Ravindra, G. H. R., Sigtryggsdottir, F. G., & Lia, L. (2018b). Protection of embankment dam toe and abutments under overtopping conditions. *3rd International Conference on Protection against Overtopping, UK*, *June*.

Salahi, M.-B., AsI, M. S., & Parvizi, M. (2015). Nonlinear Flow through a Packed-Column Experiment. *Journal of Hydraulic Engineering*, *20(9):0401*.

Sand, K. (2002). *Stabiliy and Failure Mechanisms of Dams, Sub Project No.2*.

Scheidegger, A. E. (1963). The physics of flow through porous media. *University of Toronto Press, Toronto, Canada*.

Siddiqua, S., Blatz, J. A., & Privat, N. C. (2011). Evaluating Turbulent Flow in Large Rockfill. *Journal of Hydraulic Engineering*, *137*, 1462–1469.

Siddiqua, S., Blatz, J. A., & Privat, N. C. (2013). Evaluating the behaviour of instrumented prototype rockfill dams. *Canadian Geotechnical Journal*, *50*, 298–310.

Sidiropoulou, M. G. (2007). Determination of Forchheimer equation coefficients a and b. *Hydrol Processes*, *21(4)*, 534–554.

Siebel, R. (2007). Experimental investigations on the stability of riprap layers on overtoppable earthdams. *Environmental Fluid Mechanics*, *7*(6), 455–467. https://doi.org/10.1007/s10652-007-9041-8

Sigtryggsdóttir, F. G., Snæbjörnsson, J. T., Grande, L., & Sigbjörnsson, R. (2016). Interrelations in multi-source geohazard monitoring for safety management of infrastructure systems. *Structure and Infrastructure Engineering*, *12*(3), 327–355.

Solvik, O. (1991). Throughflow and stability problems in rockfill dams exposed to exceptional loads. *Sixteenth International Congress on Large Dams*, 333–343.

Sommer, P. (1997). Uberstrombare Deckwerke/ Overtoppable erosion protections. *Unpublished Report No. DFG-Forschungsbericht La 529/8-1*, *Universita*.

Soni, J. P., Islam, N., & Basak, P. (1978). An experimental evaluation of non-Darcian flow in porous media. *Journal of Hydrology*, *38*(3–4), 231–241.

Thielicke, W. (2014). The flapping flight of birds Summary and Conclusions. *PhD Thesis, Rijksuniversiteit Groningen*.

Thielicke, W, & Stamhuis, E. . (2014). PIVlab - Time-Resolved Digital Particle Image Velocimetry Tool for MATLAB (version: 2.02). *Published under the BSD License, Programmed with MATLAB 7.0.246 (2014): R14*.

Thielicke, William, & Stamhuis, E. J. (2014). *PIVlab – Towards User-friendly , Affordable and Accurate Digital Particle Image Velocimetry in MATLAB*.

Thornton, C. I., Abt, S. R., Scholl, B. N., & Bender, T. R. (2014). Enhanced Stone Sizing for Overtopping Flow. *Journal of Hydraulic Engineering*, *140*(4), 06014005– 1 to 4.

Toledo, M. Á., & Morera, L. (2015). Design of overtopping-resistant rockfill dams. *Dam Protections against Overtopping and Accidental Leakage-2015*, 133–141.

Townsend, R. D., Garga, V., & Hansen, D. (1991). Finite difference modelling of the variation in piezometric head within a rockfill embankment. *Canadian Journal of Civil Engineering*, *18*(2), 254–263.

Venkataraman, P., & Rama Mohan Rao, P. (1998). Darcian, transitional and turbulent flow through porous media. *Journal of Hydraulic Engineering*, *124*, 840–846.

Wang, C. M., & Wang, C. Y. (2004). *Exact solutions for buckling of structural members* (Volume 6). CRC Press.

WHO. (2004). Guidelines for drinking-water quality: recommendations. *World Health Organization*, *1*.

Wilkins, J. K. (1955). Flow of water through rockfill and its application to design of dams. *New Zealand Engineering*, *01*, 382–387.

Wilkins, J. K. (1963). *The stability of overtopped rockfill dams*.

Worman, A. (1993). Seepage induced mass wasting on coarse soil slopes. *Journal of Hydraulic Engineering*, *119*(10), 1155–1168.

Zech, Y., & Soares-Frazao, S. (2007). Dam-break flow experiments and real-case data. A database from th European Impact research. *Journal of Hydraulic Research*, *45*, *Extra*, 5–7.

Zingg, T. (1935). *Beitrag Zur Schotteranalyse, Doctoral Thesis, ETH Zurich*.

Paper I

Buckling analogy for 2D deformation of placed ripraps exposed to overtopping

Ravindra, G.H.R., Sigtryggsdottir, F.G and Lia, L (2020).
Journal of Hydraulic Research
DOI: https://doi.org/10.1080/00221686.2020.1744745.

Buckling analogy for 2D deformation of placed ripraps exposed to overtopping

GANESH H R RAVINDRA, PhD Student, *Department of Civil and Environmental Engineering, Norwegian University of Science and Technology (NTNU), Trondheim, Norway*

Email: ganesh.h.r.ravindra@ntnu.no (author for correspondence)

FJOLA G SIGTRYGGSDOTTIR, Associate Professor, *Department of Civil and Environmental Engineering, Norwegian University of Science and Technology (NTNU), Trondheim, Norway*

Email: fjola.g.sigtryggsdottir@ntnu.no

LEIF LIA (IAHR Member), Professor, *Department of Civil and Environmental Engineering, Norwegian University of Science and Technology (NTNU), Trondheim, Norway*

Email: leif.lia@ntnu.no

Running Head: Buckling analogy for 2D deformation of placed ripraps

Buckling analogy for 2D deformation of placed ripraps exposed to overtopping

ABSTRACT

A novel approach quantitatively describing two-dimensional displacements of placed riprap stones exposed to overtopping flows is developed and validated coupling experimental data with Euler's buckling theory for columns. Past studies investigating the failure mechanisms of placed ripraps with toe support have analysed unidirectional displacements of riprap stones parallel to the slope. 2D description of this process is currently not available in the literature. To address this issue, data sets obtained from a physical modelling investigation conducted on model ripraps constructed with angular stones on a slope of 1:1.5 (vertical : horizontal) were further analysed along with additional experimental data. Investigation results demonstrated that placed ripraps supported at the toe underwent progressive deformations in 2D when exposed to overtopping flows. The deformation behaviour closely resembled buckling of a slender-long column pinned at one end and free at the other and this ultimately led to total riprap failure at the upstream section of the riprap.

Keywords: Buckling; flow-structure interactions; hydraulic models; hydraulic structure design & management; laboratory studies; riprap stability

1 Introduction

Riprap is one of the most widely used erosion protection measure for various in-stream hydraulic structures such as embankment dams, spillways, streambeds, river banks, bridge piers and abutments (e.g. Hiller et al., 2018a; Thornton et al., 2014; Abt et al., 2013; Khan & Ahmad, 2011; Siebel, 2007). Ripraps are also used in coastal protection structures such as dikes, embankments and jetties against wave action (Kobayashi & Jacobs, 1985). Ripraps can be broadly classified into two categories based on the method of construction; Dumped ripraps comprise of randomly placed stones while placed ripraps are characterized by stones arranged in a specific interlocking pattern. Although dumped ripraps could be considered as a more viable alternative from an economic standpoint, placed ripraps have been found to offer a significantly higher degree of stability against overtopping in comparison with dumped ripraps (Hiller et al., 2018a). This is attributed to the formation of a bearing structure due to interlocking of stones, which results in increased stability compared to randomly dumped stones. In this article, primary emphasis is laid on placed ripraps constructed on steep slopes subjected to overtopping flows.

Placed ripraps protect the downstream slopes of rockfill dams against erosion due to leakage, overtopping and violent attacks (Hiller et al., 2018b). Comprehending the underlying failure mechanism of placed ripraps when exposed to overtopping flows is of importance for improving existing state of design and construction techniques of placed ripraps. Past studies

investigating stability of placed riprap with toe support under overtopping flows have described unidirectional displacement of stones along the slope. However, analysis of 2D displacements of placed riprap stones has not been incorporated in past investigations. This article is aimed at addressing this issue through experimental investigations conducted to better understand the underlying 2D failure mechanism in placed ripraps exposed to overtopping flows.

The research discipline of riprap design under overtopping conditions has advanced since its inception with the classic study of Isbash (1936). Since this early effort to determine the size and thickness of a resistant stone layer, more than 21 stone-sizing relationships for overtopping have been developed (Abt & Thornton, 2014) with major contributions from Olivier (1967), Abt et al. (1991), Frizell et al. (1998), Chang (1998) and others. Majority of these studies have been dedicated towards investigating stability of dumped ripraps on moderately steep slopes complying with international construction practice. Available literature describing the stability aspects of placed ripraps under overtopping conditions is limited. Since dumped and placed ripraps are characterized by different failure mechanisms under overtopping conditions, understanding the stability aspects of placed ripraps is of much importance to arrive at effective riprap design from an economical and safety point of view.

Major contributors to the research area of placed riprap design are Knauss (1979), Larsen et al. (1986), Sommer (1997), Dornack (2001), Peirson et al. (2008) and Hiller et al. (2018a). Their experimental investigations were conducted with toe support structures. The studies conducted by Sommer (1997) and Larsen et al. (1986) were specifically aimed at comprehending the underlying failure mechanisms of placed ripraps exposed to overtopping flows on mild to moderately steep slopes (S = 0.125 to 0.50; S is the ratio of the vertical to the horizontal slope dimensions). They introduced a technique of measurement of displacement of select stones in a direction parallel to the slope with incremental overtopping flows. Hiller et al. (2018a) adopted the same technique to analyse the failure mechanisms of placed ripraps on a steeper slope (S = 0.67). These investigations concluded that unidirectional stone displacements along the chute direction leading to formation of a gap at the upstream section of the riprap was the underlying failure mechanism in placed riprap supported at the toe.

This study further extends past findings describing unidimensional failure mechanisms in placed ripraps to 2D by providing qualitative and quantitative descriptions of a unique process interrelating the disciplines of hydraulic and structural research. Experimental data sets accumulated by Hiller et al. (2018a) through physical modelling investigation conducted on model ripraps constructed with angular stones on a steep slope of S = 0.67 have been further analysed along with additional experimental data. Results from the analysis are presented wherein 2D displacement of placed riprap stones are described to better understand the underlying failure mechanism in placed ripraps exposed to overtopping flows.

2 Experimental setup and methodology

A detailed description of the employed experimental setup and methodology are presented in Hiller et al. (2018a). For ease of reference, a brief overview of the same has been presented in this section. Overtopping tests were conducted on model ripraps constructed in a flume (25 m long, 2 m high and 1 m wide) at the hydraulic laboratory at NTNU (Hiller, 2017). Discharge to the flume was supplied by pumps with a combined capacity of $q = 0.4$ m^2 s^{-1}.

A conceptual 1:10 model setup consisting of a single-layered placed riprap section of width 1 m and chute length of $L_S = 1.8$ m constructed over a base frame inclined at 1:1.5 ($S = 0.67$) (Figs 1 and 2) was designed by Hiller et al. (2018a). The test setup was designed assuming Froude similarity. Quarry stones of rhyolite with median diameter of $d_{50} = 0.057$ m and density of $\rho_s = 2710$ kg m^{-3} were employed as riprap stones. The median stone size was computed as $d_{50} = (abc)^{1/3}$ (Hiller et al., 2018a) averaged over a sample size of 500 stones, where a, b and c represent the longest, intermediate and shortest axis respectively. The respective axes lengths were measured employing a calliper and the mean values were obtained as $a = 0.091$ m, $b = 0.053$ m and $c = 0.038$ m. The employed stones could be considered angular to sub-angular (average $a\ b^{-1} = 1.7$) and uniformly graded ($C_u = d_{60}\ d_{10}^{-1} = 1.17$). Test ripraps were placed on a 0.1 m thick filter layer comprised of geotextile and angular stones of size $d_{50,F} = 0.025$ m and density $\rho_{s,F} = 3050$ kg m^{-3}. The dimensions of the filter and the riprap were chosen in accordance with guidelines offered by the Norwegian Water Resources and Energy Directorate (NVE, 2012).

Placed ripraps were constructed by manual placement of stones in an interlocking pattern commencing at the toe progressing upstream to the crest. The test setup required 1200 stones on average. Riprap stones on the slope were deliberately placed with the longest axis (a-axis) inclined at $\beta \approx 60^o$ with respect to the chute bottom and with an inclination of $\beta \approx 90^o$ for stones placed on the horizontal crest to account for practical considerations (Fig. 1) (Lia et al., 2013). The ripraps were supported at the toe section with a metallic support structure and the entire test setup was elevated from the flume bottom to avoid backwater effects (Figs 1 and 2). The experimental setup was situated sufficiently downstream of the inflow section to achieve calm flow upstream of the test ripraps.

Hiller et al. (2018a) employed the packing factor P_c in their study to obtain a quantitative measure of density of riprap stone placement as this can have an impact on overall riprap stability and this parameter has further been incorporated in this study. The term packing factor was defined as Eq. (1) by Olivier (1967).

$$P_c = \frac{1}{N.\ d_{50}^2} \tag{1}$$

where N represents the number of stones per m^2 surface area of the riprap and d_{50} signifies the median stone size. P_c is lower for a densely placed riprap compared to a loosely packed riprap (Hiller et al., 2018a).

The location co-ordinates of select riprap stones were measured employing a laser traverse system in a 3D Cartesian coordinate system with its origin situated at the fixed toe support (Fig. 1). The x-axis was aligned in a direction parallel to the chute (33.7º to the flume bottom) pointing in the upstream direction and the z-axis was set perpendicular to the chute. Location coordinates could be measured to an accuracy of ± 0.1 mm in the x-direction and ± 1 mm in the z-direction. The selected stones were located along the centreline of the flume (y = 0.5) at specific positions of x = 0, 0.4, 0.8, 1.2, 1.6 and 1.8 m. The chosen riprap stones were identified as MSm (Fig. 1), with m = 0, 1, 2, 3, 4 and 5 for stones located at x = 0, 0.4, 0.8, 1.2, 1.6 and 1.8 m respectively. The marked stone placed on the horizontal crest of the model was labelled MC (Fig. 1). Stone displacements were considered only along the x and z-directions as any possibility of encountering lateral flows prompting stone displacements in the y-direction was ruled out.

Discharge was supplied to the flume in stepwise increments of q_i = 0.02 - 0.05 $m^2 s^{-1}$ for a specific time interval Δt. Prior to further increment in q_i, location co-ordinates of the former selected stones were measured. This procedure was repeated until total failure of the riprap structure was achieved. The overtopping discharge magnitude at which complete collapse or bulk erosion of the riprap occurred was defined as the critical unit discharge (q_c) in this experimental study. Continuous monitoring of erosion of individual stones was not possible due to highly aerated and turbulent flow over the riprap surface.

Riprap stones placed on the horizontal crest upstream of the transition to chute cannot be considered part of the riprap structure. This is because the riprap stones placed on the steep slope are exposed to larger destabilizing forces when compared with stones on the horizontal crest. Also, as per the findings of Hiller et al. (2018a), displacements of stone identified as MC (Fig. 1) were negligible. Hence, measurements for MC are not considered part of further analysis in this study.

Herein, data sets from seven different tests are compiled and results from the analysis are presented in the subsequent sections of this article. Table 1 presents a brief overview of the testing procedure and critical unit discharges. Data sets for tests 5 to 7 were obtained from Hiller et al. (2018a) with the addition of data sets from four new tests (tests 1 to 4). Tests 5, 6 and 7 were referred to as P01, P02 and P04 respectively within the article Hiller et al. (2018a).

As can be inferred from Table 1, the critical unit discharges for the tested ripraps varied over the range q_c = 0.12 $m^2 s^{-1}$ to 0.4 $m^2 s^{-1}$. Variability in stability of placed ripraps against

overtopping has been described by Hiller et al. (2018a) as dependent on factors such as the packing density of placement and skill level of labour. All tests were conducted by exposing the ripraps to incremental overtopping in regular discharge and time steps. Test 7 from Table 1 is a special case as riprap failure could not be achieved even after application of the maximum possible unit discharge. Reference is made to Hiller et al. (2018a) for further details regarding testing procedures and discussions.

3 Data analysis

Acquired data sets from the overtopping tests were employed to compute the 2D displacements, Δx_m and Δz_m of selected riprap stones with incremental overtopping. The subscript m denotes the position of the stone along the respective axes with m = 0, 1, 2, 3, 4 and 5 for stones located at x = 0, 0.4, 0.8, 1.2, 1.6 and 1.8 m respectively. The displacements (Δx_m and Δz_m) are defined as the difference in stone positions compared to their initial location along the x and z-axes respectively. Description of stone displacements along the x-axis has been presented in Hiller et al. (2018a). This article extends the findings to provide a 2D representation of the failure mechanism.

Figure 3 illustrates analysis results from a single test, test 1 presented in Table 1. The dimensionless forms of stone displacements in 2D were analysed for incremental unit discharges normalized over the critical unit discharge ($q_i\, q_c^{-1}$). The horizontal axis of the plot ($L_m\, L_s^{-1}$) represents the distance to the respective selected riprap stones from the riprap stone placed adjacent to the fixed toe structure along the x-axis ($L_m = x_m - x_0$) (Fig. 1) normalized over the total riprap length ($L_s = x_5 - x_0$ at $q_i\, q_c^{-1} = 0$). Stone displacements were computed with respect to the position of selected riprap stone adjacent to the fixed toe structure as the displacement of the stone identified as MS0 were moderate in comparison with the displacements measured for the other stones. The vertical axis of the plot represents the progressive stone displacements along the z-axis normalized over the median riprap stone diameter ($\Delta z_m\, d_{50}^{-1}$).

From Fig. 3, it can be observed that the selected riprap stones underwent progressive displacements in the x-z plane with incremental overtopping. The displacements along the x-axis can be seen as gradual translation of selected riprap stones in the downstream direction. The magnitude of displacements along the x-axis are proportional to the magnitude of overtopping discharge and the distance of the respective stones from the downstream toe, further validating the findings of Hiller et al. (2018a). Further, riprap stones undergo progressive displacements along the z-direction in a manner directly proportional to the applied overtopping flow magnitude. Also, magnitude of displacements in the z-direction are dependent on the distance of the respective selected stones from the toe support as depicted in Fig. 3. The 2D displacements further led to compaction of the riprap layer resulting in the development of a gap at the upstream end of the riprap leading to total failure of the riprap structure.

Figure 4 presents results from the cumulative statistical analysis carried out with data sets obtained from all the seven tests presented in Table 1. Similar methodology as outlined for test 1 (Fig. 3) has been adopted to compute the 2D stone displacements for the remainder of the tests. Fig. 4 depicts the mean trends of 2D stone displacements for all the tests represented by average values of $\Delta z_m\, d_{50}^{-1}$ and $L_m\, L_s^{-1}$ computed for the seven tests at uniform intervals of overtopping ($q_i\, q_c^{-1} = 0.20$). Variability in test results are presented as 95% confidence intervals.

The process of 2D displacements of selected stones previously demonstrated by Fig. 3 for test 1 was observed for all seven tests. Cumulative analysis results presented in Fig. 4 further corroborate the observations made from Fig. 3 of progressive 2D displacements of selected riprap stones as a function of both the overtopping flow magnitude and distance of the respective stones from the fixed toe structure. Total riprap failure in the conducted tests was found to be initiated at the upstream section of the riprap when the maximum displacement of riprap stones along the *x*-axis exceeded the size of the longest axes of the riprap stones at MS5 ($\Delta x_5 \approx a \approx 1.6\, d_{50}$) (Hiller et al., 2018a). This further corresponds to displacement of 0.3 - 0.35 times the median stone diameter of riprap stones at MS5 ($\Delta z_5 \approx 0.3\, d_{50}$ to $0.35\, d_{50}$) along the *z*-axis (Fig. 4).

To further evaluate stone displacements in the *z*-axis, numerical values of the average dimensionless stone displacements along the *z*-axis ($\overline{\Delta z_m d_{50}^{-1}}$) for all the seven tests are tabulated in Table 2 for the individual riprap stones as a function of incremental overtopping unit discharges normalized over the critical unit discharge ($q_i\, q_c^{-1}$). As can be observed from Table 2, $\overline{\Delta z_m d_{50}^{-1}}$ underwent increments and attained peak values at MS2 ($x = 0.8$ m, $L_m\, L_s^{-1} = 0.44$) for $q_i\, q_c^{-1} < 0.20$ and $q_i\, q_c^{-1} = 0.21$ - 0.40 and further experienced reductions progressing towards MS5 ($x = 1.8$ m, $L_m\, L_s^{-1} = 1.00$). Further, for $q_i\, q_c^{-1} > 0.41$, $\overline{\Delta z_m d_{50}^{-1}}$ can be seen to attain nearly comparable values at MS2 and MS3 with subsequent reductions progressing upstream towards MS5. This demonstrates that the peak of riprap deformation along the *z*-axis undergoes a shift from MS2 ($x = 0.8$ m, $L_m\, L_s^{-1} = 0.44$) for lower overtopping magnitudes and translates in the upstream direction towards MS3 ($x = 1.2$ m, $L_m\, L_s^{-1} = 0.67$) for higher overtopping magnitudes.

The uncertainty in stone displacements along the *z*-axis are quantified as ±95% interval values presented in Table 2 for the selected riprap stones as a function of the overtopping unit discharges ($q_i\, q_c^{-1}$). From Table 2, it can be inferred that the uncertainty in stone displacements along the *z*-axis for the respective selected stones in general are larger for the overtopping intervals $q_i\, q_c^{-1} < 0.2$ and $q_i\, q_c^{-1} > 0.6$ as compared with intermediate overtopping magnitudes. ±95% interval values also occasionally attain high values for MS4 at $q_i\, q_c^{-1} = 0.21$ - 0.40 (Table 2). However, the uncertainty values are in general lower for overtopping intervals of $q_i\, q_c^{-1} =$ 0.21 - 0.60 in compared with other intervals.

4 Deformation behaviour related to buckling process

The approach presented in this section demonstrates the mechanism of progressive 2D deformation of placed riprap stones discussed in Section 3 as comparable to the mechanism of buckling observed in a slender-long column, pinned at one end and free at the other. Referring to the model setup in Fig. 1, the riprap toe is supported in the axial direction (the *x*-axis), but is free to rotate in the positive *xz*-plane. Moreover, sliding of the toe in the positive *z*-direction is possible, however restrained by frictional forces generated between the toe stones and the support steel structure. The intention of the analysis presented is to demonstrate the similarities between the two mechanisms in the simplest possible manner by implementing the well-established Euler's theory for column buckling (Timoshenko & Gere, 2009). In this simplified process, a pinned support at the toe will be assumed, although this is not ideal considering the sliding possibility in the positive *z*-direction at the toe. Nonetheless, this support condition serves the purpose of the intended demonstration. Herein, an empirical methodology quantitatively describing the process of buckling in placed ripraps is introduced and verified with experimental data.

The mechanism of buckling of an Euler column exposed to external loading can be quantitatively described employing the governing fourth order differential equation (Eq. (2)) (Wang & Wang, 2004). Solving Eq. (2) to obtain the buckling modes of the specific case of a column pinned at one end and free at the other in accordance with the methodology described by Wang and Wang (2004) resulted in Eq. (3).

$$\frac{\mathrm{d}^4 w(r)}{\mathrm{d}r^4} + \alpha \frac{\mathrm{d}^2 w(r)}{\mathrm{d}r^2} = 0 \tag{2}$$

$$w(r) = K \sin\left(k \,.\, \pi \,.\, \frac{r}{R} \,.\, f\right) \tag{3}$$

where, $w(r)$ represents the lateral deflection of the column at a distance of r from the fixed end, the total length of the column is represented as R, parameter k denotes the buckling mode (k = 0, 1, 2, ...) and α, and f are numeric constants. The constant α relates to the external axial load as well as the column stiffness parameters. Further, K denotes the amplitude of deflection and is a calibration parameter with the unit 'm' to maintain the dimensional homogeneity of the equation.

Equation (3), in a non-dimensional form can be applied to quantitatively describe the buckling modes of placed ripraps by considering a conceptual column with lateral deformations defined as $\Delta z_m \, d_{50}^{-1}$ at a distance of L_m from the pinned end (Fig. 1). The column length ratio, r/R from Eq. (3) is replaced with $L_m \, L_s^{-1}$ (Eq. (4)). Parameter A is a dimensionless numeric constant, obtained through calibration.

$$\frac{\Delta z_m}{d_{50}} = A \sin\left(k \,.\, \pi \,.\, \left(\frac{L_m}{L_s}\right) .\, f\right) \tag{4}$$

Equations (3) and (4) only provide description of the buckling mode (shape) of the column. The magnitude of deformation is considered directly proportional to the magnitude of the applied external load. Hence, to incorporate the loading conditions into the criteria, the hydraulic load acting on the conceptual column is considered as the dimensionless term $q_i\, q_c^{-1}$ (Fig. 1) introduced in Eq. (4) resulting in Eq. (5).

$$\left(\frac{\Delta z_m}{d_{50}}\right)_i = A \quad \frac{q_i}{q_c} \sin\left(k \,.\, \pi \,.\, \left(\frac{L_m}{L_s}\right)_i .f\right) \tag{5}$$

It should be noted that $L_m\, L_s^{-1}$ is incorporated in Eq. (5) as a function of $q_i\, q_c^{-1}$ to account for riprap stone displacements along the *x*-axis with incremental overtopping where the iterative variable *i* denotes a discharge step ($i = 0$ for $q_i\, q_c^{-1} = 0$ and $i = n$ for $q_i\, q_c^{-1} = 1$). The term $(L_m\, L_s^{-1})_{i=0}$ represents the original positions of the selected riprap stones prior to being exposed to overtopping.

Relationship for quantifying the displacement of stones along the *x*-axis with incremental overtopping is required to use Eq. (5). Hiller et al. (2018a) demonstrate that the relative displacements ($\Delta x_m\, L_m^{-1}$), on an average could be considered as being similar for all the selected riprap stones at a particular overtopping discharge magnitude. To further validate this statement, a regression analysis of the relative stone displacements along the *x*-axis against the dimensionless discharge ratio was conducted. The analysis demonstrated that there exists an exponential relationship correlating these parameters given as Eq. (6) with a correlation to the parent data expressed in terms of the Nash-Sutcliffe coefficient of $R^2 = 0.81$ (Fig. 5). It can be observed from Fig. 5 that the relative displacements for the stones show a larger degree of spread for higher overtopping magnitudes ($q_i\, q_c^{-1} > 0.60$) in comparison with lower magnitudes. This observation is in line with earlier findings of Hiller et al. (2018a). This was explained as a consequence of variation in aeration pattern over the riprap during testing in turn influencing stone displacements. Reference is made to Hiller et al. (2018a) for further details in this regard. From Fig. 5, it can be observed that the relative displacements ($\Delta x_m\, L_m^{-1}$) for the stones as a function of overtopping flow magnitude follow a clear trend. An approximate estimation of relative displacements for the stones can be obtained employing Eq. (6) with a reasonable degree of accuracy, considering the uncertainty imparted by scattering of the data. It should be noted that Eq. (6) is valid for $i > 0$ as $(\Delta x_m\, L_m^{-1})_{i=0} = 0$ for all stones.

$$\left(\frac{\Delta x_m}{d_{50}}\right)_i = 0.0035\, e^{\left(2.97 \,.\, \frac{q_i}{q_c}\right)} \tag{6}$$

The term $(L_m\, L_s^{-1})_i$ in Eq. (5), which is a function of the applied overtopping load can be computed employing Eq. (7). The variable $(\Delta x_m\, L_s^{-1})_i$ for a particular overtopping flow can be obtained with the help of modified form of Eq. (6) presented as Eq. (8). Equation (7) is valid for $i = 0$ to $i = n$ whereas Eq. (8) is valid for $i > 0$ and $(L_m\, L_s^{-1})_{i=0}$ represents the initial positions of

the riprap stones prior to overtopping exposure and $(\Delta x_m \, L_s^{-1})_{i=0} = 0$ for all stones.

$$\left(\frac{L_m}{L_S}\right)_{i+1} = \left(\frac{L_m}{L_S}\right)_i - \left(\frac{\Delta x_m}{L_S}\right)_{i+1} \tag{7}$$

$$\left(\frac{\Delta x_m}{L_S}\right)_i = \left(\frac{L_m}{L_S}\right)_{i=0} 0.0035.\, e^{(2.97\,.\,\frac{q_i}{q_c})} \tag{8}$$

Equation (5) needs calibration with experimental data to obtain values of the numerical constants A and f for the buckling mode considered. This was done employing the cumulative experimental data presented in Fig. 4. Equation (5) was used to predict the 2D displacements of riprap stones for the corresponding values of $q_i \, q_c^{-1}$ considered as average for the respective measurement intervals. Numeric values of parameters A and f were subjected to a multivariate analysis with stepwise modifications to the respective parametric values and the corresponding goodness of fit, quantified by R^2 values were analyzed to arrive at optimal performance.

The calibration resulted in Fig. 6 with values for calibration constants as $A = 0.38$ and $f = 0.70$ for the first buckling mode ($k = 1$). This corresponded to correlation between the observed and the predicted displacements of $R^2 = 0.89$ and $R^2 = 0.99$ for $\Delta z_m \, d_{50}^{-1}$ and $L_m \, L_s^{-1}$ respectively. Further, Eq. (5), with $A = 0.38$, $f = 0.70$ and $k = 1$, was used to compute the continuous profiles of the buckling progression also presented in Fig. 6.

Investigation outcomes presented in Fig. 6 suggest a reasonable correlation between the predictions and the observations for the x and the z-displacements upon initial visual observation. The empirical predictions obtained from employing Eq. (5) are presented in Table 2 for detailed evaluation of the goodness of fit between predictions and observations. It can be observed from Table 2 that the values projected by Eq. (5) are in good agreement with observations for stones MS3, MS4 and MS5 for all overtopping intervals. The predictions agree well with $\overline{\Delta z_m d_{50}^{-1}}$ values and lie within the ±95% confidence bands (Table 2). However, as can be deduced from Fig. 6 and Table 2, Eq. (5) underestimates the stone displacements along the z-axis for MS1 and for MS2. That is, the correlation between the observed and predicted z-displacements was considerably better for the upstream section of the riprap (MS2 to MS5, $L_m \, L_s^{-1} > 0.44$) in comparison with the downstream section (MS0 to MS2, $L_m \, L_s^{-1} < 0.44$).

Discussions presented in this section describe the calibration of Eq. (5). However, further validation of the performance of the proposed equation is necessary to corroborate validity of the equation in predicting 2D deformation behavior of placed ripraps and this is recommended in future studies.

This comparative evaluation supports the hypothesis that the structural behavior of placed ripraps exposed to overtopping resembles the structural response of a slender-long column with the earlier specified support boundary conditions.

5 Discussions

5.1 Theoretical description of 2D deformations

The results obtained from this study demonstrate that placed ripraps constructed on steep slopes exposed to overtopping flows undergo a 2D buckling process closely resembling the buckling profile of a long-slender column under compression pinned at one end and free at the other end. This can be explained as a direct consequence of the interlocking forces generated between the individual riprap stones forming a bearing structure capable of withstanding certain degree of deformations.

Upon exposure to overtopping flows, the individual riprap stones are subjected to numerous forces such as the hydraulic drag and lift forces, gravitational force, interlocking forces setup between the individual stones and the frictional forces setup at the interface between the bottom of the riprap layer and the underlying filter zone. A riprap stone is subjected to hydraulic drag forces acting parallel to the chute in the downstream direction. The component of the gravitational force acting along the same direction further reinforces this effect. The sum of these forces is countered by the combination of interlocking forces generated between the riprap stone and the frictional forces setup at the interface between the riprap stone and the underlying filter zone, both acting parallel to the chute in the upstream direction. The resultant of these forces lead to downward displacement of the stone along the chute, in turn resulting in compaction along the *x*-direction.

Further, stone displacements along the *z*-axis can be attributed to two disparate mechanisms acting simultaneously. The hydraulic lift forces acting on the riprap stones perpendicular to the flow direction results in an upward pull on the stones and this force is countered by the vertical interlocking resistive forces generated between the stones. The resultant of these forces may result in stone displacements along the *z*-axis. Furthermore, analyzing the scenario from a structural standpoint, the horizontal and vertical interlocking forces generated within the placed riprap result in the formation of a bearing structure capable of withstanding some degree of deformation under compressive loading. So, stone displacements along the *x*-axis due to compressive forces results in generation of bending moments within the riprap layer leading to stone displacements along the *z*-axis.

Hence, the observed buckling mechanism can be considered possible due to the formation of a bearing structure as a consequence of the interlocking forces setup within placed ripraps. Ultimate riprap structural failure can be considered the consequence of combined effect of compressive forces causing stone displacements along the *x* and the *z*-axes. This in turn results in compression of the riprap through compaction (*x*-displacement) and development of bending moment due to the *z*-displacements, ultimately resulting in total collapse of the structure

in a buckling like manner.

Further, numerous past studies investigating placed riprap stability have concluded that the erosion of single stones in a placed riprap does not necessarily result in the loss of the structural integrity of the placed riprap structure (Hiller et al., 2018a; Dornack, 2001; Sommer, 1997; Larsen et al., 1986). The findings of this article provide evidence in support of this statement. Since placed ripraps exposed to overtopping loads form a unified structure as a consequence of the generated interlocking effect, detachment of a single loosely placed stone from the structure does not necessarily entail loss of structural integrity as the configuration of the neighboring stones can still offer a considerable degree of resistance against the destabilizing force.

5.2 Explanations for observations from the study

Observations from Section 3 of this article concerning regarding uncertainties in stone displacements and translation of peak of riprap deformation profile are explained as consequences of combined effects of variation in aeration patterns over the ripraps during testing and compaction of stones when exposed to initial overtopping flows. Uncertainty in stone displacements along the z-axis for the respective selected stones in general were found to be larger for overtopping intervals $q_i\, q_c^{-1} < 0.2$ and $q_i\, q_c^{-1} > 0.6$ as compared with intermediate overtopping magnitudes. Further, the peak of riprap deformation profile along the z-axis was found to undergo a shift from a downstream location (MS2, $L_m\, L_s^{-1} = 0.44$) for lower overtopping magnitudes, translating upstream (MS3, $L_m\, L_s^{-1} = 0.67$) for higher overtopping magnitudes.

The observed uncertainty in stone displacements for lower discharges ($q_i\, q_c^{-1} < 0.20$) can be attributed to initial readjustment of stones within the riprap when exposed to preliminary small magnitude overtopping flows. This is mainly dependent on stone placing efficiency as the riprap is loosely packed during construction with intermediate voids and initial exposure to overtopping leads to compaction of the stones forming a bearing structure. Subsequently, with exposure to incremental overtopping flows, the riprap behaves a structural member. Further, higher degree of uncertainty in stone displacements along the z-axis at higher overtopping magnitudes ($q_i\, q_c^{-1} > 0.6$) can be explained as a consequence of change in the aeration pattern over the riprap during different phases of testing. Hiller et al. (2018a) analyzed relative stone displacements patterns along the x-axis ($\Delta x_m\, L_s^{-1}$) for the riprap stones and found that the dimensionless relative displacements in general followed a consistent trend for all the stones. They also observed higher degree of spread in the relative displacement values for the individual stones at high discharge magnitudes ($q_i\, q_c^{-1} > 0.6$) and explained this as a consequence of variation in aeration pattern over the riprap at different testing phases. This reasoning can be extended to stone displacements along the z-direction as change in aeration pattern results in

modification to fluid density in turn leading to variation in development of flow forces with incremental overtopping. At low discharges where large degree of aeration is observed, flow forces may be diminished in comparison with higher overtopping magnitudes where aeration is absent. This can result in more pronounced development of stone displacements at higher overtopping magnitudes due to absence of air entrainment, which leads to higher flow force concentration.

The shift in peak of the deformation profile along the z-axis from MS2 at lower overtopping magnitudes to MS3 at high overtopping magnitudes can be explained as due to the combined effect of the previously described phenomenon. Upon exposure to initial overtopping ($q_i\, q_c^{-1} < 0.20$), individual stones undergo initial compaction due to presence of intermediate voids. That is, the 2D riprap deformation pattern is governed by compaction through individual stone displacements at this stage of testing. Also, flow forces acting on the riprap stone placed at the upstream section of the riprap are higher compared to stones placed on the lower sections at this stage due to higher degree of air entrainment at the downstream section of the riprap and also due to attenuation of flow velocities and forces due to roughness of the riprap layer. This entails that the upstream riprap section is pushed against the downstream section leading to a temporary bulge in the riprap deformation profile as can be observed from Fig. 4 for MS2. This trend is further amplified for $q_i\, q_c^{-1} = 0.21\text{-}0.40$ as further compaction takes place within the riprap. Upon formation of a more unified bearing structure through compaction, the placed riprap behaves similar to a structural member further undergoing consistent out of the plane displacements, ultimately leading to buckling.

Correlation between the observed and the predicted z-displacements employing Eq. (5) was considerably better for the upstream section of the riprap (between MS2 to MS5, $L_m\, L_s^{-1} > 0.44$) in comparison with the downstream section (MS0 to MS2, $L_m\, L_s^{-1} < 0.44$). This variation can be explained as a consequence of assumption of an ideal pinned support at the downstream toe. Derivation of Eq. (5) in accordance with the Euler's buckling theorem requires the assumption of an ideal pinned support permitting no displacements in the x-z plane. From Fig. 6, it can be observed that the riprap stones placed adjacent to the fixed toe support (MS0) did undergo some degree of displacement along the z-axis. Although the toe stones are constrained to move horizontally owing to the resistance offered by the fixed toe support, the hydraulic lift forces acting against vertical frictional force from the toe support still results in some degree of displacements along the z-axis. Since this effect is not incorporated within Eq. (5), stone displacements along the z-axis for the downstream section of the riprap (MS0 to MS2 , $L_m\, L_s^{-1} < 0.44$) are underestimated in comparison with the upstream section of the riprap (MS2 to MS5 ($L_m\, L_s^{-1} > 0.44$).

5.3 Study limitations and recommendations

The findings presented in this study are derived through experimental investigations conducted on a special placed riprap structure constructed on a steep slope ($S = 0.67$) with angular stones ($a\ b^{-1} = 1.7$) placed at an angle of $\beta = 60^{o}$. Validity of experimental results considering different material and site-specific properties should be further looked into to address scaling concerns and to improve confidence for general applicability of study findings.

- Conduction of similar investigations as performed as part of this study on placed ripraps built on milder slopes is recommended to better understand the importance of embankment slope on the buckling process.
- Further research is recommended on investigating similar tests conducted with sub-angular or rounded stones to study the differences in behavior of ripraps constructed with such stones.
- Inclination of the riprap stones with respect to the chute (β) can also influence placed riprap stability (Lia et al., 2013). Further studies with regards to influence of riprap stone inclination on 2D stone displacements is recommended.
- Since P_c values for the tests incorporated in this study lie within a narrow range of 0.52 - 0.58, evaluation of the impact of P_c on overall riprap stability or the 2D stone displacements is not possible from this study. However, it is recommended that future investigations in this regard look into the significance of P_c on the x and the z-displacements of riprap stones and in turn, on overall placed riprap stability.
- Carrying out large-scale overtopping field tests with placed ripraps constructed on rockfill dam structures are recommended to evaluate the validity of the observed failure mechanism at larger scales and to better understand the combined influence of throughflow and overflow on placed riprap stability.
- Toe support conditions for placed ripraps can be considered a key factor influencing the overall failure mechanism. Further research in understanding the behavior of placed ripraps with unrestrained toe structures is recommended, as this is relevant from a practical standpoint.

6 Concluding remarks

Experimental data sets obtained from overtopping tests conducted on model placed ripraps placed on slope of $S = 0.67$ and supported at the toe have been analyzed in this study to comprehend the underlying failure mechanism. Investigation results demonstrated that placed ripraps supported at the toe underwent progressive deformations in 2D when exposed to overtopping flows. The deformation behaviour closely resembled buckling of a slender-long column pinned at one end and free at the other and this ultimately led to total riprap failure at the

upstream section of the riprap. The formation of a bearing structure was described as a consequence of the interlocking forces generated within the placed riprap structure offering a certain degree of resistance against the external destabilizing forces. The magnitude of stone displacements were found to be correlated with the applied overtopping flow magnitude and also to the position of the stones along the chute length. Empirical relationships describing the 2D buckling phenomenon observed in placed ripraps with toe support have been introduced coupling experimental results with the well-established Euler's theory for column buckling. The criteria were calibrated against the experimental data with reasonable correlation.

Existing approaches for the determination of stability of riprap take into account the geometrical and flow boundary conditions, riprap material characteristics and fluid properties within the design criteria considering stone size as the primary design parameter. Findings of the present study document the fact that stability of placed ripraps with toe support is a predictable mechanism. This leads to the possibility of incorporation of buckling like 2D deformations of placed ripraps as a failure mechanism within the design process, which can enhance the effectiveness of the design practice. This is considering that numerous design parameters such as stone size and chute length, can be strategically designed to accommodate or impede the formation of these deformations.

The configuration of the toe structure has been identified as the key factor governing the failure mechanism as either sliding or buckling like 2D deformation and further research in this regard to understand the effects of toe configuration on riprap stability is recommended in future investigations.

Acknowledgements

The support and co-operation from Dr. Priska Helene Hiller, NVE, Norway and Prof. Jochen Aberle, TU Braunschweig, Germany in designing the experimental setup and making available their experimental data sets is highly appreciated. The assistance offered by master student Ms. Guri Veslegard is appreciated.

Funding

The authors acknowledge the financial support offered by HydroCen, Norway.

Notation

a, b, c = longest, intermediate and shortest axes lengths of riprap stones respectively (m)
C_u = coefficient of uniformity (-)
d_j = riprap stone diameter corresponding to j% finer (m)

$d_{j,F}$ = filter stone diameter corresponding to j% finer (m)

i = iterative variable representing a discharge step (-)

K = Numeric constant (m)

L_m = distance from downstream toe (m)

L_s = total length of the riprap (m)

m = iterative variable representing position of stones along the x-axis (-)

n = number of discharge steps (-)

N = number of riprap stones per unit area of the riprap (m^{-2})

P_c = Packing factor (-)

q = maximum unit discharge delivery capacity ($m^3 s^{-1} m^{-1}$)

q_c = critical unit discharge ($m^3 s^{-1} m^{-1}$)

q_i = unit discharge at i^{th} step ($m^3 s^{-1} m^{-1}$)

r = distance from pinned end of the column (m)

R = total column length (m)

S = slope (-)

Δt = time interval (s)

$w(r)$ = deformation at a distance r from the pinned end of the column (m)

x, y, z = coordinate axes (m)

α, A, f, k = numeric constants (-)

β = angle of a-axis of riprap stones with respect to the slope (º)

ρ_s = density of riprap stone ($kg\ m^{-3}$)

$\rho_{s,F}$ = density of filter stone ($kg\ m^{-3}$)

Δx_m, Δz_m = displacements along the respective axes for riprap stones located at position m (m)

References

Abt, S R, & Thornton, C. I. (2014). Riprap Design for Overtopping – Man Do I Need a Martini! *World Environment and Water Resources Congress 2014*, (1936), 1191–1198.

Abt, Steven R., Thornton, C. I., Scholl, B. A., & Bender, T. R. (2013). Evaluation of overtopping riprap design relationships. *Journal of the American Water Resources Association*, *49*(4), 923–937.

Abt, Steven R, Terry L, J., & Members, A. (1991). Riprap Design for Overtopping Flow. *Journal of Hydraulic Engineering*, *119*, 959–972.

Chang, H. H. (1998). Riprap Stability on Steep Slopes. *International Journal of Sediment Research*.

Dornack, S. (2001). Uberstrombare Damme-Beitrag zur Bemessung von Deckwerken aus Bruchsteinen/ Overtopping dams-Design criteria for riprap. *PhD Thesis, Technische Universitat Dresden*.

Frizeii, K. H., Ruff, J. F., & Mishra, S. (1998). Simplified Design Guidelines for Riprap Subjected To Overtopping Flow. *In Proceedings of the Annual Conference of the Assoc. Of State Dam Safety Officials.*, 301–312.

Hiller, P. H. (2017). Riprap design on the downstream slopes of rockfill dams,. *Doctoral Thesis,*

Norwegian University of Science and Technology, Trondheim.

Hiller, P. H., Aberle, J., & Lia, L. (2018a). Displacements as failure origin of placed riprap on steep slopes. *Journal of Hydraulic Research*, *56*(2), 141–155.

Hiller, P. H., Lia, L., & Aberle, J. (2018b). Field and model tests of riprap on steep slopes exposed to overtopping. *Journal of Applied Water Engineering and Research*, *0*(0), 1–15.

Isbash, S. (1936). Construction of Dams by Depositing Rock in Running Water. *International Congress on Large Dams*.

Khan, D., & Ahmad, Z. (2011). Stabilization of Angular-Shaped Riprap under Overtopping Flows. *World Academy of Science, Engineering and Technology, International Journal of Civil, Environmental, Structural, Construction and Architectural Enfineering*, *5*(11), 550–554.

Knauss, J. (1979). Computation of maximum discharge at overflow rockfill dams (a comparison of different model test results). In *13th Congress on Large Dams* (Vol. Q50, pp. 143–159).

Kobayashi, N., & Jacobs, B. K. (1985). Riprap Stability Under Wave Action. *Journal of Waterway, Port, Coastal, and Ocean Engineering*, *111*(3), 552–566.

Larsen, P., Bernhart, H. H., Schenk, E., Blinde, A., Brauns, J., & Degen, F. P. (1986). Uberstrombare Damme, Hochwasserentlastung uber Dammscharten/ Overtoppable dams, spillways over dam notches. *Unpublished Report Prepared for Regierungsprasidium Karlsruhe*, *Universita*.

Lia, L., Vartdal, E. A., Skoglund, M., & Campos, H. E. (2013). Riprap protection of downstream slopes of rockfill dams-a measure to increase safety in an unpredictable future climate. *European Club Symposium of the International Comission on Large Dams*.

NVE. (2012). Veileder for fyllingsdammer. *Norwegian Water Resources and Energy Directorate*, 21–25.

Olivier, H. (1967). Through and Overflow Rockfill Dams-New Design Techniques. *Proceedings of the Institution of Civil Engineers*, 433–471.

Peirson, W. L., Jens, F., Steven E, P., & Ronald J, C. (2008). Placed Rock as Protection against Erosion by Flow down Steep Slopes. *Journal of Hydraulic Engineering*, *134*, 1370–1375.

Siebel, R. (2007). Experimental investigations on the stability of riprap layers on overtoppable earthdams. *Environmental Fluid Mechanics*, *7*(6), 455–467.

Sommer, P. (1997). Uberstrombare Deckwerke/ Overtoppable erosion protections. *Unpublished Report No. DFG-Forschungsbericht La 529/8-1*, *Universita*.

Thornton, C. I., Abt, S. R., Scholl, B. N., & Bender, T. R. (2014). Enhanced Stone Sizing for Overtopping Flow. *Journal of Hydraulic Engineering*, *140*(4), 06014005–.

Timoshenko, S. P., & Gere, J. M. (2009). *Theory of Elastic Stability*. Mineola, NY: Dover Publication, INC.

Wang, C. M., & Wang, C. Y. (2004). *Exact solutions for buckling of structural members* (Volume 6). CRC Press.

Table 1 Testing procedure for the documented tests incorporating the discharge q_i given as range, number of discharge steps n, time intervals Δt, initial packing factor P_c and the critical unit discharge q_c representing loading condition at total riprap failure.

Test	q_i (m^2 s^{-1})	n (-)	Δt (s)	P_c (-)	q_c (m^2 s^{-1})
1	0.05-0.30	9	1800	0.58	0.30
2	0.05-0.20	7	1800	0.56	0.20
3	0.05-0.12	3	1800	0.57	0.12
4	0.05-0.15	4	1800	0.54	0.15
5 (P01*)	0.05-0.24	9	1800	0.56	0.24
6 (P02*)	0.05-0.36	11	3600	0.55	0.36
7 (P04*)	0.10-0.40, 0.35, 0.40	6	3600, 17h	0.53	0.40

*Original labels for the respective tests as employed within Hiller et al. (2018a).

Table 2 Results from analysis of the experimental data sets. Numerical values of the average dimensionless stone displacements along the z-axis ($\overline{\Delta z_m d_{50}^{-1}}$) for marked stones with indices MSm computed for all the seven tests. The displacements are presented as a function of incremental overtopping unit discharge intervals ($q_i\, q_c^{-1}$). ± 95% confidence intervals are presented along with confidence bands computed about the mean. Empirical projections obtained by employing Eq. (5) are presented.

$q_i\, q_c^{-1}$ (-)	Stone Index (-)	$\overline{\Delta z_m d_{50}^{-1}}$ (-)	±95% Confidence interval (-)	95% Confidence band (-)	Eq. (5)
< 0.20	MS0	0.04	0.04	0.00 – 0.08	0.00
	MS1	0.06	0.04	0.02 – 0.10	0.02
	MS2	0.09	0.06	0.03 – 0.15	0.03
	MS3	0.07	0.04	0.03 – 0.10	0.04
	MS4	0.05	0.04	0.01 – 0.08	0.04
	MS5	0.03	0.03	0.00 – 0.06	0.03
0.21-0.40	MS0	0.07	0.02	0.05 – 0.09	0.00
	MS1	0.11	0.01	0.09 – 0.12	0.05
	MS2	0.15	0.03	0.12 – 0.18	0.09
	MS3	0.12	0.02	0.10 – 0.14	0.11
	MS4	0.10	0.04	0.05 – 0.14	0.11
	MS5	0.08	0.02	0.05 – 0.10	0.09
0.41-0.60	MS0	0.06	0.03	0.03 – 0.09	0.00
	MS1	0.14	0.02	0.11 – 0.16	0.09
	MS2	0.19	0.03	0.16 – 0.21	0.15
	MS3	0.20	0.02	0.18 – 0.22	0.19
	MS4	0.18	0.02	0.16 – 0.21	0.18
	MS5	0.16	0.02	0.14 – 0.18	0.16
0.61-0.80	MS0	0.08	0.03	0.05 – 0.11	0.00
	MS1	0.20	0.02	0.18 – 0.22	0.12
	MS2	0.26	0.03	0.23 – 0.29	0.21
	MS3	0.25	0.06	0.19 – 0.31	0.26
	MS4	0.24	0.03	0.22 – 0.27	0.26
	MS5	0.24	0.03	0.20 – 0.27	0.22
0.81-1.00	MS0	0.09	0.04	0.05 – 0.12	0.00
	MS1	0.27	0.04	0.23 – 0.30	0.15
	MS2	0.32	0.04	0.28 – 0.36	0.27
	MS3	0.32	0.04	0.28 – 0.37	0.33
	MS4	0.32	0.03	0.29 – 0.34	0.33
	MS5	0.30	0.06	0.24 – 0.35	0.29

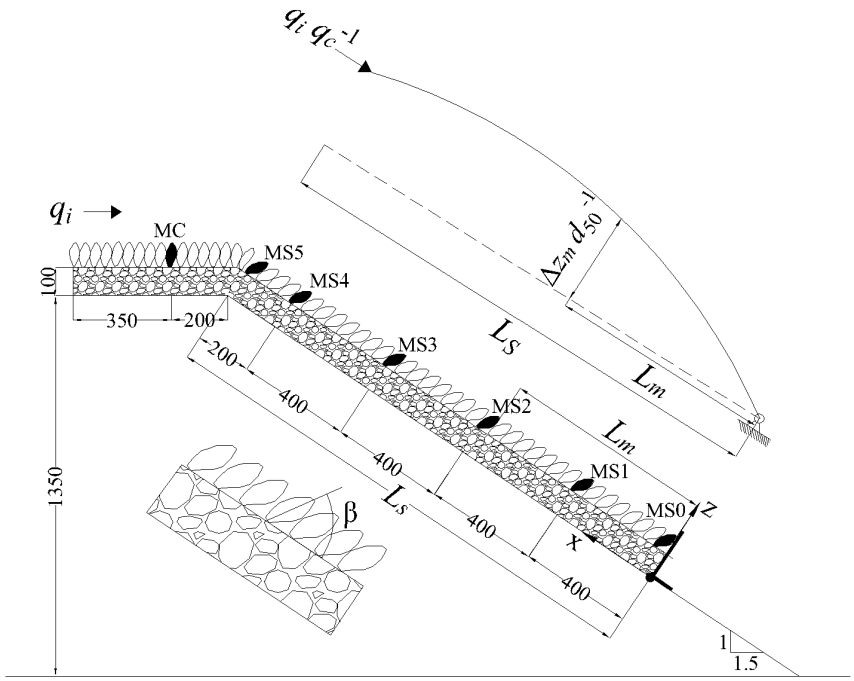

Fig. 1 Depiction of experimental setup of model placed riprap with chute length of L_s = 1.8 m supported at the toe along with portrayal of inclination angle (β) of a-axis of the stones with respect to the chute direction. Illustration of buckling process in the riprap is depicted for a conceptual column pinned at one end and free at the other. All measurements are in mm, flow direction from left to right. This depiction of the experimental setup is a modified form of Fig. 3 from Hiller et al. (2018a) with the addition of conceptual illustration of the buckling process.

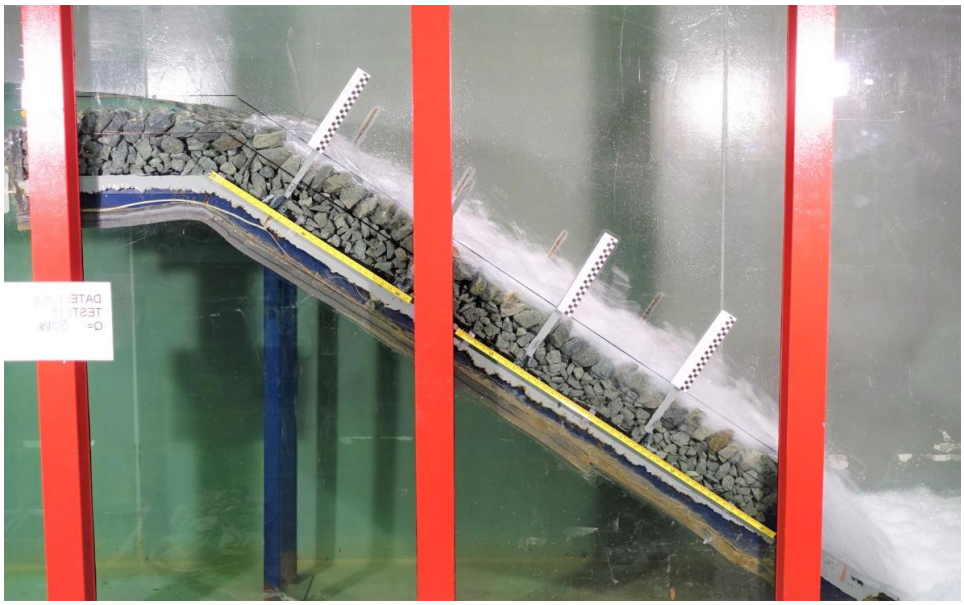

Fig. 2 Image of the experimental setup during testing (test 5, q_i = 0.1 m^2 s^{-1}). The riprap model is situated at the hydraulic lab of NTNU, Trondheim.

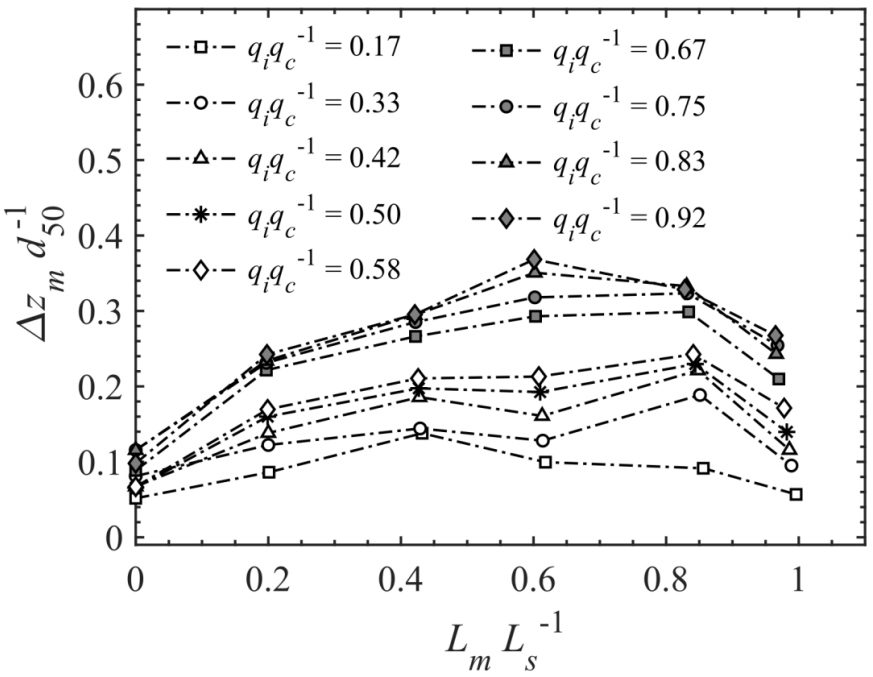

Fig. 3 Depiction of 2D displacements of selected riprap stones for test 1 with the vertical plot axis represents normalized stone displacements along the z-axis ($\Delta z_m d_{50}^{-1}$). The horizontal plot axis represents normalized stone displacements along the x-axis accounted for within the term $L_m L_s^{-1}$. The displacements are presented for incremental overtopping discharge magnitudes represented by the dimensionless term $q_i q_c^{-1}$.

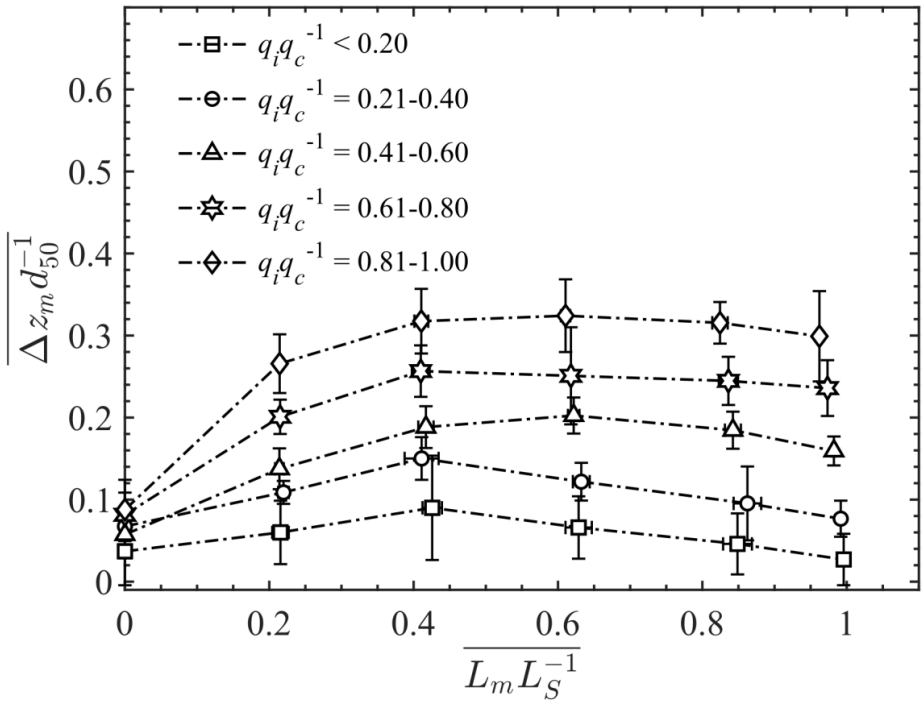

Fig. 4 Results from the cumulative analysis carried out on data sets from seven tests representing average stone displacements in 2D. The vertical plot axis represents normalized average stone displacements along the z-axis ($\Delta z_m\, d_{50}^{-1}$). The horizontal plot axis represents normalized average stone displacements along the x-axis accounted for within the term $L_m\, L_s^{-1}$. The displacements are presented for incremental overtopping discharge magnitudes represented by the dimensionless term $q_i\, q_c^{-1}$. Uncertainty in displacements shown as 95% confidence intervals.

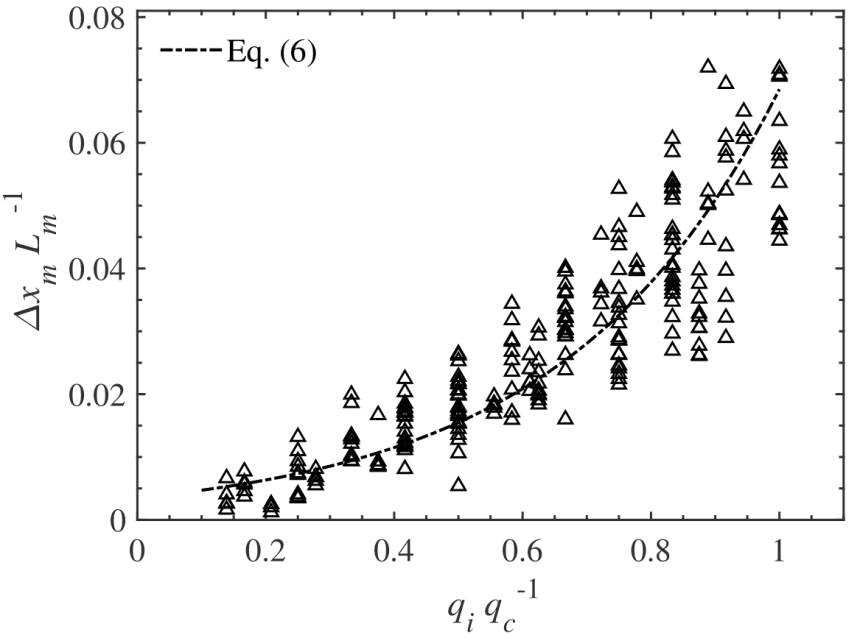

Fig. 5 Results from the statistical regression analysis carried out to obtain relationship between the relative displacement of stones along the *x*-axis applied overtopping discharge magnitudes. The vertical plot axis represents the relative displacement of stones along the *x*-axis ($\Delta x_m L_m^{-1}$). The horizontal plot axis represents the dimensionless form of overtopping discharge magnitudes ($q_i q_c^{-1}$).

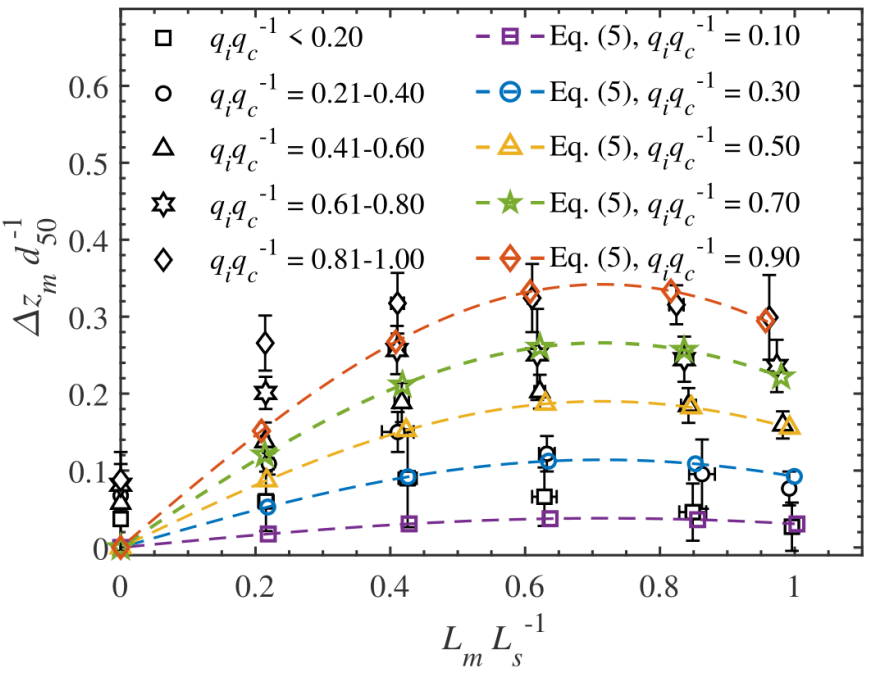

Fig. 6 Observed 2D stone displacements from Fig. 4 juxtaposed with predicted values from Eq. (5). The vertical plot axis represents normalized average stone displacements along the z-axis ($\Delta z_m d_{50}^{-1}$). The horizontal plot axis represents normalized average stone displacements along the x-axis accounted for within the term $L_m L_s^{-1}$. The displacements are presented for incremental overtopping discharge magnitudes represented by the dimensionless term $q_i q_c^{-1}$. Uncertainty in observed displacements shown as 95% confidence intervals. The continuous 2D displacement profiles computed from Eq. (5) for the corresponding values of $q_i q_c^{-1}$ considered as average for the respective measurement intervals.

Paper II

Toe support conditions for placed ripraps on rockfill dams- A field survey.
Ravindra, G.H.R., Sigtryggsdottir, F.G., Asbølmo, M.F and Lia, L (2019).
Vann 2019 (3), pp. 185- 199.

Toe support conditions for placed ripraps on rockfill dams – A field survey

Av Ganesh H R Ravindra, Fjola G Sigtryggsdottir, Malin F Asbølmo og Leif Lia

Ganesh H R Ravindra is a PhD Candidate at the Department of Civil and Environmental Engineering, Norwegian University of Science and Technology (NTNU), Trondheim.
Fjola G Sigtryggsdottir is an Associate Professor at the Department of Civil and Environmental Engineering, NTNU, Trondheim.
Malin F Asbølmo is an MSc Student at the Department of Civil and Environmental Engineering, NTNU, Trondheim and
Leif Lia is a Professor at the Department of Civil and Environmental Engineering, NTNU, Trondheim.

Summary

Riprap toe stabilization is of significance to ensure adequate overall stability of the riprap structure exposed to extreme overtopping conditions. From economical and stability points of view, it is of importance to investigate current state of toe support conditions for placed ripraps on rockfill dams. This article presents findings from field surveys investigating construction aspects of placed ripraps built on several Norwegian rockfill dams. Key parameters describing quality of placement of riprap and toe stones such as size, shape and inclination have been analysed as part of this study. Further, details concerning current state of riprap toes have been outlined. In addition, conformity of construction practices with Norwegian dam safety guidelines is also looked into. Study findings suggest that construction practices adopted for placed ripraps meet the requirements of Norwegian dam safety regulations. However, investigation outcomes also show that construction practices adopted at present do not prioritize on addressing additional recommendations put forward by the dam safety authorities with regards to placed riprap stability. Furthermore, detailed survey of riprap toe sections revealed that well-defined toe support measures stabilizing riprap toes are currently not implemented at any of the surveyed rockfill dams. Further experimental research in this regard to better understand failure mechanism of placed ripraps with realistic toe support conditions is recommended. Also, experimental investigations to arrive at methodologies to provide ideal toe support for placed ripraps on rockfill dams is recommended.

Sammendrag

Tåstøtte til plasting på steinfyllingsdammer – en feltstudie

Sikringstiltak ved damtå har betydning for stabilitet til plastring som blir utsatt for overtopping. Fra et økonomisk og stabilitetsmessig ståsted, er det viktig å studere hvordan tåstein faktisk er plassert på plastrede steinfyllingsdammer. Denne artikkelen presenterer funn fra feltkartlegging, gjennomført for å undersøke utforming av nedstrøms plastring og tå på

eksisterende norske steinfyllingsdammer. Ulike parametere som beskriver kvaliteten til plastringen, slik som størrelse, form og helning av tå- og plastringsstein, har blitt analysert som en del av denne studien. Videre blir detaljer vedrørende praksis for sikring av tåstein beskrevet. I tillegg blir samsvar mellom eksisterende fyllingsdammer og norsk regelverk for bygging av fyllingsdammer undersøkt. Funn fra studien antyder at plastring på eksisterende fyllingsdammer oppfyller kravene som er gitt i damsikkerhetsforskriften. Derimot viste resultatene fra kartleggingen at ytterligere anbefalinger for å sikre en stabil plastring, gitt i Veileder for fyllingsdammer, ikke er oppfylt. Dessuten viste studier av nedre del av skråningene at ingen av de kartlagte steinfyllingsdammene er bygd med ekstra sikringstiltak for tåstein. Videre studier anbefales for å bedre kunne forstå bruddmekanismene til plastring som ikke er sikret ved damtå. I tillegg anbefales det å utføre fysiske modell- og storskalaforsøk med et formål om å utvikle metoder for sikring av tåstein som gir tilstrekkelig stabilitet av plastring på fyllingsdammer.

1.0 Introduction

Dams are essential for hydropower development as they enable storage of water in reservoirs, in turn assisting stable power production. There are over 360 large dams in Norway at present (over 15 m high) and over 180 of these are rockfill dams. Several of the existing Norwegian rockfill dams are poised to be upgraded in the near future to meet requirements of revised dam safety regulations. Upgrading of rockfill dams often includes expensive reconstruction of the downstream riprap. Riprap is one of the most common measures for erosion protection of downstream slopes of rockfill dams (e.g. Abt et al., 2013, Ravindra et al., 2018a, Hiller et al., 2018a and Ravindra et al., 2019). Ripraps can be broadly classified into two categories based on the method of construction. Dumped ripraps comprise of randomly placed stones while placed ripraps are characterized by stones arranged in a specific interlocking pattern (Hiller et al., 2018a and Ravindra et al., 2019).

Evaluation of stability aspects of placed ripraps constructed on rockfill dams is important from economical and safety standpoints. Although extensive literature is available within the discipline of dumped riprap design, available international literature on the stability and design aspects of placed ripraps in connection with rockfill dams is limited (Ravindra et al., 2018a). Past studies such as Knauss (1979), Larsen et al. (1986), Sommer (1997), Dornack (2001), Peirson et al. (2008), Hiller et al. (2018a) and Ravindra et al. (2019) have been aimed at investigating the underlying failure mechanisms of placed ripraps exposed to overtopping flows. These experimental investigations were conducted on model placed ripraps constrained at the toe using metallic support structures.

It should be noted that toe section of the riprap in this article refers to the last row of riprap stones placed on the downstream dam foundation (Figure 1). On the other hand, the term rockfill dam toe refers to either an internal or an external structure constructed in tandem with the downstream rockfill shoulder comprising of coarser material as compared with the rockfill shoulder material. This facilitates expulsion of seepage or accidental leakage flows from within the dam structures thereby preventing build up of excess pore pressures. Hence, rockfill dam toe is constructed to assure enhanced stability of the downstream shoulder under extremely high through-flow conditions (Morán et al., 2019). This article is intended at investigating construction aspects of only the toe sections of placed ripraps on rockfill dams.

Several past investigations looking into the stability of ripraps under overtopping situations have suggested that the probability of initiation of failure at the toe section of ripraps can be significant (Figure 1). Hiller et al. (2018b) and Lia et al. (2013) present findings concerning placed riprap stability from large-scale overtopping tests stating that none of the tested ripraps failed as a consequence of breach of the riprap structure in itself. All failures were observed to have initiated at the toe or along the sidewalls of the ripraps. Further along similar lines, Solvik

(1991) based on model studies has argued that special attention should be directed towards stabilizing toe section of ripraps.

These observations can be considered to be a consequence of the toe stones and stones placed along the abutments being exposed to higher magnitude hydrodynamic forces during overtopping events in comparison with riprap stones placed on the dam slopes. Flow concentration at the toe section of ripraps under throughflow conditions result in highly erosive hydrodynamic drag and lift forces on the toe stones (Figure 1). Further under overflow conditions, the destabilizing forces on the riprap toe are amplified as the toe has to deal with dynamic forces transferred by the overlying riprap layer in addition to the destabilizing drag and lift forces (Figure 1) (Ravindra et al., 2018b). Hence, the riprap toe stones need to be provided with adequate support to inhibit removal of the stones under the influence of destabilizing hydrodynamic forces.

In order to safeguard dams against accidental overtopping events, dam safety regulations in Norway prescribe construction of single-layered placed ripraps on the downstream slopes of rockfill dams. The individual riprap stones are to be placed in an interlocking pattern with their longest axis inclined towards the dam (OED, 2009; NVE, 2012). Placed ripraps on rockfill dams exposed to overtopping can fail as a consequence of sliding or structural collapse of the riprap structure depending on the toe support conditions. In case of a constrained toe support, the riprap structure may fail because of structural collapse as a fixed support is provided to avoid sliding of the riprap structure (Ravindra et al., 2019). However, in case of an unrestrained toe, the riprap section could undergo sliding along the steep slope as a result of limited frictional resistance offered at the foundation (Ravindra et al., 2019). Hence, configuration of the toe section of placed riprap can be considered a key factor influencing the overall failure mechanism of placed ripraps exposed to overtopping flows.

The Norwegian Water Resources and Energy Directorate (NVE, 2012) recommend design specifications for placed ripraps in general. However, protocols addressing specifics on the design aspects of toe support for the riprap structures are currently unavailable. The available references within the NVE recommendations pertinent to riprap toe stability state that it may be necessary to secure the lowermost part of the downstream slope and the abutments of rockfill dams with larger stones, or other reinforcing measures based on the dam cross-section and overtopping flow magnitude. It is also stated that rock foundation should provide good support against sliding of the toe stones. If the foundation should provide good support against sliding of the toe stones, one has to blast a trench or cast a foot, especially for foundations with inclinations larger than 10°. Although these statements point out key design considerations

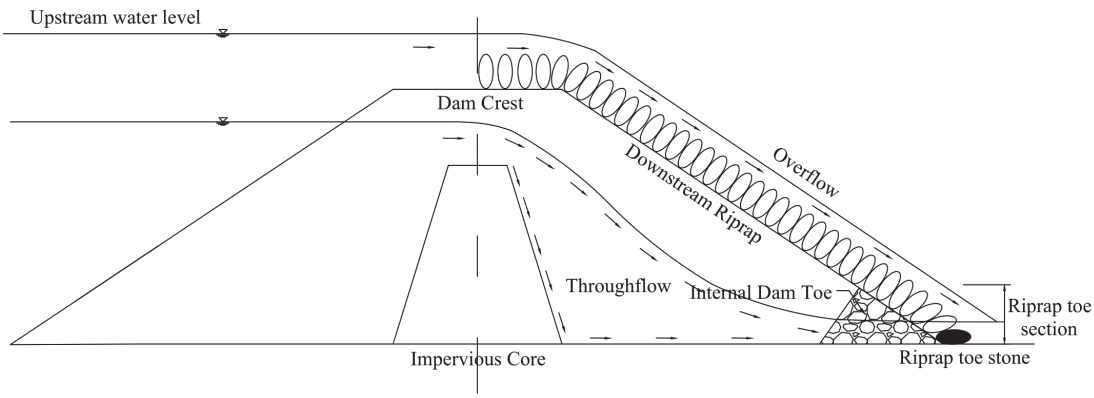

Figure 1. Description of throughflow and overflow scenarios in rockfill dams

with regards to riprap design, technical details of design and construction of riprap toe support structures is currently not provided. But, earlier discussions with regards to riprap toe brings forth the possibility that probability of initiation of unraveling riprap failure could be high at the toe section. Since previous studies conducted to investigate placed riprap stability under overtopping conditions have been conducted with placed riprap structures constrained at the toe section using rigid support structures, it is of relevance to comprehend existing toe support conditions on rockfill dams. This would help facilitate development of experimental studies for realistic evaluation of stability of placed ripraps exposed to overtopping flows.

The present field survey was intended at investigating toe structures and construction aspects of placed ripraps and riprap toe conditions of several Norwegian rockfill dams. As part of the survey, key parameters describing quality of placement of riprap and toe stones such as size, shape and inclination were recorded and these have been further analysed and discussed in the present article. Further, conformity of placed riprap toe construction with official dam safety guidelines are evaluated as part of the present study. Observations from the field survey concerning existing toe conditions for placed ripraps are also presented. This article is primarily aimed at facilitating evaluation of practical applicability of findings from past experimental investigations.

2.0 Study methodology

A field survey of placed ripraps on 33 different Norwegian rockfill dams was conducted by Hiller (2016). The present study adds to the findings of Hiller (2016) through investigation conducted to study details concerning toe construction of placed ripraps on nine Norwegian rockfill dams. Details regarding the dam location, consequence classification, height and length are presented in Table 1. The rockfill dams chosen for the field surveys consisted of varying sizes of dams from 5 m up to 142 m in height (H) and from 70 m to 1400 m in length (L). The criteria for dam selection was presence of well-defined toe structures within the dam structure. The selections included Oddatjørndammen (H = 142 m and L = 466 m) which is the highest rockfill dam in Norway and Storvassdammen (H = 90 m and L = 1400 m) which is the largest Norwegian rockfill dam by volume. Further, the selection also comprised of dams belonging to different Norwegian dam safety consequence classes (2 to 4). The classification considers potential for damage to life and property in case of dam breach (NVE, 2012). Class 4 designates dams with very high potential for damage in case of dam failure. Class 3 indicates dams with high damage potential and class 2 signifies dams with medium damage potential (Midttømme et al., 2012). The variability in dam sizes was considered as an important parameter in order to obtain a representative picture of placed riprap toe construction in Norwegian rockfill dams.

The methodology adopted by Hiller (2016) with regards to their field survey of placed riprap construction on Norwegian rockfill dams has further been incorporated in this study to investigate construction aspects of both the riprap and the toe structures. The nominal stone size (d_n) has been employed to quantify sizing of the riprap stones as this can be considered as the representative size of individual riprap stones (equation 1). Computation of d_n requires measurements of the longest, intermediate and the shortest axes dimensions of the riprap stones (a, b and c stone axes dimensions) (Hiller et al., 2018a). The median stone size (d_{50}) for the stones is further computed as the average of individual nominal stone sizes. Furthermore, the placement angle of the riprap stones with respect to the downstream dam slope is characterized through the parameter (α) (Figure 2), which is the sum of the downstream embankment slope (θ) and the inclination of the longest stone axis with respect to the horizontal (β) (equation 2).

$$d_n = (abc)^{1/3} \quad (1)$$

$$\alpha = \beta + \theta \quad (2)$$

Table 1. Details of the dams surveyed as part of the study

Dam Index	Dam name	Location	Consequence class	Dam Height (*H*) (m)	Dam Length (*L*) (m)
1	Vessingsjø Secondary dam	Tydal, Trøndelag	2	5	70
2	Skjerjevatnet Secondary dam 1	Masfjord, Hordaland	2	18.7	101.2
3	Skjerjevatnet main dam	Masfjord, Hordaland	3	29.5	251
4	Nesjø main dam	Tydal, Trøndelag	4	45	1030
5	Fjellhaugvatn dam	Kvinnherad, Hordaland	2	52	72.8
6	Akersvass dam	Rana, Nordland	4	53	485
7	Førreskar dam	Suldal, Rogaland	3	81	640
8	Storvass dam	Suldal, Rogaland	4	90	1400
9	Oddatjørn dam	Suldal, Rogaland	3	142	466

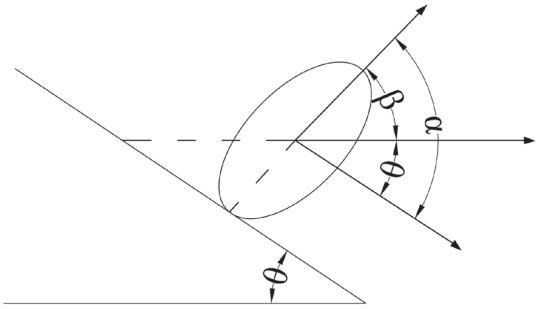

Figure 2. Portrayal of stone inclination with respect to the dam slope (α) as sum of inclination with respect to the horizontal (β) and embankment slope (θ)

The field measurements were subdivided into two different measurement phases. The first phase included measurements conducted to study the properties of the riprap section and the second phase was primarily intended at investigating properties of the toe stones and the toe support conditions. During the first phase of measurements, sizing of the riprap stones (*a*, *b* and *c*) and the inclination of the stones with respect to the horizontal (β) were measured for individual stones lying within a random 5 m x 5 m strip of the riprap. The stone dimensions were measured employing standard rulers and the inclinations were measured using a digital inclinometer. During the second phase of the survey, the dimensioning and the placement inclination of toe stones placed along the length of the dam toe were measured at regular distance intervals dependent on the dam length. Also, details regarding existing support conditions for the toe stones were recorded during this phase of the survey.

3.0 Data analysis

The data sets accumulated as part of the field survey of placed ripraps have been subjected to a statistical evaluation in this section of the article. Measurements of stone sizes (*a*, *b* and *c*) have been used to analyse the size distribution and angularity of the riprap and the toe stones. Further, measurements of inclination of the stones with respect to the horizontal (β) have been employed to compute the angle of placement of the stones with respect to the downstream slope (α). These results have further been subjected to a comparative evaluation with Norwegian dam safety requirements and recommendations to comprehend compatibility between construction practices and official guidelines.

The Norwegian Ministry of Petroleum and Energy (OED, 2009) is the official body providing

Table 2. Summary of official regulations and recommendations with respect to placed ripraps

Parameter	OED (2009) regulations	Additional NVE recommendations
Minimum stone size (d_{min})	The downstream slope should have slope protection which ensures that the dam can withstand large overtopping due to accidental loads or damage to the dam. Stones within the riprap must have satisfactory size and quality and be arranged in a stable manner.	$d_{min} = 1.0\ S^{0.43}\ {q_f}^{0.78}$ (3)*
Uniformity of stone size (d_{max}/d_{min})		$d_{max}/d_{min} < 1.7$*
Angularity		The stones be situated within the bladed to rod shape regimes within the Zingg diagram (Zingg, 1935) to ensure optimum interlocking with minimal void formation**.
Stone placement	The individual riprap stones are to be placed in an interlocking pattern with their longest axis inclined towards the dam.	As stated in the OED (2009) regulations*

*Obtained from NVE (2012) and ** from the presentation Hyllestad (2007).

where d_{min} and d_{max} denote the minimum and maximum riprap stone sizes; S stands for the downstream embankment slope (S is the ratio of the vertical to the horizontal slope dimensions) and q_f represents recommended minimum design discharge value for the respective dam consequence classifications.

regulations regarding design and construction of rockfill dams in Norway and the NVE puts forward additional technical recommendations in this regard (NVE, 2012). Table 2 succinctly summarizes the official regulations and recommendations concerning design and construction of placed ripraps.

3.1 Stone sizing

The size distribution of the stones were computed as fractions of individual stone weights to the cumulative weight of the measured stones (Figure 3). Individual stone weights (W) were computed employing Equation 4 with the nominal stone size (d_n) obtained employing equation 1.

$$W = d_n C_f \gamma_S \quad (4)$$

with C_f representing the form factor for the stones, generally assumed as 0.6 (NVE, 2012) and γ_S denoting stone density (assumed herein as 26 kN/m^3).

To conduct a comparative evaluation between field measurements of riprap stone sizes and official dam safety recommendations with regards to minimum required sizing of riprap stones, the minimum stone sizing recommendations obtained from equation 3 have been compared with the computed gradation curves within Figure 3. As per the recommendations of NVE dam safety guidelines of 2012, placed ripraps need to be constructed with stones of volume of minimum 0.15 m^3 (d_{min} = 0.64 m) for dams classified within consequence class 4. To determine the minimum median riprap stone sizing for dams in classes 3 and 2, NVE prescribes equation 3 assuming minimum unit discharges 'q_f' of 0.5 m^3/s for class 3 and 0.3 m^3/s for class 2 respectively (NVE, 2012).

Figures 3a, 3c and 3e depict size distributions for riprap stones from the surveyed placed ripraps constructed on different dams classified within dam safety classes 2, 3 and 4 respectively and Figures 3b, 3d and 3f present size distributions for toe stones from the respective dams. Furthermore, minimum stone sizing recommendations for the respective dam safety classes (equation 3) are presented within the respective plots. It can be observed from the depictions that all dams meet the recommended minimum sizing criteria for all dam safety classes. It should also be noted that the sizing of the riprap stones was in general closely resembling the sizing of the toe stones with $d_{50,T}/d_{50,RR}$ ranging from 1 to

1.25 with $d_{50,\,T}$ / $d_{50,\,RR}$ representing the ratio of median toe stone size to that of the riprap stones. However, for Fjellhaugvatn dam (Figures 3a and 3b) and for Storvass dam (Figures 3e and 3f), the toe stones were found to be of comparatively larger sizing than the riprap stones with $d_{50,\,T}$ / $d_{50,\,RR}$ of 1.53 and 1.45 respectively.

Further, the NVE guidelines for design and construction of placed ripraps also recommend that the ripraps should be comprised of uniform sized stones conforming to the criteria d_{max} /d_{min} < 1.7 (NVE, 2012). Figures 4a and 4b portray the ratio of the maximum to the minimum stone diameters for the riprap and the toe stones respectively from all the surveyed dams. The NVE guideline in this regard has also been overlaid within these plots. The depictions demonstrate that none of the dams meet the criteria considering size distribution of the riprap stones (Figure 4a). Two of the dams, Vessingsjø secondary dam and Fjellhaugvatn dam met the recommendation with regards to size distribution of the toe stones (Figure 4b).

3.2 Shape

The Zingg shape classification scheme (Zingg, 1935) is widely employed within numerous research disciplines to classify particles into different form categories such as spheroids, discs, rods and blades based on the *b*/*a* and *c*/*b* ratios. This technique has been employed in this study to determine the angularity of the measured

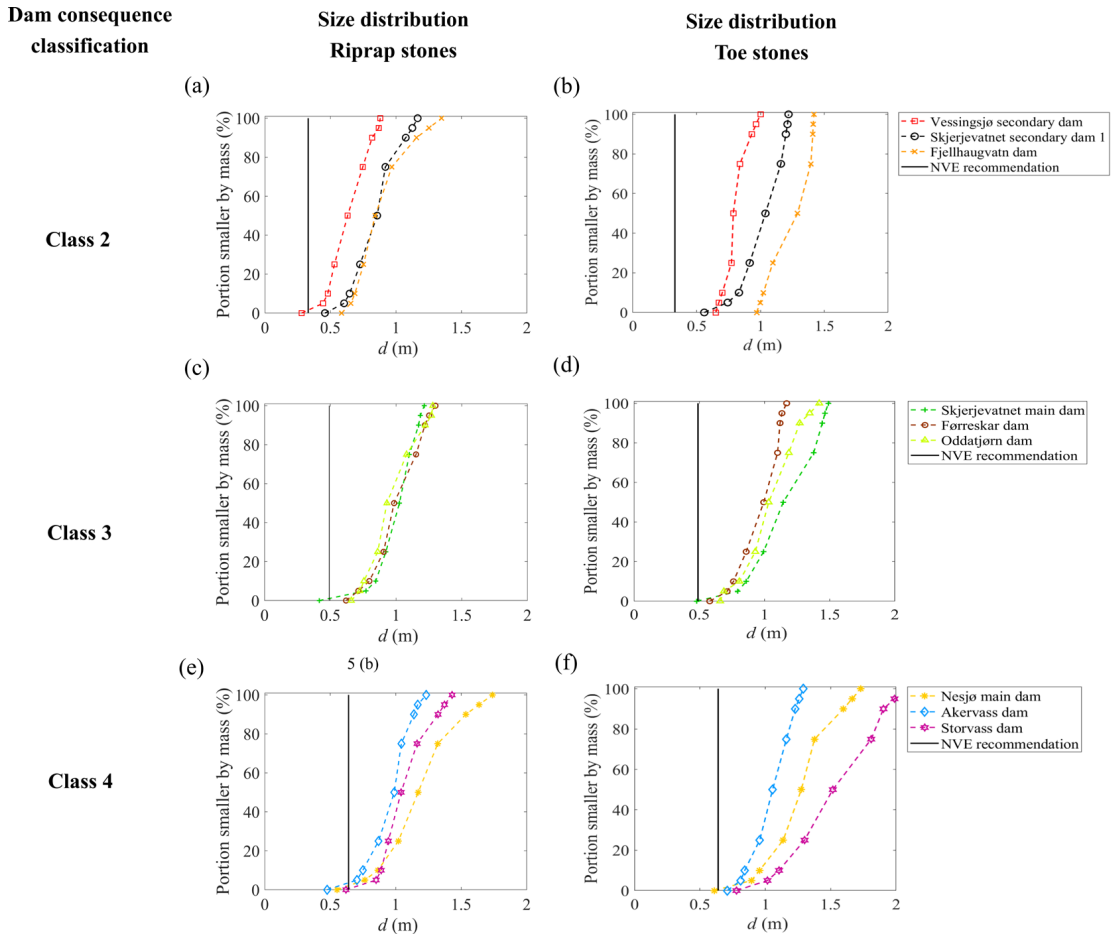

Figure 3. Panels a, c and e present size distributions for riprap stones from dams classified within consequence classes 2, 3 and 4 respectively. Panels b, d and f present size distribution for toe stones from dams classified within consequence classes 2, 3 and 4 respectively.

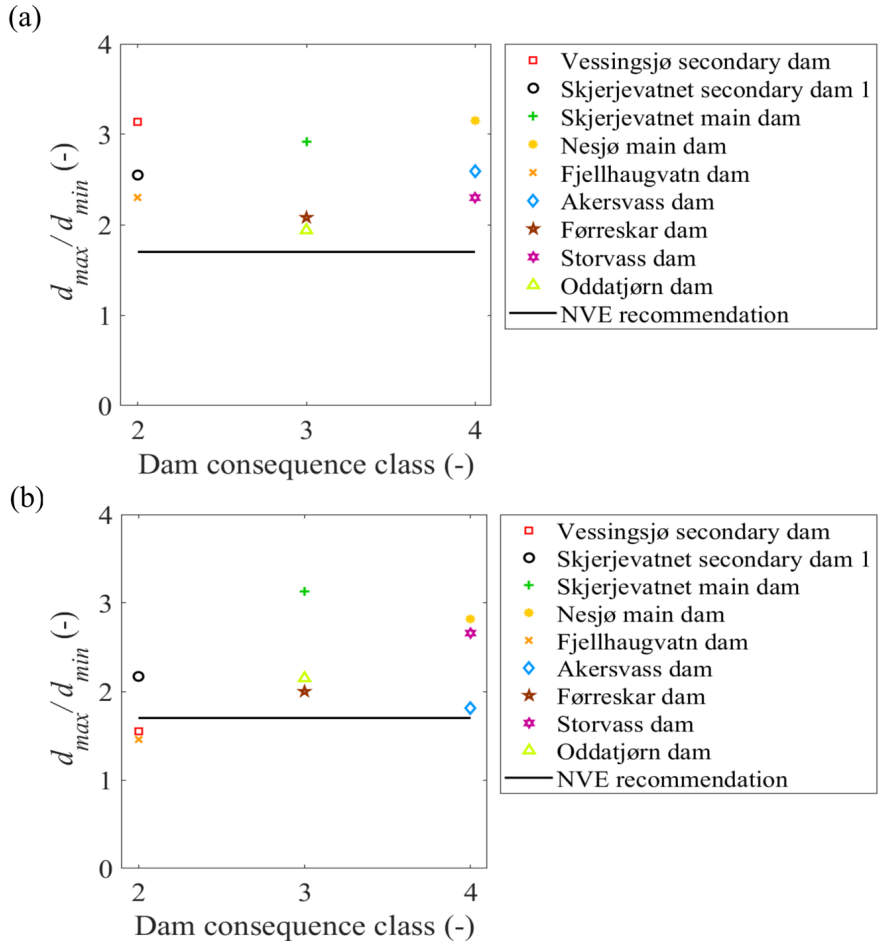

Figure 4. Panel a present plots depicting the ratio of the maximum to minimum stone diameters for the riprap stones for all the surveyed dams. Panel b presents the ratio of the maximum to minimum stone diameter for the toe stones for all the surveyed dams.

stone in line with the technique demonstrated by Hiller (2016). The NVE recommends that the stones should be situated within the bladed to rod shape regimes within the Zingg diagram (Figure 5) in order to ensure optimum interlocking with minimal void formation.

Figures 5a and 5b portray Zingg diagrams for all the measured riprap and toe stones respectively from the surveyed dams. Majority of the measured riprap stones (67 %) lie outside of the NVE specified region within the Zingg diagram with dense clusters formed at the disc to the spheroidal regions (Figure 5a). This was a trend observed also for the toe stones with 69% of the measured toe stones lying outside of the NVE recommended region with cluster formation closely resembling that of the riprap stones (Figure 5b).

3.3 Stone placement and inclination

Measurements of inclination of the stones with respect to the horizontal (β) obtained from field survey of the riprap and the toe stones have been employed to compute the angle of placement of the stones with respect to the downstream slope (α) as part of this study.

Figures 6a and 6b present the computed inclinations (α) for the riprap and the toe stones respectively for all the surveyed dams. The dam index in the respective plots represent the designations assigned for the individual dams as shown in Table 1. As can be inferred, the computed α

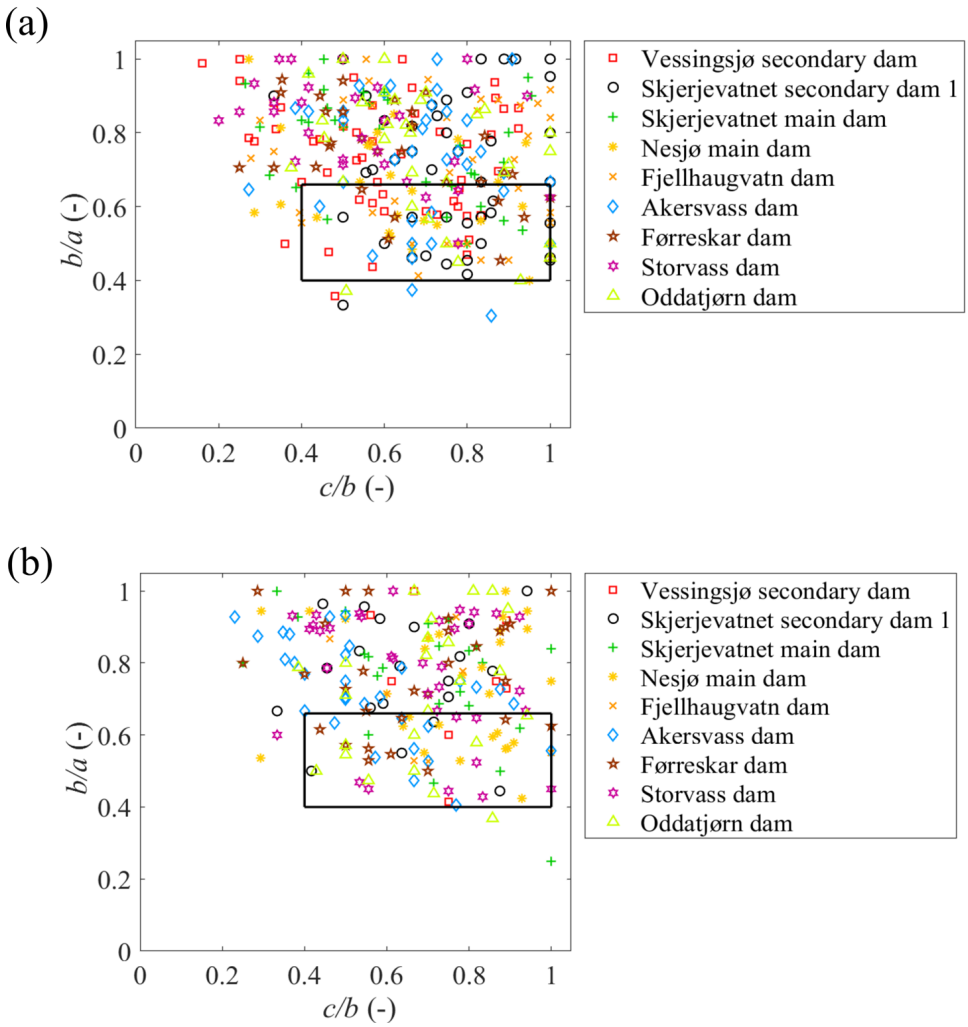

Figure 5. Panel a presents a Zingg diagram for all the measured riprap stones, and panel b presents a Zingg diagram for all the measured toe stones.

angles varied over broad ranges of 30° to 120° for the riprap stones and from 0° to 60° for the toe stones. The average placement inclinations for the riprap and the toe stones from all the surveyed dams were found to be α_{RR} = 56° and α_{T} = 16° with α_{RR} and α_{T} representing mean inclination for the riprap and the toe stones for all the surveyed dams respectively.

As stated in Table 2, the official dam safety guidelines put forward by OED (2009) or NVE (2012) state that the individual riprap stones are to be placed in an interlocking pattern with their longest axis inclined towards the dam. However, no angle of placement for the stones is specified. The conducted field surveys revealed that the riprap stone placement in general were in accordance with this requirement.

4.0 Toe classification

Details concerning toe construction of the placed ripraps charted as part of the present study were recorded during the survey of toe stones placed along the length of the dam toes. Based on these observations, toe conditions for the surveyed dams have been classified into five different categories (Table 3). The following discussions intend to describe the current state of riprap toes and outline various construction

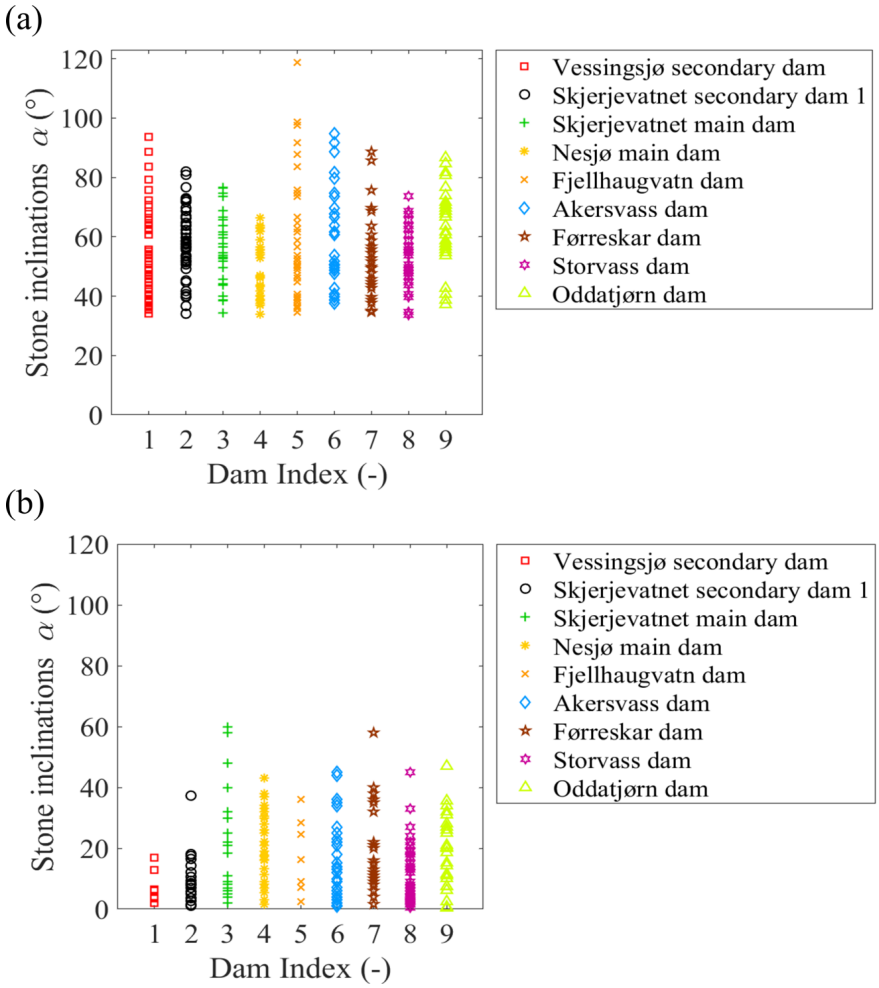

Figure 6. Panel a presents computed inclinations (α) for the riprap stones from all the surveyed dams. Panel b presents computed inclinations (α) for the toe stones from all the surveyed dams.

and stabilizing methods observed during the field inspections.

The first category of riprap toe construction includes ripraps built with no toe support. This entails that the toe stones were either lying on bare rock surfaces or buried underneath moderate amounts of soil cover. Placed ripraps buried with earth/grass cover are considered to have no toe support considering the fact that under overtopping conditions, highly turbulent throughflow and overflow forces would lead to rapid erosion of the soil/grass cover. All the surveyed ripraps can be classified under this category as majority of the toe sections were resting on bare rock surfaces or buried with moderate amount of soil cover. Illustrations of these toe support conditions are presented for dams Fjellhaugvatn, Oddatjørn and Skjerjevatnet main dam in Figure 7a, 7b and 7c respectively. Toe stones at Fjellhaugvatn dam and Skerjavatnet main dam were found to be resting on rock surfaces whereas toe stones at Oddatjørn dam were buried under moderate soil cover.

The second category of observed riprap toe conditions at the surveyed dams consists of submerged riprap toe sections. This was the case at certain reaches of riprap toe sections of Skjerjevatnet main dam and Skerjevatnet secondary dam 1. An illustration of the scenario at Skjerjevatnet main dam is depicted in Figure 7d.

Table 3. Classification of different riprap toe conditions

Category	Description of toe condition	Dam name
1	No toe support	All surveyed dams (Table 1)
2	Submerged toe	Skjerjevatnet main dam Skjerjevatnet secondary dam 1
3	Larger stones at the toe	Fjellhaugvatn dam Storvass dam
4	Tie back rods	Storvass dam
5	Concrete wall	Akersvass dam

Figure 7. Depiction of existing conditions of placed riprap toe sections. Category 1 at dams (a) Fjellhaugvatn dam (b) Oddatjørn dam and (c) Skjerjevatnet main dam. Category 2 at (d) Skjerjevatnet main dam. Category 4 at (e) Storvass dam. Category 5 at (f) Akersvass dam.

Accumulation of water at the downstream toe section of the dams could be due to a variety of causes such as seepage from the dam, snowmelt and rainfall.

Further, the third classification of riprap toe conditions observed was the placement of larger sized stones at the toe section of the riprap. Fjellhaugvatn dam and Storvass dam fall under this category as larger size stones ($d_{50,\,T}$ / $d_{50,\,RR}$ = 1.53 and 1.45 respectively) were found to be placed at the toe sections of these dams. For the rest of the surveyed dams, stone sizing at the toe and the riprap were found to be comparable.

The fourth category of riprap toe construction observed was the use of steel bars for stabilization of the toe stones. A small section of the riprap toe at Storvass dam was observed to be supported employing reinforcing steel bars (Figure 7e) measuring 25 mm in diameter with average outcrop length of 0.3 m. Although majority of the riprap toe sections of Storvass dam were observed to be unsupported, the reinforcing bars were used to stabilize toe sections of the riprap close to the right abutment where the foundation was observed to be at a steep inclination.

At Akersvass dam, a small stretch of the riprap toe section was seen to be supported with a concrete wall (Figure 7f) and this is classified as the fifth riprap toe state observed as part of this field study. The concrete wall was constructed in tandem with a leakage measuring station and hence, it was evident that riprap toe stabilization was not the primary intention of constructing the structure but rather to facilitate leakage measurements from the dam.

5.0 Discussions

The size distributions for the riprap and the toe stones presented as Figure 3 demonstrate that the stones employed for construction are of larger sizing in comparison with NVE recommendations. Further, Figure 4 depicting the ratio of the maximum to the minimum stone dimensions show that sizing of riprap and the toe stones were non-uniform in nature (d_{max} / d_{min} > 1.7) as opposed to the NVE recommended d_{max} / d_{min} < 1.7. Furthermore, majority of the measured riprap and toe stones were found to be disc to spheroidal in shape (Figure 5). These observations are further corroborated by the findings of Hiller (2016). The stone size distribution plots from Hiller (2016) also show that sizing of riprap stones is larger than the NVE recommendations. The d_{max} / d_{min} ratios for the measured riprap stones were documented to be larger than 1.7 in all of the surveyed dams. Further, the Zingg diagrams from the present study correspond well with those documented within Hiller (2016).

As stated in Table 2, the official dam safety regulations (OED, 2009) only stipulate that the downstream slope should have slope protection which ensures that the dam can withstand large overtopping due to accidental loads or damage to the dam and that the stones within the riprap must have satisfactory size and quality and be arranged in a stable manner. It is evident from the outcomes of the present study that the OED (2009) requirements for placed riprap construction have been met at all of the surveyed dams. This is considering that the riprap stones employed for constuction were of sufficient sizing (Figure 3) and the stones were observed to be placed with good interlocking with the longest stone axes towards the dam slopes. Furthermore, analysis results also show that additional recommendations presented within the NVE guidelines with regards to uniformity and angularity of stones are not strictly adhered to. Placed riprap construction is a labor and resource intensive activity and thus can influence overall economical viability of the project. Hence, existing placed riprap constrution practices take into account the most important parameters influencing riprap stability and additional recommendations with regards to uniformity and angularity of stones are not prioritized. This is considering that obtaining large volumes of stones from the quarrey strictly adhering to such criteria can add significant costs to construction.

Analysis of obtained field measurements on riprap and toe stone placement inclinations revealed that the average placement inclinations

for the riprap and the toe stones from all the surveyed dams were found to be $\alpha_{RR} = 56°$ and $\alpha_T = 16°$ respectively. Placement inclinations for toe stones are considerable lower in comparison with riprap stones because ripraps are constructed by placing individual stones commencing at the toe section progressing in the upstream direction. The stones placed at the toe section of the ripraps are generally laid on the ground or at the inclination of the downstream foundation, thereby resulting in low inclinations. Further, stones are placed at incremental inclinations progressing upwards, resulting in higher stone inclinations with respect to the dam slope. Furthermore, findings from large scale field tests conducted by Lia et al. (2013) show that placing riprap stones at an inclination of $\alpha \approx 60°$ resulted in considerable stability gain as compared to stones placed at flatter inclinations. Hence, existing placement techniques for placed riprap stones can be considered as adequate from a stability point of view.

Riprap toe stones at Fjellhaugvatn dam and Storvass dam were found to be of relatively larger size as compared with the riprap stones ($d_{50,T} / d_{50,RR} \approx 1.5$). Certain sections of the riprap toes at Skjerjevatnet main dam and Skerjevatnet secondary dam 1 were found to be in a submerged state. A small section of the riprap toe at Storvass dam was observed to be supported employing tie back rods. Further, at Akersvass dam, a small stretch of the riprap toe section was seen to be supported with a concrete wall.

Albeit the sizing of the toe stones are comparatively larger than the riprap stones at Fjellhaugvatn dam and Storvass dam ($d_{50,T} / d_{50,RR} \approx 1.5$), they can still be considered of comparable scale. Further, Fjellhaugvatn dam is constructed in a narrow channel thereby giving rise to possibility of flow concentration at the dam toe under throughflow and overtopping conditions. To achieve favorable degree of toe stability, adoption of more robust toe support structures would be necessary. Further, certain reaches of riprap toe sections of Skjerjevatnet main dam and Skerjevatnet secondary dam 1 were found to be in submergence states. However, raised downstream water level elevates the point of exit of the phreatic surface (under which the rockfill dam is saturated with water) of the seepage water under throughflow or overtopping conditions, in turn resulting in exposure of larger area of the downstream riprap to flow forces. Raising tail water level can also lead to issues with leakage measurements from the dams. Further, 25 mm steel bars were employed to stabilize the key stones at a certain stretch of riprap toe at Storvass dam with steep foundation inclination. Considering that Storvass dam is a 90 m high rockfill dam with riprap comprised of stones of the order of $d_{50} = 1$ m, use of such reinforcement bars can be considered to offer insignificant stability increment against overtopping flow forces. Furthermore, a concrete retaining wall has been constructed along a small reach of the riprap toe section at Akervass dam. Although this may offer certain degree of resistance against hydrodynamic forces in case of accidental overtopping events, the capacity of the wall to withstand the high magnitude hydrodynamic forces needs to be ascertained.

Observations made with regards to toe support conditions for placed ripraps on the surveyed dams suggest that none of the ripraps are currently equipped with well-defined toe support structures. Since the current understanding of failure mechanisms of placed ripraps stems from experimental investigations conducted on model ripraps with fixed toe supports, it seems necessary to investigate the importance of toe support in discerning the failure mechanism and in turn, overall stability of placed ripraps. To address this concern, experimental overtopping tests on model placed ripraps with unconstrained toe sections have been recently conducted at the hydraulic laboratory of NTNU, Trondheim. Investigation outcomes suggest sliding as the failure mechanism in placed ripraps without a fixed toe support in contrast with the buckling failure mechanism described by Ravindra et al. (2019) for the same placed riprap model coupled with a fixed toe support structure. Further, the average ratio of failure discharges for placed ripraps with and without

toe supports was found to be 4.2 suggesting significant reduction in stability. Furthermore, critical discharges for placed ripraps without toe support were found to be similar to those for dumped ripraps whereas Hiller et al. (2018a) documented ratios of failure discharges between 5 and 10 between placed ripraps with toe supports and dumped ripraps. Toe support was found to have minimal effect on stability of dumped ripraps. Further details in this regard will be presented within a seperate article.

These observations suggest that toe support conditions can have significant impact on overall stability of placed ripraps. Since existing placed ripraps on Norwegian rockfill dams are constructed without any form of toe support, it is essential to stabilize toe sections of these structures to enhance overall stability. Further experimental investigations in this regard to arrive at ideal methods for providing toe support for existing placed ripraps is recommended.

6.0 Conclusions

This study is intended at shedding light on a key issue related to placed riprap stability which can place findings from experimental studies into a practical framework and also facilitate further research in this study discipline. This article presents findings from a field survey conducted to investigate construction aspects of placed ripraps on rockfill dams. Key parameters describing quality of placement of riprap and toe stones such as size, shape and inclination with respect to the dam slope have been analysed as part of this study. Details concerning existing state of toe conditions for the surveyed riprap structures have been outlined. Further, conformity of construction practices with Norwegian dam safety guidelines is also addressed.

Study findings suggest that construction practices adopted for placed ripraps meet the requirements of Norwegian dam safety regulations. However, investigation outcomes also show that construction practices adopted at present do not prioritize on addressing additional recommendations put forward by the dam safety authorities with regards to placed riprap stability. Furthermore, observations from the present study document the fact that placed ripraps built on Norwegian rockfill dams are currently not equipped with well-defined toe support structures stabilizing the toe stones. However, outcomes from recent experimental tests conducted at the hydraulic laboratory of NTNU, Trondheim suggest configuration of the toe section of placed riprap as a key factor influencing the overall failure mechanism in placed ripraps exposed to overtopping flows. Hence, it is essential to stabilize toe sections of existing placed riprap structures to enhance overall stability. Further experimental investigations in this regard to arrive at design criteria for the toe support of existing placed ripraps is recommended.

Acknowledgements

The authors acknowledge the financial support provided by HydroCen, Norway. The support and co-operation offered by all the dam owners BKK, SKL and Statkraft during the field surveys is greatly appreciated.

References

Dornack, S., 2001. Uberstrombare Damme-Beitrag zur Bemessung von Deckwerken aus Bruchsteinen/ Overtopping dams-Design criteria for riprap. PhD thesis, Tech. Univ. Dresden.

Hiller, P.H., 2016. Kartlegging av plastring på nedstrøms skråning av fyllingsdammer. Trondheim.

Hiller, P.H., Aberle, J., Lia, L., 2018a. Displacements as failure origin of placed riprap on steep slopes. J. Hydraul. Res. 56, 141–155.

Hiller, P.H., Lia, L., Aberle, J., 2018b. Field and model tests of riprap on steep slopes exposed to overtopping. J. Appl. Water Eng. Res. 0, 1–15.

Hyllestad, E., 2007. Retningslinjer for fyllingsdammer. Presentasjon under EBLs vårmøte 23.5.2007: Norges vassdrags- og energidirektorat.

Knauss, J., 1979. Computation of maximum discharge at overflow rockfill dams (a comparison of different model test results), in: 13th Congress on Large Dams. pp. 143–159.

Larsen, P., Bernhart, H.H., Schenk, E., Blinde, A., Brauns, J., Degen, F.P., 1986. Uberstrombare Damme,

Hochwasserentlastung uber Dammscharten/ Overtoppable dams, spillways over dam notches. Unpubl. Rep. Prep. Regierungsprasidium Karlsruhe Universita.

Lia, L., Vartdal, E.A., Skoglund, M., Campos, H.E., 2013. Riprap protection of downstream slopes of rockfill dams-a measure to increase safety in an unpredictable future climate. Eur. Club Symp. Int. Com. Large Dams.

Midttømme, G.H., Isomäki, E., Meyer, A.E., Bartsch, M., 2012. Regulations and guidelines for dam safety in Finland , Norway and Sweden, in: ICOLD, European Club. Venice, Italy.

Morán, R., Toledo, M.Á., Larese, A., Monteiro-alves, R., 2019. A procedure to design toe protections for rock fi ll dams against extreme through- fl ows 195, 400–412.

NVE, 2012. Veileder for fyllingsdammer. Nor. Water Resour. Energy Dir. 21–25.

OED, 2009. Forskrift om sikkerhet ved vassdragsanlegg (Damsikkerhetsforskriften). Oljeog energidepartementet.

Peirson, W.L., Jens, F., Steven E, P., Ronald J, C., 2008. Placed Rock as Protection against Erosion by Flow down Steep Slopes. J. Hydraul. Eng. 134, 1370–1375.

Ravindra, G.H.R., Sigtryggsdottir, F.G., Lia, L., 2019. Buckling analogy for 2D deformation of placed ripraps exposed to overtopping. J. Hyd. Res.

Ravindra, G.H.R., Sigtryggsdottir, F.G., Lia, L., 2018a. Evaluation of Design Criteria for Downstream Riprap of Rockfill Dams, in: Proceedings of the 26th Congress on Large Dams. Vienna.

Ravindra, G.H.R., Sigtryggsdottir, F.G., Lia, L., 2018b. Protection of embankment dam toe and abutments under overtopping conditions, in: 3rd International Conference on Protection against Overtopping, UK.

Solvik, O., 1991. Throughflow and stability problems in rockfill dams exposed to exceptional loads. Sixt. Int. Congr. Large Dams 333–343.

Sommer, P., 1997. Uberstrombare Deckwerke/ Overtoppable erosion protections. Unpubl. Rep. No. DFG-Forschungsbericht La 529/8-1 Universita.

Zingg, T., 1935. Beitrag Zur Schotteranalyse, Doctoral Thesis, ETH Zurich.

Paper III

Failure mechanism in placed riprap on steep slope with unsupported toe.

Ravindra, G.H.R, Gronz, O, Dost, B and Sigtryggsdottir, F.G (2020).

Engineering structures, Volume 221, DOI: https://doi.org/10.1016/j.engstruct.2020.111038

Engineering Structures 221 (2020) 111038

Contents lists available at ScienceDirect

Engineering Structures

journal homepage: www.elsevier.com/locate/engstruct

Description of failure mechanism in placed riprap on steep slope with unsupported toe using smartstone probes

Ganesh H.R. Ravindra[a,*], Oliver Gronz[b], Bastial Dost[b], Fjóla G. Sigtryggsdóttir[a]

[a] Department of Civil and Environmental Engineering, S P Andersens veg 5, Norwegian University of Science and Technology, Trondheim 7031, Norway
[b] Department of Physical Geography, Behringstraße/Campus II, Trier University, 54296 Trier, Germany

ABSTRACT

This article is aimed at investigating the influence of toe support conditions on stability aspects of placed ripraps on steep slopes exposed to overtopping flows. All past experimental model studies investigating placed riprap stability under overtopping conditions have been conducted with ripraps constrained at the toe section. However, ripraps constructed on the downstream slopes of rockfill dams are generally not provided with any form of toe support. Hence, it is of importance from stability and economical standpoints to understand the failure mechanism in placed ripraps with realistic toe support conditions. This article presents findings from experimental overtopping tests conducted on model placed ripraps unsupported at the toe section. Employing Smartstone probes, a new technology in stone movement monitoring, laser measurement techniques and Particle Image Velocimetry (PIV) techniques, detailed description of failure mechanism in placed ripraps under overtopping conditions is presented within this study. Study findings demonstrate sliding as the underlying failure mechanism in placed ripraps with unsupported toes. Further, comparison of experimental results with past findings revealed that placed ripraps with unrestrained toes experience a fivefold reduction in stability, characterized by the critical overtopping magnitude as compared with placed ripraps provided with fixed toe supports. Furthermore, toe support conditions were found to have no effects on either the failure mechanism nor the overall stability of dumped ripraps. Further research is recommended to arrive at well-defined methodologies for design and construction of toe supports for placed ripraps.

1. Introduction

Ripraps are widely used as erosion protection measures against the impacts of currents and waves for various hydraulic structures such as river banks, bridge piers, upstream and downstream slopes of embankment dams, spillways, dykes and breakwaters (e.g. [9,7,30,1,11,25;12]). One application of ripraps within the discipline of dam engineering is to protect the downstream slopes of embankment dams against erosion due to accidental leakage or overtopping events [31]. Ripraps can be broadly classified as either dumped or placed based on the adopted method of construction. Dumped ripraps consist of randomly dumped stones whereas placed ripraps comprise of stones arranged in an interlocking pattern [7]. In order to increase the resistance against erosion from accidental leakage and overtopping events, the downstream slopes of rockfill dams built in Norway are secured with single layer placed ripraps (Fig. 1). The individual riprap stones are to be placed in an interlocking pattern with their longest axis inclined towards the dam [19] and [18]. Many rockfill dams are poised to be upgraded in the near future due to enforcement of more stringent dam safety regulations. This in turn necessitates refurbishment of placed ripraps constructed on these dams. Hence, it is of relevance from stability and economical standpoints to better understand the stability aspects of placed ripraps under overtopping conditions and this forms the primary focus of this study.

Investigation of stability aspects and failure mechanisms in placed ripraps is an intricate task as the failure process is influenced by multitudes of parameters. Factors such as riprap material properties, interlocking effect generated between the individual riprap elements, frictional forces setup at the riprap-filter interface, toe support conditions and overtopping flow magnitude and directionality can have significant influence in discerning the failure characteristics. Placed ripraps exposed to overtopping can undergo failure in several forms such as sliding of the riprap structure, erosion of individual elements leading to exposure of the underlying filter, toe scouring and 2D deformations leading to structural failure. Hence, understanding of these various failure mechanisms is essential to achieve efficient design of these structures.

Available literature describing the stability aspects of placed ripraps under overtopping conditions is rather limited as compared with the extensive research database available with respect to design and construction of dumped ripraps. Notable contributors to the research area of placed riprap design are Hiller et al. [7], Peirson et al. [21], Dornack [2], Sommer [26] and Larsen et al. [13]. An in-depth literature review into the state of the art in placed riprap design is presented within Hiller

* Corresponding author.
E-mail addresses: ganesh.h.r.ravindra@ntnu.no (G.H.R. Ravindra), gronz@uni-trier.de (O. Gronz), s6jodost@uni-trier.de (B. Dost), fjola.g.sigtryggsdottir@ntnu.no (F.G. Sigtryggsdóttir).

https://doi.org/10.1016/j.engstruct.2020.111038
Received 23 November 2019; Received in revised form 10 June 2020; Accepted 29 June 2020

Nomenclature

a, b, c	longest, intermediate and shortest axes lengths of riprap stones respectively
C_u	coefficient of uniformity
d_i	riprap stone diameter corresponding to i% finer
$d_{i,f}$	filter stone diameter corresponding to i% finer
H_p	height of the horizontal platform
L_s	riprap chute length
n	number of discharge steps
N	number of riprap stones per unit riprap surface area
P	packing factor
q_c	critical unit discharge
q_i	unit discharge at i^{th} step
q_m	combined discharge capacity of the pumps
S	slope (V: H)
t	time
u, v, w	orthogonal Smartstone axes
w_p	width of the horizontal platform
x, y, z	coordinate axes for riprap
α_u, α_v, α_w	respective angles between the u, v, w axes and the gravity vector.
β	angle of a-axis of riprap stones with respect to the slope
ρ_s	density of riprap stones
$\rho_{s,F}$	density of filter stones
Δq	discharge steps
Δt	time interval

et al. [7]. Majority of these past experimental model studies have been aimed at comprehending the underlying 1D failure mechanism in placed ripraps exposed to overtopping flows on mild to moderately steep slopes, S = 0.125 (1:8) to 0.50 (1:2). Furthermore, Hiller et al. [7] conducted experimental overtopping tests on model placed ripraps to analyse the 1D failure mechanism in placed ripraps on a steeper slope, S = 0.67 (1:1.5). These studies concluded that unidirectional stone displacements along the chute direction leading to formation of a gap at the upstream section of the riprap was the underlying failure mechanism in placed ripraps. Also, Hiller et al. [7] stated that placing riprap stones in an interlocking pattern resulted in significant stability gain as compared to randomly dumped riprap. Furthermore, Ravindra et al. [24] continued the experimental research conducted by Hiller et al. [7] to assess 2D failure mechanism in placed ripraps on steep slopes S = 0.67 (1:1.5). Ravindra et al. [24] concluded progressive stone displacements in 2D resulting in buckling like deformation of the riprap structure as the underlying failure mechanism in placed ripraps with restrained toes.

All past studies investigating stability aspects of placed riprap under overtopping conditions have been carried out with ripraps constrained at the toe section with fixed toe support structures. In large-scale practical applications, toe sections of ripraps could be supported employing several toe stabilization techniques. Commencement of riprap construction from a trench excavated into the rock foundation at the toe section, placement of larger size stones at the toe section, increasing the size (volume) of the toe section, and toe blocks of concrete anchored to the foundation with rockbolts or similar, represent some of the toe stabilization measures. Fixed toe support entails enhanced resistance against sliding at the riprap toe section. However, a field survey of existing state of toe support conditions for placed ripraps constructed on several Norwegian rockfill dams was conducted by Ravindra et al. [23] and the study findings demonstrated that none of the surveyed ripraps were currently provided with well-defined toe support measures. Majority of placed riprap toe sections were found to be either lying on bare rock surfaces or buried underneath moderate amounts of soil cover (Fig. 1). Furthermore, several past studies investigating rockfill dam and riprap stability aspects under overtopping conditions such as Morán et al. [17], Jafarnejad et al. [8], Javadi and Mahdi [10] and Morán and Toledo [16] have demonstrated toe section of rockfill dams and ripraps as a critical location for initiation of progressive dam failure. Thus, conducting experimental overtopping investigations on model placed ripraps with realistic toe support conditions is of significance to obtain representative findings concerning the stability aspects of placed ripraps exposed to overtopping flows. This would also facilitate evaluation of the validity of findings from past research works describing stability of placed ripraps under overtopping conditions.

Fig. 1. Placed riprap constructed on Dam Oddatjørn, Suldal, Norway.

This article presents findings from experimental overtopping tests conducted on model placed ripraps unsupported at the toe section. This study is aimed at investigating the influence of toe support conditions on stability aspects of placed ripraps on steep slopes exposed to overtopping flows. Using Smartstone probes[5], a new technology in stone movement monitoring, laser measurement techniques and Particle Image Velocimetry (PIV) techniques, detailed description of failure mechanism in placed ripraps unsupported at the toe is presented within this study. Furthermore, results from this investigation are evaluated against past findings describing stability of placed ripraps exposed to overtopping.

2. Experimental setup and testing program

2.1. Physical model description

A conceptual 1:10 model setup comprising of a single-layered placed riprap section of width w = 1 m and chute length of L_s = 1.8 m constructed over a base frame inclined at a steep slope of 1:1.5 (S = 0.67) was originally designed and constructed by Hiller [6] at the hydraulic laboratory of NTNU, Trondheim, Norway. The setup was designed assuming Froude similarity. This experimental testing facility was further employed in past studies investigating stability aspects of placed ripraps on steep slopes such as Hiller et al. [7] and Ravindra et al. [24]. However, this model consisted of a fixed metallic toe support structure fastened to the base frame at the downstream end of the riprap chute providing resistance against sliding of the riprap structure. A modified version of the model setup originally designed by Hiller [6] was adopted in the present study, wherein the fixed toe support structure was replaced with a horizontal platform at the downstream extremity of the riprap chute to facilitate construction of placed riprap models with unrestrained toes (Fig. 2). The modifications to the

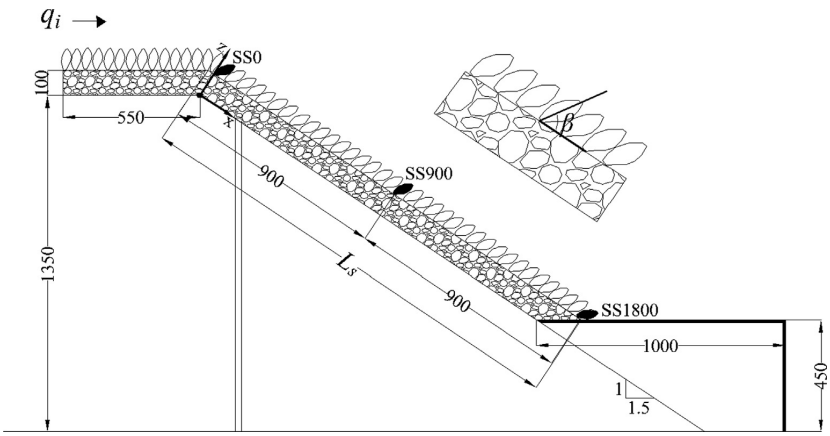

Fig. 2. Illustration of experimental setup of model placed riprap with chute length of L_s = 1.8 m along with portrayal of inclination angle (β) of a-axis of the stones with respect to the chute direction (All measurements in mm). The riprap stones mounted with the smartstone probes are represented as SS_x with x representing distances to the respective stones from the origin along the x-direction.

experimental rig were so designed as to maintain the original dimensioning of the riprap structure as used in past studies such as Hiller et al. [7] and Ravindra et al. [24] to enable comparison of experimental findings.

The model setup was constructed within a 25 m long, 2 m high and 1 m wide horizontal flume. Discharge to the flume was supplied by pumps with a combined capacity of q_m = 0.4 $m^2\ s^{-1}$. The pumps were equipped with Siemens Sitrans Mag 5000 (Nordberg, Denmark) discharge meters and controlled by valves [7] and [24]. The test setup consisted of a base frame comprising of a 0.55 m long horizontal crest and a 2.43 m long chute along the flow direction, inclined at S = 0.67 (1:1.5) (Fig. 2). A horizontal platform with height H_p = 0.45 m and width w_p = 1 m was coupled with the base frame to facilitate placement of ripraps with unrestrained toes (Fig. 2). The platform also helped elevate the downstream end of the riprap against the flume bottom to avoid backwater effects. This is considering that that the focus of the investigation was on erosion of riprap due to overtopping and not failure due to scour development at the transition to the tail water zone. The surface of the horizontal platform was covered with a layer of geotextile to provide realistic friction for the toe stones. The model setup was located sufficiently downstream of the inflow section to ensure calm flow conditions upstream of the test ripraps [24].

For the construction of model ripraps, quarry stones of rhyolite [14] with median diameter of d_{50} = 0.057 m and density of ρ_s = 2710 kg m^{-3} were used. The median riprap stone size was computed as $d_{50} = (abc)^{1/3}$ averaged over a sample size of 500 stones, where a, b and c represent the longest, intermediate and shortest axis respectively. The respective axes lengths were manually measured employing a calliper and the mean values were recorded as a = 0.091 m, b = 0.053 m and c = 0.038 m. The riprap stones could be considered angular to sub-angular with average $a\ b^{-1}$ = 1.7 and uniformly graded with $C_u = d_{60}\ d_{10}^{-1}$ = 1.17. Test ripraps were placed on a 0.1 m thick filter layer comprised of geotextile and angular stones of size $d_{50,f}$ = 0.025 m and density $\rho_{s,f}$ = 3050 kg m^{-3}. The dimensions of the filter and the riprap were chosen in accordance with guidelines offered by the Norwegian Water Resources and Energy Directorate [18].

Overtopping tests were carried out with both placed and dumped ripraps to better understand the fundamental differences and similarities in failure mechanisms between the two structures (Fig. 3). The test ripraps covered the 0.55 m long horizontal crest and the 1.8 m long chute. Placed riprap models were constructed by manual placement of stones in an interlocking pattern commencing at the toe, progressing upstream to the crest (Fig. 3a). The individual riprap stones were deliberately placed with the longest axis (a-axis) inclined at $\beta \approx 60^\circ$ with respect to the chute bottom and at an inclination of $\beta \approx 90^\circ$ on the horizontal crest to account for practical considerations (Fig. 2) [15]. It should be noted that the last row of riprap stones, which constitute the toe of the riprap were placed flat on the horizontal platform ($\beta \approx 0^\circ$) (Figs. 2 and 3). Subsequent rows of stones were placed at incremental inclinations to attain the required stone inclinations of $\beta \approx 60^\circ$. This was also in alignment with the findings from field surveys of riprap toes conducted by Ravindra et al. [23], wherein mean placement inclinations (β) for the toe stones were found to be much lower in comparison with those for the riprap stones. Further, single layer dumped ripraps were constructed by randomly dumping the riprap stones on the slope with arbitrary orientations and without any interlocking pattern (Fig. 3b).

Riprap stones placed on the horizontal crest cannot be considered part of the riprap structure. This is considering that the riprap stones placed on the steep slope are exposed to higher destabilizing forces as compared with stones on the horizontal crest [24]. Hence, riprap stones

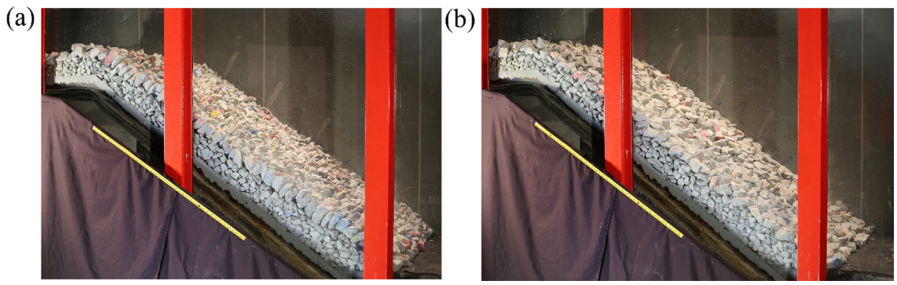

Fig. 3. Depiction of experimental model setups with (a) placed and (b) dumped ripraps at the hydraulic laboratory of NTNU, Trondheim, Norway.

covering the 0.55 m horizontal crest are not considered part of further analysis in this study and are incorporated within the model setup to simulate realistic flow transitions from the crest onto the riprap structure.

The packing factor (P) originally defined by Olivier [20] has been utilized in several past investigations concerning placed riprap stability to obtain a quantitative measure of density of riprap stone placement as this can have an impact on overall riprap stability. This has further been incorporated within this study as Eq. (6).

$$P = \frac{1}{N\, d_{50}^{2}} \tag{6}$$

where N represents the number of stones per m^2 surface area of the riprap and d_{50} signifies the median stone size. P is lower for a placed riprap compared to dumped riprap [7].

2.2. Laser traverse system

A 3D laser traverse system situated overhead of the model setup was employed to measure location co-ordinates of select riprap stones. The traverse operated within a 3D Cartesian coordinate system with its origin situated at the transition from the horizontal crest to the inclined chute (Fig. 2). The x-axis was aligned in a direction parallel to the chute (33.7° to the flume bottom) pointing in the downstream direction and the z-axis was set perpendicular to the chute. Measurement accuracies were ± 0.1 mm and ± 1 mm in the x and z-directions respectively. Stone displacements were considered only along the x and z-directions as any possibility of encountering lateral flows prompting stone displacements in the y-direction was ruled out [7] and [24].

2.3. Smartstone probes

Monitoring of stone movements prior to and during structural collapse of the riprap is of importance to gain better understanding of the underlying failure mechanism. However, due to flow aeration in the model and the sudden nature of riprap collapse, conventional stone displacement measurement techniques could not be used for monitoring stone motions during the tests. To obtain quantitative descriptions of stone displacement in the tested riprap structures prior to and during riprap failure, new technology in stone displacement monitoring named as Smartstone probes (Smartstone probe v2.1) (Fig. 4), developed at the University of Trier, Germany has been used within this study.

It is an advancement from the former version that was presented by Gronz et al. [5]. The current probe features thre triaxial sensors manufactured by Bosch Sensortec GmbH. The BMI 160 [4] is placed centric within the Smartstone probe and holds the acceleration sensor (ACC) and the gyroscope (GYR). The measuring range of the current ACC is increased from ± 4 g to ± 16 g (1 mg noise) within the present Smartstone version from the earlier probe version 1.1. The GYR records rotational velocity within the range of ± 2000 $^{\circ}s^{-1}$ (0.04 $^{\circ}s^{-1}$ noise). Additionally, it contains the magnetic sensor (MAG) BMC 150 [4], which has not been put to use in this study.

Motion data and the corresponding time stamps are stored on a 1 MB internal memory. Data can be read out wirelessly by means of active radio frequency identification (active RFID) technology. Moreover, the entire communication between a computer and the sensor is carried out via RFID and an USB-gateway. A software with graphical user interface (GUI) allows for easy handling and control of different sensor settings (sampling rate, record threshold etc.). The current probe version is encased in a 50 mm long and 10 mm wide plastic tube that is sealed at the ends with plastic plugs. Due to the non-metal casing, an internal antenna can be installed, which makes the probe more practicable under experimental conditions. Energy for recording and data exchange is supplied by a standard 1.5 V button cell (type AG5). The Smartstone probe prototype was designed and manufactured in cooperation with the company Smart Solutions Technology GbR, Germany and is still under further development.

The length of the plastic tube is variable, so the battery can be adapted to a specific application. The button cell is small resulting in the length of 50 mm. But its capacity is limited to one run of the experiment and should thus be replaced after each run. Data transmission after the experimental run further contributes towards exhaustion of battery life. For other applications with larger stones, a longer plastic tube and an AAAA battery could be used, allowing for more than one year of active waiting for trigger. The memory size allows for up to 8 min of constant movement with 100 Hz sampling rate. Commencement of data acquisition is marked by exceedance of stone movements over a user-defined threshold.

In order to equip select riprap stones with Smartstone probes within the present study, cylindrical holes of diameter 10 mm and length 50 mm were drilled within the stones utilizing a mechanical drill. The drill holes were aligned with the longest stone axes (a-axes). The probes were encased in watertight rubber envelopes and mounted within the cylindrical drill holes. The openings were further sealed using waterproof sealing agents.

Three riprap stones were mounted with Smartstone probes and placed within the test ripraps at the crown, the center and at the toe sections of the riprap structure. Stones implanted with the probes are herein referred to as 'Smartstones'. This was to monitor stone movements at these locations as this could provide details regarding initiation and progression of riprap failure. The respective stones were identified as SS_0, SS_{900} and SS_{1800} (Fig. 2) respectively with the indices representing the distance to the respective stones from the origin along the x-direction. The selected stones were located along the centreline of the flume (y = 0.5) to address concerns of wall effects.

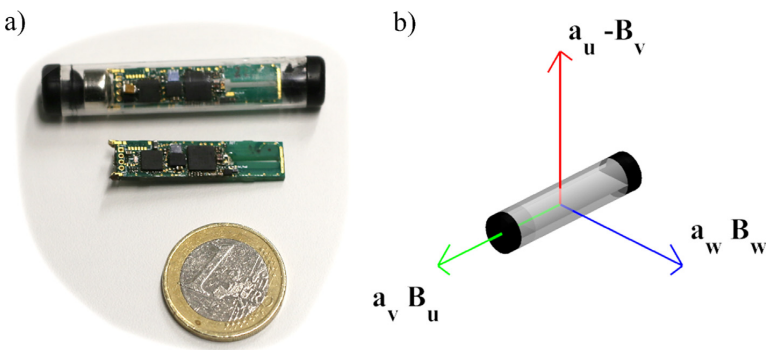

Fig. 4. (a) The Smartstone probe in a plastic tube with button cell on the left end and the circuit board with sensors underneath. (b) The probe's coordinate system.

2.4. Particle Image Velocimetry (PIV)

High-speed video footages of the overtopping tests were recorded over the course of the experimental testing program. The video footages were in turn subjected to Particle Image Velocimetry (PIV) analysis to enable cross corroboration of investigation results. PIV analysis allows for estimation of the velocity distribution in image pairs. The direction and the velocity of particles in these image pairs result from cross-correlation functions. The tool PIVlab [28,29,27,3], which is available for MATLAB was implemented to carry out the analysis. The recorded video footages were split into images and were further stored as single greyscale images within the PIV toolbox using MATLAB's rgb2gray function. The distance between the bars at the flume's sidewalls was used to calibrate distance. Besides this, PIVlab's standard parameterization was used in the analysis.

2.5. Testing methodology

In previous studies such as Hiller et al. [7] and Ravindra et al. [24], overtopping tests on model placed and dumped ripraps with toe support were conducted by exposing the riprap structures to incremental overtopping flows in step-wise increments of $\Delta q = 0.02–0.05\ m^2\ s^{-1}$ over specific time intervals of $\Delta t = 1800$ s. However, due to limitations with the Smartstone probes with respect to battery life and inbuilt memory, adoption of similar testing methodology as employed within previous investigations to conduct extended overtopping tests was not possible within the present study. Hence, testing methodology was modified to accommodate the limitations of the probes. This was done also considering changes in the behavior of placed riprap models with unsupported toes concerning deformations and critical discharges.

To begin with, several pilot overtopping tests with placed and dumped ripraps were conducted without incorporation of the Smartstone probes. Details from illustrative tests, P01 and D01 conducted with placed and dumped ripraps respectively are presented in Table 1. The pilot tests on model ripraps were carried out by exposing the riprap structures to incremental overtopping with discharge steps of $\Delta q = 0.02\ m^2\ s^{-1}$. The initial overtopping discharge magnitude was set to $q_i = 0.02\ m^2\ s^{-1}$ as this was the minimum required flow to achieve submergence of the riprap stones. The discharge levels were maintained constant over regular time intervals of $\Delta t = 1800$ s.

The 3D location co-ordinates of several marked stones were measured in between overtopping steps using the 3D laser traverse system as described within Hiller et al. [7] and Ravindra et al. [24]. This procedure was further repeated over n discharge steps until ultimate riprap collapse was achieved (q_c). The critical overtopping magnitudes for placed and dumped ripraps were consistently found to $q_c = 0.06$ and $0.04\ m^2\ s^{-1}$ respectively. The pilot tests provided measurements regarding riprap deformations prior to failure initiation and also, probable critical discharges for initiation of irreversible riprap collapse.

Further, for tests conducted with placed and dumped ripraps implanted with Smartstone probes, the riprap structures were directly exposed to the critical discharge (q_c) levels obtained from the pilot tests in order to achieve riprap failure in the shortest possible time. This was to obtain measurements regarding the motion of riprap stones during riprap collapse, also accommodating limitations of the Smartstone probes. Furthermore, video footages from the tests were captured using a high-speed camera stationed next to the viewing gallery of the flume. In essence, the adopted testing procedure results in measurements describing motion of the riprap stones prior to and during riprap collapse thereby providing a comprehensive description of the underlying failure mechanisms in the tested placed and dumped ripraps.

3. Results

3.1. Stability aspects

Details regarding the experimental testing program are presented within Table 1. The table presents particulars regarding construction and testing procedures adopted for experiments conducted on placed (P01 - P06) and dumped (D01 - D03) ripraps. The critical overtopping discharge levels for initiation of irreversible riprap failure (q_c) were found to be higher for placed ripraps as compared with dumped ripraps. Unraveling riprap failures were found to be initiated at overtopping discharge magnitudes of $q_c = 0.06\ m^2\ s^{-1}$ and $0.04\ m^2\ s^{-1}$ respectively for placed and dumped ripraps (Table 1). This ratio of critical discharge values between placed and dumped ripraps was hence found to be 1.5.

Further, the 2D deformations within placed riprap structures were analyzed with respect to incremental overtopping discharge magnitudes using laser measurements of location co-ordinates of six marked stones. Reference is made to Ravindra et al. [24] for further details regarding the analysis procedure. Analysis results revealed that the marked riprap stones placed on the riprap chute underwent only minor displacements along and normal to the chute direction (x and z axes respectively) prior to initiation of progressive riprap failure. Further, the toe stones placed on the horizontal platform experienced insignificant downstream displacements along the platform surface. Furthermore, no definite correlations were found between the stone displacements and the overtopping discharge magnitudes.

3.2. Initiation and progression of riprap failure

As stated previously, the Smartstone probes were employed within this study to better understand the mechanisms of failure initiations and progression in placed and dumped ripraps with unsupported toes. Also, Particle Image Velocimetry (PIV) analysis using the recorded video footages (provided as a supplementary video file) were also conducted to further validate results derived from the Smartstones. Cumulative results from the analyses conducted implementing these two techniques are presented herein.

Referring to Table 1, tests P02 - P06 and D02 - D03 were carried out with Smartstones on placed and dumped ripraps respectively. Prior to exposure of the riprap structure to overtopping, the Smartstone probes were configured to record measurements of accelerations and orientations using the in-built accelerometer and gyroscope. The data acquisition protocol was set to commence upon reaching a threshold trigger acceleration of 48 mg, as this would limit excessive recording of minor stone vibrations prior to failure initiation thereby preserving battery life and memory. Data acquisition rates for the probes were set to 100 Hz. Measurements from Smartstone probes implanted within stones identified as SS_0, SS_{900} and SS_{1800} (Fig. 2) were further time synchronized to enable comparison of measurements between sensors in time to gain a better understanding of stone displacements at different locations within the riprap structures.

Table 1
Description of the experimental testing procedure.

Test	P_e (-)	q_i ($m^2\ s^{-1}$)	n (-)	Δt (s)	q_c ($m^2\ s^{-1}$)
P01*	0.53	0.02–0.06	3	1800	0.06
P02	0.53	0.06	1	–	0.06
P03	0.54	0.06	1	–	0.06
P04	0.48	0.06	1	–	0.06
P05	0.49	0.06	1	–	0.06
P06	0.52	0.06	1	–	0.06
D01*	0.91	0.02 – 0.04	2	1800	0.04
D02	0.83	0.04	1	–	0.04
D03	0.74	0.04	1	–	0.04

* Pilot tests conducted without incorporation of the Smartstone probes.

3.2.1. Phases of riprap failure

Detailed analysis of the accelerometer and gyroscope data revealed that riprap failure takes place in uniquely identifiable phases. To illustrate the sequence of events leading up to and further progressing as total riprap collapse, depictions of stone acceleration and orientation measurements for an overtopping test conducted on a model placed riprap are presented as Fig. 5). Recorded measurements from the Smartstone placed at the riprap crest (S_0 from Fig. 2) from test P05 are portrayed in Fig. 5. Further, the individual phases of stone motions within the time series are labelled with capital letters. To better illustrate the failure mechanism, a video footage demonstrating the initiation and progression of placed riprap failure has been provided as a supplementary video file along with the article.

Phase A: Upon exposure to overtopping flow, the water level upstream of the model increases and eventually overtops the riprap structure. The start of Phase A ($t = 0$) represents the trigger point of the probe subsequent to which the probe initiates the data recording protocol. That is, at $t = 0$, the water flow reaches a magnitude that results in accelerations of the sensor-equipped stone that exceed the pre-set acceleration threshold of 48 mg. This acceleration can be a result of minor changes in stone inclination by fractions of a degree, as a change of inclination changes the fraction of gravity measured along each probe axis. This effect can be considered a consequence of vibrations generated due to initial flow attack on the stone. The threshold trigger acceleration was set to 48 mg within our tests basing on results from pilot tests. This can be considered an important parameter as setting a high threshold would lead to the risk of missing out on data gathering during riprap failure and a low threshold could result in filling up of the internal sensor memory prior to riprap failure. Hence, it was of essence to conduct pilot studies to discern the optimal threshold acceleration magnitude based on the experimental conditions. Further, the concerned riprap stone was found to not undergo major displacements during the remainder of phase A. Similar observations were made for Smartstones placed at the centre (S_{900}) and at the toe of the riprap (S_{1800}).

Before the next phase is described, influence of gravity on the probe's measurements should be explained. Under stationary conditions, acceleration measurements from the probes along each axis only shows a fraction of the gravitational acceleration, depending on the angle between this axis and the gravity vector (pointing vertically downwards). Let α_u be the angle between the probe u-axis and the gravity vector, α_v be the angle between the v-axis and the gravity vector and α_w be the angle between the w-axis and the gravity vector. If the stone is not moved at all, acceleration measurements from the probes along these axes will then show $a_u = \cos(\alpha_u) \cdot 1$ g, $a_u = \cos(\alpha_v) \cdot 1$ g and $a_w = \cos(\alpha_w) \cdot 1$ g. Resulting from this, small changes in the sensor's orientation are visible in changing levels of readings of the three axes. Further, if the sensor is moved, the acceleration readings will represent the sum of the gravity induced accelerations and those induced due to stone movements. Furthermore, there is only one possible scenario that results in zero measurements from the probes along all the measurement axes: free fall.

Phase B: The hydrodynamic drag and lift forces generated by incremental overtopping flows reach higher magnitudes resulting in strong vibrations as can be seen from the accelerometer plot in Fig. 5. The mean deviation in accelerations from the average acceleration values are between 0.095 g and 0.102 g for the u and w probe axes respectively. The impinging flow forces and the resulting vibrations further lead to small reorganizations of the stones within the riprap structure, as demonstrated by minor changes in stone inclinations. These are visible within the acceleration plots for the u and w axes (the blue and red lines) presented in Fig. 5. These are on different levels prior to phase B and almost on the same level after phase B. This entails that the stone underwent rotation along the u-w plane to attain a final configuration for Phase C. This conclusion can also be further corroborated through inspection of the video footage that reveals that during phase B, the riprap layer in its entirety undergoes slight compaction and the stones experience changes in orientation, tilting towards the downstream direction. The Smartstone placed at the centre (S_{900}) of the riprap displays a similar behaviour. However, the stones placed at the toe (S_{1800}) do not appear to experience significant displacements or rotations during this phase. These observations are also in line with

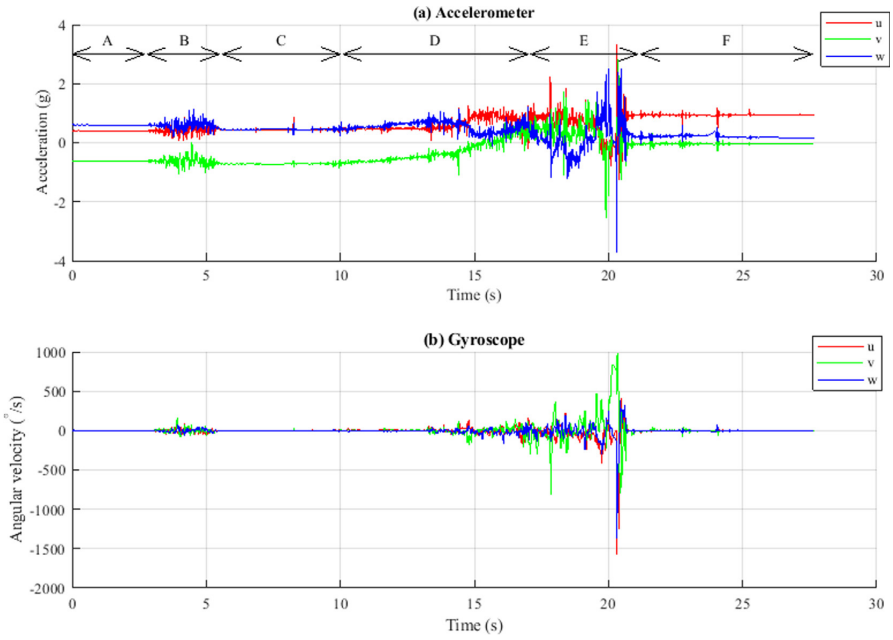

Fig. 5. Depictions of (a) accelerometer and (b) gyroscope measurements from the Smartstone placed at the riprap crest (S_0) from test P05.

findings from section 3.1 wherein 2D displacements of select stones prior to riprap collapse were monitored by adopting the laser traverse system. Only minor displacements along and normal to the chute direction (x and z axes respectively) were recorded prior to failure initiation.

Phase C: After this initial readjustment phase leading to compaction of the riprap structure, there is a phase of relative rest with only occasional single small spikes in the acceleration data. In this phase, the overtopping flow magnitude is gradually increasing.

Phase D: The failure begins quite slowly during several seconds with a tilting of the stones in the riprap layer. This tilting is visible by the changing levels of the different acceleration time series. It can be observed that the absolute values at the v axis (green line) gradually decrease while the w axis values increase (blue line). Thus, the sensor's end indicated by the blue w axis moves downwards. This effect is also documented in the video as the whole top layer tilts within this phase of failure initiation.

Phase E: Initiation of progressive collapse of the riprap structure, which will be further discussed in greater depth using more detailed depictions (Fig. 6).

Phase F: The riprap stones further collapse to form a pile on top of the horizontal platform. The pile is still overrun by water, resulting in small spikes in measurements. The pile is continually undergoing rearranged as a consequence of flow attack after a pause of several seconds.

In Fig. 6, the collapse (phase E of Fig. 5) is shown in detail. In the accelerometer plot, the resultant (black line) and the filtered resultant (thick grey line) are overlaid. The resultant is the length of the vector $u + v + w$ (without sign). If the sensor is not moved, the resultant is always 1 g (gravity). In any other case, the value will be the sum of gravity and the accelerations resulting due to displacements of the stone. In free fall and without aerodynamic drag, resultant acceleration of 0g is expected. Further, as sporadic spikes in data impede the interpretation of the resultant, the filtered resultant is also added in Fig. 6. For the resultant, a high pass has been applied (removes gravity) and afterwards a low pass has been applied (smooths spikes). The high pass removes low frequencies and constant components from the time series. This is mainly the gravity induced fraction of the signal as long as the stone is not moving or only vibrating or moving at constant velocity. Afterwards, a low pass has been applied, which removes single peaks and high frequency noise from the signal. In the filtered resultant, stationary periods, accelerations and decelerations are much easier to identify as a sequence.

The collapse begins slowly at approximately 17.5 s. The filtered resultant acceleration plot shows increasing magnitudes of up to 0.37 g at 18.4 s. Afterwards, it decreases to almost 0 g, indicating a constant collapse velocity. At 19.7 s, the filtered resultant increases again as this represents the instant when the Smartstone reaches the pile which has been formed on the horizontal platform. It seems to rebound from the pile at 20 s, as a small period of free fall is visible afterwards between 20.2 and 20.3 s (u, v and w axes show nearly 0 g). This assumption is also supported by the strong acceleration peaks observed subsequently, when the stone impacts with the pile once again. During the rebound, the stone rotates quickly at $800°s^{-1}$, which lasts for 0.2 s. Finally, the stone remains somewhere on or within the pile. The orientation is different from before the collapse, as the different acceleration levels in the axes in phases A and F in Fig. 5 indicate.

The acceleration and the gyroscope measurements were subjected to further analysis to derive displacement velocities of the Smartstone during riprap failure. The initial position and the gyroscope data were used to account for stone rotations within the acceleration data. Using integration of the acceleration values, a velocity time series was obtained. The resulting velocity plot is shown in Fig. 7. The probe-equipped stone is seen to be gradually accelerated, reaching velocities of up to 0.66 m s^{-1} at $t = 19.7$ s. When the stone reaches the pile formed on the horizontal platform, rapid decelerations can be observed.

A brief summary of salient features of the different phases involved in the failure process of placed ripraps as detailed previously has been presented within Table 2 for easy reference.

The velocities derived from Smartstone data should be further

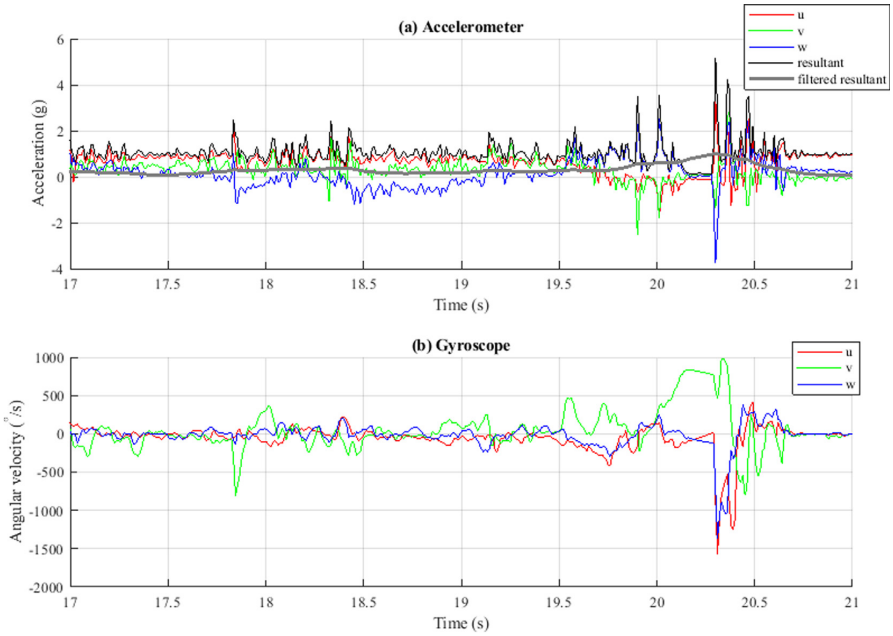

Fig. 6. Detailed plots of (a) accelerometer and (b) gyroscope measurements from the Smartstone placed at the riprap crest (S_0) from test P05 during total riprap collapse (Phase E).

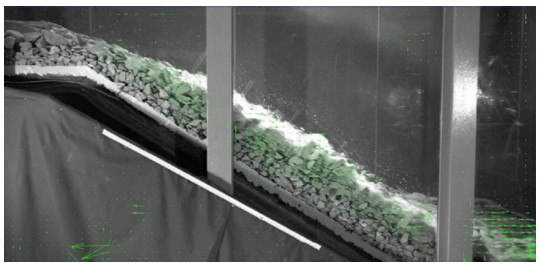

Fig. 7. Single frame from PIV analysis. Green vectors indicate direction of flow and the length indicate the velocity (From Test P05).

confirmed using different techniques. To accomplish this, Particle Image Velocimetry (PIV) analysis was conducted on the video footage (Supplementary video file) to obtain velocity distributions during the overtopping test. For each frame, the estimated velocities are stored in a matrix for the horizontal component and a second matrix for the vertical component. Fig. 7 shows a sample frame, where the matrix cell's resultant is represented by vectors. A cell next to the bar approximately in the center of the frame and in the middle of the stone layer was selected. The peak of the time series of the PIV-derived velocities (Fig. 8) in this cell were compared to Smartstone derived velocities. In all runs that were compared, excellent correlation between the Smartstone derived maximum velocities and the PIV derived peak velocities were observed. Deviations between PIV and Smartstone velocities ranged between 0.01 and 0.06 m s^{-1}.

In total, three runs of placed ripraps and three runs of dumped ripraps were examined. The observations in these two groups were found to be similar within each group and also the differences between the groups are obvious. The general findings are: Placed ripraps collapse was found to occur more abruptly than dumped ripraps. The peak velocities were also found to be higher (between 0.66 and 1.008 m s-1) for placed ripraps as compared with velocities computed for dumped ripraps (between 0.31 and 0.52 m s-1). Also, placed riprap acceleration time series show more frequent and higher magnitude peaks, while the gyroscope time series show less rotations. This in turn entails that placed ripraps are characterized by high degree of vibrations within the riprap structure and that placed ripraps collapse as a unit in the sense that the whole riprap layer slides down the slope as a unified structure. However, for dumped ripraps, less acceleration peaks were visible and significantly higher stone rotations were recorded by the gyroscope. This further suggests that dumped riprap failures entail lower degree of vibrations and that the failure progresses randomly with erosion of individual stones from the slope.

4. Discussions

4.1. Description of the failure mechanism

Cumulative analysis of data obtained from different independent measurement techniques such as laser tracking, Smartstones and video records provide a comprehensive description of the underlying failure mechanism in placed ripraps with unsupported toes. As demonstrated by the gyroscope and the accelerometer data sets, placed riprap stones experience minor degree of reorientations and displacements along the downstream chute direction following initial exposure of the riprap structure to overtopping flows (Phases A and B in Fig. 5). These observations were further supported by inspection of the video footage, which revealed that during phase B, the riprap layer as a whole undergoes compaction and reorganization along the downstream direction. Furthermore, monitoring of stone displacements using the 3D laser traverse system also support these findings as minor displacements along the x and z axes were recorded prior to failure initiation. These can be explained as a consequence of the manual stone placing efficiency during construction of the riprap models. Although individual stones are manually placed one after another, the riprap structure could be loosely packed with intermediate voids. Hence, upon initial exposure to overtopping, the incremental hydraulic drag and lift forces and the resulting vibrations lead to rearrangements of the individual stones wherein the riprap structure undergoes compaction to fill the voids. Similar observations describing compaction of placed riprap structures upon exposure to initial low magnitude overtopping flows were also documented within Ravindra et al. [24].

Further during phase C (Fig. 5), no displacements or reorientations of the riprap stones were observed. This entails that upon undergoing minor deformations leading to compaction of the riprap structure, the individual stones achieve a stable configuration leading to the formation of a unified structure. This can be explained as due to generation of interlocking forces between the individual riprap stones. With further increments in overtopping magnitude, the riprap structure is exposed to higher destabilizing hydraulic forces. These are in part transferred on to the underlying filter layer as frictional forces. The remainder is directed towards the riprap toe where the static frictional forces setup between the toe stones and the geotextile membrane laid on the horizontal platform increase in magnitude to counter the incremental hydrodynamic forces transferred towards the toe. Furthermore, initiation of riprap collapse marks the point of time at which the magnitude of the impacting hydrodynamic forces exceed the limiting values of the static frictional forces between the toe stones and the horizontal platform. This frictional yield results in displacements of the toe stones and following this event, the riprap structure in its entirety undergoes a progressive slide on the underlying filter layer, further forming a pile on the flume bottom.

Siebel [25], Dornack [2], Sommer [26] and Larsen et al. [13] investigating the 1D behavior of placed ripraps stated that the interlocking of riprap stones allows for the transfer of longitudinal forces

Table 2
Different phases involved in the failure of placed ripraps with unsupported toes.

Phase	Features
A	• Exposure to overtopping leading to submergence of the riprap structure. • The flow forces result in accelerations of the sensor-equipped stone exceeding the pre-set threshold of 48 mg.
B	• Incremental hydrodynamic drag and lift forces lead to strong vibrations. • These result in small reorganizations of the stones within the riprap structure. • The toe stones do not experience significant displacements or rotations.
C	• Period of relative rest during exposure to incremental overtopping.
D	• The failure begins during several seconds with tilting of the stones in the riprap layer.
E	• Initiation and further progression of collapse of the riprap structure.
F	• The riprap stones further collapse to form a pile on top of the horizontal platform. • The pile continually undergoes rearrangements as a consequence of flow attack after a pause of several seconds.

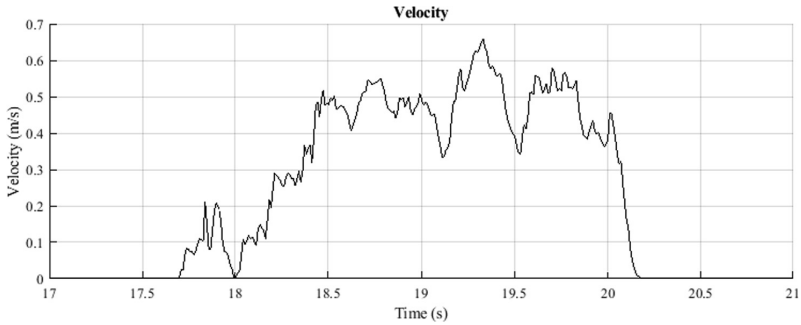

Fig. 8. Smartstone probe derived velocity for Smartstone (SS_0) from Test P05.

within the placed ripraps. They concluded that these forces, when large enough, could either cause sliding or rupture of the riprap layer. This paper describes sliding as the underlying failure mechanism in placed ripraps with unsupported toes. However, Ravindra et al. [24] demonstrated a buckling like structural collapse as the failure mechanism in placed ripraps on steep slopes provided with fixed toe support. Juxtaposition of these two disparate failure mechanisms helps bring out the importance of toe support conditions in discerning the failure mechanism in placed ripraps. In case of a constrained toe structure as adopted in Ravindra et al. [24], the riprap structure is likely to fail as a consequence of structural collapse or buckling as the toe support structure provides unlimited resistance stabilizing the toe, in turn eliminating the possibility of sliding of the riprap structure. Under such conditions, the riprap structure experiences some degree of compaction during initial stages of overtopping exposure and further, following the formation of a unified riprap structure, incremental overtopping flows give rise to development of progressive 2D deformation profiles in ripraps resembling the buckling process in a slender-long column as demonstrated by Ravindra et al. [24]. However, in case of an unrestrained toe, the placed riprap section slides along the steep slope as a result of limited frictional resistance offered at the toe section. Hence, the current investigation explains that the configuration of the toe section of placed riprap as a key factor influencing the overall failure mechanism. Further, Hiller et al. [7] investigated 1D displacement of riprap stones in placed riprap with supported toes and showed that compaction of the riprap structure at the downstream end leads to formation of a gap at the upstream crest of the riprap. However, this was not observed within this study as the limited frictional forces setup at the interface between the toe stones and the horizontal platform do not allow for such a high degree of compaction to occur. The riprap structure experiences sliding failure due to toe yield before any major compaction or 2D deformation of the riprap structure could occur.

It was earlier demonstrated that dumped and placed ripraps are characterized by distinct failure mechanisms when exposed to overtopping. Dumped ripraps were found to go through a surface erosion process where individual stones were eroded by the action of destabilizing turbulent flow forces. This was in contrast to failure initiation in placed ripraps wherein the riprap structure as a whole was found to undergo a slide. This difference in the failure mechanisms can be described as due to the absence of interlocking forces between individual riprap stones. Since dumped ripraps comprise of randomly arranged stones, individual stones are not interlocked with the adjacent elements. When the dumped riprap structure is exposed to overtopping flow forces, the individual stones counter the flow attack primarily through self-weight of the individual elements and the bottom frictional forces generated at the riprap-filter interface. Failure initiation marks the instant at which the magnitude of the destabilizing hydrodynamic forces exceed the resultant of the stabilizing self-weight and the frictional forces. Hence, dumped riprap failure can be stated as the resultant of progressive unraveling erosion of individual riprap elements whereas placed riprap failure entails sudden slide of the entire riprap structure. This also provides an explanation for higher velocities measured for stone displacements in placed ripraps during failure as compared to dumped riprap stones. Placed ripraps experience an instantaneous slide following toe yield wherein the riprap structure moves down the slope as a unit. Whereas dumped riprap failure entails erosion of discreet riprap elements wherein individual stones suffer collisions with one another during the erosion process thereby resulting in loss of kinetic energy. Further, placed riprap failures were found to be initiated at higher overtopping magnitudes as compared with dumped ripraps. As a combined effect of these two causes, placed riprap stones travel on the slope at higher velocities than dumped riprap stones. Furthermore, a similar mode of failure was described for dumped ripraps within Hiller et al. [7] wherein model studies were conducted with placed ripraps provided with fixed toe supports. This in turn suggests that toe support conditions have no effect on the failure mechanism in dumped ripraps exposed to overtopping.

4.2. Importance of toe support for riprap stability

The critical overtopping discharge magnitudes for initiation of riprap collapse (q_c) were found to be $q_c = 0.06\ m^2\ s^{-1}$ and $0.04\ m^2\ s^{-1}$ for placed and dumped ripraps respectively constructed with stones of dimension $d_{50} = 0.057$ m within the present experimental study (Table 1). Considering Froude scaling with a scaling ratio of 1:10, for ripraps built with stones of mean diameter of $d_{50} = 0.57$ m at the prototype scale, the critical overtopping discharges would translate to $q_c = 1.9\ m^2\ s^{-1}$ and $1.3\ m^2\ s^{-1}$ respectively for placed and dumped ripraps with unsupported toes. This in turn entails that placed ripraps unsupported at the toe offer 1.5 times higher stability, characterized by the critical overtopping magnitude as compared with dumped riprap. Past experimental studies conducted on placed riprap models provided with fixed toe supports such as Hiller et al. [7], Peirson et al. [22], Dornack [2] and Larsen et al. [13] have also demonstrated that placed ripraps offer higher stability as compared to dumped riprap, especially at steep slopes. Hiller et al. [7] conducted experimental overtopping investigations with 1: 10 scale model placed ripraps with fixed toe supports constructed with riprap stones of average diameter $d_{50} = 0.057$ m. Hiller et al. (2018a) documented average critical overtopping magnitudes of $q_c = 0.30\ m^2\ s^{-1}$ and $0.04\ m^2\ s^{-1}$ respectively for placed and dumped ripraps ($9.5\ m^2\ s^{-1}$ and $1.3\ m^2\ s^{-1}$ respectively at the prototype scale) resulting in a ratio of average critical discharge values of 7.5. The fivefold reduction in placed riprap stability in terms of average critical overtopping discharge magnitude required to achieve placed riprap from $q_c = 0.30\ m^2\ s^{-1}$ within Hiller et al. [7] to $q_c = 0.06\ m^2\ s^{-1}$ within the present study can be attributed to the absence of a toe support structure. At prototype scales, this would entail a reduction in critical overtopping magnitude from $q_c = 9.5\ m^2$

s^{-1} to 1.9 m^2 s^{-1}. However, dumped riprap stability can be stated as being unaffected by toe support conditions as the critical discharge for failure initiation remained constant at $q_c = 0.04$ m^2 s^{-1} between model setups (1.3 m^2 s^{-1} at prototype scales). These findings further add to the earlier statement that toe support conditions can have considerable impacts on placed riprap stability and not on the stability aspects of dumped ripraps.

4.3. Smartstones

The Smartstone probes represent state of the art technology in stone movement monitoring. Adoption of this sophisticated technique within the experimental model setup facilitated in obtaining better understanding of the failure mechanisms in placed and dumped ripraps exposed to overtopping. The probes have been found to be versatile and reliable with broad ranging capabilities. A major advantage of the technique is concerning elimination of undesirable effects on flow hydraulics within the model. Results from the present study clearly demonstrate that the Smartstones probes are capable of capturing several important details regarding initiation and progression of failure in ripraps such as acceleration and angular velocities of the stones thereby providing an overarching picture of the underlying failure mechanisms. However, the probes currently face limitations with regards to limited battery life and internal memory capabilities. Further improvements to the probes addressing these limitations could greatly enhance potential for implementation of the probes within practical and experimental applications.

4.4. Limitations and recommendations

- The experimental testing program employed within this study utilizes a distinct setup with placed riprap models built on a steep slope, $S = 0.67$ (1:1.5) with angular stones ($a\,b^{-1} = 1.7$) placed at an angle of $\beta = 60^{\circ}$. Validity of experimental results considering different material properties and construction methods should be studied in future investigations to address scaling concerns and to improve confidence for wide-ranging applicability of study findings.
- The packing factor (P_c) values for the tests incorporated in this study vary within a narrow range of 0.49–0.54 for placed ripraps and hence, detailed evaluation of the influence of P_c on overall placed riprap stability is not possible from this study. Further research in this regard is recommended in future investigations.
- Investigation of impacts of air-entrainment on overall riprap stability is beyond the scope of the present study and inclusion of this as a study parameter in future research works is recommended.
- With respect to scaling of study findings, large-scale overtopping field tests with placed ripraps constructed on rockfill slopes are recommended to evaluate the validity of the observed failure mechanism at larger scales.
- Toe support conditions for placed ripraps have been demonstrated as a key factor influencing the overall failure mechanism. Further research to arrive at design criteria and solutions as well as construction methodologies for riprap toes is highly recommended for future investigations.

5. Concluding remarks

This study adds to the state of the art within the study discipline of placed riprap stability exposed to overtopping conditions. The investigation is aimed at obtaining better understanding of the importance of toe support conditions on stability aspects of placed ripraps through experimental overtopping tests conducted on 1:10 scale model placed riprap structures with unsupported toes constructed on steep slopes of 1:1.5 (vertical: horizontal slope dimensions).

Employing Smartstone probes, the state of the art in stone movement monitoring, detailed description of the underlying failure mechanism in placed ripraps with unsupported toes is presented. Study findings demonstrate sliding as the underlying failure mechanism in placed ripraps with unsupported toes. This was found to be the resultant of limited frictional resistance available at the toe section of the riprap. The sliding failure observed within this study for placed ripraps with unsupported toes was in contrast to the buckling like 2D structural deformations documented within Ravindra et al. [24] for placed ripraps provided with fixed toe supports. Further, comparison of critical discharge magnitudes from the present study with those of Hiller et al. [7] revealed that placed ripraps with unrestrained toes experience a five-fold reduction in stability as compared with placed ripraps provided with fixed toe supports. Further, toe support conditions were found to have no effects on either the failure mechanism or the overall stability of dumped ripraps.

Findings from the present study suggest that toe support conditions can have significant impact on the overall stability aspects of placed ripraps under overtopping conditions. However, recent findings from Ravindra et al. [23] revealed the fact that existing placed ripraps built on rockfill dams are generally not provided with any well-defined form of toe support. Findings from the present study lead to the conclusion that coupling existing riprap structures with toe supports can lead to considerable gain in overall stability. Since multitude of rockfill dams are poised to be upgraded in the near future, arriving at criteria and measures for the toe support design and construction is of significance from placed riprap stability standpoint. Hence, further research addressing this vital feature influencing placed riprap stability is highly recommended.

CRediT authorship contribution statement

Ganesh H.R. Ravindra: Conceptualization, Methodology, Investigation, Writing - original draft, Writing - review & editing. **Oliver Gronz:** Software, Formal analysis, Investigation, Data curation, Visualization. **Bastial Dost:** Software, Formal analysis, Investigation, Data curation, Visualization. **Fjóla G. Sigtryggsdóttir:** Conceptualization, Methodology, Writing - original draft, Writing - review & editing.

Declaration of Competing Interest

The authors declare that they have no known competing financial interests or personal relationships that could have appeared to influence the work reported in this paper.

Acknowledgements

The authors acknowledge the financial support offered by HydroCen, Norway. The support and co-operation from Dr. Priska Helene Hiller, NVE, Norway and Prof. Jochen Aberle, TU Braunschweig, Germany in designing the original experimental setup is appreciated. The authors appreciate the assistance of Dr. Andreas Krein, Luxembourg Institute of Science and Technology. The authors would also like to thank the MSc student Malin F Asbølmo for the assistance offered during the experimental testing program.

Appendix A. Supplementary material

Supplementary data to this article can be found online at https://doi.org/10.1016/j.engstruct.2020.111038.

References

[1] Abt SR, Thornton CI, Scholl BA, Bender TR. Evaluation of overtopping riprap design relationships. J Am Water Resour Assoc 2013;49(4):923–37.
[2] Dornack S. Überströmbare Dämme – Beitrag zur Bemessung von Deckwerken aus Bruchsteinen/ Overtopping Dams-Design Criteria for Riprap PhD thesis Technische

Universitat Dresden; 2001.
[3] Garcia D. A fast all-in-one method for automated post-processing of PIV data. Exp Fluids 2011;50:1247–59.
[4] Bosch Sensortech GmbH. “BMC150 and 150”; 2019. URL: https://www.bosch-sensortec.com/bst/products/all_products/bmc150, https://www.bosch-sensortec.com/bst/products/all_products/bmc160, retrieved: 15/Oct/2019.
[5] Gronz O, et al. Smartstones: A small 9-axis sensor implanted in stones to track their movements. Catena 2016;142:245–51.
[6] Hiller PH. Riprap design on the downstream slopes of rockfill dams. Doctoral Thesis. Trondheim: Norwegian University of Science and Technology; 2017.
[7] Hiller PH, Aberle J, Lia L. Displacements as failure origin of placed riprap on steep slopes. J Hydraul Res 2018;56(2):141–55.
[8] Jafarnejad M, Franca MJ, Pfister M, Schleiss AJ. Time-based failure analysis of compressed riverbank riprap. J Hydraul Res 2017;55(2):224–35.
[9] Jafarnejad M, Franca MJ, Pfister M, Schleiss AJ. Design of riverbank riprap using large, individually placed blocks. J Hydraul Eng 2019;145(12):1–12.
[10] Javadi N, Mahdi T-F. Experimental investigation into rockfill dam failure initiation by overtopping. Nat Hazards 2014;74:623–37.
[11] Khan D, Ahmad Z. Stabilization of angular-shaped riprap under overtopping flows. World Acad Sci, Eng Technol, Int J Civil, Environ, Struct, Construct Architectural Eng 2011;5(11):550–4.
[12] Kobayashi N, Jacobs BK. Riprap stability under wave action. J Waterw Port Coastal Ocean Eng 1985;111(3):552–66.
[13] Larsen P, et al. Uberstrombare Damme, Hochwasserentlastung Uber Dammscharten/ Overtoppable Dams, Spillways over Dam Notches. Unpublished report prepared for Regierungsprasidium Karlsruhe Universita; 1986.
[14] Lev V, Anantharamu V. Estimating the elastic properties of mica and clay minerals. Geophysics 2020;85(2). MR83–95.
[15] Lia, Leif, Vartdal EA, Skoglund M, Campos HE. Riprap protection of downstream slopes of rockfill dams-a measure to increase safety in an unpredictable future climate. European club symposium of the international comission on large dams; 2013.
[16] Morán R, Toledo MA. Reserarch into protection of rockfill dams from overtopping using rockfill downstream toes. Can J Civ Eng 2011;38(12):1314–26.
[17] Morán, Rafael, Miguel Á Toledo, Antonia Larese, and Ricardo Monteiro-alves. 2019. “A Procedure to Design Toe Protections for Rock Fi Ll Dams against Extreme Through- Fl Ows.” 195: 400–412.
[18] NVE. Veileder for fyllingsdammer/guidelines for rockfill dams. Norwegian water resources and energy directorate; 2012. 21–25.
[19] OED. Forskrift Om Sikkerhet Ved Vassdragsanlegg (Damsikkerhetsforskriften). Oljeog Energidepartementet; 2009.
[20] Olivier, Henry. Through and overflow rockfill dams-new design techniques. Proc Inst Civil Engineers; 1967. p. 433–71.
[21] Peirson WL, Figlus J, Pelles SE, Cox RJ. Placed rock as protection against erosion by flow down steep slopes. J Hydraul Eng 2008;134(9):1370–5.
[22] Peirson WL, Jens F, Pells Steven E, Cox RJ. Placed rock as protection against erosion by flow down steep slopes. J Hydraul Eng 2008;134:1370–5.
[23] Ravindra GHR, Sigtryggsdottir FG, Asbølmo MF, Lia L. Toe support conditions for placed ripraps on rockfill dams- a field survey. Vann 2019;3.
[24] Ravindra GHR, Sigtryggsdottir FG, Lia L. Buckling analogy for 2D deformation of placed ripraps exposed to overtopping. J Hydraul Res 2020.
[25] Siebel R. Experimental investigations on the stability of riprap layers on overtoppable earthdams. Environ Fluid Mech 2007;7(6):455–67.
[26] Sommer P. Überströmbare Deckwerke/ Overtoppable Erosion Protections. Unpublished report No. DFG-Forschungsbericht La 529/8-1 Universita; 1997.
[27] Thielicke W. The flapping flight of birds summary and conclusions PhD Thesis Rijksuniversiteit Groningen; 2014.
[28] Thielicke W, Stamhuis EJ. PIVlab - Time-Resolved Digital Particle Image Velocimetry Tool for MATLAB (Version: 2.02). Published under the BSD license, programmed with MATLAB 7.0.246 (2014): R14; 2014.
[29] Thielicke, William, Stamhuis Eize J. PIVlab – towards user-friendly, affordable and accurate digital particle image velocimetry in MATLAB; 2014.
[30] Thornton CI, Abt SR, Scholl BN, Bender TR. Enhanced stone sizing for overtopping flow. J Hydraul Eng 2014;140(4):06014005–9.
[31] Toledo MÁ, Moran R, Onate E. Dam protection against overtopping and accidental leakage. London: CRC Press/Balkema; 2015.

Paper IV

Non-linear flow through rockfill embankments

Ravindra, G.H.R., Sigtryggsdottir, F.G and Høydal, Ø (2019).
Journal of Applied Water Engineering and Research, 7:4, 247-262,
DOI: https://doi.org/10.1080/23249676.2019.1683085.

Non-linear flow through rockfill embankments

GANESH H R RAVINDRA, PhD Candidate, *Department of Civil and Environmental Engineering, Norwegian University of Science and Technology (NTNU)*, *Trondheim, Norway*

Email: ganesh.h.r.ravindra@ntnu.no (author for Correspondence)

FJOLA G SIGTRYGGSDOTTIR, Associate Professor, *Department of Civil and Environmental Engineering, Norwegian University of Science and Technology (NTNU), Trondheim, Norway*

Email: fjola.g.sigtryggsdottir@ntnu.no

ØYVIND A HØYDAL, Principal Engineer, *Norwegian Geotechnical Institute (NGI), Oslo, Norway*

Email: oyvind.armand.hoydal@ngi.no

Running Head: Non-linear flow through rockfill embankments

Non-linear flow through rockfill embankments

ABSTRACT

This article considers experimental data from throughflow investigations conducted on rockfill dams and adds to the state of the art in the study discipline of non-linear flow through rockfill medium, which previously has been limited to permeameter studies. The experimental program consisted of throughflow tests conducted on three different rockfill dam model setups comprising of a large-scale test conducted on a 6 m high homogenous rockfill dam and 1:10 and 1:5 scale models of the same tested in laboratory settings. The test dams were composed of uniformly graded rockfill with median particle sizes ranging from 10.2 mm to 350 mm. Based on statistical analysis conducted on the experimental data sets, a general non-Darcy type power-law describing non-linear flow through homogenous rockfill dams is proposed. Also, some of the well-known power-law relationships from the available literature are validated employing the experimental data sets.

Keywords: Hydraulic structures; Rockfill embankments; Throughflow; Non-linear flow

1.0 Introduction

Rockfill dams are vulnerable to extreme flood events leading to accidental overtopping of the dam core or even the dam crest as the dam structure is primarily composed of pervious and erodible material. Highly turbulent flow through the downstream embankment structure of rockfill dams can result in internal erosion and also destabilize the downstream slope due to dynamic pore pressure generation (Ravindra et al. 2018b). Several instances of embankment dam failures resulting as a consequence of flow through the embankment structure are documented in international literature (e.g. Leps (1975), Cruz et al. (2009) and Foster et al. (2000)). Comprehending turbulent throughflow hydraulic properties of rockfill dams facilitates effective safety assessment (e.g. Morán and Toledo (2011), Siddiqua et al. (2011), Ferdos and Dargahi (2016a), Ferdos and Dargahi (2016b) and Ravindra et al. (2018b)). Furthermore, it is also of relevance for

development of numerical models predicting rockfill dam breach process as this can assist in effective design of components of rockfill dam overtopping protection system such as the dam toe resulting in reduced risk of dam failure.

This article presents findings from experimental investigations conducted on homogenous rockfill embankments exposed to throughflow conditions to analyze non-linear throughflow properties of rockfill embankments. This is intended at adding to the state of the art in the study discipline of non-linear flow through rockfill medium, which previously has been limited to permeameter studies in laboratory settings. Extensive literature is available in the study discipline of non-linear flow through rockfill as several past studies have investigated non-Darcian throughflow aspects of rockfill medium adopting theoretical approaches and also through experimental throughflow tests conducting in varying sizes of permeameters. This has led to accumulation of various empirical equations describing the non-linear relationship between velocity and gradient of flow through rockfill. Although these different studies have provided valuable insight into throughflow hydraulics in rockfill material, research into quantitative physical validation of these relationships in actual rockfill dams is currently unavailable in international literature. This can be considered as the missing link in the process of development of a sophisticated numerical model simulating rockfill dam breach (Fig. 1). The present study is intended at addressing this issue through analysis of throughflow hydraulics in homogenous rockfill embankments.

Table 1 succinctly summarizes the fundamental differences between the various methodologies available for investigating flow through hydraulic properties of rockfill dams ranging from theoretical approaches to large scale field testing. It is evident that any findings originating from theoretical studies or from experimental investigations conducted in permeameters inevitably require validation within actual rockfill dam models at laboratory and large scales to enhance confidence in the findings for practical implementation. Due to the resource intensive nature of testing rockfill dam models, especially at large scales, research in this area has seldom been conducted and this article is conceived with the intention of bridging this gap.

It is vital to understand the significance of large-scale validation of experimental results obtained from investigations conducted in laboratory settings. Since most laboratory experiments are conducted on downscaled models, concerns regarding validity of these findings as applied to prototype scales are generally encountered in engineering applications. Fig. 2 presents a depiction of comparison of sizes of the different model setups employed in this study along with illustrative examples of permeameter setups from past investigations juxtaposed with a representative large rockfill dam of height 40 m. The large-scale field test rockfill dam model of 6 m height [a] as part of this study is presented in Fig. 2 along with two laboratory model setups [b] including (a) 1.2 m high and (b) 0.6 m high rockfill dam models. Further, Permeameter setups employed in past investigations [c] such as (a) 1.90 m x 1.0 m permeameter employed by Ferdos et al. (2015) (b) 1.5 m x 0.76 m permeameter from Siddiqua et al. (2011) and (c) 1.0 m x 0.2 m permeameter setup used in Salahi et al. (2015). It can be inferred from Fig. 2 that the laboratory test setups commonly employed in experimental studies are of significantly smaller scale in comparison with prototype rockfill dams leading to scaling concerns. Hence, test findings need validation from large-scale field tests which can be considered to be of more comparable size.

The European research project dubbed IMPACT (Investigation of Extreme Flood Processes and Uncertainties) was undertaken during the period 2001-2004 by a consortium of 11 institutions across Europe. The primary research focus of the project was the assessment and reduction of risks from extreme flooding caused by natural events or the failure of dams and flood defense structures (e.g. Zech and Soares-Frazao (2007) and Morris and Park (2007)). Experimental throughflow tests were conducted on a 6 m high prototype homogenous rockfill dam in Rossvatn, Norway as part of the IMPACT project. In a parallel study conducted by NTNU, Trondheim and SINTEF, Trondheim, model studies on 1:5 and 1:10 scaled models of the large scale test dam were conducted at the hydraulic testing facility of NTNU, Trondheim (EBL Kompetanse (2003), EBL Kompetanse (2006) and EBL Kompetanse (2007)). The test dams were composed of uniformly graded rockfill with median particle sizes ranging from d_{50} = 10.2 mm to 350 mm.

Experimental data pertaining to throughflow hydraulic behavior of rockfill embankments were accumulated as part of these studies and these have further been employed in the present study to better understand non-linear flow through actual rockfill embankments. A statistical analysis has been conducted on the obtained data sets which resulted in a general power-law of the non-Darcy form describing non-linear throughflow within the tested rockfill embankments. Furthermore, some of the well-known empirical relationships from the available literature are validated employing the experimental data sets. This study is aimed at providing a realistic description of non-linear flow through homogenous rockfill embankments and also at addressing scaling issues with regards to flow through rockfill dams and also at facilitating further development of numerical modelling tools.

1.1 Background

Flow through porous media is generally characterized as either Darcy or non-Darcy type based on confirmation of flow properties with the linear Darcy flow theory (equation 1) widely implemented in soil mechanics. Deviations from the linear trend requires the flow to be classified as non-Darcian type.

$$V = K\ i \tag{1}$$

where, V = Bulk flow velocity, K = Coefficient of permeability and i = hydraulic gradient.

Darcian or linear flow through rockfill is seldom encountered in practical applications (Leps, 1975). Penman (1971) states that for flow through rockfill to be characterized as Darcian, the permeability of the material should be of the order of $K = 10^{-5}$ m/s. To ensure such a low permeability in highly porous rockfill embankments, the interstitial voids must be completely filled with fine material to regulate the flow (Cruz et al. 2010). Wilkins (1955) states that applicability of the linear Darcy flow theory is limited to flow through small grains of the order of 0.5 mm. Flow in rockfill structures depart from the linear flow regime because of the highly porous characteristic of rockfill material resulting in large interconnected void spaces leading to high velocity flows (Siddiqua et al. 2011). When the flow regime is laminar and steady state, a linear relationship between discharge and hydraulic gradient exists and Darcy's law is applicable. Increased

flow velocity, irregularities and excessive momentum transfer perturb the flow regime and gradually the flow becomes Non-Darcian (Salahi et al. 2015). Hence, it can be concluded that Darcy's law does not adequately describe throughflow hydraulics in coarse-grained porous media especially at high velocities (e.g. Hansen et al. (1995), Venkataraman and Rama Mohan Rao (1998), Siddiqua et al. (2011) and Ferdos and Dargahi (2016a)).

Pertaining to throughflow hydraulic characteristics of rockfill dams, flow through the core as well as through the sand filter can be considered to be laminar confirming with the linear Darcy flow theory owing to considerably low permeability. However, these low velocity flows do not necessarily pose considerable threat to the integrity of the rockfill embankment. But, flow through the transition zone and the supporting fill is more problematic as the state of flow is highly turbulent as a consequence of large permeability resulting in generation of highly destabilizing forces with high internal erosion potential (e.g. Solvik (1991) and Cruz et al. (2009)). Hence, it is of importance to better understand turbulent throughflow hydraulics in rockfill embankments as this can facilitate effective design of rockfill slopes and components of rockfill dam overtopping protection system such as the dam toe.

Description of non-Darcian or turbulent flow through porous media is generally represented as a power-law function (equation 2), as demonstrated by past investigations such as Izbash (1931), Escande (1953), Wilkins (1955), Scheidegger (1963), Parkins (1966) and Siddiqua et al. (2011).

$$V = a\ i^b \tag{2}$$

where, a and b are empirical coefficients to be determined experimentally. Coefficient a depends on the properties of fluid and porous media such as porosity, particle shape, particle size, roughness, tortuosity of void structure and viscosity of fluid. Parameter b *is* dependent upon the state of flow or the level of flow turbulence (Siddiqua et al. 2011).

Numerous past studies have investigated non-Darcian throughflow properties of rockfill employing varying sizes of permeameters. In depth reviews of the exhaustive literature available in this research discipline is available in studies such as Leps (1975), Venkataraman and Rama Mohan Rao (1998), Sidiropoulou (2007), Cruz et al. (2009) and Salahi et al. (2015)). Key findings from the state of the art in the study discipline pertinent to the investigations conducted in the present article are succinctly summarized herein along with details concerning some of the well-established empirical criteria describing non-linear flow through rockfill.

1.2 Permeameter Studies

Escande (1953) conducted some of the first transmissibility tests on rockfill material with median particle size d_{50} = 38 mm in a vertical constant head permeameter of diameter D = 0.4 m and length L = 4 m. Based on experimental test results, Escande (1953) concluded that flow through the tested material was turbulent obeying a power law function (equation 2) with b = 0.5.

Engelund (1953), based on a theoretical study presented a power-law (equation 3) to describe turbulent flow through porous medium along with a general relationship for turbulent permeability of flow (equation 4).

$$i = \frac{V^2}{k_t} \tag{3}$$

$$k_t = \frac{n^3 g\, d_i}{\beta_o\,(1-n)} \tag{4}$$

with k_t signifying turbulent permeability, β_o representing the particle shape coefficient (3.6 for blasted or crushed rock) and d_i indicating the characteristic dimension or the representative particle size of the porous medium. A relationship for d_i is presented in publications such as Solvik (1991) and Cruz et al. (2009) as d_i = 1.7 d_{10}. However, some recent studies such as EBL Kompetanse (2006) and Siddiqua et al. (2011) argue on behalf of a different relationship d_i = 1.22 d_{20} .

Wilkins (1955) conducted permeameter studies on rockfill with median particle sizes ranging from d_{50} = 19 mm to 76 mm with the objective of estimating flow through capacity of rockfill embankments. Studies conducted by Wilkins (1955) employed a permeameter of dimensions D = 0.20 m and L = 0.69 m for his main series of experimental investigations. A few tests were also conducted with a permeameter of D = 0.56 m. Based on data accumulated from an elaborate testing program, Wilkins (1955) proposed a power-law (equation 5) to describe turbulent flow through rockfill.

$$V = W n m^{0.50} i^{0.54} \tag{5}$$

where, n signifies the porosity of the medium, m denotes the hydraulic mean radius defined as the ratio of the void ratio (e) to the specific surface area of the stones (S_o) and W represents a material dependent coefficient with a value of 5.243 for crushed rocks. Further, Wilkins (1963) based on additional experimental data proposed a revised version of equation 5 with W = 6.693. It should be noted that equation 5 proposed by Wilkins (1955, 1963) are of the form of equation 2 with experimentally derived empirical coefficients $a = W n m^{0.5}$ and b = 0.54.

Wilkins (1955) noted measurement of the surface area of irregular stones (S_o) as a difficult problem. To address this concern, Leps (1975) carried out an investigation to obtain a general empirical relationship to relate parameter m with the median stone size (d_{50}) of the rockfill material. Leps (1975) tabulated the values of parameter m for rock particles of median diameter ranging over a broad interval of d_{50} = 19 mm to 1220 mm which in turn translates to equation 6 (Cruz et al. 2009).

$$m = \frac{d_{50}}{8} \tag{6}$$

Further, several studies have conducted experimental testing programs in permeameters for further validation of performance of the Engelund (1953) approach (equations 3 and 4) and the Wilkins (1955, 1963) approach (equation 5). Parkins (1963, 1966) performed tests on d_{50} = 10 mm to 20 mm homogenous angular gravel and concluded that the performance of the Wilkins (1955) approach was satisfactory in

predicting the experimental results. Further, a recent study conducted by Siddiqua et al. (2011) on rockfill material with median particle size ranging over d_{50} = 10 mm to 150 mm in a large scale permeameter (D = 0.76 m and L = 2.7 m) further corroborated the performance of the Wilkins (1955, 1963) and the Engelund (1953) approaches in describing non-linear flow through coarse rockfill. The ability of the Engelund (1953) and the Wilkins (1955, 1963) approaches in describing the non-linear throughflow characteristics of rockfill embankments is further evaluated in this article as these are widely implemented in practical applications concerning throughflow hydraulics of rockfill material.

Furthermore, most past studies have not assessed throughflow hydraulic properties in sufficiently coarse rockfill material of sizes commonly employed in dam construction especially at extremely high turbulence levels. To address this concern, recent studies conducted by Ferdos et al. (2015), Ferdos and Dargahi (2016a) and Ferdos and Dargahi (2016b) have focused on investigating flow through properties in large rockfill with d_{50} = 100 mm to 240 mm at high turbulence levels. Large-scale field studies (in injection wells) and permeameter studies in laboratory settings were undertaken in this regard, aimed at calibration and validation of numerical simulation tools.

Although considerable number of investigations have investigated non-Darcian flow through rockfill material in permeameters of varying sizes, experimental validation of these past findings in rockfill embankments exposed to throughflow conditions is still of relevance. This is particularly vital considering the fact that flow through a rockfill embankment is analogous to open channel flow as the phreatic surface is exposed to atmospheric pressure whereas flow through rockfill material tested in permeameters can be considered to resemble pipe flow devoid of a well-defined phreatic surface.

2.0 Experimental setups and testing methodology

The experimental program developed as part of the IMPACT and EBL Kompetanse studies consisted of tests conducted on homogeneous rockfill dams constructed at three different scales (1:1 model of dam height H = 6 m, 1:10 and 1:5 scaled models with H = 0.6 and 1.2 m respectively). The test rockfill dams

were comprised of rockfill material with median particle sizes varying over a broad range of d_{50} = 10.2 mm to 350 mm.

Experimental throughflow tests were conducted on a 6 m high prototype homogenous rockfill dam constructed in a temporary testing location in Rossvatn, Norway. Furthermore, 1:10 and 1:5 scaled model tests of the same were conducted at the hydraulic testing facility of NTNU, Trondheim (EBL Kompetanse (2003), EBL Kompetanse (2006) and EBL Kompetanse (2007)). The following discussions outline the experimental setups employed for the testing program. The large-scale test setup, the 1:10 and 1:5 scale models of the same are termed as models setups M1, M2 and M3 respectively herein.

2.1 Large-scale field test experimental setup

The large scale field testing site was located 600 m downstream of Rossvatn dam, Norway which is a 20 m high and 300 m long combined rockfill and gravity dam. The dam spillway consists of three identical bottom outlet gates with a combined capacity of 450 m^3/s at full supply level. The gates were used to regulate inflow to the testing location (EBL Kompetanse, 2006). Two water level gauges were situated upstream of the test dam to monitor water level in the reservoir formed upstream of the test embankment and furthermore, two gauges were positioned downstream of the test dam for discharge measurements from the test site.

The planar, cross-sectional and the longitudinal sectional design details of the test homogenous rockfill embankment are depicted in Figs. 3a, 3b and 3c respectively. The 6m high homogenous rockfill embankment (M1) was constructed in a channel with mean top width of 42.8 m. The cross-sectional geometric outline consisted of crest and bottom widths of 2 m and 20 m respectively with upstream and downstream inclinations of S = 1:1.5 (V: H). The inclination of the embankment side slope was chosen in accordance with Norwegian rockfill dam construction practice (e.g. NVE (2012), Hiller et al. (2018) and Ravindra et al. (2018a)). The abutment profiles at the test location were steep resulting in a trapezoidal channel cross-section (Figs. 3c and 4a). The rockfill embankment of volume $V_E \approx 2000$ m^3 was constructed

of uniformly graded rockfill material with median stone size of d_{50} = 350 mm. During embankment construction, a set of 4 piezometers (P_1 to P_4) were installed within the embankment structure at an elevation of 2 m from the channel bottom at a spacing of 4 m along the flow direction for throughflow depth measurements (Fig. 3). Images from the test site depicting the test embankment prior to and during testing are presented in Figs. 4a and 4b respectively. In addition, an illustrative throughflow phreatic surface is presented in Fig. 3b with parameter $h\,(k)_j$ denoting the total throughflow depth at the respective piezometer locations (k = 1 to 4) for a particular discharge step (j = 1 to Ω with Ω being the discharge step at dam failure). Parameter $h\,(m,\ k,\ k+1)_j$ signifies the mean flow depth between two consecutive piezometer locations (P_k and P_{k+1}) at a particular discharge step j (Fig. 3b). Δx stands for the horizontal distance between two consecutive piezometers along the flow direction. Construction details of the test dam were obtained from EBL Kompetanse (2006).

2.2 Model tests experimental setup

The 1:10 and 1:5 scale models of the large-scale test dam were constructed in flumes available at the hydraulic testing facilities of NTNU, Trondheim. The 0.6 m high dams (M2) were constructed in a 2.2 m wide and 10 m long stepped flume and the 1.2 m high dams (M3) were constructed in a 4 m wide and 10 m long flume. Construction details of the 0.6 m and the 1.2 m test dams are presented in Figs. 5 and 6 respectively. Pumps with combined capacities of 0.3 m^3/s and 0.9 m^3/s supplied discharge to the upstream flume reservoirs of model setups M2 and M3 respectively. Perforated walls were situated upstream of the test dams to reduce flow turbulence and fluctuations ensuring calm inflow. The stepped longitudinal profile of the flume for M2 assisted with avoiding downstream tail water build-up and for M3, short distance to the flume outlet addressed this concern.

All test dams for model setup M2 were built with upstream and downstream inclinations of 1:1.5. However, due to limited availability of space within the flume, test dams for model setup M3 were constructed as partial dam structures with only the downstream embankment built with an inclination of

1:1.5 (Fig. 6). From a dam safety standpoint, it is of importance to comprehend the throughflow properties within the downstream shoulder of a rockfill dam in comparison with the upstream embankment as the downstream slope of rockfill embankments are exposed to higher degree of destabilizing forces under turbulent throughflow conditions. Also, the large-scale field test model (M1) consisted of piezometers installed at the center and within the downstream half of the embankment. Hence, model setups for M3, influenced by limited availability of space in the flume, were constructed as half dams with only the downstream half of the embankment structure.

Further, the flume sidewalls for both setups were sloped at 1:1 transforming the flume cross-section to a trapezoidal profile. This was done to account for the steep abutment profile observed at the test location in Rossvatn, Norway which resulted in a trapezoidal channel cross-section. For model setup M2, a total of 7 piezometers were positioned along the centerline of the dam sections with uniform spacing of 0.3 m for throughflow depth measurements and 2 piezometers were placed upstream of the test dam sections for water level measurements. For M3, 5 piezometers with even spacing of 0.5 m were installed within the embankment structures of the test dams and a single piezometer was installed upstream of the test embankments. Construction details of the experimental setup were obtained from EBL Kompetanse (2006).

2.3 Testing methodology and material properties

A series of 7 tests were conducted on the model dams described in earlier discussions. A single throughflow test was conducted on the 6 m high rockfill embankment which was constructed of uniformly graded rockfill material (with coefficient of uniformity, $C_u = d_{60}/d_{10} = 1.2$) with $d_{50} = 350$ mm. Further, a set of 6 throughflow tests were carried out on the 1:10 and 1:5 models comprised of uniformly graded rockfill material ($C_u = 1.3$ to 2.0) with median stone sizes ranging over the interval $d_{50} = 10.8$ mm to 203.7 mm. The measured porosities for the employed rockfill material were consistent within the range, $n = 0.40$ to 0.52. Mean grain density of the employed rockfill material was $\rho_s = 3060$ kg/m^3. The test embankments were exposed to incremental throughflow discharges in steps of ΔQ (Table 2). The discharge levels were maintained constant over regular time intervals of 10 minutes to ensure attainment of steady state flow

within the dam structure. The process was repeated until the development of total embankment breach characterized by the breach discharge represented as Q_b. However, for the tested dams constructed with large size rockfill with $d_{50} > 87.5$ mm, ultimate dam breach could not be achieved even with application of maximum flow (Q_{max}) considering capacity of the channel for the large-scale test and the capacities of the flumes for the model tests. The piezometric pressure head measurements at the individual piezometers located within the dam structure were recorded for the corresponding throughflow magnitudes. Further details regarding the construction aspects of the test dams, rockfill material properties and particulars of testing procedure are presented in Table 2. For additional information regarding rockfill material properties employed in this study, reference is made to technical reports EBL Kompetanse (2006) for model setup M1, Kjellesvig (2002) for M2 and Sand (2002) for M3.

In Table 2, the individual tests are denoted as Mα-Tθ, where α represents the model index and θ signifies the test number. Parameters H and W_{cr} represent the height and crest width of the rockfill embankments respectively. S denotes the upstream and downstream embankment slope values. For tests conducted with model setup M3, S represents only the downstream slope as the embankments were constructed as partial dams incorporating only the downstream embankment structures. Details regarding rockfill material properties such as the specific gravity (SG), median stone diameter (d_{50}), coefficient of uniformity (C_u) and porosity are also presented in Table 2. The testing procedures are described through the parameter ΔQ symbolizing the throughflow discharge intervals. Furthermore, the particle size distribution curves for the materials used in the different tests are presented in Fig. 7.

3.0 Data analysis

3.1 Throughflow gradient-velocity relationship within the test dams

The accumulated data sets from the individual tests conducted on test rockfill dams (Table 2) are subjected to a statistical evaluation to comprehend the throughflow i-V characteristics within the rockfill embankments. As stated previously, throughflow depths at individual piezometric locations were recorded

as a function of incremental discharges as part of the testing procedure (Fig. 3b). The measured depths were in turn used to compute the flow gradients and average throughflow velocities within the test embankments. A conceptual representation of the phreatic surface for throughflow is presented in Fig. 3b for illustration of adopted terminologies. The gradient driving throughflow between any two consecutive piezometers at a particular throughflow magnitude is computed as the ratio of drop in head between the respective piezometer locations to the horizontal distance between them (equation 7). Further, the corresponding average bulk flow velocity was computed as the ratio of throughflow magnitude to the mean cross-sectional area of the flow between the two consecutive piezometric locations (Fig. 3b) (equation 8).

$$i\,(k, k+1)_j = \frac{h\,(k)_j - h\,(k+1)_j}{\Delta x} \tag{7}$$

$$V\,(m, k, k+1)_j = \frac{Q_j}{A\,(m,k,k+1)_j} = \frac{Q_j}{h\,(m,k,k+1)_j .\ w\,(m,k,k+1)_j} \tag{8}$$

where $i\,(k,\ k+1)_j$ and $V\,(m,\ k,\ k+1)_j$ represent the hydraulic gradient and mean bulk throughflow velocity between two consecutive piezometer locations designated as k and $k + 1$ at a particular throughflow magnitude Q_j. $A\,(m,\ k,\ k+1)_j$, $h\,(m,\ k,\ k+1)_j$ and $w\,(m,\ k,\ k+1)_j$ represent the mean cross-sectional area of flow, mean flow depth and mean flow cross-section width between the two successive piezometer locations k and $k + 1$. It should be noted that variation of dam width with depth as a result of trapezoidal longitudinal-section of the dam is accounted for within the term $w\,(m,\ k,\ k + 1)_j$. The mean flow depth ($h\,(m,\ k,\ k+1)_j$) between two successive piezometer positions is computed as $(h\,(k)_j + h\,(k+1)_j)/2$ with $h\,(k)_j$ and $h\,(k+1)_j$ representing the flow depths at the respective piezometer locations. Further, the mean flow cross-section width ($w\,(m,\ k,\ k+1)_j$) between two successive piezometer positions is computed as $(w\,(k)_j + w\,(k+1)_j)/2$ with $w\,(k)_j$ and $w\,(k+1)_j$ representing the mean flow cross-section widths at the respective piezometer locations.

The porosity of the rockfill medium has considerable impact on throughflow hydraulic properties and to incorporate this in the analysis, the term void velocity ($V_n = V/n$) is adopted henceforth, giving rise to a modified version of the power-law (equation 2) presented as equation 9.

$$V_n = a\, i^b \tag{9}$$

The hydraulic gradients and the corresponding void velocities within the test dams at incremental throughflow magnitudes were computed between consecutive piezometers for all the tests outlined in Table 2 up to dam breach (Q_b) or until the maximum applied flow (Q_{max}). Further analysis of the i-V_n trends within the different test dams were conducted over the range of applied through flows for which the test dams were stable. The term stability herein refers to the ability of the rockfill dams to withstand incremental hydraulic gradients as a function of incremental through flows. Investigation of the development of hydraulic gradients within the tested rockfill embankments revealed that hydraulic gradients at different locations within the test dams underwent gradual increments as a function of incremental applied through flows. This trend was observed up to a point of inflection after which a decrease in hydraulic gradient was observed with further increments of the applied through flows. Similar observations with respect to evolution of hydraulic gradients within rockfill dams with incremental throughflow are documented within Javadi and Mahdi (2014). Further analysis with the i-V_n trends in this study were conducted over stable states of the tested dams or up to the point of transition of the computed i-V_n trends at different locations within the embankment structure from an increasing trend to a decreasing trend. Investigation of internal stability of rockfill embankments is beyond the scope of the present study.

The computed i-V_n trends for the tests over the range of flows for which the dams were stable are presented in Fig. 8a and 8b for model setups M2 and M3 respectively and in Fig. 9 for model setup M1. It can be inferred from the depictions that the computed i-V_n trends for the tests followed non-linear trends in general. Although some degree of variability in the i-V_n trends were observed at different locations within the tested dam structures, the trends in general were in good agreement with each other. The observed

variability could be explained as a consequence of local variations in porosity or packing density of rockfill medium at the different piezometric locations due to disparities in manual construction efficiency. The i-V_n trends are presented over a broad range of hydraulic gradients (i = 0.01 to 0.5) for tests conducted with model setups M3 and M2. But, for model setup M1, i-V_n trends are presented over a narrower hydraulic gradient range of i = 0.24 to 0.40 as a consequence of unavailable measurements of flow depths for lower throughflow magnitudes as the piezometers were located at 2 m elevation from the dam bottom.

To discern consistency with throughflow properties across models, a comparative evaluation between tests M2-T4 and M3-T1 was carried out. This was considering that tests M2-T4 and M3-T1 were conducted with 0.6 m and 1.2 m high dams respectively and both the test dams were constructed with the same rockfill material with median particle size of d_{50} = 0.876 m and material properties n = 0.49 and C_u = 1.4. Fig. 10 presents the computed i-V_n trends within the two test dams and as can be inferred, the plots agree well with one another thereby demonstrating consistency with throughflow properties across the models.

Trend lines of the form $y = a\,x^b$ were added to the individual i-V_n plots demonstrating excellent correlation with the parent data sets as presented in Table 3. Further, the obtained values of parameters a and b for the respective tests are also tabulated in Table 3. It could be observed from Table 3 that the parameter b for all the tests was consistently placed within the range of 0.48 to 0.55 except for Test M3-T2, wherein a lower value of parameter b = 0.41 was found. The average of the obtained b values was found to be b = 0.51. As stated earlier, parameter b within the power-law (equation 2) represents the degree of flow turbulence. The obtained average value of parameter b = 0.51 signifies fully developed turbulent flow regime. This finding is in line with conclusions of several past studies such as Escande (1953), Soni et al. (1978) and Siddiqua et al. (2011) with regards to parameter b that $b \approx 0.5$ represents post-linear or non-Darcian flow regime. Furthermore, correlation between material properties such as C_u and n and parameter b were evaluated and no definitive relationships could be observed in this regard between the parameters. Considering the anomalous value of b = 0.41 for test M3-T2, although the exact reason for the observation

is not apparent, the large size of the rockfill particles used for the test (d_{50} = 0.203 m) could offer a possible explanation in this regard as the mean stone diameter for this particular test was oversized considering the dam height (H = 1.2 m). This could inhibit complete development of flow turbulence resulting in a lower value of b. Furthermore, the porosity of the dam material for M3-T2, n = 0.52 was slightly higher in comparison with other materials which fall within a range of 0.40 – 0.49 and this could also influence flow turbulence levels within the test dam.

Further, Fig. 11 represents the correlation between parameters a and d_{50} for the respective tests. A clear exponential trend can be observed in this regard quantitatively described by a symmetrical sigmoidal trend line represented as equation 10. The trend line demonstrates good correlation with the parent dataset with an R^2 = 0.95.

$$a = \left(72.987 - \frac{73.613}{\left(1+\left(\frac{d_{50}}{1.136\,.\,10^{9}}\right)^{0.179}\right)}\right) \tag{10}$$

To obtain a general power-law describing the non-linear i-V_n trend for throughflow in rockfill embankments, the experimentally derived results for parameters a and b were substituted in equation 9 resulting in equation 11. The value for parameter b is adopted as 0.51 as this represents the average for all tests.

$$V_n = \left(72.987 - \frac{73.613}{\left(1+\left(\frac{d_{50}}{1.136\,.\,10^{9}}\right)^{0.179}\right)}\right) i^{0.51} \tag{11}$$

3.2 Performance based evaluation of power-law relationships

The proposed power-law relationship describing the correlation between hydraulic gradient and void-velocity of flow through rockfill embankments (equation 11) has further been subjected to a comparative performance based evaluation in the present section along with some well-establish power-law relationships from international literature. The Engelund (1953) (equations 3 and 4) and the Wilkins (1955, 1963)

(equation 5) power-law relationships obtained from experimental studies conducted in permeameters, describing non-linear flow through rockfill medium are widely implemented in various disciplines of hydraulic engineering. These criteria have been included in the present study to investigate their validity in describing throughflow properties in actual rockfill embankments.

The Engelund (1953) and the Wilkins (1955, 1963) power laws in i-V_n form are presented as equations 12 and 13 respectively with terminologies defined earlier. Some of the long-standing research questions attached to these criteria were introduced earlier. Considering equation 12, consideration of the representative characteristic dimension of the porous medium has been in question as whether d_i =1.7 d_{10} or d_i =1.22 d_{20}. Further, considering equation 13, two different values for the material dependent empirical coefficient W have been proposed in Wilkins (1955) and Wilkins (1963) as 5.243 and 6.693 respectively. The present analysis is intended at validating the performance of these individual criteria by quantifying the ability of these power-laws in accurately describing observations from the experimental testing program and also at addressing the associated research questions.

$$V_n = \sqrt{\frac{n\, g\, d_i}{\beta_o\,(1-n)}}\; i^{0.50} \tag{12}$$

$$V_n = W\, m^{0.50}\, i^{0.54} = W\, \left(\frac{d_{50}}{8}\right)^{0.50} i^{0.54} \tag{13}$$

Equations 11, 12 and 13 are employed herein to predict the void velocities (V_n) within the tested rockfill dam sections with measured hydraulic gradients as inputs. Two distinct versions of equation 12 are adopted as Engelund (1953)-a and Engelund (1953)-b with d_i =1.7 d_{10} or d_i =1.22 d_{20} respectively and two separate versions of equation 13 are considered as Wilkins (1955) and Wilkins (1963) with W = 5.243 and 6.693 respectively. The required d_i values within Engelund (1953)-a and Engelund (1953)-b equations were computed employing the particle gradation curves available for consideration within EBL Kompetanse (2006), Sand (2002) and Kjellesvig (2002). The parameter m within Wilkins (1955) and Wilkins (1963) was computed as per equation 6 in line with the recommendations of Leps (1975).

To quantify the effectiveness of the individual criteria in predicting the experimental data and to select the best relationship for non-linear flow through rockfill, the normalized objective function (NOF) criteria will be employed herein as demonstrated by Salahi et al. (2015), Gikas et al. (2006) and Kornecki et al. (1999). The NOF is defined as the ratio of root mean square error (RMSE) to the overall mean (X_m) of the experimental data (Salahi et al. 2015).

$$\text{NOF} = \frac{\text{RMSE}}{X_m} \tag{14}$$

$$\text{RMSE} = \sqrt{\frac{\sum_{r=1}^{N}(P_r - O_r)^2}{N}} \tag{15}$$

with N representing the number of experimental data points, X_m signifying the mean of experimental data, P_r and O_r representing the predicted and the observed values. As per Kornecki et al. (1999), the ideal value of NOF is 0.0 which suggests that lower values of NOF entails better performance.

Table 4 summarizes the results from the comparative analysis conducted to analyze and rank the performance of the various criteria. The proposed power-law relationship (equation 11) demonstrated the lowest NOF of 0.1685 suggesting the best performance (Rank 1) among the analyzed criteria closely followed by the Engelund (1953)-b approach with NOF of 0.1850 (Rank 2). Engelund (1953)-a and Wilkins (1955) criteria with higher NOF values of 0.2654 and 0.3113 were ranked at number 3 and 4 respectively followed by the Wilkins (1963) approach ranked fifth with a high NOF of 0.6435.

Depiction of the correlation between the observed void velocities (V_n (O)) and the predicted void velocities (V_n(P)) employing equation 11 is presented in Fig. 12. As can be inferred from the depiction, the majority of the predictions were in good agreement with the observations falling within a 5% and 10% error intervals with few data points lying outside the 10% error interval. The proposed equation 11 successfully predicted the void velocities within all tests from models M1 and M2 as all data points found to lie within the 5% error interval for these tests. All of the outliers were found to be from tests M3-T2 and M3-T1. As stated earlier, the value of parameter b was found to be 0.41 for test M2-T2, which was lower as compared

to the average of 0.51 for all the tests. Equation 11 was developed assuming an average value for b as 0.51 and this could offer an explanation for outliers observed from test M2-T2. Further, outliers from M3-T1 represent sporadic peaks in measurements (Fig. 8b) which are not simulated by the proposed equation 11.

4.0 Discussions

Findings from the experimental study program investigating non-linear throughflow hydraulic characteristics of rockfill embankments add to the state of the art in the study discipline of non-linear flow through rockfill medium, which has been limited to permeameter studies in laboratory settings. The experimental testing program consisting of large-scale field studies and hydraulic modelling studies in laboratory settings resulted in a power-law relationship (equation 11) describing the i-V_n trends within rockfill embankments. Since the experimental study program was comprised of large-scale field studies on a 6 m high rockfill dam and hydraulic model studies on 1:10 and 1:5 scale models of the same, the study findings address scaling concerns generally encountered in engineering applications by demonstrating a consistent trend in experimental results over three disparate model scales. Furthermore, since the test rockfill dams comprised of rockfill material of particle sizes spanning over a wide spectrum (d_{50} = 10.8 mm to 350 mm), the study findings establish confidence in the documented results for implementation in large-scale applications.

Comprehension of throughflow hydraulic properties of rockfill embankments can assist in the design process of rockfill embankments considering accidental leakage or overtopping events. It can also facilitate the design of overtopping protection elements of rockfill dams such as the dam toe, which acts as a defense mechanism for rockfill structures under unanticipated overtopping events. Sound knowledge of the i-V behavior of flow through rockfill embankments can enable the development of effective numerical modelling techniques for simulating rockfill dam breach mechanisms thereby enhancing design efficiency.

The proposed power-law (equation 11) describing the non-linear relationship between the hydraulic gradient (i) and the throughflow void velocity (V_n) has been validated for gradient values $i < 0.5$

and d_{50} spanning over a broad range of 10.8 mm to 350 mm and implementation of the criteria beyond these ranges should be considered with caution. The material properties of the employed rockfill material such as the porosity and the coefficient of uniformity were within the range of of n = 0.40 to 0.52. These parameter can play major roles in discerning throughflow properties within rockfill embankments. Validation of the performance of the criteria beyond these limits is recommended in future investigations. Although the C_u values within this study vary over a range of 1.2 to 2.0, the rockfill material are still classified as uniformly graded material. For the material to be considered well graded, C_u would have to be larger than 4 or 6. Hence, the research findings are limited to uniformly graded rockfill material and study of flow through behavior in rockfill dams constructed of well-graded rockfill is recommended.

The performance based comparative evaluation of the various power-law relations based on the normalized objective function (NOF) indicated that the proposed power-law (equation 11) followed by Engelund (1953)-b approaches best predicted the experimental results corroborated by the lowest NOF values. Further, the performance of Engelund (1953)-b approach was better in comparison with Engelund (1953)-a criteria suggesting that the relationship d_i =1.22 d_{20} can be considered to better represent the characteristic dimension of porous medium when juxtaposed with d_i =1.7 d_{10}. Furthermore, the performance of Wilkins (1955) approach was found to be better in comparison with Wilkins (1963) with signifying better characterization of material dependent coefficient W = 5.243 in comparison with W = 6.693. Also, good performance of equations conceived and validated through investigations conducted in permeameters in describing non-linear flow through actual rockfill embankments demonstrate the validity of permeameter testing in simulating throughflow conditions in practical applications.

Conclusions

This article presents findings from experimental investigations conducted on homogenous rockfill embankments exposed to throughflow conditions to analyze non-linear throughflow properties of rockfill embankments. This was intended at adding to the state of the art in the study discipline of non-linear flow

through rockfill medium, which previously has been limited to permeameter studies in laboratory settings. The experimental program consisted of 7 tests conducted on three different setups including a large-scale test conducted on a 6 m high homogenous rockfill embankment and 1:10 and 1:5 scale models of the same tested in laboratory settings. The test dams were composed of uniformly graded rockfill with median particle size ranging from 10.2 mm to 350 mm. A statistical analysis conducted on the obtained data sets resulted in a general non-Darcy power law (equation 11) describing the non-linear i-V_n trend for throughflow within rockfill embankments.

Some of the well-established power-law relationships obtained in permeameter studies such as the Engelund (1953) and the Wilkins (1955, 1963) approaches are validated employing the experimental data sets demonstrating the validity of permeameter testing in simulating throughflow conditions in actual rockfill dams. The characteristic dimension of the rockfill medium within the Engelund (1953) approach was found to be best represented by the relationship d_i =1.22 d_{20} when juxtaposed with d_i =1.7 d_{10}. Considering the material dependent coefficient in the Wilkins (1955, 1963) approach, the analysis results indicate better performance with W = 5.243 in comparison with W = 6.693.

Since the experimental testing program consisted of large-scale field studies and hydraulic modelling studies in laboratory settings, the study findings address scaling concerns generally encountered in engineering applications by demonstrating a consistent trend in experimental results over three different model scales. Furthermore, since the test rockfill dams comprised of rockfill material of particle sizes spanning over a wide spectrum (d_{50} = 10.8 mm to 350 mm), the study findings establish confidence in the documented results for implementation in large-scale applications.

Comprehension of throughflow hydraulic properties of rockfill embankments can assist in the design process of rockfill embankments and components of the overtopping protection system for rockfill dams such as the dam toe under unanticipated overtopping events thereby assisting in enhancement of

rockfill dam safety. This can also support the development of numerical modelling tools and techniques for simulating rockfill dam breach mechanisms thereby enhancing design efficiency.

Acknowledgements

The support and co-operation of organizations EnergiNorge, Norway, Sweco, Trondheim and SINTEF, Trondheim in making available the experimental data sets is highly appreciated. The contributions of all partner institutions involved in conduction of the experimental programs is acknowledged.

Funding

The authors acknowledge the financial support offered by EnergiNorge, Norway and HydroCen, Norway.

Notations

A = Flow cross-section area (m^2)
a = Empirical coefficient ($m\ s^{-1}$)
b = Empirical coefficient (-)
C_u = Coefficient of uniformity (-)
D = Diameter of permeameter (m)
d_i = Characteristic particle size (m)
d_p = Stone diameter corresponding to p % finer (m)
e = Void ratio (-)
g = Acceleration due to gravity ($m\ s^{-2}$)
H = Dam height (m)
h = Total throughflow depth (m)
i = Flow gradient (-)
k_t = Turbulent permeability ($m^2\ s^{-2}$)
L = Length of permeameter (m)
m = Hydraulic mean radius (m)
N = Number of data points (-)
NOF = Normalized objective function (-)
n = Porosity (-)

O_r = Observed values with index r (m s^{-1})

P_r = Predicted values with index r (m s^{-1})

Q_b = Embankment breach discharge (m^3 s^{-1})

Q_j = Discharge magnitude at step (j) (m^3 s^{-1})

Q_{max} = Maximum applied flow (m^3 s^{-1})

RMSE = Root mean square error (-)

S = Slope (-)

S_o = Surface area of the stones (m^2)

SG = Specific gravity (-)

V = Bulk flow velocity (m s^{-1})

V_E = Volume of the embankment (m^3)

V_n = Void velocity (m s^{-1})

V_n (O) = Observed Void velocity (m s^{-1})

V_n (P) = Predicted Void velocity (m s^{-1})

W = Material dependent coefficient for rockfill (m-s)

W_{cr} = Crest width of test dams (m)

w = Mean flow cross-section width (m)

X_m = Mean of experimental data (m s^{-1})

α = Model index (-)

β_o = Particle shape coefficient (-)

ΔQ = Discharge steps (m^3 s^{-1})

Δx = Horizontal distance between piezometers (m)

θ = Test number (-)

ρ_s = Density of stones (kg m^{-3})

Ω = Final discharge step (-)

References

Cruz, P.T., Materon, B., Freitas, M., 2010. Concrete Face Rockfill Dams. CRC Press, Taylor and Francis Group.

EBL Kompetanse AS. 2007. Stability and breaching of dams, Report on Sub-Project 3: Breaching of Embankment Dams.

EBL Kompetanse, A., 2006. Stability and breaching of embankment dams, Report on Sub-project 2: Stability of downstream shell and dam toe during large through-flow.

EBL Kompetanse AS. 2003. Stability and breaching of dams, Report on Sub-Project 1: Shear strength of Rockfill and Stability of Dam Slopes.

Engelund, F., 1953. On the laminar and turbulent flows of groundwater through homogeneous sand. Trans. Dan. Acad. Tech. Sci., 3, 1–105.

Escande, L., 1953. Experiments Concerning The Infiltration Of Water Through A Rock Mass. Proc. Minnesota Int. Hydro Conv.

Ferdos, F., Dargahi, B., 2016a. A study of turbulent flow in large-scale porous media at high Reynolds numbers. Part I: numerical validation. J. Hydraul. Res. 54, 663–677.

Ferdos, F., Dargahi, B., 2016b. A study of turbulent flow in large-scale porous media at high Reynolds numbers. Part II: flow physics. J. Hydraul. Res. 54, 678–691.

Ferdos, F., Worman, A., Ekstrom, I., 2015. Hydraulic Conductivity of Coarse Rockfill used in Hydraulic Structures. Transp. Porous Media 108, 367–391.

Foster, M., Fell, R., Spannagle, M., 2000. The statistics of embankment dam failures and accidents. Can. Geotech. J. 37, 1000–1024.

Gikas, G.D., Yiannakopoulou, T., Tsihrintzis, V.A., 2006. Modeling of non-point source pollution in a Mediterranean drainage basin. Environ. Model. Assess. 11, 219–233.

Hansen, D., Garga, V.K., Townsend, D.R., 1995. Selection and application of a one-dimensional non-Darcy flow equation for two-dimensional flow through rockfill embankments. Can. Geotech. J. 32, 223–232.

Hiller, Priska H, Jochen Aberle and Leif Lia. Displacements as failure origin of placed riprap on steep slopes. J Hyd Res 56.2 (2018): 141-155.

Izbash, S. V, 1931. O filtracii v krupnozernistom materiale, in: Izv. Nauchno Issled. Inst. Gidro-Tekh. (NILG). Leningrad, Russia.

Javadi N, Mahdi, T F. 2014. Experimental investigation into rockfill dam failure initiation by overtopping. Nat. Hazards. 74 (2): 623–637.

Kjellesvig HM. 2002. Stability and Failure Mechanisms of Dams, Data Report No. 1. Laboratory tests at Department of Hydraulic and Environmental Engineering, NTNU, Trondheim.

Kornecki, T.S., Sabbagh, G.J., Storm, D.E., 1999. Evaluation of runoff, erosion, and phosphorus modeling system - SIMPLE. J. Am. Water Resour. Assoc. 35, 807–820.

Leps, T.M., 1975. Flow through rockfill: In Embankment-dam Engineering, Vol 12, No. ed, John Wiley and Sons INC., Pub., NY, 1973, 22P.

Morán, R., Toledo, M.A., 2011. Reserarch into protection of rockfill dams from overtopping using rockfill downstream toes. Can. J. Civ. Eng. 38 (12), 1314–1326.

Morris, M.W., Park, H., 2007. Breach formation : Field test and laboratory experiments Formation d ' une brèche dans une barrage : Test sur le terrain et expériences en laboratoire. J. Hyd. Res. 45, 9–17.

NVE, 2012. Veileder for fyllingsdammer. Nor. Water Resour. Energy Dir. 21–25.

Parkin AK. 1963. Rockfill dams with inbuilt spillways. Water Res. Edn. Aust., Bull. No.6.

Parkin AK, Trollope DH and Lawson JD. Rockfill structures subject to water flow. Journal of Soil Mechanics & Foundations Div 92.ASCE# 4973 Proceeding (1966).

Penman, A.D.M., 1971. Rockfill. Build. Res. Stn. Curr. Pap. Dep. Environ. CP 15/71.

Ravindra, G.H.R., Sigtryggsdottir, F.G., Lia, L., 2018a. Protection of embankment dam toe and abutments under overtopping conditions, in: 3rd International Conference on Protection against Overtopping, UK.

Ravindra, G.H.R., Sigtryggsdottir, F.G., Lia, L., 2018b. Evaluation of Design Criteria for Downstream Riprap of Rockfill Dams, in: Proceedings of the 26th Congress on Large Dams. Vienna.

Salahi, M.-B., AsI, M.S., Parvizi, M., 2015. Nonlinear Flow through a Packed-Column Experiment. J. Hydraul. Eng. 20(9):0401.

Sand K. 2002. Stability and Failure Mechanisms of Dams, Sub Project No. 2. Laboratory tests at SINTEF Energy Research, Trondheim.

Scheidegger, A.E., 1963. The physics of flow through porous media. Univ. Toronto Press. Toronto, canada.

Siddiqua, S., Blatz, J.A., Privat, N.C., 2011. Evaluating Turbulent Flow in Large Rockfill. J. Hydraul. Eng. 137, 1462–1469.

Sidiropoulou, M.G., 2007. Determination of Forchheimer equation coefficients a and b. Hydrol Process. 21(4), 534–554.

Solvik, O., 1991. Throughflow and stability problems in rockfill dams exposed to exceptional loads. Sixt. Int. Congr. Large Dams 333–343.

Soni, J.P., Islam, N., Basak, P., 1978. An experimental evaluation of non-Darcian flow in porous media. J. Hydrol. 38, 231–241.

Venkataraman, P., Rama Mohan Rao, P., 1998. Darcian, transitional and turbulent flow through porous media. J. Hydraul. Eng. 124, 840–846.

Wilkins, J.K., 1963. The stability of overtopped rockfill dams.

Wilkins, J.K., 1955. Flow of water through rockfill and its application to design of dams. New Zeal. Eng. 01, 382–387.

Zech, Y., Soares-Frazao, S., 2007. Dam-break flow experiments and real-case data. A database from th European Impact research. J. Hydraul. Res. 45, Extra, 5–7.

List of Tables

Table 1. Summary of the fundamental differences between various methodologies available for investigating flow through hydraulic properties of rockfill dams

Test method	Advantages	Disadvantages
Large scale field test with rockfill dams	a. Allows for large scale validation of theoretical and laboratory test findings b. Dam size and rockfill material particle size comparable with full-scale dams thereby addressing scaling concerns c. Includes realistic flow features as found within full-scale dams	a. Resource intensive b. Field testing can result in reduced control over test conditions
Laboratory tests with rockfill dam models	a. Allows for preliminary validation of theoretical and permeameter findings b. Includes realistic flow features c. Economical d. Laboratory testing allows for good control over test conditions	a. Inability to address scaling concerns with respect to size of the dam and rockfill material size b. Requires large scale validation
Laboratory tests with permeameters	a. Allows for preliminary validation of theoretical predictions b. Can incorporate rockfill material of particle size comparable with prototype dams c. Economical d. Laboratory testing allows for good control over test conditions	a. Unrealistic flow features as it resembles pipe flow rather than free surface flow through a dam b. Inability to incorporate realistic dimensioning of the dam structure c. Requires validation within dams d. Inability to address scaling concerns
Theoretical approaches	a. Ability to consider full scale dimensioning for dam size and rockfill medium particle size b. Can incorpoate realistic flow physics c. Economical d. Scaling concerns are minimized	a. Flow physics too complex to fully incorporate all details b. Inevitably requires experimental validation

Table 2. Details of embankment construction aspects, rockfill material properties and testing procedures

Test No.	H (m)	S (-)	W_{cr} (m)	SG (-)	d_{50} (mm)	C_u (-)	n (-)	ΔQ ($m^3 s^{-1}$)	Q_b ($m^3 s^{-1}$)	Q_{max} ($m^3 s^{-1}$)
M1-T1	6	1: 1.5	2	2.78	350	1.2	0.40	5	-	30.5
M2-T1	0.6	1: 1.5	0.4	3.06	51.4	1.8	0.44	0.005	0.10	0.10
M2-T2	0.6	1: 1.5	0.4	3.06	10.8	2.0	0.45	0.005	0.025	0.025
M2-T3	0.6	1: 1.5	0.4	3.06	18.5	1.3	0.45	0.005	0.045	0.045
M2-T4	0.6	1: 1.5	0.4	3.06	87.6	1.4	0.49	0.01	-	0.15
M3-T1	1.2	1: 1.5	1.0	3.06	87.6	1.4	0.49	0.025	-	0.30
M3-T2	1.2	1: 1.5	1.0	3.06	203.7	1.7	0.52	0.05	-	0.50

Table 3. Values of experimentally derived parameters *a* and *b* for the conducted tests

Test No.	d_{50} (mm)	a (m s^{-1})	b (-)	R^2 (-)
M1-T1	350	0.83	0.55	0.92
M2-T1	51.4	0.33	0.54	0.94
M2-T2	10.8	0.13	0.52	0.71
M2-T3	18.5	0.24	0.53	0.94
M2-T4	87.6	0.51	0.48	0.90
M3-T1	87.6	0.56	0.56	0.81
M3-T2	203.7	0.58	0.41	0.82

Table 4. Summary of results from the comparative analysis

Methodology	RMSE (-)	X_m (-)	NOF (-)	Rank (-)
Equation 11	0.0396	0.2353	0.1685	1
Engelund (1953)-a	0.0625	0.2353	0.2654	3
Engelund (1953)-b	0.0435	0.2353	0.1850	2
Wilkins (1955)	0.0733	0.2353	0.3113	4
Wilkins (1963)	0.1514	0.2353	0.6435	5

List of Figures

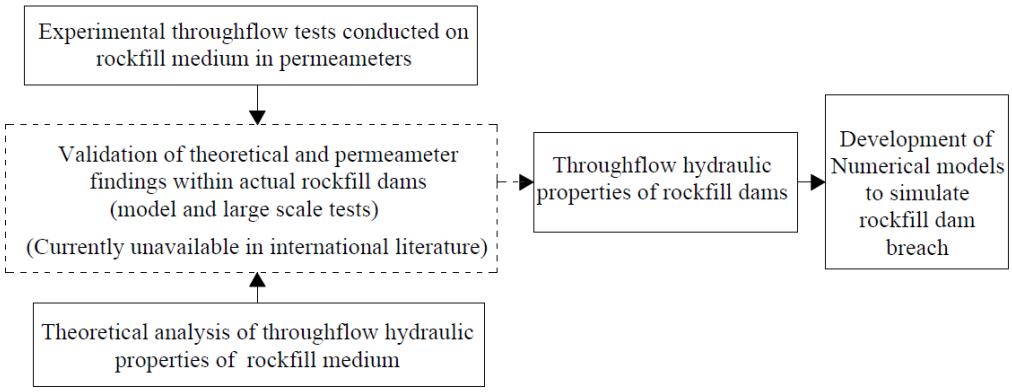

Figure 1 Illustration of processes involved in the development of a numerical rockfill dam breach model and the missing link currently unavailable in international literature which forms the subject of this article

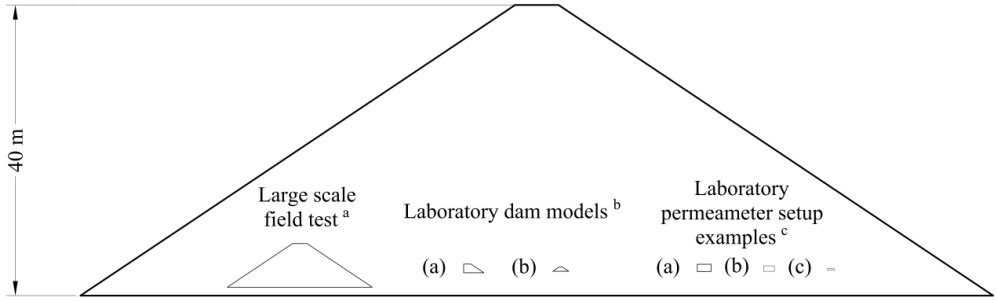

Figure 2 Illustrates size differences in disparate model setups with [a] representing the 6 m high large-scale rockfill dam model tested as part of this study; [b] Representing rockfill dam models tested in laboratory settings as part of this study; [c] Depicting representative permeameter setups used in past studies. The disparate setups are nested within a representative large rockfill dam of height 40 m.

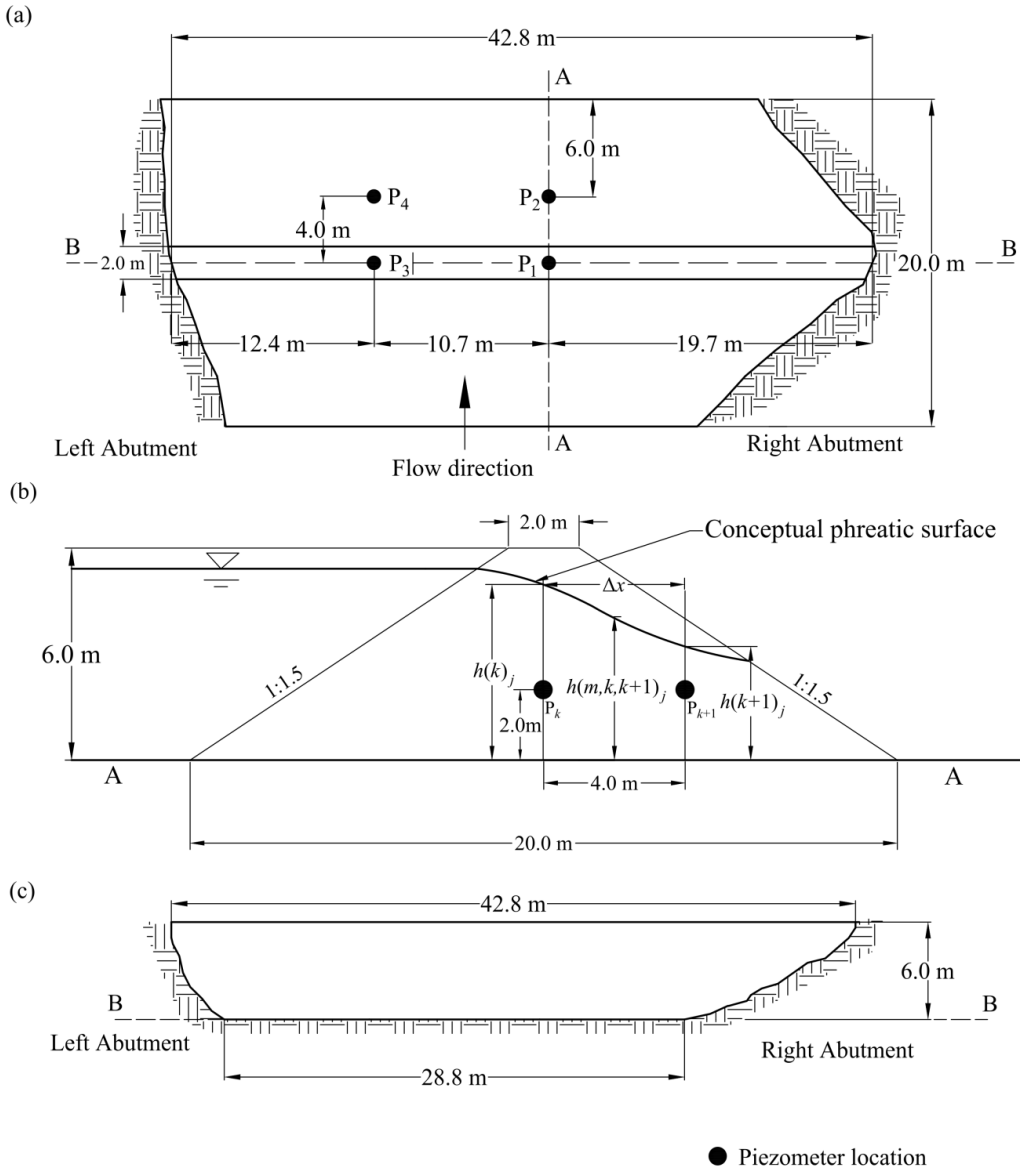

Figure 3 (a) Planar design details; (b) Cross-sectional design details (along axis A-A); (c) Longitudinal-sectional design details (along axis B-B) of the 6 m high test rockfill dam (M1).

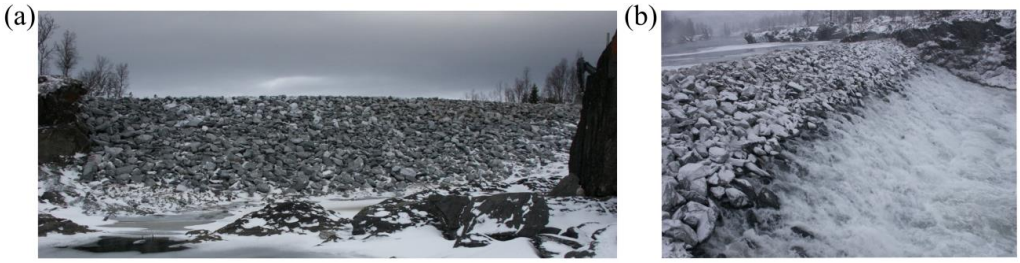

Figure 4 (a) Image of the test rockfill embankment (M1) from the test site at Rossvatn, Norway prior to testing; (b) Image of the test dam during testing (Image courtesy: EBL Kompetanse (2006)).

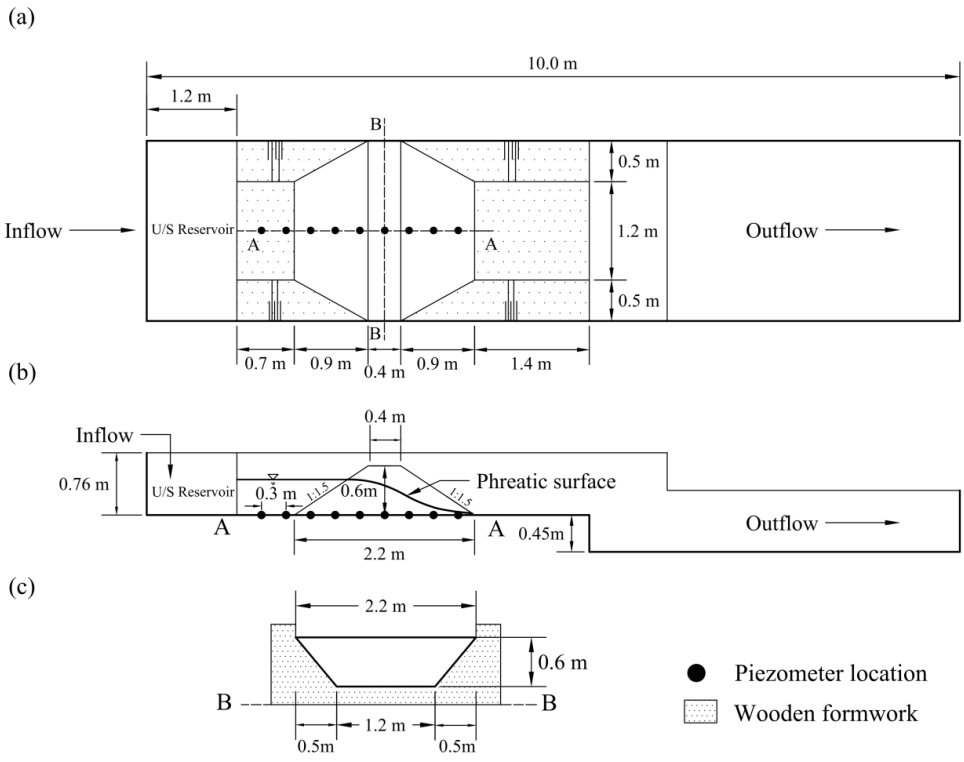

Figure 5 (a) Depiction of the planar design details; (b) Cross-sectional design details (along axis A-A); (c) Longitudinal-sectional design details (along axis B-B) of the 0.6 m test rockfill dam (M2) constructed at the hydraulic laboratory of NTNU, Trondheim.

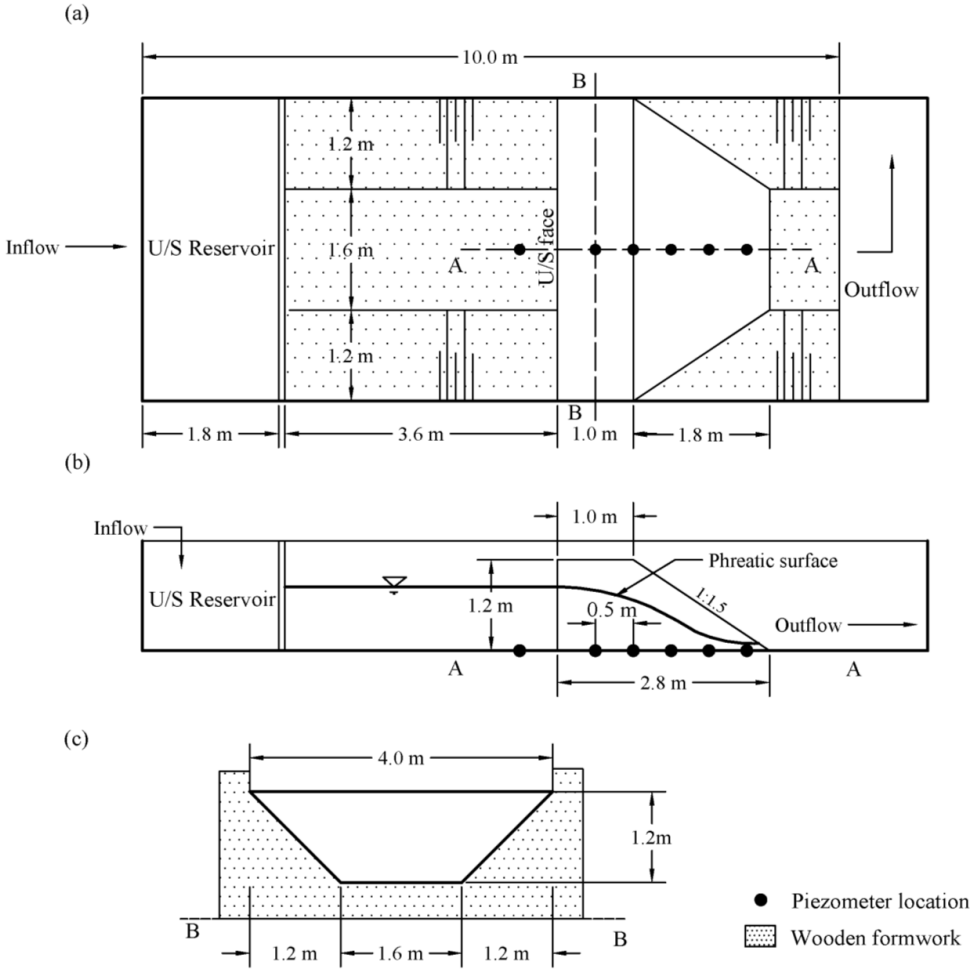

Figure 6 (a) Depiction of the planar design details; (b) Cross-sectional design details (along axis A-A); (c) Longitudinal-sectional design details (along axis B-B) of the 1.2 m test rockfill dam (M3) constructed at the hydraulic laboratory of NTNU, Trondheim.

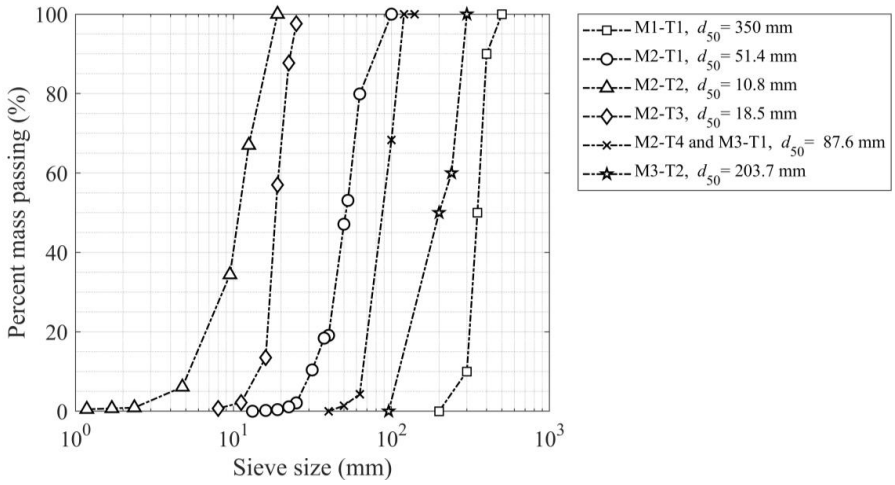

Figure 7 Particle size distribution curves for the materials employed for construction of different test dam models.

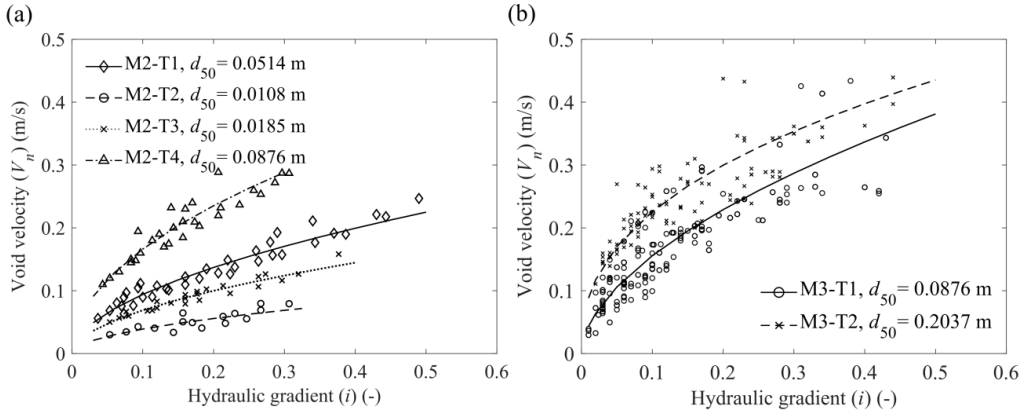

Figure 8 (a) Computed i-V_n trends - model setup M2 (b) Computed i-V_n trends - model setup M3

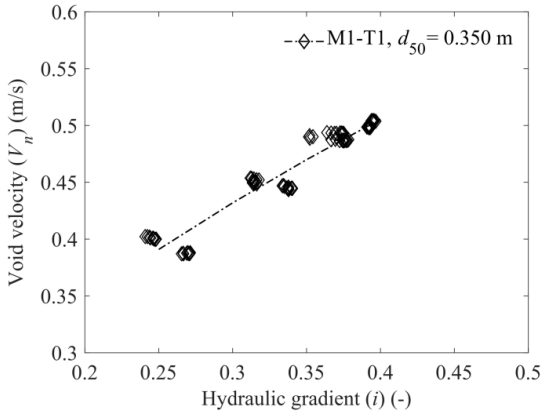

Figure 9 Computed i-V_n trends - model setup M1

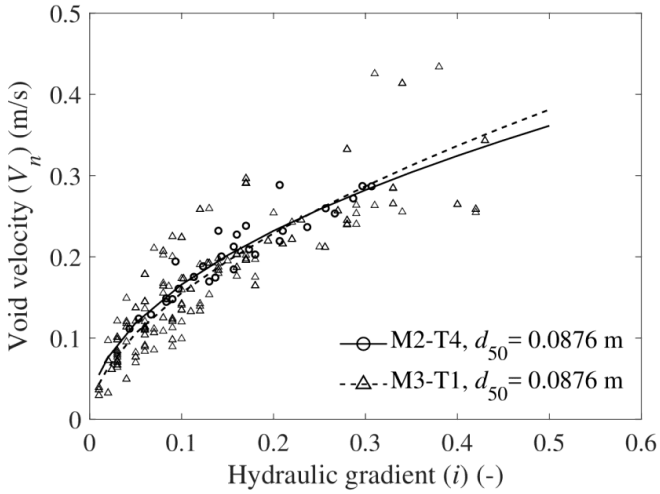

Figure 10 Comparative evaluation of i-V_n trends within model setups M2-T4 and M3-T1

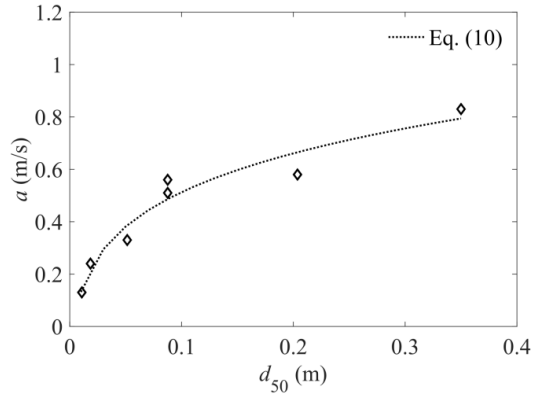

Figure 11 Relationship between parameter a and the mean rockfill particle sizes (d_{50})

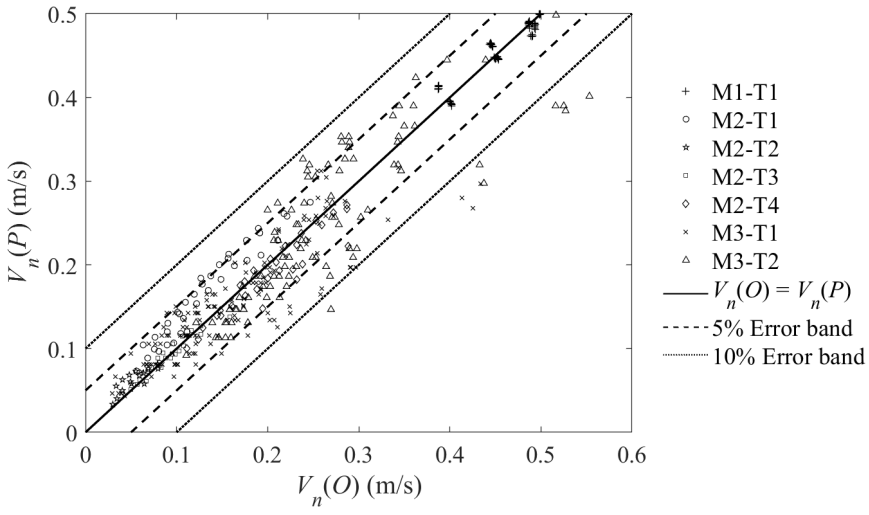

Figure 12 Depiction of correlation between the observed void velocities ($V_n(O)$) and the predicted void velocities ($V_n(P)$) for the proposed equation 11

Paper V

Effects of toe configuration on throughflow hydraulic properties of rockfill dams

Kiplesund, G. H, Ravindra, G.H.R, Rokstad, M.M, Sigtryggsdottir, F.G (2020).

Under review in the *Journal of Applied Water Engineering and Research*

Effects of toe configuration on throughflow properties of rockfill dams

Geir H Kiplesund[a], Ganesh H R Ravindra[a], Marius M Rokstad[a] and Fjóla G. Sigtryggsdóttir[a]

[a] Department of Civil and Environmental Engineering, S P Andersens veg 5, Norwegian University of Science and Technology, Trondheim, Norway, 7031

Email addresses: geir.h.kiplesund@ntnu.no (Geir H Kiplesund, author for correspondence), ganesh.h.r.ravindra@ntnu.no (Ganesh H R Ravindra), marius.rokstad@ntnu.no (Marius M Rokstad) and fjola.g.sigtryggsdottir@ntnu.no (Fjóla G. Sigtryggsdóttir).